Synthesis and Characterization of Regioregular, Amphiphilic Semifluoroalkyl-Substituted Polythiophenes and Cofacial Bis(oligothienyl)naphthalenes

A Dissertation
Presented To
The Academic Faculty

By

Shannon Watt

In Partial Fulfillment
Of the Requirements for the Degree
Doctor of Philosophy in the
School of Chemistry and Biochemistry

Georgia Institute of Technology

December 2007

Synthesis and Characterization of Regioregular, Amphiphilic Semifluoroalkyl-Substituted Polythiophenes and Cofacial Bis(oligothienyl)naphthalenes

Approved by:

Dr. David M. Collard, Advisor
School of Chemistry & Biochemistry
Georgia Institute of Technology

Dr. Laren Tolbert
School of Chemistry & Biochemistry
Georgia Institute of Technology

Dr. Anselm Griffin
School of Polymer, Textile, and Fiber Engineering
Georgia Institute of Technology

Dr. Marcus Weck
School of Chemistry & Biochemistry
Georgia Institute of Technology

Dr. Seth Marder
School of Chemistry & Biochemistry
Georgia Institute of Technology

Date Approved: October 30, 2007

For my husband Terry, my sister Ashley, and my grandfather Henry

ACKNOWLEDGEMENTS

I cannot sufficiently thank my advisor, Dr. David Collard, for providing extraordinary support, encouragement, and assistance for every undertaking during my years at Georgia Tech. His dedication to and excellence in science, mentoring, and education have inspired me to become a better scientist, mentor, and educator.

I would like to acknowledge members of the Collard group, past and present, for their assistance and support, including Dr. Michael Hibbs, Dr. Genara Andrade, Dr. Susi Coons, Dr. Ling Li, Dr. Jeffrey Capadona, Dr. Kurt Knoblock, Mr. David Noga, Ms. Reagan Charney, Ms. Jareesa Tucker, Mr. Rakesh Nambiar, Mr. Brad Carson, Ms. Catherine Silvestri, Ms. Whitney Komorner, and Ms. Anjli Kumar. Special thanks to Dr. Glen Brizius for assistance with cyclic voltammetry and to Dr. Bing Wang for sharing her synthetic expertise. Ms. Jenny Raynor and Ms. Kathy Beckner Woody have offered much-appreciated friendship and encouragement.

Members of my thesis committee (Dr. Anselm Griffin, Dr. Seth Marder, Dr. Laren Tolbert, and Dr. Marcus Weck) have been generous with their time and assistance throughout my graduate career.

Many members of the School of Chemistry and Biochemistry provided access to and help with instrumentation, including Dr. Les Gelbaum (training, 2-D, and variable temperature NMR assistance), Dr. Robert Braga (IR assistance), the Bunz, Beckham, and Tolbert groups (instrument access), and the Georgia Tech Mass Spectrometry Laboratory (MS experiments). The MALDI-TOF experiments described in Chapter 2 were performed by the Center for Molecular Analysis at Carnegie Mellon University. The wide-angle X-ray scattering experiments described in Chapter 3 were performed with the assistance of Ms. Marilyn Minus and Dr. Satish Kumar (Georgia Tech School of Polymer, Textile, and Fiber Engineering). My understanding of organic field effect

transistors was greatly enhanced by Dr. Benoit Domercq and Dr. Bernard Kippelen (Georgia Tech School of Electrical and Computer Engineering) and by Ms. Ranbel Sun (REU student from the Massachusetts Institute of Technology).

Numerous School of Chemistry and Biochemistry faculty and staff have supplied appreciated encouragement and support during all of my endeavors here. Special thanks go to Dr. Cam Tyson, Ms. Kathy Huggins, and Ms. Denisha Thomas for all of their hard work involving the graduate program. Dr. Julia Kubanek provided invaluable mentoring and support.

I would like to thank past and present members of the Georgia Tech Women in Chemistry Committee for their collaboration in developing and carrying out the program described in Appendix A. Miss Ashley Ringer, Dr. Lauren Schwimmer, Dr. Susie Eustis, Dr. Nicole Poulsen, Ms. MaryNell Higley, Ms. Jenny Raynor, Dr. Catherine Santai, and Ms. Myneeka Cook played a special part in this project. A number of faculty and staff, both from the School of Chemistry and Biochemistry and from across campus, assisted the Committee in a variety of ways. Dr. David Collard, Dr. Seth Marder, Dr. Keith Oden, Dr. Julia Kubanek, Ms. Yvette Upton, Dr. Dana Hartley, Ms. Billiee Pendleton-Parker, Dr. Cam Tyson, Dr. Rigoberto Hernandez, and Dr. Thomas Orlando have provided valuable support for the Committee's work.

I would like to thank Ms. Caroline Burd, Ms. Maria-Isabel Carnasciali, Ms. Teena Carroll, Ms. Karen Feigh, Ms. Janine Johnson, Miss Ashley Ringer, Ms. Eliane Traldi, and Ms. Farhana Zaman for their continued friendship, support, and laughter. Stephanie, P.J., and Noah George help me to remember that life exists outside of the lab. Your friendship means more to me than I can ever express.

I would like to thank my parents, Jack and Faith Sisk, for raising me to be a strong individual and for supporting me during my studies. My sisters, Andrea and Ashley Sisk, are wonderful sources of love and laughter. My grandparents, Eda and the

late Henry Jonocco, supplied a lifetime of unconditional love and support. Stan and Karen Watt, Sheila Watt, Julie Watt and Matt Brun, and Ellen Watt made me a part of their family. Thanks also go to the extended Sisk, Jonocco, Watt, and Pfankuch families for their encouragement.

I could never adequately express my gratitude to my husband Terry for always believing in and encouraging me, especially during those times when I could not do those things for myself. Terry, you taught me to dream ambitious dreams and to pursue those dreams in the face of any and all challenges. You're my best friend, and my accomplishments would not have been possible without your sacrifices, love, and support.

TABLE OF CONTENTS

Acknowledgements iv

List of Tables x

List of Figures xi

List of Abbreviations and Symbols xvi

Summary xx

Chapter 1: Background 1

1.1: Conjugated Materials 1

1.2: Liquid Crystalline Polymers 1

1.3: Semifluoroalkyl-substituted Polythiophenes 3

1.4: Conjugated Oligomers as Models for Interchain Charge Transfer 4

1.4.1: The Nature of Charge Carriers in One- and Two-Dimensional Conjugated Systems 4

1.4.2: Charge Carriers in π-stacked Conjugated Oligomers 6

1.5: Scope of Work 7

1.6: References 8

Chapter 2: Synthesis of Poly(3-semifluoroalkylthiophene)s 12

2.1: Introduction 12

2.2: Experimental 12

2.2.1: General Methods 12

2.2.2: Representative Synthetic Procedures 13

2.3: Results and Discussion 36

2.3.1: Synthetic Approach to Semifluroalkylthiophene Monomers 36

2.3.2: Synthetic Approach to Poly(3-semifluoroalkylthiophene)s 37

2.3.3: Structural Characterization of Poly(3-semifluoroalkylthiophene)s 40

2.4: Conclusions 45

2.5: References 45

Chapter 3: Characterization of Semifluoroalkyl-substituted Polythiophenes 47

3.1: Introduction 47

3.2: Experimental 47

3.3: Results and Discussion 48

3.3.1: Solution-state Characterization of Poly(3-semifluoroalkylthiophene)s 48

3.3.2: Characterization of Solid-State Polymer Properties 49

3.4: Conclusions 55

3.5: References 57

Chapter 4: Synthesis and Characterization of Cofacial 1,8-Bis(oligothiophene)-Substituted Naphthalenes as Models for Interchain Charge Transfer 59

4.1: Background 59

4.2: Experimental 62

4.3: Results and Discussion 70

4.3.1: Synthetic Approaches to 1,8-Bis(oligothiophene)-substituted Naphthalenes 70

4.3.2: Structural Characterization of 1,8-Bis(oligothiophene)-substituted Naphthalenes 74

4.3.3: Absorption and Emission Spectroscopy of 1,8-Bis(oligothiophene)-substituted Naphthalenes 95

4.3.4: Effects of Structure on Electronic Properties of 1,8-Bis(oligothiophene)-substituted Naphthalenes 95

4.4: Conclusions 100

4.5: References 101

Chapter 5: Future Work 102

5.1: Future Directions for Poly(3-semifluoroalkylthiophene)s 102

5.2: Future Directions for Cofacial 1,8-Bis(oligothiophene)-Substituted Naphthalenes 103

5.3: References 104

Appendix A: Students Repairing the Leaky Pipeline: The Georgia Tech Women in Chemistry Committee 106

A.1: Introduction 106

A.2: Program Description 109

A.3: Committee Accomplishments 109

A.4: Future Work 112

A.5: Conclusion 113

A.6: References 113

Appendix B: Detailed Procedures for the Synthesis of 3-(Iodo-semifluoroalkyl) Thiophenes. 115

Appendix C: ^{1}H and ^{13}C NMR Spectra of Intermediates in the Synthesis of Poly(3-semifluoroalkylthiophene)s 122

Appendix D: DSC Thermograms of Six Poly(3-semifluoroalkylthiophene) Homologues 150

Appendix E: Cyclic Voltammagrams of 1,8-Bis(oligothienyl)naphthalenes 158

Appendix F: Supplemental information for conformational analysis of N-$(Th_2Me)_2$ by NMR 168

LIST OF TABLES

Table 2.1	Reaction progress for synthesis of **2(5,4)**.	17
Table 2.2	Polymer characterization data.	38
Table 3.1	Optical and thermotropic data.	48
Table 3.2	Thermal transitions for liquid crystalline homologues of **Rg(Th-m,n)**.	49
Table 3.3	Polymer **Rg(Th-11,6)** *d*-spacing as a function of temperature.	53
Table 4.1	Absorption and emission maxima for **3 N-(ThMe)$_2$**, **5 N-(Th$_2$Me)$_2$**, and **7 N-(Th$_3$Me)$_2$**.	95
Table 4.2	Oxidation and reduction potentials of **3 N-(ThMe)$_2$**, **5 N-(Th$_2$Me)$_2$**, and **7 N-(Th$_3$Me)$_2$**.	96
Table A.1	Percentage of female tenure-track faculty at top 50 funded chemistry departments.	106
Table B.1	Reaction progress for the synthesis of **2(5,8)**.	116
Table B.2	Reaction progress for the synthesis of **2(5,6)**.	117
Table B.3	Reaction progress for the synthesis of **2(11,8)**.	118
Table B.4	Reaction progress for the synthesis of **2(11,6)**.	119
Table B.5	Reaction progress for the synthesis of **2(11,4)**.	120
Table B.6	Reaction progress for the synthesis of **2(8,4)**.	121
Table B.7	Reaction progress for the synthesis of **2(8,3)**.	121
Table F.1	Possible conformations of **5 N-(Th$_2$Me)$_2$** and maximum number of corresponding NMR signals.	168
Table F.2	Effect of various parameters on coalescence temperature T_c.	169

LIST OF FIGURES

Figure 1.1	Examples of fluoroalkyl- and semifluoroalkyl-substituted polythiophenes.	3
Figure 1.2	Structure of regioregular **Rg(Th-5,4)**.	3
Figure 1.3	Positive doping of polyacetylene.	4
Figure 1.4	Schematic representing the fate of conjugated radical cations.	5
Figure 1.5	Oxidative states resulting from p-doping of π-stacked oligomers.	6
Figure 1.6	Structure of methyl-terminated 1,8-bis(oligothienyl)naphthalenes.	7
Figure 1.7	Structure of regioregular poly(3-semifluoroalkylthiophene)s **Rg(Th-m,n)**.	8
Figure 2.1	Structure of regioregular poly(3-semifluoroalkylthiophene)s **Rg(Th-m,n)**.	12
Figure 2.2	Synthesis of 2,5-dibromo-3-(semifluoroalkyl)thiophenes **4(m,n)**.	14
Figure 2.3	Synthesis of regiorandom (top) and regioregular (bottom) poly(3-semifluoroalkylthiophene)s.	38
Figure 2.4	Transmetallation and initiation intermediates in Grignard metathesis (GRIM). The semifluoroalkyl side chain is abbreviated R.	39
Figure 2.5	^{1}H NMR spectra of regiorandom **Rn(Th-5,4)** (top) and regioregular **Rg(Th-5,4)** (bottom).	41
Figure 2.6	^{13}C spectra of poly(3-semifluoroalkyl)thiophenes. Top: Regiorandom **Rn(Th-5,4)** vs. regioregular **Rg(Th-5,4)**. Center: Regioregular **Rg(Th-11,6)**. Bottom: the fluoromethylene region of the **Rg(Th-8,3)** spectrum.	42
Figure 2.7	^{19}F NMR spectra of **Rg(Th-11,6)** in $CHCl_3$ at 60 ºC.	43
Figure 2.8	MALDI-TOF spectrum of regioregular **Rg(Th-5,4)**. **Inset:** distribution of polymer end groups in the m/z region 5550-5725.	44
Figure 3.1	DSC thermogram of regioregular **Rg(Th-11,4)** (heating and cooling at 10 ºC/min).	50
Figure 3.2	DSC thermogram of regioregular **Rg(Th-11,6)** (heating and cooling at 10 ºC/min).	51
Figure 3.3	Interdigitated lamellar architecture for **Rg(Th-11,6)** consistent with X-ray diffraction data.	53

Figure 3.4	Wide-angle X-ray diffractogram of **Rg(Th-11,6)** powder, heating from 90 ºC to 210 ºC.	54
Figure 3.5	UV-visible spectra of a **Rg(Th-5,4)** thin film, cooling from 245 ºC to 61 ºC.	55
Figure 3.6	Polarized optical micrographs of a **Rg(Th-11,6)** thin film, at 40 ºC (top), 140 ºC (middle), and 176 ºC (bottom). Scale bar corresponds to 50 μm.	56
Figure 4.1	Hydrogen terminated oligomers synthesized by Nakayama: cofacial bis (oligomers) (left) and mono(oligomers) (right).	59
Figure 4.2	Hydrogen-terminated multi-stacked oligomers examined by Nakayama.	61
Figure 4.3	Hydrogen terminated multi-stacked system examined by Iyoda.	61
Figure 4.4	Structure of methyl-terminated 1,8-bis(oligothienyl)naphthalenes.	62
Figure 4.5	Synthesis of 1,8-dibromonaphthalene **1** via a Sandmeyer reaction.	70
Figure 4.6	Synthesis of **3 N-(ThMe)$_2$** by Kumada coupling.	71
Figure 4.7	Synthesis of 1,8-bis(2-thienyl)naphthalene **2** and 1,8-bis(5-bromo-2-thienyl) naphthalene **4**.	72
Figure 4.8	Synthesis of **5 N-(Th$_2$Me)$_2$** by Negishi coupling.	73
Figure 4.9	Wolff-Kischner synthesis of 5-methyl-2,2'-bithiophene, **6**.	74
Figure 4.10	Synthesis of **7 N-(Th$_3$Me)$_2$** by Negishi coupling.	74
Figure 4.11	HSQC spectrum of the aromatic region of **3 N-(ThMe)$_2$**.	75
Figure 4.12	HMBC spectrum of **3 N-(ThMe)$_2$**.	77
Figure 4.13	COSY spectrum of **5 N-(Th$_2$Me)$_2$.**	78
Figure 4.14	NOE (top) and ^{1}H NMR (bottom) spectra of **5 N-(Th$_2$Me)$_2$**.	80
Figure 4.15	Relevant portion of the HSQC spectrum of **5 N-(Th$_2$Me)$_2$**.	81
Figure 4.16	HMBC spectrum of **5 N-(Th$_2$Me)$_2$**.	82
Figure 4.17	COSY spectrum of **7 N-(Th$_3$Me)$_2$**.	83
Figure 4.18	NOE (top) and ^{1}H NMR (bottom) spectra of **7 N-(Th$_3$Me)$_2$**.	84
Figure 4.19	HSQC spectrum of **7 N-(Th$_3$Me)$_2$**.	86
Figure 4.20	HMBC spectrum of **7 N-(Th$_3$Me)$_2$**.	87
Figure 4.21	^{1}H NMR spectra of **3 N-(ThMe)$_2$** at 60 ºC (top), 25 ºC (center), and –40 ºC (bottom).	88

Figure 4.22	^{13}C NMR spectra of **3 N-(ThMe)$_2$** at 60 ºC (top), 25 ºC (center), and –40 ºC (bottom).	89
Figure 4.23	^{1}H NMR spectra of **5 N-(Th$_2$Me)$_2$** at 25 ºC (top) and –40 ºC (bottom).	90
Figure 4.24	^{13}C NMR spectra of **5 N-(Th$_2$Me)$_2$** at 25 ºC (top) and –40 ºC (bottom).	91
Figure 4.25	^{1}H NMR spectra of **7 N-(Th$_3$Me)$_2$** at 25 ºC (top) and –40 ºC (bottom).	92
Figure 4.26	^{13}C NMR spectra of **7 N-(Th$_3$Me)$_2$** at 25 ºC (top) and –40 ºC (bottom).	92
Figure 4.27	Calculated energy barrier to inner thiophene ring rotation for **5 N-(Th$_2$Me)$_2$**.	93
Figure 4.28	Calculated energy barrier to outer thiophene ring rotation for **5 N-(Th$_2$Me)$_2$**.	94
Figure 4.29	CV of **7 N-(Th$_3$Me)$_2$**.	97
Figure 4.30	CV of **5 N-(Th$_2$Me)$_2$**.	98
Figure 4.31	CV of **3 N-(ThMe)$_2$**.	99
Figure 5.1	Possible unstacked oligomer model compounds.	103
Figure 5.2	Example of a proposed multi-stacked system, which extends (gray) Iyoda's existing system (black). R = alkyl.	104
Figure A.1	Representation of the 'leaky pipeline' characterizing the exodus of women from careers in STEM. Here, a 'full' pipeline corresponds to 50% women entering Ph.D. programs.	107
Figure C.1	^{1}H (top) and ^{13}C (bottom) spectra of **1(5)**.	123
Figure C.2	^{1}H (top) and ^{13}C (bottom) spectra of **1(11)**.	124
Figure C.3	^{1}H (top) and ^{13}C (bottom) spectra of **1(8)**.	125
Figure C.4	^{1}H (top) and ^{13}C (bottom) spectra of **2(5,4)**.	126
Figure C.5	^{1}H (top) and ^{13}C (bottom) spectra of **2(5,8)**.	127
Figure C.6	^{1}H (top) and ^{13}C (bottom) spectra of **2(5,6)**.	128
Figure C.7	^{1}H (top) and ^{13}C (bottom) spectra of **2(11,8)**.	129
Figure C.8	^{1}H (top) and ^{13}C (bottom) spectra of **2(11,6)**.	130
Figure C.9	^{1}H (top) and ^{13}C (bottom) spectra of **2(11,4)**.	131
Figure C.10	^{1}H (top) and ^{13}C (bottom) spectra of **2(8,4)**.	132
Figure C.11	^{1}H (top) and ^{13}C (bottom) spectra of **2(8,3)**.	133

Figure C.12	^{1}H (top) and ^{13}C (bottom) spectra of **3(5,4)**.	134
Figure C.13	^{1}H (top) and ^{13}C (bottom) spectra of **3(5,8)**.	135
Figure C.14	^{1}H (top) and ^{13}C (bottom) spectra of **3(5,6)**.	136
Figure C.15	^{1}H (top) and ^{13}C (bottom) spectra of **3(11,8)**.	137
Figure C.16	^{1}H (top) and ^{13}C (bottom) spectra of **3(11,6)**.	138
Figure C.17	^{1}H (top) and ^{13}C (bottom) spectra of **3(11,4)**.	139
Figure C.18	^{1}H (top) and ^{13}C (bottom) spectra of **3(8,4)**.	140
Figure C.19	^{1}H (top) and ^{13}C (bottom) spectra of **3(8,3)**.	141
Figure C.20	^{1}H (top) and ^{13}C (bottom) spectra of **4(5,4)**.	142
Figure C.21	^{1}H (top) and ^{13}C (bottom) spectra of **4(5,8)**.	143
Figure C.22	^{1}H (top) and ^{13}C (bottom) spectra of **4(5,6)**.	144
Figure C.23	^{1}H (top) and ^{13}C (bottom) spectra of **4(11,8)**.	145
Figure C.24	^{1}H (top) and ^{13}C (bottom) spectra of **4(11,6)**.	146
Figure C.25	^{1}H (top) and ^{13}C (bottom) spectra of **4(11,4)**.	147
Figure C.26	^{1}H (top) and ^{13}C (bottom) spectra of **4(8,4)**.	148
Figure C.27	^{1}H (top) and ^{13}C (bottom) spectra of **4(8,3)**.	149
Figure D.1	DSC thermogram of regioregular **Rg(Th-11,8)** (heating and cooling at 10ºC/min).	151
Figure D.2	DSC thermogram of regioregular **Rg(Th-5,4)** (heating and cooling at 10ºC/min).	152
Figure D.3	DSC thermogram of regioregular **Rg(Th-5,6)** (heating and cooling at 10ºC/min).	153
Figure D.4	DSC thermogram of regioregular **Rg(Th-5,8)** (heating and cooling at 10ºC/min).	154
Figure D.5	DSC thermogram of regioregular **Rg(Th-8,3)** (heating and cooling at 10ºC/min).	155
Figure D.6	DSC thermogram of regioregular **Rg(Th-8,4)** (heating and cooling at 10ºC/min).	156
Figure D.7	DSC thermogram of regioregular **Rg(Th-8,0)** (heating and cooling at 10ºC/min).	157
Figure E.1	CV of **N-(Th_3Me)$_2$**, first run.	159
Figure E.2	CV of **N-(Th_3Me)$_2$**, second run.	160
Figure E.3	CV of **N-(Th_3Me)$_2$**, third run.	161

Figure E.4 CV of **N-($Th_2Me)_2$**, first run. 162

Figure E.5 CV of **N-($Th_2Me)_2$**, second run. 163

Figure E.6 CV of **N-($Th_2Me)_2$**, third run. 164

Figure E.7 CV of **N-($ThMe)_2$**, first run. 165

Figure E.8 CV of **N-($ThMe)_2$**, second run. 166

Figure E.9 CV of **N-($ThMe)_2$**, third run. 167

Figure F.1 ^{1}H NMR of a dilute (5 mg/mL) sample of **5 N-($Th_2Me)_2$** at –50 °C. 168

Figure F.2 ^{13}C NMR of a dilute (5 mg/mL) sample of **5 N-($Th_2Me)_2$** at –40 °C. 169

LIST OF ABBREVIATIONS AND SYMBOLS

δ	chemical shift
Δ	reflux
λ	wavelength
μ	micro
μA	microampere
Å	Angstrom
abs	absorption
AcOH	acetic acid
AIBN	2,2'-azo-bis(isobutyronitrile)
Ar	aromatic
br	broad
Bu	butyl
COSY	correlation spectroscopy
CV	cyclic voltammetry
d	doublet
dd	doublet of doublets
ddt	doublet of doublet of triplets
dec.	decomposed
di(EG)	di(ethylene glycol)
DMF	dimethyl formamide
DMSO	dimethyl sulfoxide
DP	degree of polymerization
dq	doublet of quartets
DSC	differential scanning calorimetry
d-spacing	diffraction spacing
EI	Electron Ionization

em	emission
E_{ox}	oxidation potential
E_{red}	reduction potential
ESR	electron spin resonance
Et_2O	diethyl ether
EtOH	ethanol
FET	field effect transistor
FTIR	Fourier-Transform Infrared Spectroscopy
g	grams
GC	gas chromatography
GC-MS	gas-chromatography-mass spectrometry
GPC	gel-permeation chromatography
GRIM	Grignard metathesis
h	hour
HH	head-to-head
HMBC	heteronuclear multiple bond correlation spectroscopy
HRMS	high-resolution mass spectrometry
HSQC	heteronuclear single quantum correlation spectroscopy
HT	head-to-tail
Hz	Hertz
I	isotropic
IR	infrared
J	coupling constant
L	liter
LC	liquid crystalline
LC-CP	liquid crystalline conjugated polymer
LCD	liquid crystal display
LCP	liquid crystalline polymer

LEDs	light emitting diodes
m	multiplet or medium
M	molar
m/z	mass to charge ratio
M^+	molecular ion
MALDI	matrix-assisted laser desorption ionization
MALDI-TOF	matrix-assisted laser desorption ionization time of flight mass spectrometry
MeOH	methanol
mg	milligrams
MHz	Megahertz
mL	milliliters
mM	millimolar
mM	millimolar
mmol	millimoles
M_n	number-average molecular weight
mol	moles
mp	melting point
MS	mass spectrometry
mV	millivolts
M_w	weight-average molecular weight
N_2	nitrogen
NBS	*N*-bromosuccinimide
n-BuLi	n-butyllithium
Ni(dppp)Cl_2	[1,3-bis(diphenylphosphino)propane]dichloronickel(II)
NMR	nuclear magnetic resonance spectroscopy
NOE	nuclear Overhauser effect
OPM	optical polarized microscopy
p	pentet

$Pd(PPh_3)_4$	tetrakis(triphenylphosphine)palladium(0)
PDI	polydispersity index
POT	poly(3-octylthiophene)
ppm	parts per million
qt	quartet of triplets
R	alkyl
RMgBr	alkyl magnesium bromide
RPM	revolutions per minute
RT	room temperature
s	strong
s	second
s	singlet
S.C.E.	standard calomel electrode
SC	semicrystalline
Th	thiophene
THF	tetrahydrofuran
TMEDA	*N*,*N*,*N*′,*N*′-tetramethylethylenediamine
tt	triplet of triplets
TT	tail-to-tail
UV	ultraviolet
UV-vis	ultraviolet-visible
V	volts
WAXS	wide-angle X-ray scattering
w	weak
$\overline{X}$	degree of polymerization

SUMMARY

Conjugated polymers and oligomers have been widely studied based on their wide range of useful properties and applications. Given the importance of self-assembly and charge transfer in the development of conjugated materials for use in electronic applications, it is crucial to: (i) prepare functional materials by molecular design, (ii) evaluate the structure-property relationships of new materials, and (iii) develop fundamental understanding of electronic structure and charge transport behavior.

The use of conjugated polymeric materials in electronic applications relies on control of the assembly and orientation of the polymer chains in the solid state. Conjugated polymers with liquid crystalline behavior could be used to implement an additional level of control over orientation and resultant properties. Substitution of the conjugated polythiophene backbone with semifluoroalkyl side chains (i.e., the diblock -$(CH_2)_m(CF_2)_nF$) has afforded materials with unusual properties. The mutual immiscibility of the aromatic backbone, the alkyl side-chain segments, and the fluoroalkyl side-chain termini provides control over supramolecular packing. A series of eight polymers has been synthesized, in which the lengths of the alkyl (m) and fluoroalkyl (n) segments are varied. One regiorandom analogue and two poly(3-alkylthiophene)s were also synthesized for comparative purposes. The structure, molecular weight, and regioregularity of the polymers were evaluated using a variety of techniques.

The semifluoroalkyl-substituted polymers have been systematically studied to determine the effect of side chain length and m:n block ratios on their solution state, liquid crystalline, and solid state properties. The effect of side chains on conjugation was determined, where solubility allowed, by solution-state UV-visible and fluorescence spectroscopy. The thermal and liquid crystalline properties of the homopolymers were

evaluated by DSC, variable-temperature X-ray diffraction, and polarized optical microscopy. Several semifluoroalkyl-substituted polythiophene homologues show liquid crystalline behavior.

Molecular packing and charge transport are key factors governing the use of conjugated materials in electronic applications. A wide variety of oligomers have been studied as models for charge migration in conjugated polymers. One-dimensional models do not adequately represent two-dimensional charge transport; thus, a variety of two-dimensional, covalently-linked models have been developed. Previous work by our group, and others, led to the proposal of bis(oligothienyl) compounds as models to study the interaction of the π-conjugated chains. Previous reports by other researchers described the synthesis and characterization of hydrogen-terminated analogues of 1,8-bis(oligothienyl)naphthalenes. However, these materials proved to be unsuitable for use as charge transport models, as they were subject to irreversible polymerization upon oxidation. Installation of methyl groups at the terminal α-positions of 1,8-bis(oligothienyl)naphthalenes allowed us to create a series of models in which conjugated chains are held in close proximity. This provides access to multiple redox states, and future systems based on these molecules may be used as models for charge transport or as functional materials for incorporation into devices.

CHAPTER 1: BACKGROUND

1.1: Conjugated Materials

The 1977 discovery that polyacetylene can be electrically conductive[1] gave rise to the field of conjugated materials.[2] Conjugated polymeric materials have been studied for incorporation into such (opto)electronic applications as biological and chemical sensing, light harvesting, energy storage, communications, and nanoelectronics because they may be easily processed, lightweight, and tunable compared to their inorganic counterparts.[3] The use of conjugated polymers in these applications relies on the solid-state assembly and orientation of the polymer chains;[4] for example, the orientation of polymer chains perpendicular to the gate electrode, so as to maximize the source-drain current, is key to their use in field effect transistors (FETs).[5,6]

Polythiophenes have been studied extensively because of their conductivity, field-effect mobility, stability under various thermal and environmental conditions, and versatility in myriad applications. Alkyl substitution of the thiophene monomer at the 3-position greatly enhances the solubility of the resulting polymer. However, substitution also introduces an additional level of complexity arising from the polymerization of an asymmetric monomer. Regioregular, or head-to-tail coupled, poly(3-alkylthiophene)s exhibit enhanced coplanarity, conductivity, and mechanical properties compared to their regiorandom counterparts, in which some fraction of monomers are linked in a head-to-head or tail-to-tail arrangement. The effect of regioregularity on the optical, electronic, and physical properties of poly(3-alkylthiophene)s is ascribed to the supramolecular assembly of the polymer chains in highly-ordered solid-state structures.[7]

1.2: Liquid Crystalline Polymers

The supramolecular order of polymer films may be influenced by processing conditions (e.g., solvent, temperature, deposition method) or by molecular design (e.g.,

substitution, copolymerization, incorporation of mesogens). Polymers bearing rod-like mesogenic units may form liquid crystalline phases, which may be responsive to thermal, chemical, mechanical, or electrical stimuli, thereby providing additional opportunities to influence molecular packing and orientation.[8] The existence of liquid crystalline phases depends on several factors, including the structure (e.g., axial ratio and relative volume fraction) of the mesogenic segment.[9] Main chain liquid crystalline polymers (LCPs) incorporate mesogenic units into the polymer backbone itself; the backbone may contain only rigid monomers or a combination of rigid and flexible units. Side-chain LCPs incorporate mesogens as substituents attached to the polymer backbone; often a flexible spacer decouples the two units and allows each to move and align independently. The formation of lyotropic mesophases and smectic-like structures from amphiphilic semifluorinated alkanes (i.e., $H(CH_2)_m(CF_2)_nF$, with $m, n \geq 6$) led to the development of side-chain liquid crystal polymers with methacrylate and siloxane backbones.[10-13]

Development of liquid crystalline conjugated polymers (LC-CPs) affords the potential to enhance control over polymer self-assembly and consequent optical and electronic properties. Examples of main chain LC-CPs include poly(9,9-dialkylfluorene)s,[14] poly(2,5-dialkylphenylene ethynylene)s,[15] poly(2,5-dialkoxyphenylene ethynylene)s,[16] poly(2,5-dialkoxyphenylene vinylene)s,[17,18] and poly(2,5-dialkoxy-1,4-phenylene-2,5-thiophene)s.[19] Side-chain LC-CP materials and non-conjugated polymer backbones with conjugated mesogenic side chains have been incorporated into electroluminescent devices.[20-22] While LC-CPs may be used in liquid crystal displays (LCDs) and electroluminescent devices due to their ability to emit polarized light, the potential for enhanced supramolecular order also lends itself to incorporation into FETs.[23-27]

1.3: Semifluoroalkyl-substituted Polythiophenes

Substitution of the conjugated polymer backbone with mesogenic semifluoroalkyl side chains, i.e., the amphiphilic diblock $-(CH_2)_m(CF_2)_nF$, has afforded materials with unusual properties due to the mutual immiscibility of the aromatic backbone, the alkyl side chain segments, and the fluoroalkyl side chain termini.[28-30] Several classes of perfluoroalkyl- and semifluoroalkyl-substituted polythiophenes (Figures 1.1 and 1.2) have been synthesized, including regioregular and regiorandom homopolymers and copolymers, to examine structure-property relationships, such as the effect of side chain length and composition on material properties. These materials have exhibited n-dopability and solubility in supercritical CO_2 (**A**);[31,32] significant solution and solid-state fluorescence (**B**);[33] and highly-ordered bilayer lamellar assemblies (**C**).[30,34] We have also previously reported one homologue of regioregular poly(3-semifluoroalkyl thiophene) (**Rg(Th-5,4)**, Figure 1.2), which exhibited a weakly ordered nematic mesophase.[29]

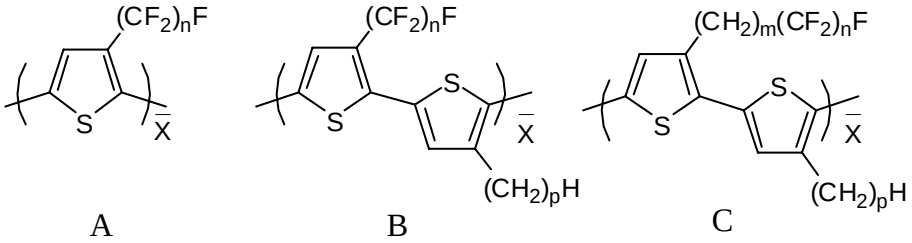

Figure 1.1. Examples of fluoroalkyl- and semifluoroalkyl-substituted polythiophenes.

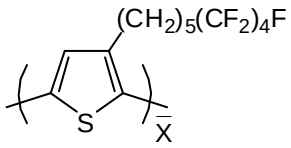

Rg(Th-5,4)

Figure 1.2. Structure of regioregular **Rg(Th-5,4)**.

1.4: Conjugated Oligomers as Models for Interchain Charge Transfer

Molecular packing and charge transport are key factors governing the use of conjugated materials in (opto)electronic applications.[4] However, the fundamental examination of charge transport in conjugated polymers is often complicated by a number of factors, including polydispersity, semicrystallinity, and structural imperfection.

Consequently, a wide variety of oligomers have been studied as models for charge migration in conjugated polymers. A number of studies have focused on one-dimensional linear oligomers as model systems for polymeric counterparts.[35-37] Such models are inherently limited because they do not take into account two-dimensional transport via π-stacking. Thus, a variety of two-dimensional, covalently linked models have been developed, including oligothiophenes linked by cyclophane, bicyclic, and linear moieties, to gain insight into charge transfer in conjugated systems.[38-43]

1.4.1: The Nature of Charge Carriers in One- and Two-Dimensional Conjugated Systems

As the conjugation length of a linear molecule increases, a density of states due to increasingly overlapping between π orbitals gives rise to the electronic band structure characteristic of conjugated materials. In such systems, the filled valence band is

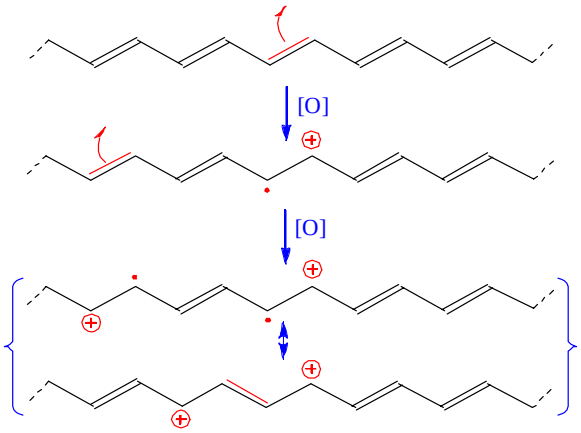

Neutral polymer

Radical cation (polaron)
ESR active

Dication (bipolaron)
ESR inactive

Figure 1.3. Positive doping of polyacetylene.

separated from the conduction band by an intrinsic band gap. One-electron oxidation of a neutral conjugated chain by p-doping with an electron acceptor results in a positively charged polaron species (Figure 1.3). A positive polaron, or radical cation, is stabilized by delocalization of the positive charge and the unpaired electron over several repeat units, which undergo a corresponding change from aromatic to quinoidal geometry. The presence of a radical cation renders the system ESR active and gives rise to new optical absorptions.[44] Comparable stabilization processes occur when the conjugated chain is subjected to reductive (or n-) doping with an electron donor.

Further p-doping results in the formation of a bis(radical cation), whose component free electrons can combine to form a dication (or bipolaron) with 2+ charge, as shown in Figure 1.3. The loss of spin associated with bipolaron formation renders the system ESR inactive.[45,46]

In an isolated conjugated molecule, charge is only delocalized along the individual conjugated chain. In the case of two or more conjugated molecules, there are a number of processes that radical cations might undergo (Figure 1.4).

A radical cation on one molecule, M, may undergo an electron transfer reaction with a second radical cation (Figure 1.4, example 1). This disproportionation process

DISPROPORTIONATION

$$M^{+\cdot} + M^{+\cdot} \rightarrow M^{2+} + M^{0}$$

BIS(RADICAL CATION) COMBINATION

$$M^{2(+\cdot)} \rightarrow M^{2+}$$

σ-DIMERIZATION

$$M^{+\cdot} + M^{+\cdot} \rightarrow M^{+}\text{—}M^{+}$$

π-DIMERIZATION

$$M^{+\cdot} \text{- - -} M^{+\cdot} \rightarrow (M \text{- - -} M)^{2+/0}$$

Figure 1.4. Schematic representing the fate of conjugated radical cations.

results in the formation of one oxidized species (a dication) and one reduced species (a neutral, uncharged molecule). The existence of these two species is supported by optical and ESR spectroscopy in the case of tetrathiafulvalene systems.[44] A single conjugated molecule bearing a bis(radical cation) may also undergo an intramolecular disproportionation, corresponding to combination of unpaired electrons to form a spinless dication (Figure 1.4, example 2).[46]

A radical cation may also undergo two types of dimerization (Figure 1.4, examples 3 and 4). In the first case, alignment of sp^2 orbitals on adjacent chains may facilitate formation of a reversible σ-bond between the two molecules, as seen in the case of the redox switch 1,3,5-tripyrrolidinobenzene.[47] Evidence also exists that two conjugated oligomer chains bearing radical cations may associate in solution to form a π-dimer.[42,48-50] In both cases, the resultant dimers are spinless.

1.4.2: Charge Carriers in π-stacked Conjugated Oligomers

In a system of two π-stacked oligomers, oxidation may proceed as illustrated in Figure 1.5. The first oxidation produces a species with one radical cation chain and one neutral chain; electron transfer between the two conjugated tiers would result in the identical species. The second oxidation could occur either on the previously oxidized chain or on the neutral chain, resulting in either a bis(radical cation) or a bipolaron. The third and fourth oxidations can occur in the same manner. Characterization of the nature

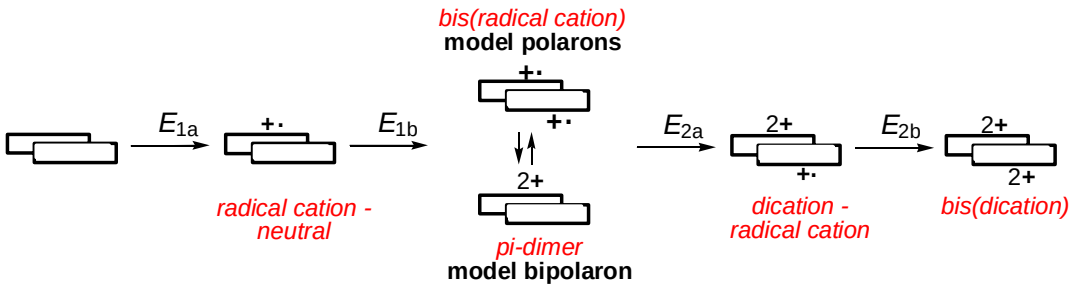

Figure 1.5. Oxidative states resulting from p-doping of π-stacked oligomers.

of the charged species formed upon oxidation of well-defined two-dimensional systems is key to understanding charge transport in conjugated polymers. Examination of such oxidative processes in the 1,8-bis(oligothienyl) naphthalene systems described in Chapter 4 (Figure 1.6) will afford insights into the behavior of charged species in conjugated systems.

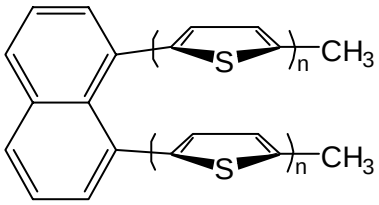

n = 1: **N-(ThMe)$_2$**
n = 2: **N-(Th$_2$Me)$_2$**
n = 3: **N-(Th$_3$Me)$_2$**

Figure 1.6. Structure of methyl-terminated 1,8-bis(oligothienyl)naphthalenes.

1.5: Scope of Work

Given the importance of self-assembly and charge transfer in the development of conjugated materials for use in (opto)electronic applications, it is crucial to: (i) prepare functional materials by molecular design, (ii) evaluate the structure-property relationships of new materials, and (iii) enhance the fundamental understanding of electronic structure and charge transport behavior. The body of work to be described herein builds on existing knowledge in these areas.

Hong and coworkers reported a single liquid crystalline homologue of regioregular poly(3-semifluoroalkyl)thiophene (**Rg(Th-5,4)** Figure 1.2).[29] Enhanced understanding of structure-property relationships is key to the use of such materials in (opto)electronic applications. In Chapter 2, we describe the synthesis of a homologous series of regioregular semifluoroalkyl-substituted polythiophenes, **Rg(Th-m,n)**, with various side chain lengths and m:n ratios (Figure 1.7). The effect of side-chain structure on the self-assembly and liquid crystalline properties of these materials is explored in Chapter 3.

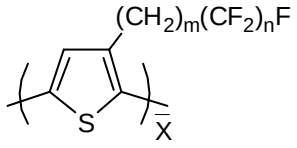

Rg(Th-m,n)

m = 5, n = 4	**Rg(Th-5,4)**
m = 5, n = 6	**Rg(Th-5,6)**
m = 5, n = 8	**Rg(Th-5,8)**
m = 8, n = 3	**Rg(Th-8,3)**
m = 8, n = 4	**Rg(Th-8,4)**
m = 11, n = 4	**Rg(Th-11,4)**
m = 11, n = 6	**Rg(Th-11,6)**
m = 11, n = 8	**Rg(Th-11,8)**

Figure 1.7. Structure of regioregular poly(3-semifluoroalkylthiophene)s **Rg(Th-m,n)**.

Chapter 4 concentrates on extending models for charge transport from one dimension to the second dimension by the synthesis and analysis of covalently linked, cofacially-held conjugated oligothiophenes. As discussed in Section 4.1, Nakayama explored the structural, optical, and electronic properties of a series of hydrogen-terminated 1,8-bis(oligothienyl) naphthalenes.[51-54] Due to the absence of a terminal blocking group, these materials undergo irreversible polymerization upon oxidation, which precludes their incorporation into electronic devices. Chapter 4 describes a series of methyl-capped bis(oligothienyl)naphthalenes designed to stabilize oxidative states (Figure 1.6).

1.6: References

1. Shirakawa, H.; Louis, E. J.; MacDiarmid, A. G.; Chiang, C. K.; Heeger, A. J. *J. Chem. Soc., Chem. Commun.* **1977**, 578.

2. Shirakawa, H. *Angew. Chem.* **2001**, *40*, 2575.

3. Skotheim, T. A.; Elsenbaumer, R. L.; Reynolds, J. R.; Eds. *Handbook of Conducting Polymers, Second Edition, Revised and Expanded*; Marcel Dekker: New York, N. Y., **1997**.

4. Taliani, C.; Blinov, L. M. *Adv. Mater.* **1996**, *8*, 353.

5. Katz, H. E.; Bao, Z. *J. Phys. Chem. B* **2000**, *104*, 671.

6. Sirringhaus, H.; Brown, P. J.; Friend, R. H.; Nielsen, M. M.; Bechgaard, K.; Langeveld-Voss, B. M. W.; Spiering, A. J. H.; Janssen, R. A. J.; Meijer, E. W.; Herwig, P.; De Leeuw, D. M. *Nature* **1999**, *401*, 685.

7. McCullough, R. D. *Adv. Mater.* **1998**, *10*, 93.

8. Suarez, M.; Lehn, J.-M.; Zimmerman, S. C.; Skoulios, A.; Heinrich, B. *J. Amer. Chem. Soc.* **1998**, *120*, 9526.

9. Tschierske, C. *J. Mater. Chem.* **2001**, *11*, 2647.

10. Höpken, J.; Pugh, C.; Richtering, W.; Moeller, M. *Makromolekulare Chemie* **1988**, *189*, 911.

11. Kuwahara, H.; Hamada, M.; Ishikawa, Y.; Kunitake, T. *J. Amer. Chem. Soc.* **1993**, *115*, 3002.

12. Jariwala, C. P.; Mathias, L. J. *Macromolecules* **1993**, *26*, 5129.

13. Johansson, G.; Percec, V.; Ungar, G.; Zhou, J. P. *Macromolecules* **1996**, *29*, 646.

14. Grell, M.; Bradley, D. D. C.; Long, X.; Chamberlain, T.; Inbasekaran, M.; Woo, E. P.; Soliman, M. *Acta Polym.* **1998**, *49*, 439.

15. Kloppenburg, L.; Jones, D.; Claridge, J. B.; Zur Loye, H.-C.; Bunz, U. H. F. *Macromolecules* **1999**, *32*, 4460.

16. Steiger, D.; Smith, P.; Weder, C. *Macromol. Rapid Commun.* **1997**, *18*, 643.

17. Bao, Z.; Amundson, K. R.; Lovinger, A. J. *Macromolecules* **1998**, *31*, 8647.

18. Bao, Z.; Chen, Y.; Cai, R.; Yu, L. *Macromolecules* **1993**, *26*, 5281.

19. Yu, L.; Bao, Z.; Cai, R. *Angew. Chem.* **1993**, *105*, 1392.

20. Park, J. H.; Lee, C. H.; Akagi, K.; Shirakawa, H.; Park, Y. W. *Synth. Met.* **2001**, *119*, 633.

21. Yao, Y.-H.; Yang, S.-H.; Hsu, C.-S. *Polymer* **2006**, *47*, 8297.

22. Grell, M.; Bradley, D. D. C. *Adv. Mater.* **1999**, *11*, 895.

23. Fujiwara, T.; Locklin, J.; Bao, Z. *Appl. Phys. Lett.* **2007**, *90*, 232108/1.

24. Sirringhaus, H.; Wilson, R. J.; Friend, R. H.; Inbasekaran, M.; Wu, W.; Woo, E. P.; Grell, M.; Bradley, D. D. C. *Appl. Phys. Lett.* **2000**, *77*, 406.

25. Kim, Y. M.; Lim, E.; Kang, I.-N.; Jung, B.-J.; Lee, J.; Koo, B. W.; Do, L.-M.; Shim, H.-K. *Macromolecules* **2006**, *39*, 4081.

26. Lim, E.; Kim, Y. M.; Lee, J.-I.; Jung, B.-J.; Cho, N. S.; Lee, J.; Do, L.-M.; Shim, H.-K. *J. Polym. Sci., Part A: Polym. Chem.* **2006**, *44*, 4709.

27. Newsome, C. J.; Kawase, T.; Shimoda, T.; Brennan, D. J. *Proceedings of SPIE-The International Society for Optical Engineering* **2003**, *5217*, 16.

28. Hong, X.; Tyson, J. C.; Middlecoff, J. S.; Collard, D. M. *Macromolecules* **1999**, *32*, 4232.

29. Hong, X. M.; Collard, D. M. *Macromolecules* **2000**, *33*, 6916.

30. Hong, X. M.; Tyson, J. C.; Collard, D. M. *Macromolecules* **2000**, *33*, 3502.

31. Li, L.; Collard, D. M. *Macromolecules* **2006**, *39*, 6092.

32. Li, L.; Counts, K. E.; Kurosawa, S.; Teja, A. S.; Collard, D. M. *Adv. Mater.* **2004**, *16*, 180.

33. Li, L.; Collard, D. M. *Macromolecules* **2005**, *38*, 372.

34. Wang, B.; Watt, S.; Collard, D. M. *PMSE Prepr.* **2006**, *94*, 444.

35. Guay, J.; Kasai, P.; Diaz, A.; Wu, R.; Tour, J. M.; Dao, L.H. *Chem. Mater.* **1992**, *4*, 1097.

36. Bauerle, P.; Segelbacher, U.; Maier, A.; Mehring, M. *J. Am. Chem. Soc.* **1993**, *115*, 10217.

37. Hotta, S.; Waragai, K. *J. Phys. Chem.* **1993**, *97*, 7427.

38. Mataka, S.; Shigaki, K.; Sawada, T.; Mitoma, Y.; Taniguchi, M.; Thiemann, T.; Ohga, K.; Egashira, N. *Angew. Chem. Int. Ed.* **1998**, 2532.

39. Salhi, F.; Lee, B.; Metz, C.; Bottomley, L. A.; Collard, D. M. *Org. Lett.* **2002**, *4*, 3195.

40. Salhi, F.; Collard, D. M. *Adv. Mater.* **2003**, *15*, 81.

41. Grimme, W.; Kaemmerling, H. T.; Lex, J.; Gleiter, R.; Heinze, J.; Dietrich, M. *Angew. Chem. Int. Ed. Engl.* **1991**, *30*, 205.

42. Knoblock, K.; Silvestri, C. J.; Collard, D. M. *J. Am. Chem. Soc.* **2006**, *128*, 13680.

43. Sakai, T.; Satou, T.; Kaikawa, T.; Takimiya, K.; Otsubo, T.; Aso, Y. *J. Am. Chem. Soc.* **2005**, *127*, 8082.

44. Frere, P.; Allain, M.; Elandaloussi, E. H.; Levillain, E.; Sauvage, F.-X.; Riou, A.; Roncali, J. *Chem. Eur. J.* **2002**, *8*, 784.

45. Kaufman, J. H.; Colaneri, N. S.; Scott, J. C.; Street, G. B. *Phys. Rev. Lett.* **1984**, *53*, 1005.

46. Bredas, J. L.; Street, G. B. *Acc. Chem. Res.* **1985**, *18*, 309.

47. Heinze, J.; Willmann, C.; Bauerle, P. *Angew. Chem. Int. Ed.* **2001**, *40*, 2861.

48. Miller, L. L.; Mann, K. R. *Acc. Chem. Res.* **1996**, *29*, 417.

49. Nessakh, B.; Horowitz, G.; Garnier, F.; Deloffre, F.; Srivastava, P.; Yassar, A. *J. Electroanal. Chem.* **1995**, *399*, 97.

50. Zotti, G.; Schiavon, G.; Berlin, A.; Pagani, G. *Synth. Met.* **1993**, *61*, 81.

51. Kuroda, M.; Nakayama, J.; Hoshino, M. *Tetrahedron Lett.* **1992**, *33*, 7553.

52. Kuroda, M.; Kosho, N.; Nakayama, J.; Hoshino, T. *Jpn. Kokai Tokkyo Koho* **1993**, *Patent JP 92-52963 19920312*.

53. Kuroda, M.; Nakayama, J.; Hoshino, M.; Furusho, N.; Kawata, T.; Ohba, S. *Tetrahedron* **1993**, *49*, 3735.

54. Kuroda, M.; Nakayama, J.; Hoshino, M.; Furusho, N.; Ohba, S. *Tetrahedron Lett.* **1994**, *35*, 3957.

CHAPTER 2: SYNTHESIS OF POLY(3-SEMIFLUOROALKYLTHIOPHENE)S

2.1: Introduction

A previous report described the synthesis of a single, liquid-crystalline homologue of poly(3-semifluoroalkyl)thiophene.[1] Here we report the synthesis and structural characterization of the homologous family of semifluoroalkyl-substituted polythiophenes shown in Figure 2.1. The overall length of the side chain and the ratio of alkyl to fluoroalkyl (i.e., m:n) segments was varied to determine structure-property relationships. These polymers and poly(3-octylthiophene), an alkyl-substituted analogue **Rg(Th-8,0)**, were synthesized by Grignard metathesis (GRIM) polymerization. A regiorandom analogue **Rn(Th-5,4)** was synthesized for the purposes of comparison. All polymers were characterized by ^{1}H, ^{13}C, and ^{19}F nuclear magnetic resonance spectroscopy (NMR); matrix-assisted laser desorption ionization time of flight mass spectrometry (MALDI); and gel permeation chromatography (GPC), where solubility allowed.

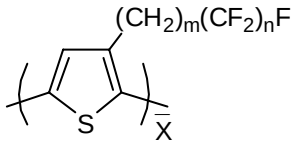

Rg(Th-m,n)

m = 5, n = 4	**Rg(Th-5,4)**
m = 5, n = 6	**Rg(Th-5,6)**
m = 5, n = 8	**Rg(Th-5,8)**
m = 8, n = 3	**Rg(Th-8,3)**
m = 8, n = 4	**Rg(Th-8,4)**
m = 11, n = 4	**Rg(Th-11,4)**
m = 11, n = 6	**Rg(Th-11,6)**
m = 11, n = 8	**Rg(Th-11,8)**

Figure 2.1. Structure of regioregular poly(3-semifluoroalkylthiophene)s **Rg(Th-m,n)**.

2.2: Experimental

2.2.1: General Methods

2,2'-Azo-bis(isobutyronitrile) (AIBN) was recrystallized from EtOH. Dimethyl sulfoxide (DMSO) was purified by fractional distillation under reduced pressure and

subsequently dried and stored over 4 Å molecular sieves. Et_2O and THF were purified by distillation from sodium or potassium benzophenone ketyl. Concentration of Grignard reagents was determined by titration with 2-butanol in xylenes with *N*-phenyl-1-naphthylamine as indicator. All other reagents were used as received from Fisher, VWR, or Aldrich. Column chromatography was performed using silica gel (60 Å, 230 x 400 mesh, Sorbent Technologies). Room temperature ^{1}H NMR spectra were recorded on a Varian Mercury Vx 300 MHz instrument using $CDCl_3$ as a solvent. ^{13}C NMR spectra were obtained at 75.5 MHz. High-temperature ^{1}H and ^{13}C NMR spectra were obtained on a Bruker AMX400 instrument at 400 MHz and 100 MHz, respectively, or on a Bruker DRX 500 instrument at 500MHz and 125 MHz, respectively, using $CDCl_3$ or 1,1,2,2-tetrachloroethane-d_2 as a solvent. ^{19}F NMR spectra were obtained on a Varian Mercury Vx 400 instrument at 376 MHz using $CDCl_3$ or 1,1,2,2-tetrachloroethane-d_2 as a solvent. Chemical shifts for ^{1}H and ^{13}C spectra are reported relative to internal tetramethylsilane; those for ^{19}F spectra are reported relative to internal trifluoroacetic acid. Infrared spectra were recorded on a Thermo Electron Nicolet 4700 FTIR as neat solids or liquids. Elemental analyses were performed by Atlantic Microlabs (Norcross, GA). GC-MS spectra and HRMS data were recorded on a Hewlett-Packard 5890 GC coupled to a VG 70SE EI spectrometer with split (100/1 split ratio) and splitless injections.

MALDI-TOF spectra were obtained on a PerSeptive Biosystems Voyager STR instrument with a terthiophene matrix at the Carnegie Mellon University Center for Molecular Analysis. GPC chromatograms were obtained on a Waters 2690 instrument with Waters 2487 Dual λ absorbance detector using THF as eluent.

2.2.2: Representative Synthetic Procedures

Representative synthetic procedures and spectroscopic data for the synthetic scheme in Figure 2.2 are illustrated below for the *m = 5, n = 4* homologue. Procedures are modified from literature,[2-7] as noted in the Discussion section. Spectroscopic data for

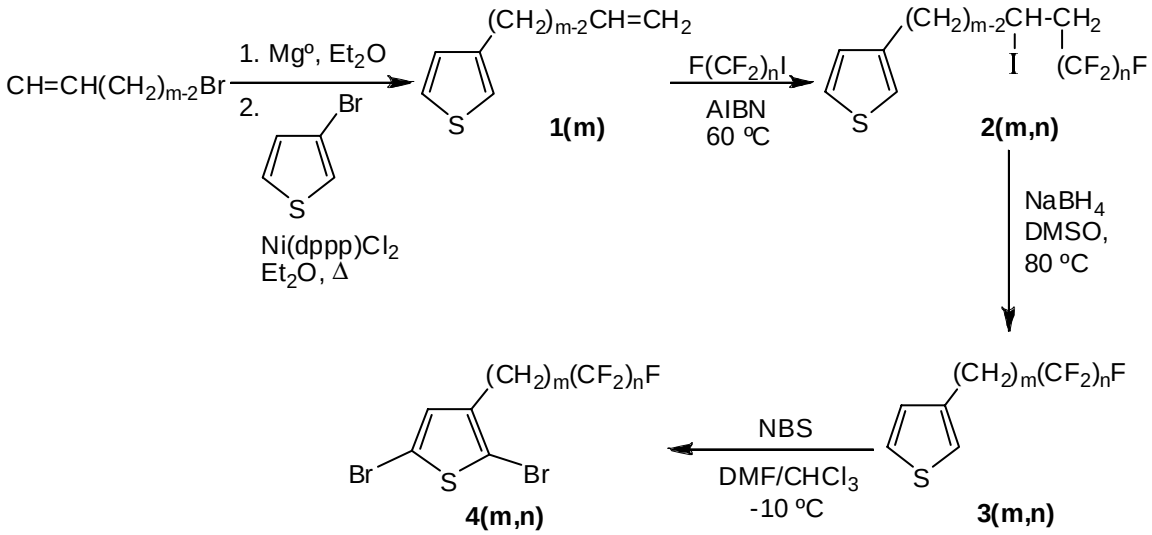

Figure 2.2. Synthesis of 2,5-dibromo-3-(semifluoroalkyl)thiophenes **4(m,n)**.

other homologues is provided. ^{1}H and ^{13}C NMR spectra are reproduced in Appendix C as proof of purity where elemental analysis is unavailable.

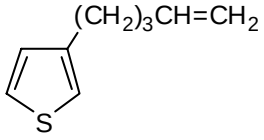

3-(ω-Alkenyl)thiophenes, 1(m). *3-(Penten-1-yl)thiophene, 2(m = 5).* A solution of 5-bromo-1-pentene (23.78 g, 159.5 mmol) in anhydrous Et_2O (80 mL) was added dropwise to magnesium (10.25 g, 421.7 mmol) in anhydrous Et_2O (80 mL) at 0 °C over 2 h using Schlenk techniques. The mixture was allowed to warm to room temperature and sonicated for 1 h. The resulting solution was transferred via cannular to an addition funnel and added dropwise to a solution of 3-bromothiophene (25.0 mL, 154 mmol) and $Ni(dppp)Cl_2$ (1.36 g, 2.56 mmol) in anhydrous Et_2O (50 mL) at 0 °C over 1 h. The mixture was allowed to warm to room temperature and then heated at reflux overnight. The reaction mixture was poured into ice water (200 mL), and the resulting solution was acidified with 10% HCl (25 mL) and extracted with petroleum ether (4 x 200 mL). The

combined extracts were dried over Na_2SO_4, and the solvent was removed on a rotary evaporator. Fractional distillation gave **1(5)** as a clear, colorless liquid (19.2 g, 82.1%). ^{1}H NMR (300 MHz, $CDCl_3$): δ 1.72 (p, *J* = 7.8 Hz, 2H, C-2 CH_2), 2.09 (qt, *J* = 7.0, 1.3 Hz, 2H, C-3 CH_2), 2.64 (t, *J* = 7.6 Hz, 2H, C-1 CH_2), 4.94-5.06 (m, 2H, C-5 CH_2), 5.82 (ddt, *J* = 16.9, 10.3, 6.7 Hz, 1H, C-4 CH), 6.90-6.95 (m, 2H, Ar-4 and Ar-2), 7.23 (dd, *J* = 4.9, 1.9 Hz, 1H, Ar-5). ^{13}C NMR (75 MHz, $CDCl_3$): δ 29.69, 29.74, 33.4 (C-1), 114.7, 119.9 (Ar-2), 125.0 (Ar-5), 128.1 (Ar-4), 138.4, 142.6 (Ar-3). IR (neat): 3075 (*sp*^{2} C-H), 2976, 2929, 2857 (*sp*^{3} C-H), 1640 (C=C), 1440 (thiophene), 991, 909 ($CH=CH_2$ bend), 759 cm^{-1} (γ-CH bend). MS (EI) m/z: 152 (M^+), 111 (M - $CH_2CH=CH_2$), 97 (M – $(CH_2)_2CH=CH_2$).

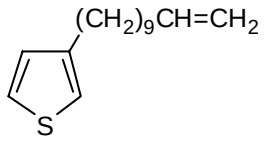

3-(Undecen-1-yl)thiophene, 1(11): Clear, colorless liquid (14.8 g, 59.9%). ^{1}H NMR (300 MHz, $CDCl_3$): δ 1.21-1.42 (m, 12H, C-3 to C-8 CH_2), 1.61 (p, *J* = 7.4 Hz, 2H, C-2 CH_2), 2.04 (qt, *J* = 7.0, 1.3 Hz, 2H, C-9 CH_2), 2.62 (t, *J* = 7.4 Hz, 2H, C-1 CH_2), 4.90-5.04 (m, 2H, C-11 CH_2), 5.81 (ddt, *J* = 17.1, 10.2, 6.7 Hz, 1H, C-10 CH), 6.90-6.95 (m, 2H, Ar-2 and Ar-4), 7.23 (dd, *J* = 4.9, 2.0 Hz, 1H, Ar-5). ^{13}C NMR (75 MHz, $CDCl_3$): δ 29.0, 29.2, 29.4, 29.53, 29.55, 29.61, 30.4, 30.6, 33.9 (C-1), 114.0, 119.7 (Ar-2), 124.9 (Ar-5), 128.2 (Ar-4), 139.1, 143.1 (Ar-3). IR (neat): 3076 (*sp*^{2} C-H), 2923, 2852 (*sp*^{3} C-H), 1640 (C=C), 1463 (thiophene), 992, 908 ($CH=CH_2$ bend), 755 cm^{-1} (γ-CH bend). MS (EI) m/z: 236 (M^+), 111 (M - $(CH_2)_7CH=CH_2$), 97 (M - $(CH_2)_8CH=CH_2$).

3-(Octen-1-yl)thiophene, 1(8). Clear, colorless liquid (14.3 g, 57.4%). ^{1}H NMR (300 MHz, $CDCl_3$): δ 1.31-1.47 (m, 6H, C-3 to C-5 CH_2), 1.66 (p, *J* = 7.2 Hz, 2H, C-2

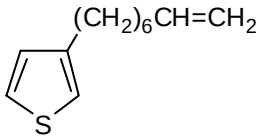

CH_2), 2.08 (qt, *J* = 7.2, 1.3 Hz, 2H, C-6 CH_2), 2.66 (t, *J* = 7.2 Hz, 2H, C-1 CH_2), 4.95-5.07 (m, 2H, C-8 CH_2), 5.84 (ddt, *J* = 17.1, 10.5, 6.6 Hz, 1H, C-7 CH), 6.93-6.97 (m, 2H, Ar-2 and Ar-4), 7.25 (dd, *J* = 2.8, 5.0 Hz, 1H, Ar-5). ^{13}C NMR (75 MHz, $CDCl_3$): δ, 28.8, 28.9, 29.1, 30.2, 30.5, 33.8 (C-1), 114.2, 119.7 (Ar-2), 125.0 (Ar-5), 128.2 (Ar-4), 139.0, 143.1 (Ar-3). IR (neat): 3074 (sp^2 C-H), 2924 (s), 2853 (m, sp^3 C-H), 1640 (C=C), 1461 (thiophene), 993, 908 ($CH=CH_2$ bend), 769 cm^{-1} (s, γ-CH bend). MS (EI) m/z: 194 (M^+), 111 (M - $(CH_2)_4CH=CH_2$), 97 (M - $(CH_2)_5CH=CH_2$).

General method for the synthesis of 3-(iodo semifluoroalkyl)thiophenes, 2(m,n). A mixture of **1(m)**, AIBN, and the corresponding perfluoroalkyl iodide was stirred under N_2 for 30 minutes in a 50 mL round-bottomed flask and then heated to 70-80 ºC. (Reactions containing perfluorobutyl iodide were heated to 60°C with a condenser to prevent loss of reagent.) The degree of conversion was monitored by ^{1}H NMR, and additional AIBN and perfluoroalkyl iodide were added when the rate of conversion leveled off. In some cases, decomposed or unreacted catalyst, perfluoroalkyl iodide, and/or perfluoroalkane byproduct were removed prior to the addition of further reagents by either filtering the reaction mixture through silica gel with petroleum ether or by subjecting the reaction mixture to reduced pressure. The dark brown reaction mixture was allowed to cool to room temperature, and unreacted perfluoroalkyl iodide and/or perfluoroalkane byproduct was removed under reduced pressure. Column chromatography (silica gel, petroleum ether) gave product **2(m,n)**.

3-(4-Iodo-6,6,7,7,8,8,9,9,9-nonafluorononyl)thiophene, 2(5,4). Treatment of **1(5)** (10.0 g, 65.8 mmol) with AIBN (540 mg, 3.29 mmol) and perfluorobutyl iodide (12.2 mL, 72.4 mmol) was followed by treatment as described in Table 2.1. Column

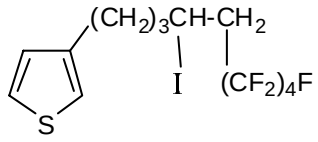

chromatography (silica gel, petroleum ether) gave **2(5,4)** as a clear, colorless liquid (19.0 g, 58.0%). ^{1}H NMR (300 MHz, $CDCl_3$): δ 1.68-1.99 (m, 4H, C-2 and C-3 CH_2), 2.57-3.04 (m, 4H, C-5 and C-1 CH_2), 4.29-4.40 (m, 1H, C-4 CH), 6.93-6.98 (m, 2H, Ar-4, Ar-2), 7.27 (dd, J = 4.9, 1.8 Hz, 1H, Ar-5). ^{13}C NMR (75 MHz, $CDCl_3$): δ 20.3 (C-4), 29.1, 30.5, 39.8, 41.6 (t, $^{2}J_{C\text{-}F}$ = 20.7 Hz, C-5), 120.3 (Ar-2), 125.5 (Ar-5), 127.9 (Ar-4), 141.6 (Ar-3). IR (neat): 3105 (w, sp^2 C-H), 2938, 2861 (sp^3 C-H), 1467 (thiophene), 1215 (s, br), 1131 cm^{-1} (s, C-F stretch). MS (EI) m/z: 498 (M^+), 371 (M - I), 111 (M - $CH_2CHICH_2(CF_2)_4F$), 97 (M – $(CH_2)_2CHICH_2(CF_2)_4F$).

Table 2.1. Reaction progress for synthesis of **2(5,4)**.

Time (h)	Conversion (%)	AIBN added (mg)	$F(CF_2)_nI$ added (mL)
0	0	542	12.20
48	59	541	5.00
96	71	547	3.50
168	80	545	2.44
240	86	--	--
264	--	540	0.85
288	--	--	0.85
312	90	538	0.61
360	93	--	--

3-(4-Iodo-6,6,7,7,8,8,9,9,10,10,11,11,12,12,13,13,13-heptadecafluorotridecyl) thiophene, 2(5,8): White solid (12.5 g, 46.1%), mp 44–46 °C. ^{1}H NMR (300 MHz, $CDCl_3$): δ 1.70-1.97 (m, 4H, C-2 and C-3 CH_2), 2.58-3.03 (m, 4H, C-5 and C-1 CH_2),

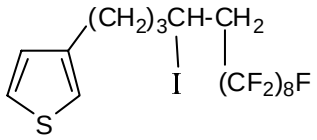

4.29-4.40 (m, 1H, C-4 CH), 6.93-6.98 (m, 2H, Ar-4, Ar-2), 7.25-7.28 (m, 1H, Ar-5). ^{13}C NMR (75 MHz, $CDCl_3$): δ 20.4 (C-4), 29.1, 30.5, 39.8, 41.7 (t, $^2J_{C\text{-}F}$ = 20.6 Hz, C-5), 120.3 (Ar-2), 125.5 (Ar-5), 127.9 (Ar-4), 141.6 (Ar-3). IR (powder): 3098 (w, sp^2 C-H), 2946, 2860 (sp^3 C-H), 1458 (thiophene), 1196 (s, br), 1144 (s), 1114 cm^{-1} (m, C-F stretch). MS (EI) m/z: 698 (M^+), 571 (M - I), 111 (M – $CH_2CHICH_2(CF_2)_8F$), 97 (M – $(CH_2)_2CHICH_2(CF_2)_8F$).

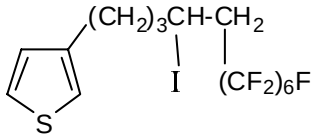

3-(4-Iodo-6,6,7,7,8,8,9,9,10,10,11,11,11-tridecafluoroundecyl)thiophene, 2(5,6): Clear, colorless liquid (5.86 g, 24.4%). ^{1}H NMR (300 MHz, $CDCl_3$): δ 1.68-1.99 (m, 4H, C-2 and C-3 CH_2), 2.60-3.04 (m, 4H, C-5 and C-1 CH_2), 4.29-4.40 (m, 1H, C-4 CH), 6.94-6.98 (m, 2H, Ar-4, Ar-2), 7.27 (dd, *J* = 4.8, 1.8 Hz, 1H, Ar-5). ^{13}C NMR (75 MHz, $CDCl_3$): δ 20.3 (C-4), 29.2, 30.5, 39.8, 41.7 (t, $^2J_{C\text{-}F}$ = 21.1 Hz, C-5), 120.3 (Ar-2), 125.5 (Ar-5), 127.9 (Ar-4), 141.6 (Ar-3). IR (neat): 3107 (w, sp^2 C-H), 2938, 2863 (sp^3 C-H), 1468 (thiophene), 1232 (s), 1189 (s, br) 1142 (s), 1122 cm^{-1} (m, C-F stretch). MS (EI) m/z: 598 (M^+), 471 (M - I), 111 (M – $CH_2CHICH_2(CF_2)_6F$), 97 (M – $(CH_2)_2CHICH_2(CF_2)_6F$).

3-(10-Iodo-12,12,13,13,14,14,15,15,16,16,17,17,18,18,19,19,19-heptadecafluorononadecyl) thiophene, 2(11,8): White solid (863 mg, 18.0%). ^{1}H NMR (300 MHz, $CDCl_3$): δ 1.23-1.45 (m, 12H, C-3 to C-8 CH_2), 1.62 (p, *J* = 7.6 Hz, 2H, C-2

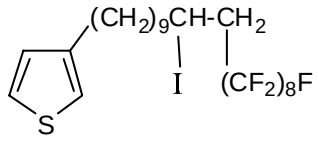

CH_2), 1.68-1.90 (m, 2H, C-9 CH_2), 2.62 (t, J = 7.5 Hz, 2H, C-1 CH_2), 2.66-3.03 (m, 2H, C-11 CH_2), 4.28-4.39 (m, 1H, C-10 CH), 6.90-6.95 (m, 2H, Ar-4, Ar-2), 7.23 (dd, J = 4.9, 2.0 Hz, 1H, Ar-5). ^{13}C NMR (75 MHz, $CDCl_3$): δ 21.0 (C-10), 28.6, 29.3, 29.43, 29.46, 29.5, 29.6, 30.4, 30.6, 40.4, 41.7 (t, $^2J_{C\text{-}F}$ = 20.7 Hz, C-11), 119.7 (Ar-2), 125.0 (Ar-5), 128.2 (Ar-4), 143.1 (Ar-3). IR (neat): 3095 (w, sp^2 C-H), 2920, 2852 (sp^3 C-H), 1466 (thiophene), 1230 (m), 1199 (s, br), 1146 (s), 1116 cm^{-1} (m, C-F stretch). MS (EI) m/z: 782 (M^+), 655 (M - I), 111 (M – $(CH_2)_7CHICH_2(CF_2)_8F$), 97 (M – $(CH_2)_8CHICH_2(CF_2)_8F$).

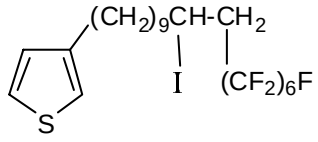

3-(10-Iodo-12,12,13,13,14,14,15,15,16,16,17,17,17-tridecafluoroheptadecyl)thiophene, 2(11,6): Clear, colorless liquid (2.31 g, 20.5%). ^{1}H NMR (300 MHz, $CDCl_3$): δ 1.22-1.48 (m, 12H, C-3 to C-8 CH_2), 1.62 (p, J = 7.7 Hz, 2H, C-2 CH_2), 1.68-1.90 (m, 2H, C-9 CH_2), 2.62 (t, J = 7.5 Hz, 2H, C-1 CH_2), 2.66-3.04 (m, 2H, C-11 CH_2), 4.27-4.39 (m, 1H, C-10 CH), 6.90-6.95 (m, 2H, Ar-4, Ar-2), 7.23 (dd, J = 4.9, 2.9 Hz, 1H, Ar-5). ^{13}C NMR (75 MHz, $CDCl_3$): δ 21.0 (C-10), 28.6, 29.38, 29.43, 29.47, 29.5, 29.7, 30.4, 30.6, 40.4, 41.7 (t, $^2J_{C\text{-}F}$ = 20.4 Hz, C-11), 119.7 (Ar-2), 124.9 (Ar-5), 128.1 (Ar-4), 143.1 (Ar-3). IR (neat): 2926, 2855 (sp^3 C-H), 1464 (thiophene), 1233 (s), 1190 (s, br), 1143 (s), 1122 cm^{-1} (m, C-F stretch). MS (EI) m/z: 682 (M^+), 555 (M - I), 139 (M - $(CH_2)_5CHICH_2(CF_2)_6F$), 111 (M - $(CH_2)_7CHICH_2(CF_2)_6F$), 97 (M -

$(CH_2)_8CHICH_2(CF_2)_6F$).

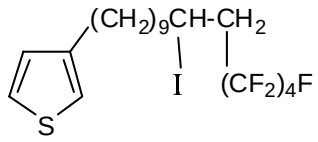

3-(10-Iodo-12,12,13,13,14,14,15,15,15-nonafluoropentadecyl)thiophene, 2(11,4): Clear, colorless liquid (1.96 g, 20.2%). ^{1}H NMR (300 MHz, $CDCl_3$): δ 1.19-1.47 (m, 12H, C-3 to C-8 CH_2), 1.62 (p, *J* = 7.8 Hz, 2H, C-2 CH_2), 1.69-1.89 (m, 2H, C-9 CH_2), 2.62 (t, *J* = 7.4 Hz, 2H, C-1 CH_2), 2.67-3.02 (m, 2H, C-11 CH_2), 4.28-4.37 (m, 1H, C-10 CH), 6.90-6.95 (m, 2H, Ar-4, Ar-2), 7.23 (dd, *J* = 4.9, 2.9 Hz, 1H, Ar-5). ^{13}C NMR (75 MHz, $CDCl_3$): δ 20.9 (C-10), 28.6, 29.37, 29.42, 29.47, 29.5, 29.6, 30.3, 30.6, 40.4, 41.6 (t, $^2J_{C\text{-}F}$ = 20.7 Hz, C-11), 119.7 (Ar-2), 124.9 (Ar-5), 128.1 (Ar-4), 143.0 (Ar-3). IR (neat): 2926, 2855 (sp^3 C-H), 1463 (thiophene), 1216 (s, br), 1132 cm^{-1} (s, C-F stretch). MS (EI) m/z: 582 (M^+), 455 (M - I), 111 (M - $(CH_2)_7CHICH_2(CF_2)_4F$), 97 (M - $(CH_2)_8CHICH_2(CF_2)_4F$).

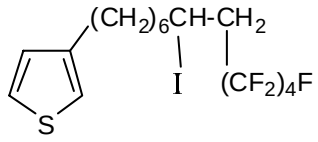

3-(7-Iodo-9,9,10,10,11,11,12,12,12-nonafluorododecylthiophene), 2(8,4). Clear, colorless liquid (4.90 g, 29.8%). ^{1}H NMR (300 MHz, $CDCl_3$): δ 1.22-1.47 (m, 6H, C-3 to C-5 CH_2), 1.62 (p, *J* = 7.7 Hz, 2H, C-2 CH_2), 1.69-1.89 (m, 2H, C-6 CH_2), 2.62 (t, *J* = 7.7 Hz, 2H, C-1 CH_2), 2.67-3.02 (m, 2H, C-8 CH_2), 4.26-4.37 (m, 1H, C-7 CH), 6.90-6.94 (m, 2H, Ar-4, Ar-2), 7.22 (dd, *J* = 5.0, 2.8 Hz, 1H, Ar-5). ^{13}C NMR (75 MHz, $CDCl_3$): δ 20.7 (C-7), 28.3, 29.0, 29.5, 30.2, 30.4, 40.2, 41.3 (t, $^2J_{C\text{-}F}$ = 20.7 Hz, C-8),

119.9 (Ar-2), 125.1 (Ar-5), 128.2 (Ar-4), 142.9 (Ar-3). IR (neat): 2929, 2856 (sp^3 C-H), 1464 (thiophene), 1216 (s, br), 1132 cm^{-1} (s, C-F stretch). MS (EI) m/z: 540 (M^+), 413 (M - I), 97 (M - $(CH_2)_5CHICH_2(CF_2)_4F$).

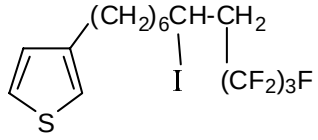

3-(7-Iodo-9,9,10,10,11,11,11-heptafluoroundecylthiophene), 2(8,3). Clear, colorless liquid (5.48 g, 38.1%). ^{1}H NMR (300 MHz, $CDCl_3$): δ 1.20-1.47 (m, 6H, C-3 to C-5 CH_2), 1.62 (p, *J* = 7.7 Hz, 2H, C-2 CH_2), 1.69-1.89 (m, 2H, C-6 CH_2), 2.62 (t, *J* = 7.7 Hz, 2H, C-1 CH_2), 2.66-3.01 (m, 2H, C-8 CH_2), 4.25-4.37 (m, 1H, C-7 CH), 6.89-6.94 (m, 2H, Ar-4, Ar-2), 7.23 (dd, *J* = 5.0, 2.8 Hz, 1H, Ar-5). ^{13}C NMR (75 MHz, $CDCl_3$): δ 20.8 (C-7), 28.3, 29.0, 29.5, 30.2, 30.4, 40.2, 41.3 (t, $^2J_{C\text{-}F}$ = 20.7 Hz, C-8), 119.8 (Ar-2), 125.1 (Ar-5), 128.2 (Ar-4), 142.9 (Ar-3). IR (neat): 2928, 2856 (sp^3 C-H), 1463 (thiophene), 1219 (s, br), 1117 cm^{-1} (s, C-F stretch). MS (EI) m/z: 490 (M^+), 363 (M - I), 111 (M - $(CH_2)_4CHICH_2(CF_2)_3F$), 97 (M - $(CH_2)_5CHICH_2(CF_2)_3F$).

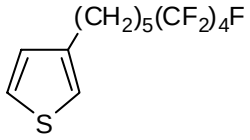

3-(Semifluoroalkyl)thiophenes, 3(m,n). *3-(6,6,7,7,8,8,9,9,9-Nonafluorononyl)thiophene, 3(5,4).* A solution of **2(5,4)** (6.00 g, 12.0 mmol) in anhydrous DMSO (7 mL) was added dropwise to a solution of $NaBH_4$ (1.82 g, 48.0 mmol) in anhydrous DMSO (5 mL) under N_2. The mixture was heated at 80 ºC overnight. The reaction mixture was allowed to cool to room temperature, water (100

mL) was added slowly, and the mixture was extracted with Et_2O (5 x 125 mL). The combined organic layers were washed with 0.5% aqueous HCl (3 x 300 mL) and dried over $MgSO_4$. The solvent was removed on a rotary evaporator to give **3(5,4)** as a clear, colorless liquid (3.93 g, 88%). ^{1}H NMR (300 MHz, $CDCl_3$): δ 1.42 (p, *J* = 7.2 Hz, 2H, C-3 CH_2), 1.56-1.74 (m, 4H, C-2 and C-4 CH_2), 1.94-2.16 (m, 2H, C-5 CH_2), 2.65 (t, *J* = 7.8 Hz, 2H, C-1 CH_2), 6.91-6.95 (m, 2H, Ar-4, Ar-2), 7.25 (dd, *J* = 4.7, 3.0 Hz, 1H, Ar-5). ^{13}C NMR (75 MHz, $CDCl_3$): δ 20.0 (t, $^3J_{C\text{-}F}$ = 3.5 Hz, C-4), 28.8 (C-3), 30.0 (C-1), 30.2 (C-2), 30.8 (t, $^2J_{C\text{-}F}$ = 22.1 Hz, C-5), 120.0 (Ar-2), 125.2 (Ar-5), 128.0 (Ar-4), 142.4 (Ar-3). IR (neat): 3108 (w, sp^2 C-H), 2935, 2681 (sp^3 C-H), 1467 (thiophene), 1216 (s, br), 1166 (m), 1130 cm^{-1} (s, C-F stretch). MS (EI) m/z: M^+ = 372, 111 (M - $(CH_2)_3(CF_2)_4F$), 97 (M - $(CH_2)_4(CF_2)_4F$).

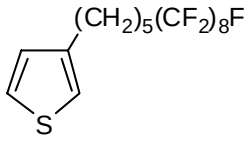

3-(6,6,7,7,8,8,9,9,9,10,10,11,11,12,12,13,13,13-Heptadecafluorotridecyl)thiophene, 3(5,8): White solid (4.51 g, 91.7%), mp = 40–41 °C. ^{1}H NMR (300 MHz, $CDCl_3$): δ 1.36-1.49 (m, 2H, C-3 CH_2), 1.59-1.73 (m, 4H, C-2 and C-4 CH_2), 2.05 (tt, *J* (^{1}H-^{19}F) = 19.1 Hz, *J* (^{1}H-^{1}H) = 8.7 Hz, 2H, C-5 CH_2), 2.65 (t, *J* = 7.4 Hz, 2H, C-1 CH_2), 6.91-6.95 (m, 2H, Ar-4, Ar-2), 7.23-7.28 (m, 1H, Ar-5). ^{13}C NMR (75 MHz, $CDCl_3$): δ 20.1 (t, $^3J_{C\text{-}F}$ = 3.6 Hz, C-4), 28.8 (C-3), 30.0 (C-1), 30.2 (C-2), 30.9 (t, $^2J_{C\text{-}F}$ = 22.3 Hz, C-5), 120.0 (Ar-2), 125.2 (Ar-5), 128.0 (Ar-4), 142.4 (Ar-3). IR (powder): 3100 (w, sp^2 C-H), 2946, 2861 (sp^3 C-H), 1468 (thiophene), 1246 (m), 1198 (s, br), 1144 (s), 1114 cm^{-1} (m, C-F stretch). MS (EI) m/z: 572 (M^+), 111 (M - $(CH_2)_3(CF_2)_8F$), 97 (M - $(CH_2)_4(CF_2)_8F$).

3-(6,6,7,7,8,8,9,9,10,10,11,11,11-Tridecafluoroundecyl)thiophene, 3(5,6): Clear,

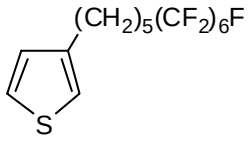

colorless liquid (4.17 g, 90.2%). ^{1}H NMR (300 MHz, $CDCl_3$): δ 1.36-1.49 (m, 2H, C-3 CH_2), 1.57-1.74 (m, 4H, C-2 and C-4 CH_2), 2.05 (tt, J (^{1}H-^{19}F) = 18.9 Hz, J (^{1}H-^{1}H) = 8.7 Hz, 2H, C-5 CH_2), 2.65 (t, J = 7.5 Hz, 2H, C-1 CH_2), 6.91-6.95 (m, 2H, Ar-4, Ar-2), 7.23-7.28 (m, 1H, Ar-5). ^{13}C NMR (75 MHz, $CDCl_3$): δ 20.1 (t, $^{3}J_{C\text{-}F}$ = 4.1 Hz, C-4), 28.8 (C-3), 30.0 (C-1), 30.2 (C-2), 30.9 (t, $^{2}J_{C\text{-}F}$ = 22.9 Hz, C-5), 120.0 (Ar-2), 125.2 (Ar-5), 128.0 (Ar-4), 142.4 (Ar-3). IR (neat): 3106 (w, sp^2 C-H), 2941, 2861 (sp^3 C-H), 1467 (thiophene), 1233 (s), 1188 (s, br), 1142 (s), 1120 cm^{-1} (m, C-F stretch). MS (EI) m/z: 472 (M^+), 111 (M - $(CH_2)_3(CF_2)_6F$), 97 (M - $(CH_2)_4(CF_2)_6F$).

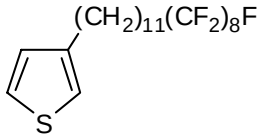

3-(12,12,13,13,14,14,15,15,16,16,17,17,18,18,19,19,19-Heptadecafluorononadecyl)thiophene, 3(11,8): White solid (1.20 g, 89.5%), mp = 56–58 °C. ^{1}H NMR (300 MHz, $CDCl_3$): δ 1.22-1.42 (m, 14H, C-3 to C-9 CH_2), 1.52-1.68 (m, 4H, C-2 and C-10 CH_2), 2.05 (tt, J (^{1}H-^{19}F) = 19.1, J (^{1}H-^{1}H) = 7.7 Hz, 2H, C-11 CH_2), 2.62 (t, J = 7.5 Hz, 2H, C-1 CH_2), 6.90-6.95 (m, 2H, Ar-4, Ar-2), 7.23 (dd, J = 4.9, 2.0 Hz, 1H, Ar-5). ^{13}C NMR (75 MHz, $CDCl_3$): δ 20.2 (t, $^{3}J_{C\text{-}F}$ = 3.6 Hz, C-10), 29.2, 29.3, 29.41, 29.45, 29.5, 29.6 (2C), 30.4 (C-1), 30.6 (C-2), 30.9 (t, $^{2}J_{C\text{-}F}$ = 22.2 Hz, C-11), 119.7 (Ar-2), 124.9 (Ar-5), 128.2 (Ar-4), 143.1 (Ar-3). IR (powder): 3098 (sp^2 C-H), 2920, 2850 (sp^3 C-H), 1470 (thiophene), 1246 (m), 1198 (s, br), 1144 (s), 1116 cm^{-1} (m, C-F stretch). MS (EI) m/z: 656 (M^+), 637 (M - F), 111 (M - $(CH_2)_9(CF_2)_8F$), 97 (M -

$(CH_2)_{10}(CF_2)_8F$).

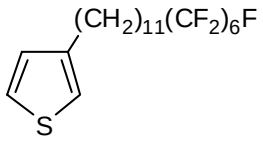

3-(12,12,13,13,14,14,15,15,16,16,17,17,17-Tridecafluoroundecyl)thiophene, 3(11,6): White solid (1.58 g, 84.0%), mp = 38-40 ºC. ^{1}H NMR (300 MHz, $CDCl_3$): δ 1.21-1.42 (m, 14H, C-3 to C-9 CH_2), 1.50-1.68 (m, 4H, C-2 and C-10 CH_2), 2.05 (tt, *J* (^{1}H-^{19}F) = 19.0 Hz, *J* (^{1}H-^{1}H) = 8.2 Hz, 2H, C-11 CH_2), 2.62 (t, *J* = 7.5 Hz, 2H, C-1 CH_2), 6.90-6.95 (m, 2H, Ar-4, Ar-2), 7.23 (dd, *J* = 5.0, 3.0 Hz, 1H, Ar-5). ^{13}C NMR (75 MHz, $CDCl_3$): δ 20.2 (t, $^3J_{C\text{-}F}$ = 3.9 Hz, C-10), 29.2, 29.3, 29.40, 29.45, 29.5, 29.6 (2C), 30.4 (C-1), 30.6 (C-2), 30.9 (t, $^2J_{C\text{-}F}$ = 22.4 Hz, C-11), 119.7 (Ar-2), 124.9 (Ar-5), 128.2 (Ar-4), 143.1 (Ar-3). IR (powder): 3104 (*sp*^{2} C-H), 2918, 2852 (*sp*^{3} C-H), 1472 (thiophene), 1247 (m), 1187 (s, br), 1138 (s), 1122 cm^{-1} (m, C-F stretch). MS (EI) m/z: 556 (M^+), 111 (M - $(CH_2)_9(CF_2)_6F$), 97 (M - $(CH_2)_{10}(CF_2)_6F$).

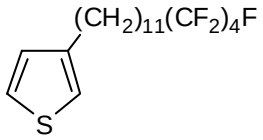

3-(12,12,13,13,14,14,15,15,15-Nonafluoropentadecyl)thiophene, 3(11,4): Clear, colorless liquid (872 mg, 56.7%). ^{1}H NMR (300 MHz, $CDCl_3$): δ 1.21-1.42 (m, 14H, C-3 to C-9 CH_2), 1.54-1.66 (m, 4H, C-2 and C-10 CH_2), 2.04 (tt, *J* (^{1}H-^{19}F) = 19.2 Hz, *J* (^{1}H-^{1}H) = 7.9 Hz, 2H, C-11 CH_2), 2.62 (t, *J* = 7.6 Hz, 2H, C-1 CH_2), 6.90-6.95 (m, 2H, Ar-4, Ar-2), 7.23 (dd, *J* = 4.9, 3.0 Hz, 1H, Ar-5). ^{13}C NMR (75 MHz, $CDCl_3$): δ 20.2 (t, $^3J_{C\text{-}F}$ = 3.9 Hz, C-10), 29.2, 29.3, 29.41, 29.45, 29.5, 29.6 (2C), 30.4 (C-1), 30.6 (C-2),

30.8 (t, $^{2}J_{C\text{-}F}$ = 22.6 Hz, C-11), 119.7 (Ar-2), 124.9 (Ar-5), 128.2 (Ar-4), 143.1 (Ar-3). IR (neat): 3103 (*sp*^{2} C-H), 2915, 2851 (*sp*^{3} C-H), 1472 (thiophene), 1246 (s), 1202 (s, br), 1167 cm^{-1} (s, C-F stretch). MS (EI) m/z: 456 (M^{+}), 139 (M - $(CH_2)_7(CF_2)_4F$), 111 (M - $(CH_2)_9(CF_2)_4F$), 97 (M - $(CH_2)_{10}(CF_2)_4F$).

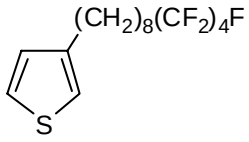

3-(9,9,10,10,11,11,12,12,12-Nonafluorododecylthiophene), 3(8,4). Clear, colorless liquid (1.03 g, 95.4%). ^{1}H NMR (300 MHz, $CDCl_3$): δ 1.18-1.44 (m, 8H, C-3 to C-6 CH_2), 1.54-1.68 (m, 4H, C-2 and C-7 CH_2), 2.03 (tt, *J* (^{1}H-^{19}F) = 18.7 Hz, *J* (^{1}H-^{1}H) = 7.7 Hz, 2H, C-8 CH_2), 2.61 (t, *J* = 7.7 Hz, 2H, C-1 CH_2), 6.88-6.94 (m, 2H, Ar-4, Ar-2), 7.22 (dd, *J* = 5.0, 2.8 Hz, 1H, Ar-5). ^{13}C NMR (75 MHz, $CDCl_3$): δ 20.0 (t, $^{3}J_{C\text{-}F}$ = 3.4 Hz, C-7), 29.06, 29.15, 29.18 (2C), 30.2 (C-1), 30.5 (C-2), 30.8 (t, $^{2}J_{C\text{-}F}$ = 21.8 Hz, C-8), 119.8 (Ar-2), 125.1 (Ar-5), 128.2 (Ar-4), 143.1 (Ar-3). IR (neat): 2927, 2856 (*sp*^{3} C-H), 1464 (thiophene), 1216 (s, br), 1202 (s, br), 1165 cm^{-1} (s, C-F stretch). MS (EI) m/z: 414 (M^{+}), 111 (M - $(CH_2)_6(CF_2)_4F$), 97 (M - $(CH_2)_7(CF_2)_4F$).

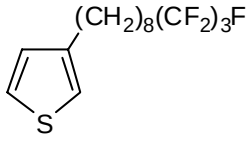

3-(9,9,10,10,11,11,11-Heptafluoroundecylthiophene), 3(8,3). Clear, colorless liquid (3.12 g, 76.6%). ^{1}H NMR (300 MHz, $CDCl_3$): δ 1.19-1.44 (m, 8H, C-3 to C-6 CH_2), 1.48-1.69 (m, 4H, C-2 and C-7 CH_2), 2.02 (tt, *J* (^{1}H-^{19}F) = 18.7 Hz, *J* (^{1}H-^{1}H) = 7.7 Hz, 2H, C-8 CH_2), 2.61 (t, *J* = 7.7 Hz, 2H, C-1 CH_2), 6.88-6.94 (m, 2H, Ar-4, Ar-2), 7.22

(dd, J = 5.0, 2.8 Hz, 1H, Ar-5). ^{13}C NMR (75 MHz, $CDCl_3$): δ 20.0 (t, $^3J_{C\text{-}F}$ = 3.4 Hz, C-7), 29.0, 29.13, 29.16 (2C), 30.2 (C-1), 30.5 (C-2), 30.6 (t, $^2J_{C\text{-}F}$ = 21.8 Hz, C-8), 119.8 (Ar-2), 125.1 (Ar-5), 128.2 (Ar-4), 143.1 (Ar-3). IR (neat): 2927, 2856 (sp^3 C-H), 1464 (thiophene), 1218 (s), 1168 cm^{-1} (s, C-F stretch). MS (EI) m/z: 364 (M^+), 111 (M - $(CH_2)_6(CF_2)_3F$), 97 (M - $(CH_2)_7(CF_2)_3F$).

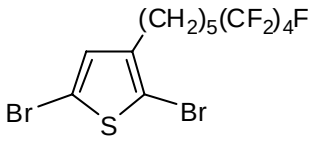

2,5-Dibromo-3-(semifluoroalkyl)thiophenes, 4(m,n). *2,5-Dibromo-3-(6,6,7,7,8,8,9,9,9-nonafluorononyl)thiophene, 5(5,4).* A solution of **3(5,4)** (5.00 g, 13.4 mmol) in DMF (12.5 mL) and chloroform (12.5 mL) was cooled to –10 °C. *N*-Bromosuccinimide (4.79 g, 26.9 mmol) was added, and the mixture was agitated at –10 °C under N_2 for 27 h. The reaction mixture was poured into water (50 mL) and the resultant mixture was extracted with hexanes (3 x 50 mL). The combined organic layers were washed with 0.5% aqueous HCl (5 x 100 mL) and dried over Na_2SO_4. The solvent was removed on a rotary evaporator. Column chromatography (silica gel, 99/1 hexanes/$CHCl_3$) gave **4(5,4)** as a clear, colorless liquid (4.69 g, 66.1%). ^{1}H NMR (300 MHz, $CDCl_3$): δ 1.35-1.46 (m, 2H, C-3 CH_2), 1.57-1.69 (m, 4H, C-2 and C-4 CH_2), 1.97-2.15 (m, 2H, C-5 CH_2), 2.54 (t, J = 7.6 Hz, 2H, C-1 CH_2), 6.77 (s, 1H, Ar-4). ^{13}C NMR (75 MHz, $CDCl_3$): δ 19.9 (t, $^3J_{C\text{-}F}$ = 3.5 Hz, C-4), 28.4 (C-3), 29.1 (C-1), 29.2 (C-2), 30.7 (t, $^2J_{C\text{-}F}$ = 22.3 Hz, C-5), 108.3 (Ar-2), 110.6 (Ar-5), 130.8 (Ar-4), 142.3 (Ar-3). ^{19}F NMR (376 MHz, $CDCl_3$): δ –81.6 (3F, C-9 CF_3), -115.2 (2F), -125.0 (2F), -126.6 (2F). IR (neat): 2945, 2861 (sp^3 C-H), 1221 (m, br), 1167 (m), 1132 cm^{-1} (m, C-F stretch). HRMS (EI): Calculated for $C_{13}H_{11}Br_2F_9S$: 527.88045, Observed 527.88411 (δ -6.9 ppm). MS

(EI) m/z: 528 (M^+), 449 (M - Br).

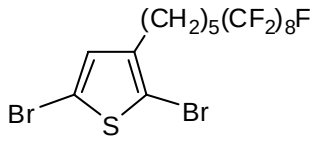

2,5-Dibromo-3-(6,6,7,7,8,8,9,9,9,10,10,11,11,12,12,13,13,13-heptadecafluorotridecyl)thiophene, 4(5,8): White solid (4.57 g, 71.8%), mp = 32-34 ºC. ^{1}H NMR (300 MHz, $CDCl_3$): δ 1.31-1.47 (m, 2H, C-3 CH_2), 1.50-1.73 (m, 4H, C-2 and C-4 CH_2), 1.92-2.17 (m, 2H, C-5 CH_2), 2.52 (t, J = 7.6 Hz, 2H, C-1 CH_2), 6.75 (s, 1H, Ar-4). ^{13}C NMR (75 MHz, $CDCl_3$): δ 19.9 (C-4), 28.4, 29.1, 29.2, 30.8 (t, $^2J_{C\text{-}F}$ = 23.0 Hz, C-5), 108.26, 110.62, 130.79 (Ar-4), 142.27 (Ar-3). ^{19}F NMR (376 MHz, $CDCl_3$): δ –81.8 (3F, C-13 CF_3), -115.5 (2F), -122.8 (2F), -123.0 (4F), -124.8 (2F), -124.6 (2F), -127.2 (2F). IR (powder): 2943, 2859 (sp^3 C-H), 1203 (s), 1149 cm^{-1} (s, C-F stretch). MS (EI) m/z: 730 (M^+), 651 (M – Br). HRMS (EI): Calculated for $C_{17}H_{11}F_{17}Br_2S$: 717.86767, Observed 727.87102 (Δ = -4.6 ppm).

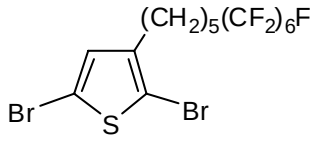

2,5-Dibromo-3-(6,6,7,7,8,8,9,9,10,10,11,11,11-tridecafluoroundecyl)thiophene, 4(5,6): White solid (3.48 g, 63.9%). ^{1}H NMR (300 MHz, $CDCl_3$): δ 1.33-1.45 (m, 2H, C-3 CH_2), 1.50-1.73 (m, 4H, C-2 and C-4 CH_2), 1.91-2.20 (m, 2H, C-5 CH_2), 2.52 (t, J = 7.7 Hz, 2H, C-1 CH_2), 6.75 (s, 1H, Ar-4). ^{13}C NMR (75 MHz, $CDCl_3$): δ 19.9 (t, $^3J_{C\text{-}F}$ = 3.9 Hz, C-4), 28.4, 29.1, 29.2, 30.8 (t, $^2J_{C\text{-}F}$ = 23.0 Hz, C-5), 108.3, 110.6, 130.8 (Ar-4), 142.3 (Ar-3). ^{19}F NMR (376 MHz, $CDCl_3$): δ –81.8 (3F, C-11 CF_3), -115.4 (2F), -123.0

(2F), -123.9 (2F), -124.6 (2F), -127.2 (2F). IR (powder): 2945, 2861 (*sp*^{3} C-H), 1543, 1466, 1419, 1240 (br), 1144 cm^{-1} (C-F stretch). MS (EI) m/z: 628 (M^+), 549 (M – Br). HRMS (EI): Calculated for $C_{15}H_{11}F_{13}Br_2S$: 627.87406, Observed 627.87225 (Δ = 2.9 ppm).

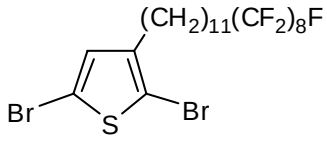

2,5-Dibromo-3-(12,12,13,13,14,14,15,15,16,16,17,17,18,18,19,19,19-heptadecafluorononadecyl)thiophene, 4(11,8): White solid (4.28 g, 58.2%), mp 33-34.5 ºC. ^{1}H NMR (300 MHz, $CDCl_3$): δ 1.17-1.41 (m, 14H, C-3 to C-9 CH_2), 1.44-1.65 (m, 4H, C-2 and C-10 CH_2), 1.91-2.15 (m, 2H, C-11 CH_2), 2.48 (t, J = 7.2 Hz, 2H, C-1 CH_2), 6.75 (s, 1H, Ar-4). ^{13}C NMR (75 MHz, $CDCl_3$): δ 20.1 (C-10), 29.07, 29.1, 29.2, 29.3 (2C), 29.5 (3C), 29.6, 30.9 (t, $^2J_{C\text{-}F}$ = 23.1 Hz, C-11), 107.9, 110.3, 131.0 (Ar-4), 143.0 (Ar-3). ^{19}F NMR (376 MHz, $CDCl_3$): δ –81.7 (3F, C-19 CF_3), -115.3 (2F), -122.7 (2F), -122.9 (4F), -123.7 (2F), -124.5 (2F), -127.1 (2F). IR (powder): 2920, 2852 (*sp*^{3} C-H), 1471 (thiophene), 1244 (m), 1198 (s, br), 1146 (s), 1115 cm^{-1} (m, C-F stretch). MS (EI) m/z: 812 (M^+), 733 (M – Br), 654 (M – Br_2). HRMS (EI): Calculated for $C_{23}H_{23}F_{17}Br_2S$: 811.96158, Observed 811.96242 (Δ = -1.0 ppm). Elem. anal. calculated for $C_{15}H_{17}F_7Br_2S$: C 33.93% H 2.85% F 39.66% S 3.94%. Observed C 34.45% H 2.84% F 39.66% S 3.94%.

2,5-Dibromo-3-(12,12,13,13,14,14,15,15,16,16,17,17,17-tridecafluoroundecyl)thiophene, 4(11,6): Clear, colorless liquid (5.01 g, 81.9%). ^{1}H NMR (300 MHz, $CDCl_3$): δ 1.18-1.42 (m, 14H, C-3 to C-9 CH_2), 1.44-1.65 (m, 4H, C-2 and C-10 CH_2), 1.92-2.14 (m, 2H, C-11 CH_2), 2.48 (t, J = 7.2 Hz, 2H, C-1 CH_2), 6.75 (s, 1H, Ar-4). ^{13}C NMR (75 MHz, $CDCl_3$): δ 20.1 (C-10), 29.1 (2C), 29.2, 29.4 (2C), 29.5

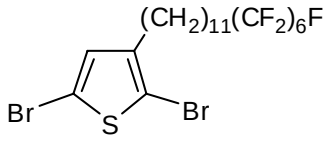

(3C), 29.6, 30.9 (t, $^{2}J_{C\text{-}F}$ = 23.1 Hz, C-11), 107.9, 110.3, 131.0 (Ar-4), 143.0 (Ar-3). ^{19}F NMR (376 MHz, $CDCl_3$): δ –81.8 (3F, C-17 CF_3), -115.4 (2F), -122.9 (2F), -123.9 (2F), -124.6 (2F), -127.1 (2F). IR (neat): 2924, 2854 (*sp*^{3} C-H), 1466 (thiophene), 1234 (m), 1187 (s, br), 1143 (s), 1121 cm^{-1} (m, C-F stretch). MS (EI) m/z: 812 (M^+), 633 (M – Br), 554 (M – Br_2). HRMS (EI): Calculated for $C_{21}H_{23}F_{13}Br_2S$: 711.96796, Observed 711.96334 (Δ = 2.3 ppm).

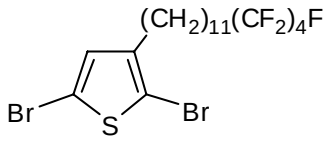

2,5-Dibromo-3-(12,12,13,13,14,14,15,15,15-nonafluoropentadecyl)thiophene, 4(11,4): Clear, colorless liquid (5.37 g, 88.4%). ^{1}H NMR (300 MHz, $CDCl_3$): δ 1.18-1.42 (m, 14H, C-3 to C-9 CH_2), 1.44-1.68 (m, 4H, C-2 and C-10 CH_2), 1.92-2.13 (m, 2H, C-11 CH_2), 2.48 (t, *J* = 7.2 Hz, 2H, C-1 CH_2), 6.75 (s, 1H, Ar-4). ^{13}C NMR (75 MHz, $CDCl_3$): δ 20.1 (C-10), 29.07, 29.10, 29.2, 29.35 (2C), 29.47 (3C), 29.56, 30.8 (t, $^{2}J_{C\text{-}F}$ = 22.9 Hz, C-11), 107.9, 110.3, 130.9 (Ar-4), 143.0 (Ar-3). ^{19}F NMR (376 MHz, $CDCl_3$): δ –81.8 (3F, C-15 CF_3), -115.4 (2F), -125.3 (2F), -126.8 (2F). IR (neat): 2925, 2855 (*sp*^{3} C-H), 1465 (thiophene), 1218 (m, br), 1165, 1121 cm^{-1} (m, C-F stretch). MS (EI) m/z: 612 (M^+), 533 (M – Br), 454 (M – Br_2).

2,5-Dibromo-3-(9,9,10,10,11,11,12,12,12-nonafluorododecylthiophene), 4(8,4). Clear, colorless liquid (3.50 g, 71.6%). ^{1}H NMR (300 MHz, $CDCl_3$): δ 1.18-1.41 (m, 8H, C-3 to C-6 CH_2), 1.44-1.63 (m, 4H, C-2 and C-7 CH_2), 2.02 (tt, *J* (^{1}H-^{19}F) = 18.8 Hz, *J*

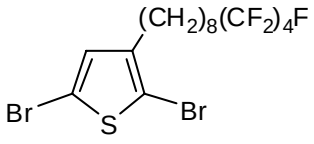

(^{1}H-^{1}H) = 7.6 Hz, 2H, C-8 CH_2), 2.49 (t, *J* = 7.6 Hz, 2H, C-1 CH_2), 6.75 (s, 1H, Ar-4). ^{13}C NMR (75 MHz, $CDCl_3$): δ 20.0 (t, $^3J_{C\text{-}F}$ = 3.4 Hz, C-7), 28.94, 29.06, 29.10 (2C), 29.4, 29.5, 30.6 (t, $^2J_{C\text{-}F}$ = 21.8 Hz, C-8), 108.0, 110.4, 130.9 (Ar-4), 142.8 (Ar-3). ^{19}F NMR (376 MHz, $CDCl_3$): δ –82.0 (3F, C-15 CF_3), -115.4 (2F), -125.2 (2F), -126.8 (2F). IR (neat): 2927, 2856 (*sp*^{3} C-H), 1464 (thiophene), 1216 (s, br), 1130 cm^{-1} (s, C-F stretch). MS (EI) m/z: 570 (M^+), 491 (M – Br), 412 (M – Br_2). HRMS (EI): Calculated for $C_{16}H_{17}F_9Br_2S$: 569.92740, Observed 569.92548 (Δ = 3.4 ppm).

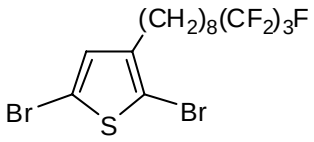

2,5-Dibromo-3-(9,9,10,10,11,11,11-heptafluoroundecylthiophene), 4(8,3). Clear, colorless liquid (1.90 g, 42.6%). ^{1}H NMR (300 MHz, $CDCl_3$): δ 1.20-1.42 (m, 8H, C-3 to C-6 CH_2), 1.45-1.64 (m, 4H, C-2 and C-7 CH_2), 2.01 (tt, *J* (^{1}H-^{19}F) = 18.2 Hz, *J* (^{1}H-^{1}H) = 7.7 Hz, 2H, C-8 CH_2), 2.49 (t, *J* = 7.2 Hz, 2H, C-1 CH_2), 6.75 (s, 1H, Ar-4). ^{13}C NMR (75 MHz, $CDCl_3$): δ 20.0 (t, $^3J_{C\text{-}F}$ = 3.4 Hz, C-7), 28.94, 29.06, 29.10 (2C), 29.4, 29.5, 30.6 (t, $^2J_{C\text{-}F}$ = 21.8 Hz, C-8), 108.0, 110.4, 130.9 (Ar-4), 142.8 (Ar-3). ^{19}F NMR (376 MHz, $CDCl_3$): δ –80.8 (3F, C-11 CF_3), -115.4 (2F), -127.8 (2F). IR (neat): 2926, 2856 (*sp*^{3} C-H), 1464 (thiophene), 1218 (s), 1168 (s), 1115 cm^{-1} (s, C-F stretch). MS (EI) m/z: 520 (M^+), 441 (M – Br), 362 (M – Br_2). HRMS (EI): Calculated for $C_{15}H_{17}F_7Br_2S$: 519.93059, Observed 519.93003 (Δ = 1.1 ppm). Elem. anal. calculated for $C_{15}H_{17}F_7Br_2S$: C 34.50% H 3.28% F 25.47% S 6.14% Br 30.61%. Observed C 34.75% H

3.30% F 25.17% S 6.18% Br 30.65%.

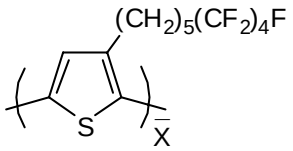

Poly(3-semifluoroalkylthiophene)s. *Poly(3-(6,6,7,7,8,8,9,9,9-nonafluorononyl)thiophene, Rg(Th-5,4).* Methylmagnesium bromide (2.78 mL, 8.34 mmol) was added to a solution of **4(5,4)** (4.40 g, 8.34 mmol) in anhydrous THF (50 mL) using Schlenk techniques. The mixture was heated at reflux for 1 h. Ni(dppp)Cl_2 (41.7 mg, 76.9 μmol) in anhydrous THF (3 mL) was added, and the mixture was heated at reflux for 45 min, allowed to cool to room temperature, and poured onto MeOH (30 mL). The resultant precipitate was isolated by filtration and fractionated by Soxhlet extraction (MeOH, hexanes, $CHCl_3$). The remaining polymer was dissolved in 1,2-dichlorobenzene at 120°C. The solution was hot-filtered, cooled, and centrifuged (4000 RPM). The solvent was decanted, and the polymer was washed with MeOH (3 x 50 mL). MeOH was removed from the polymer by rotary evaporation to give **Rg(Th-5,4)** as a purple solid (554 mg, 18.0%, 1,2-dichlorobenzene soluble fraction). ^{1}H NMR ($C_2D_2Cl_4$, 120 °C, 400 MHz): δ 1.35-1.45 (p, J = 7.0 Hz, 2H, C-3 CH_2), 1.65 (p, J = 7.2 Hz, 2H), 1.73 (p, J = 7.2 Hz, 2H), 2.06 (tt, $^3J_{H\text{-}F}$ = 18.7 Hz, J = 8.1 Hz, 2H, C-5 CH_2), 2.82 (t, J = 7.2 Hz, 2H, C-1 CH_2), 6.95 (s, 1H, Ar-4). ^{13}C NMR ($C_2D_2Cl_4$, 120 °C, 100 MHz): δ 20.3 (t, $^3J_{C\text{-}F}$ = 3.2 Hz, C-4), 29.0 (C-3), 29.2 (C-1), 30.0 (C-2), 31.3 (t, $^2J_{C\text{-}F}$ = 22.6 Hz, C-5), 129.0 (Ar-2), 131.1 (Ar-5), 134.3 (Ar-4), 139.8 (Ar-3). ^{19}F NMR (376 MHz, 60 ºC, $CDCl_3$): δ –82.4 (3F, C-9 CF_3), -115.2 (2F), -125.5 (2F), -127.0 (2F). IR (neat): 2943, 2862 (sp^3 C-H), 1220 (m, br), 1131 cm^{-1} (C-F stretch). Elemental analysis: Calculated: 42.17% C, 2.99% H, 46.12% F, 8.66% S. Observed: 42.07% C, 2.90% H, 46.33% F, 8.64% S.

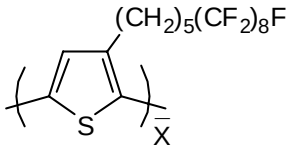

Poly(3-(6,6,7,7,8,8,9,9,9,10,10,11,11,12,12,13,13,13-heptadecafluorotridecyl)thiophene), Rg(Th-5,8): Purple solid (228 mg, 6.5%, 1,2-dichlorobenzene-soluble portion). ^{1}H NMR ($C_2D_2Cl_4$, 120 °C, 400 MHz): δ 1.09-1.44 (m, 2H, C-3 CH_2), 1.49-1.96 (m, 4H, C-2 and C-4 CH_2), 2.04-2.24 (m, 2H, C-5 CH_2), 2.82-3.01 (m, 2H, C-1 CH_2), 7.08 (br s, 1H, Ar-4). ^{13}C and ^{19}F NMR data are unavailable due to polymer insolubility, even at high temperature. IR (neat): 2943, 2859 (sp^3 C-H), 1203 (s), 1149 cm^{-1} (s, C-F stretch). Elem. anal. calculated for $C_{17}H_{11}F_{17}S$: C 35.80% H 1.95% F 56.63% S 5.62%. Observed C 36.01% H 1.82% F 56.58% S 5.57%.

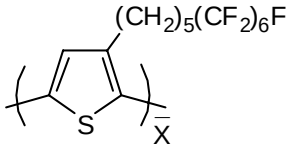

Poly(3-(6,6,7,7,8,8,9,9,10,10,11,11,11-tridecafluoroundecyl)thiophene), Rg(Th-5,6): Purple solid (113 mg, 4.6%, 1,2-dichlorobenzene-soluble portion). ^{1}H NMR ($C_2D_2Cl_4$, 120 °C, 400 MHz): δ 1.42-1.53 (m, 2H, C-3 CH_2), 1.56-1.77 (m, 4H, C-2 and C-4 CH_2), 1.94-2.14 (m, 2H, C-5 CH_2), 2.74-2.85 (m, 2H, C-1 CH_2), 6.94 (br s, 1H, Ar-4). ^{13}C and ^{19}F NMR data are unavailable due to polymer insolubility, even at high temperature. IR (neat): 2945, 2861 (sp^3 C-H), 1543, 1466, 1419, 1240 (br), 1144 cm^{-1} (C-F stretch). Elem. anal. calculated for $C_{15}H_{11}F_{13}S$: C 38.31% H 2.36% F 52.52% S 6.81%. Observed C 38.28% H 2.42% F 52.32% S 6.81%.

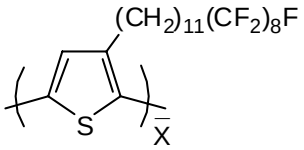

Poly(3-(12,12,13,13,14,14,15,15,16,16,17,17,18,18,19,19,19-heptadecafluorononadecyl)thiophene), Rg(Th-11,8): Purple solid (206 mg, 17.8%, $CHCl_3$-soluble portion). ^{1}H NMR ($C_2D_2Cl_4$, 120 °C, 400 MHz): δ 1.20-1.46 (m, 14H, C-3 to C-9 CH_2), 1.58 (p, *J* = 7.6 Hz, 2H), 1.70 (p, *J* = 7.6 Hz, 2H), 2.02 (tt, *J* = 18.3, 8.2 Hz, 2H, C-11 CH_2), 2.79 (br t, *J* = 7.3 Hz, 2H, C-1 CH_2), 6.96 (br s, 1H, Ar-4). ^{13}C NMR ($C_2D_2Cl_4$, 120 °C, 100 MHz): δ 20.2 (C-10), 29.2, 29.3, 29.4, 29.5, 29.6 (3C), 29.7, 30.6, 31.1 (t, $^2J_{C\text{-}F}$ = 22.5 Hz, C-11), 128.8, 130.7, 134.0, 140.1. CF_2 and CF_3 resonances appeared as complex multiplets arising from short and long-range ^{13}C-^{19}F coupling from 105 and 122 ppm. ^{19}F NMR (376 MHz, 60 ºC, $CDCl_3$): δ -81.9 (3F, C-19 CF_3), -114.9 (2F), -122.3 (2F), -122.5 (4F), -123.3 (2F), -124.1 (2F), -126.7 (2F). IR (neat): 2920, 2852 (*sp*^{3} C-H), 1471 (thiophene), 1244 (m), 1198 (s, br), 1146 (s), 1115 cm^{-1} (m, C-F stretch). Elem. anal. calculated for $C_{23}H_{23}F_{17}S$: C 42.21% H 3.54% F 49.35% S 4.90%. Observed C 42.20% H 3.61% F 49.36% S 4.84%.

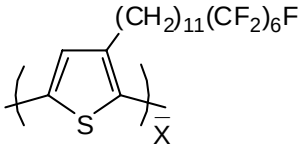

Poly(3-(12,12,13,13,14,14,15,15,16,16,17,17,17-tridecafluoroundecyl)thiophene), Rg(Th-11,6): Purple solid (995 mg, 26.5%, $CHCl_3$-soluble portion). ^{1}H NMR (400 MHz, 60 ºC, $CDCl_3$): δ 1.13-1.50 (m, 14H, C-3 to C-9 CH_2), 1.58 (p, *J* = 6.9 Hz, 2H), 1.70 (p, *J* = 6.9 Hz, 2H), 2.03 (tt, *J* = 18.0, 8.2 Hz, 2H, C-11 CH_2), 2.80 (br t, *J* = 7.3 Hz, 2H, C-1 CH_2), 6.96 (br s, 1H, Ar-4). ^{13}C NMR (125 MHz, 60 ºC, $CDCl_3$): δ 20.5 (C-10),

29.5 (2C), 29.6, 29.7 (2C), 29.8 (3C), 29.9, 30.9 (t, $^{2}J_{C\text{-}F}$ = 22.5 Hz, C-11), 129.7, 131.0, 134.2, 140.3. ^{19}F NMR (376 MHz, 60 ºC, $CDCl_3$): δ –81.9 (3F, C-17 CF_3), -115.0 (2F), -122.6 (2F), -123.6 (2F), -124.3 (2F), -126.9 (2F). IR (neat): 2921, 2851 (*sp*^{3} C-H), 1469 (thiophene), 1232 (m), 1185 (s, br), 1141 (s), 1121 cm^{-1} (m, C-F stretch). Elem. anal. calculated for $C_{21}H_{23}F_{13}S$: C 45.49% H 4.18% F 44.54% S 5.78%. Observed C 45.30% H 4.19% F 44.70% S 5.80%.

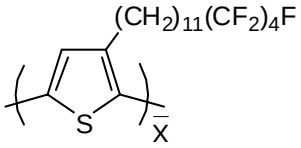

Poly(3-(12,12,13,13,14,14,15,15,15-nonafluoropentadecyl)thiophene), Rg(Th-11,4): Purple solid (203 mg, 5.1%, hexanes-soluble portion). ^{1}H NMR (300 MHz, $CDCl_3$): δ 1.14-1.46 (m, 14H, C-3 to C-9 CH_2), 1.47-1.75 (m, 4H, C-2 and C-10 CH_2), 2.01 (tt, *J* = 18.3, 8.2 Hz, 2H, C-11 CH_2), 2.78 (br t, 2H, C-1 CH_2), 6.96 (s, 1H, Ar-4). ^{13}C NMR (75 MHz, $CDCl_3$): δ 20.1 (t, *J* = 3.7 Hz, C-10), 29.1, 29.2, 29.4 (2C), 29.46, 29.49, 29.6 (3C), 30.7 (t, $^{2}J_{C\text{-}F}$ = 22.9 Hz, C-11), 128.6, 130.5, 134.4, 139.9. IR (neat): 2921, 2851 (*sp*^{3} C-H), 1468 (thiophene), 1216 (m, br), 1166, 1130 cm^{-1} (m, C-F stretch). Elem. anal. calculated for $C_{19}H_{23}F_9S$: C 50.22% H 5.10% S 7.06%. Observed C 50.49% H 5.56% F S 6.32%.

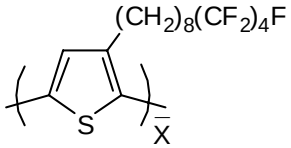

Poly(3-(9,9,10,10,11,11,12,12,12-nonafluorododecylthiophene), Rg(Th-8,4). Purple solid (260 mg, 15.0%, $CHCl_3$-soluble portion). ^{1}H NMR (300 MHz, $CDCl_3$): δ

1.18-1.48 (m, 8H, C-3 to C-6 CH_2), 1.49-1.79 (m, 4H, C-2 and C-7 CH_2), 1.92-2.11 (m, 2H, C-8 CH_2), 2.78 (t, J = 7.3 Hz, 2H, C-1 CH_2), 6.95 (br s, 1H, Ar-4). ^{13}C NMR (75 MHz, $CDCl_3$): δ 20.1 (t, J = 3.7 Hz, C-7), 29.1, 29.2, 29.3, 29.4, 29.5, 30.5, 30.8 (t, $^2J_{C\text{-}F}$ = 22.0 Hz, C-8), 128.6, 130.5, 133.7, 139.8. ^{19}F NMR (376 MHz, $CDCl_3$): δ –81.6 (3F, C-12 CF_3), -115.2 (2F), -125.0 (2F), -126.6 (2F). IR (neat): 2924, 2854 (sp^3 C-H), 1468 (thiophene), 1216 (s, br), 1129 cm^{-1} (s, C-F stretch). Elem. anal. calculated for $C_{16}H_{17}F_9S$: C 46.60% H 4.16% S 7.78%. Observed C 46.39% H 4.27% S 7.48%.

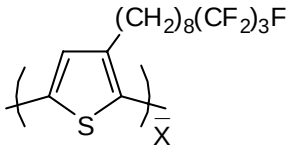

Poly(3-(9,9,10,10,11,11,11-heptafluoroundecylthiophene), Rg(Th-8,3). Purple solid (553 mg, 60.0%, $CHCl_3$-soluble portion). ^{1}H NMR (300 MHz, $CDCl_3$): δ 1.22-1.48 (m, 8H, C-3 to C-6 CH_2), 1.64-1.80 (m, 4H, C-2 and C-7 CH_2), 1.92-2.13 (m, 2H, C-8 CH_2), 2.78 (t, J = 6.9 Hz, 2H, C-1 CH_2), 6.95 (s, 1H, Ar-4). ^{13}C NMR (75 MHz, $CDCl_3$): δ 20.0 (C-7), 29.1, 29.2 (2C), 29.4, 29.5, 30.3, 30.5 (C-8), 129.4, 130.5, 133.7, 139.8. ^{19}F NMR (376 MHz, $CDCl_3$): δ –81.6 (3F, C-11 CF_3), -116.2 (2F), -128.6 (2F). IR (neat): 2923, 2853 (sp^3 C-H), 1468 (thiophene), 1216 (s), 1166 (s), 1114 cm^{-1} (m, C-F stretch). Elem. anal. calculated for $C_{15}H_{17}F_7Br_2S$: C 49.72% H 4.73% F 36.70% S 8.85%. Observed C 49.84% H 4.69% F 36.47% S 8.85%.

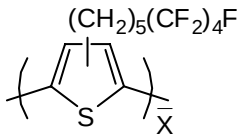

Regiorandom Poly(3-semifluoroalkyl)thiophene. *Poly(3-(6,6,7,7,8,8,9,9,9-*

nonafluorononyl)thiophene, Rn(Th-5,4). Anhydrous $FeCl_3$ (1.83 g, 11.3 mmol) and 3-(6,6,7,7,8,8,9,9,9-nonafluorononyl)thiophene **4(5,4)** (1.00 g, 2.69 mmol) were stirred in anhydrous $CHCl_3$ (6 mL) at room temperature under N_2. After 16 h, the solution was poured into MeOH (15 mL). The crude polymer was isolated by filtration and fractionated by Soxhlet extraction (MeOH, hexanes, $CHCl_3$) to afford the regiorandom polymer **Rn(5,4)** as a red-purple solid (235 mg, 23.7%, $CHCl_3$-soluble portion). ^{1}H NMR (400 MHz, 60 ºC, $CDCl_3$): δ 1.20-1.80 (m, 6H, C-2 to C-4 CH_2), 1.96-2.17 (m, 2H, C-5 CH_2), 2.52-2.54 (m, 2H, head-to-head C-1 CH_2), 2.83 (t, *J* = 7.3 Hz, 2H, head-to-tail C-1 CH_2), 6.92-7.08 (m, 1H, head-to-head and head-to-tail Ar-4). ^{13}C NMR (125 MHz, 60 ºC, $CDCl_3$): δ 20.1, 29.0, 29.1, 29.7, 30.1, 31.0 (t, *J* = 22.5 Hz, C-5), 125.2, 126.5, 127.4, 128.8, 130.1, 130.8, 131.0, 134.0, 135.3, 136.0, 139.5, 139.9, 142.5, 143.0 (all thiophene carbons). CF_2 and CF_3 resonances appeared as complex multiplets arising from short and long-range ^{13}C-^{19}F coupling at 108-121 ppm. Elem. anal. calculated for $C_{13}H_{11}F_9S$: C 42.17% H 2.99% F 46.18% S 8.66%. Observed C 42.75% H 3.47% F 42.75% S 8.01%.

2.3: Results and Discussion

2.3.1: Synthetic Approach to Semifluroalkylthiophene Monomers

The route used to prepare 3-semifluoroalkylthiophene monomers **3(m,n)** and **4(m,n)** is shown in Figure 2.2. The experimental methods given above are representative of the synthetic procedures used. However, some minor modifications were used in later syntheses, as noted below.

A series of 3-(ω-alkenyl)thiophenes **1(m)** where m>2, was synthesized by nickel-catalyzed Kumada coupling[2,3] of 3-bromothiophene and the appropriate ω-bromo-1-alkene. Use of sonication to initiate formation of the Grignard reagent resulted in the formation of appreciable quantities of two byproducts, α,ω-bisalkenes (e.g.,

$H_2C=CH(CH_2)_{2m-4}CH=CH_2$) by homocoupling of the ω-bromo-1-alkene, and internal alkenes (e.g., 3-Th-$(CH_2)_{m-3}CH=CHCH_3$) by isomerization of the desired 3(ω-alkenyl)thiophene. The formation of these byproducts was minimized by use of only the heat of addition of the alkenyl bromide to initiate and sustain formation of the Grignard reagent. Separation of the desired 3-(ω-alkenyl)thiophene from the small amount of internal alkene formed in the coupling reaction was not possible by column chromatography. However, the internal alkene is unreactive in the next step in the synthetic scheme and could be removed at a later stage.

Regioselective AIBN-catalyzed radical addition[4,5] of the appropriate perfluoroalkyl iodide across the terminal alkene affords 3-(iodo-semifluoroalkyl)thiophenes **2(m,n)**. Later reactions were carried out in a sealed, high-pressure reaction tube. The extent of reaction was monitored by NMR, and additional perfluoroalkyl iodide and catalyst were added when conversion leveled off (Table 2.1). The desired regioisomer is formed in excess of 95% (as determined by ^{1}H NMR) and isolated from the minor product during purification.

Reaction of **2(m,n)** with $NaBH_4$ provides 3-semifluoroalkylthiophene **3(m,n)**.[5] The reaction must be carried out in a rigorously dry environment to avoid elimination of H-I. The 3-substituted thiophenes **3(m,n)** were used as the monomer for oxidative regiorandom polymerization. Alternatively, subsequent reaction of **3(m,n)** with two equivalents of NBS at –10 °C results in **4(m,n)**,[1] which serves as the monomer for regioregular polymerization. Precise stoichiometry and low temperature (-10 ºC) avoid overbromination and formation of regioisomers, respectively.

2.3.2: Synthetic Approach to Poly(3-semifluoroalkylthiophene)s

Synthetic routes for polymerization are shown in Figure 2.3. For comparison purposes, the regiorandom polymer **Rn(Th-5,4)** was synthesized from **3(5,4)** according to literature methods for oxidative polymerization.[8] While the regioregular and

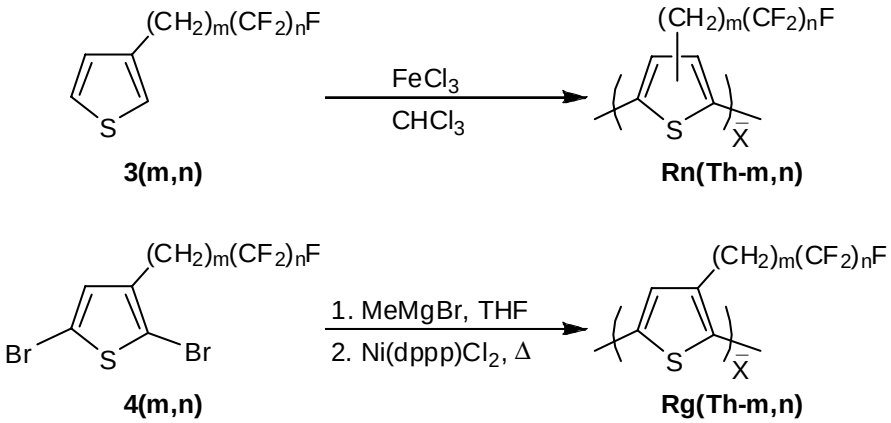

Figure 2.3. Synthesis of regiorandom (top) and regioregular (bottom) poly(3-semifluoroalkylthiophene)s.

regiorandom polymers were similar in molecular weight (Table 2.2), the regiorandom material is more soluble and higher melting than its regioregular counterpart.

Synthesis of regioregular poly(3-semifluoroalkylthiophene)s, **Rg(Th-m,n)**, was carried out by Grignard metathesis (GRIM) polymerization.[6,7] This technique, developed

Table 2.2. Polymer characterization data.

Rg(Th-m,n)	MALDI M_n	MALDI DP	MALDI PDI	GPC M_n
Rn(Th-5,4)[b]	$6.2x10^3$	17	1.13	--[d]
Rg(Th-5,4)[a]	$6.3x10^3$	17	1.27	--[d]
Rg(Th-5,6)[a]	$6.3x10^3$	13	1.12	--[d]
Rg(Th-5,8)[a]	$3.6x10^3$	6	1.12	--[d]
Rg(Th-8,3)[b]	$8.5x10^3$	23	1.36	--[d]
Rg(Th-8,4)[b]	$6.5x10^3$	16	1.30	$13.1x10^3$
Rg(Th-11,4)[c]	$5.7x10^3$	12	1.13	--
Rg(Th-11,6)[b]	$8.0x10^3$	14	1.08	--[d]
Rg(Th-11,8)[b]	$10.9x10^3$	17	1.35	--[d]
Rg(Th-8,0)[b]	$6.2x10^3$	32	1.13	$9.3x10^3$

[a] 1,2-dichlorobenzene fraction
[b] $CHCl_3$ fraction
[c] hexanes fraction
[d] unable to analyze due to insolubility at room temperature

by the McCullough group, produces highly regioregular polymers via a 'quasi-living' mechanism.[9,10] According to the literature, **4** reacts with a stoichiometric amount of Grignard reagent (e.g., RMgBr) to form primarily 2-bromo-5-bromomagnesio-3-semifluoroalkylthiophene, which then reacts with an organometallic initiator before undergoing polymerization (Figure 2.4). Complete reaction of **4** with the Grignard reagent is necessary to form high molecular weight materials.[10]

Eight semifluoroalkyl-substituted polymers, **Rg(Th-m,n)**, were synthesized. Regioregular poly(3-octylthiophene), or **Rg(Th-8,0)**, was also synthesized by GRIM for purposes of comparison. Characterization data for the polymers are summarized in Table 2.2. Early reactions produced materials with slightly lower molecular weights and yields than expected. After investigation, it was determined that the molecular weight of these polymers is limited by a number of factors. First, the extent of metallation of **4** was determined by carefully controlled NMR quenching studies, in which an aliquot of the reaction mixture was quenched with MeOH. The solvent was subsequently removed

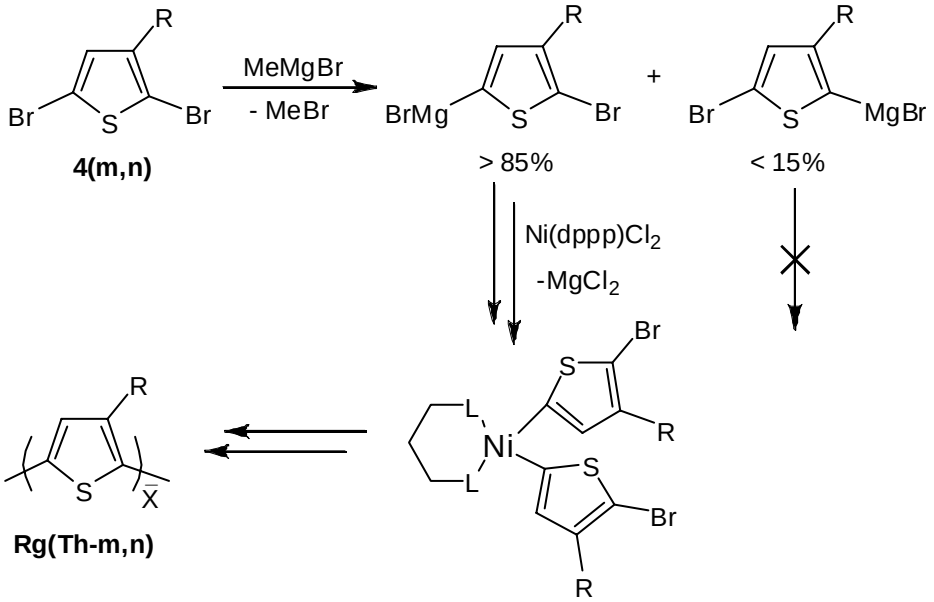

Figure 2.4. Transmetallation and initiation intermediates in Grignard metathesis (GRIM). The semifluoroalkyl side chain is abbreviated R.

from the aliquot, and the residue was characterized by ^{1}H NMR. The presence of peaks in the NMR spectra corresponding to **4** indicates incomplete metallation; this is true regardless of the concentration, reaction temperature, identity of the Grignard alkyl group, or Grignard reagent stoichiometry. The origin of this incomplete metallation is unknown, but may arise partially from the alkylation of the monomer **4** by the Grignard reagent. Evidence for this side reaction was obtained by GC-MS analysis of material that was not incorporated into the polymer chains. Additionally, the fluoroalkyl side chain segment reduces the solubility of the polymer in most organic solvents, which may result in termination of the polymerization due to aggregation. A number of **Rg(Th-m,n)** homologues formed characteristic purple precipitates during polymerization, consistent with the insolubility of high molecular weight homologues with increased fluoroalkyl content in common organic solvents, as discussed below. In an attempt to mitigate both of these factors, later GRIM procedures involved forming the Grignard intermediate at higher (approximately 1M) concentrations before polymerizing under more dilute (approximately 0.05-0.1M) conditions.

Purification of most **Rg(Th-m,n)** homologues also posed a challenge due to their limited solubility in common organic solvents. In all cases, Soxhlet extraction with methanol and hexanes removed low molecular weight material, but polymers with longer fluoroalkyl segments were resistant to solvents such as chloroform. Several homologues more readily dissolved at elevated temperatures in such solvents as 1,2-dichlorobenzene and 1,1,2,2-tetrachloroethane. In such cases, material of reasonable molecular weight was isolated by stirring in boiling solvent, hot filtering and centrifuging the solution, decanting the high-boiling solvent, and washing with methanol. Unfortunately, some high molecular weight materials with high fluoralkyl content remained intractable even under these conditions, accounting for yields of less than 10%; for example, approximately 40% of the **Rg(Th-5,8)** polymer was completely insoluble. In all cases,

the soluble fraction with the highest molecular weight was characterized.

2.3.3: Structural Characterization of Poly(3-semifluoroalkylthiophene)s

The identity, purity, and regiorgularity of all homologues were verified by NMR spectroscopy. The ^{1}H NMR spectrum of **Rg(Th-5,4)** (Figure 2.5, bottom) shows a predominant resonance for the proton on the thiophene ring and a principal triplet for the protons on C-1 of the side chain of each repeat unit. The NMR spectra of regioregular polymers each show a small, broad peak upfield of this triplet, arising from a small population of C-1 protons on the side chain of repeat units with head-to-head and tail-to-tail 'defect' arrangements.[11] Relative integration of these two C-1 signals in the spectra of each polymer indicates that homologues of **Rg(Th-m,n)** are highly regioregular. The ^{1}H NMR spectrum of **Rn(Th-5,4)** (Figure 2.5, top) shows additional 'defect' resonances in the region corresponding to the thiophene proton and a significantly larger C-1 'defect' signal. Based on analysis of NMR spectra, **Rn(Th-5,4)** is approximately 74% regioregular, whereas homologues of **Rg(Th-m,n)** are at least 90% regioregular.

Regioregularity of **Rg(Th-m,n)** was confirmed by ^{13}C NMR. The ^{13}C spectrum for **Rg(Th-5,4)** (Figure 2.6, top) shows the expected four signals in the aromatic region

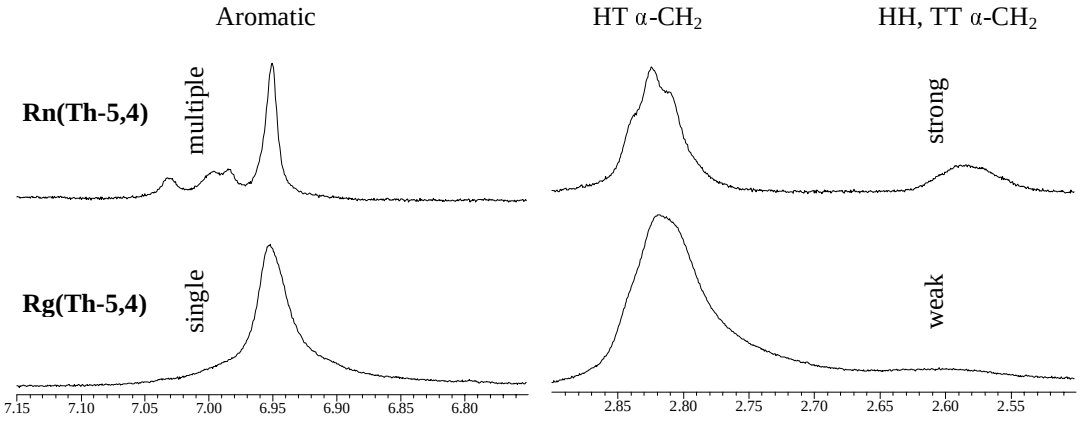

Figure 2.5. ^{1}H NMR spectra of regiorandom **Rn(Th-5,4)** (top) and regioregular **Rg(Th-5,4)** (bottom).

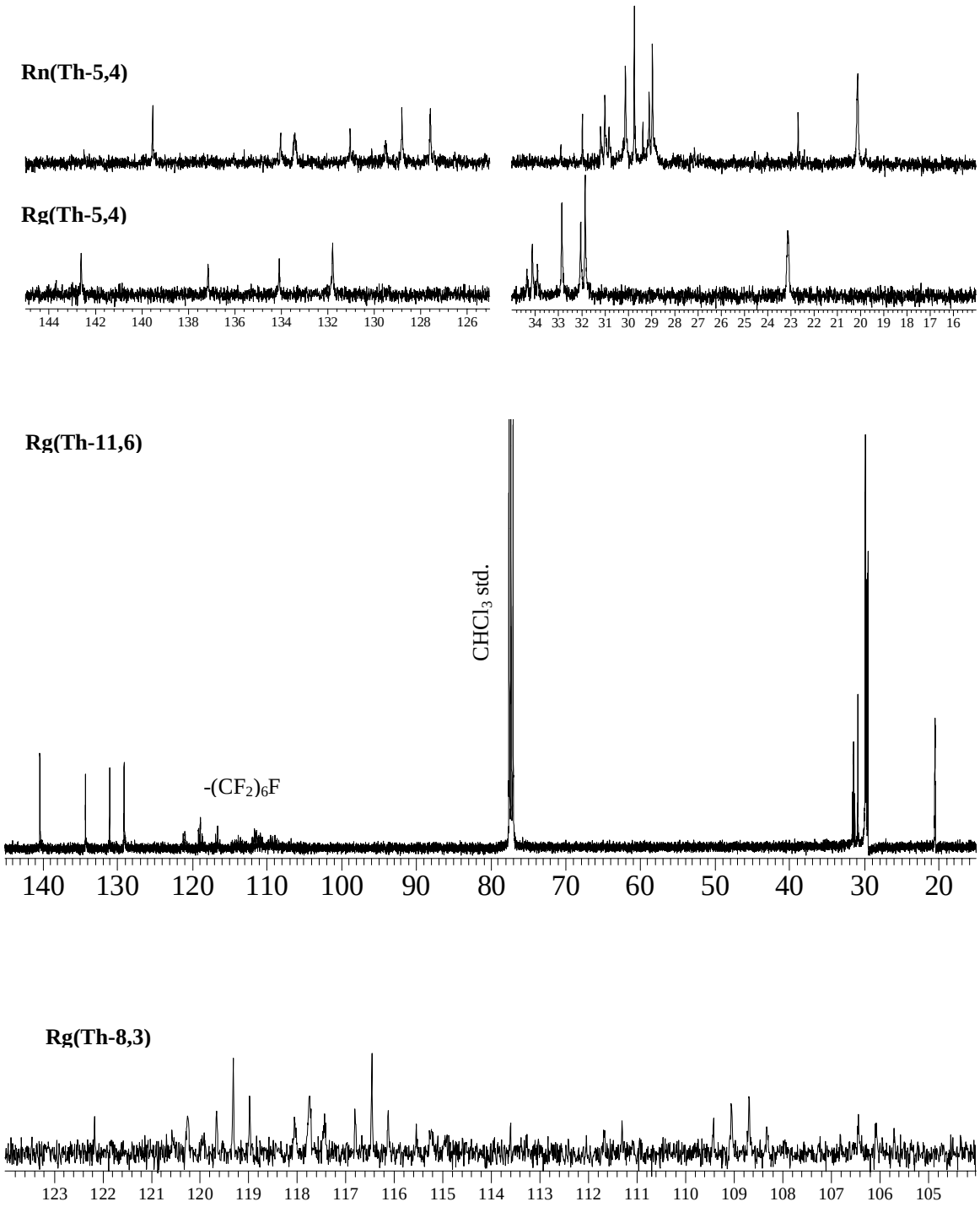

Figure 2.6. ^{13}C spectra of poly(3-semifluoroalkyl)thiophenes. Top: Regiorandom **Rn(Th-5,4)** vs. regioregular **Rg(Th-5,4)**. Center: Regioregular **Rg(Th-11,6)**. Bottom: the fluoromethylene region of the **Rg(Th-8,3)** spectrum.

and five signals in the aliphatic region, corresponding to four thiophene carbons and five side chain carbons, respectively. Regiorandom polymers display additional signals in both regions, arising from head-to-head and tail-to-tail couplings (Figure 2.6, top). The signals at 31.3 and 20.3 ppm (Figure 2.6, center) correspond to C-5 and C-4 of the side chain, respectively; each signal is split into a triplet with coupling constants (22 and 3 Hz, respectively) consistent with ^{13}C and ^{19}F two- and three- bond coupling. The resonances in the region from 105-125 ppm correspond to the fluorine-carbon coupling of the fluoromethylene carbons (Figures 2.6, center and bottom). Assignment of these peaks is precluded by the complex multiplicity caused by one-, two-, and three-bond ^{13}C-^{19}F coupling with large coupling constants (typically 285, 20, and 3 Hz, respectively); low relative signal intensity; and the overlap of signals arising from the narrow range of chemical shifts. The identity of **Rg(Th-m,n)** homologues was further confirmed by ^{19}F spectroscopy, which for the **Rg(Th-11,6)** homologue shows the expected six resonances

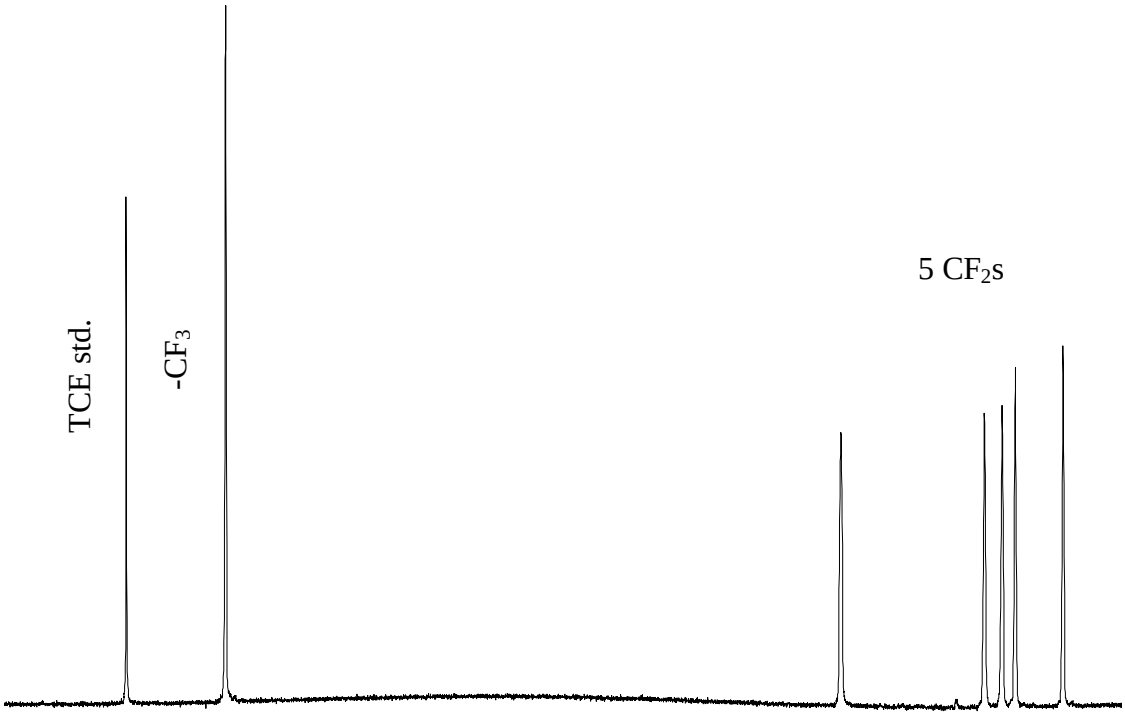

Figure 2.7. ^{19}F (right) NMR spectra of **Rg(Th-11,6)** in $CHCl_3$ at 60 ºC.

corresponding to the five CF_2s and CF_3 of the side chain (Figure 2.7).

Molecular weights and polydispersities of **Rg(Th-m,n)** homologues, obtained by MALDI-TOF MS, are shown in Table 2.2. MALDI data indicate that the polymers are of reasonable molecular weight. GPC experiments were performed where solubility allowed. The M_n values obtained by GPC are approximately 1.5-2 times higher than those obtained by MALDI. This is consistent with literature evidence that GPC overestimates the molecular weight of semi-rigid poly(3-alkylthiophene)s due to comparison with more coil-like polystyrene standards.[12] Close examination of MALDI

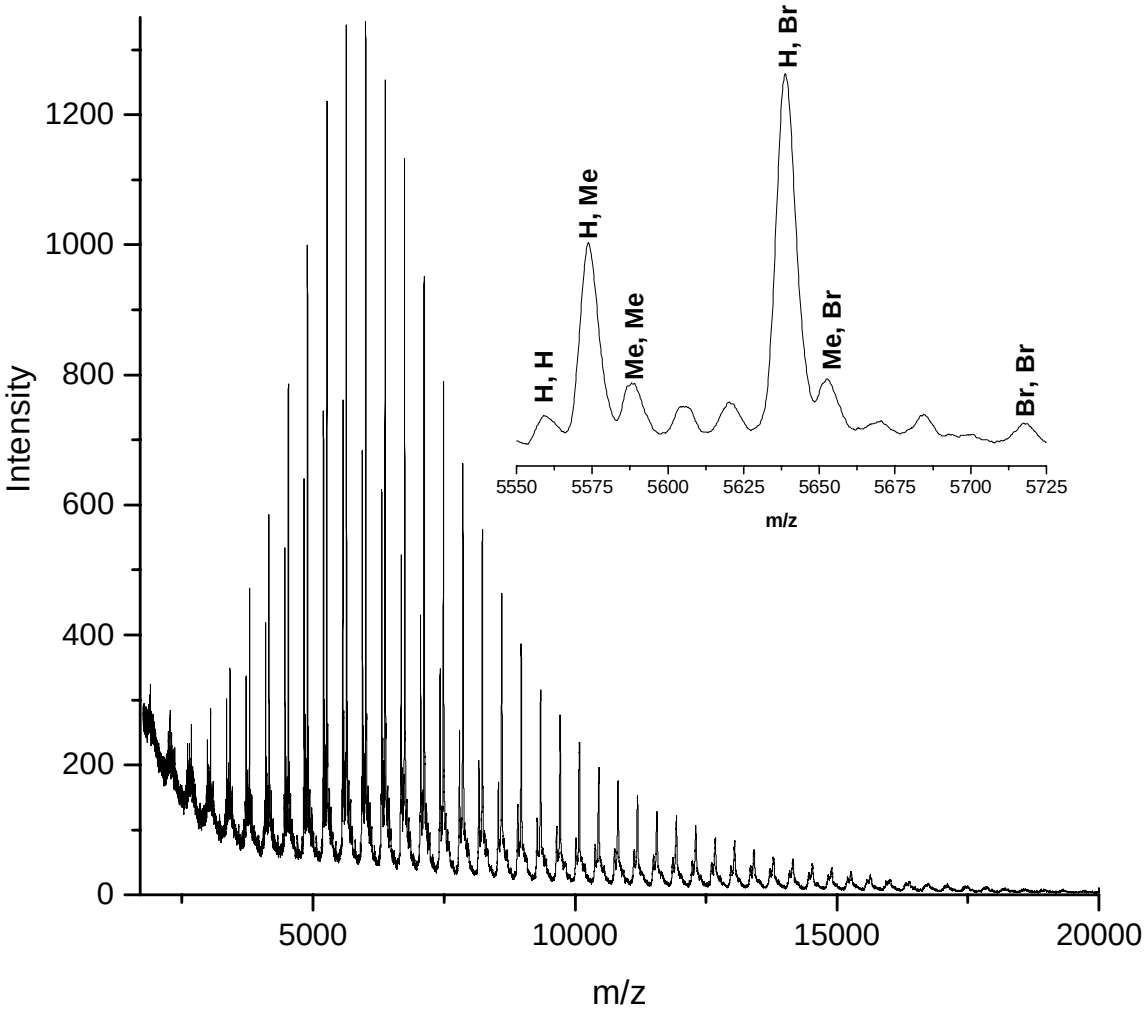

Figure 2.8. MALDI-TOF spectrum of regioregular **Rg(Th-5,4)**. **Inset:** distribution of polymer end groups in the m/z region 5550-5725.

spectra indicates the presence of a variety of H, CH_3, and Br end group combinations (Figure 2.8). Elemental analysis, in many cases, confirms the presence of Br.

2.4: Conclusions

A family of poly(3-semifluoroalkylthiophene)s **Rg(Th-m,n)** has been synthesized by GRIM polymerization. One regiorandom analogue **Rn(Th-5,4)** and one alkyl analogue **Rg(Th-8,0)** were synthesized for comparative purposes. Solubility was shown to be a limiting factor in synthesis and processing of high molecular weight materials. The materials described in Chapter 2 were characterized by optical spectroscopy, differential scanning calorimetry, variable temperature wide angle X-ray scattering, variable temperature solid-state UV-visible spectroscopy, and optical polarized microscopy, as described in Chapter 3.

2.5: References

1. Hong, X. M.; Collard, D. M. *Macromolecules* **2000**, *33*, 6916.

2. Tamao, K.; Sumitani, K.; Kiso, Y.; Zembayashi, M.; Fujioka, A.; Kodama, S.; Nakajima, I.; Minato, A.; Kumada, M. *Bull. Chem. Soc. Jpn.* **1976**, *49*, 1958.

3. Tamao, K.; Kodama, S.; Nakajima, I.; Kumada, M.; Minato, A.; Suzuki, K. *Tetrahedron* **1982**, *38*, 3347.

4. Feiring, A. E. *J. Org. Chem.* **1985**, *50*, 3269.

5. Hong, X.; Tyson, J. C.; Middlecoff, J. S.; Collard, D. M. *Macromolecules* **1999**, *32*, 4232.

6. Loewe, R. S.; Khersonsky, S. M.; McCullough, R. D. *Adv. Mater.* **1999**, *11*, 250.

7. Loewe, R. S.; Ewbank, P. C.; Liu, J.; Zhai, L.; McCullough, R. D. *Macromolecules* **2001**, *34*, 4324.

8. Sugimoto, R.; Takeda, S.; Gu, H. B.; Yoshino, K. *Chemistry Express* **1986**, *1*, 635.

9. Sheina, E. E.; Liu, J.; Iovu, M. C.; Laird, D. W.; McCullough, R. D. *Macromolecules* **2004**, *37*, 3526.

10. Iovu, M. C.; Sheina, E. E.; Gil, R. R.; McCullough, R. D. *Macromolecules* **2005**,

38, 8649.

11. McCullough, R. D. *Adv. Mater.* **1998**, *10*, 93.

12. Liu, J.; Loewe, R. S.; McCullough, R. D. *Macromolecules* **1999**, *32*, 5777.

CHAPTER 3: CHARACTERIZATION OF SEMIFLUOROALKYL-SUBSTITUTED POLYTHIOPHENES

3.1: Introduction

This chapter focuses on the characterization of the semifluoroalkyl-substituted polymers **Rg(Th-m,n)** whose synthesis is described in Chapter 2. A variety of techniques, including solution-state absorption and fluorescence spectroscopy, differential scanning calorimetry (DSC), variable temperature wide-angle X-ray scattering (WAXS), variable temperature solid-state UV-visible spectroscopy, and optical polarized microscopy (OPM) were used to investigate structure-property relationships and to determine the effect of overall side chain length and m:n side chain block ratios on liquid crystallinity.

3.2: Experimental

Solution-state absorption and fluorescence spectra were obtained on a Shimadzu UV-2401PC and RF-5301 spectrometer and fluorimeter, respectively. Differential scanning calorimetry experiments were carried out on a Mettler 822e instrument with heating and cooling rates of 10 ºC/min and a first heating/cooling cycle to erase any thermal history. Variable-temperature polarized optical microscopy was performed by heating a solvent-cast sample between glass slides on a Linkam THM600 temperature control stage. Micrographs were obtained using a Leica DMRX polarized microscope and analyzed with Image Pro Plus software (version 4.5.1.22). Variable temperature wide-angle X-ray scattering experiments were performed on a Rigaku instrument with MicroMax 002 X-ray generator (Cu K_α source) and R-axis IV++ detector system. Variable temperature solid-state absorption spectra were recorded on a Shimadzu UV-3103PC.

3.3: Results and Discussion

3.3.1: Solution-state Characterization of Poly(3-semifluoroalkylthiophene)s

The effect of side chains on conjugation was determined, where solubility allowed, by solution-state UV-visible and fluorescence spectroscopy; λ_{max} values for these materials are shown in Table 3.1. These homologues absorb and emit at similar wavelengths to regioregular poly(3-octylthiophene) **Rg(Th-8,0)**. Like poly(3-alkylthiophene)s, all **Rg(Th-m,n)** homologues are characteristically dark purple in the

Table 3.1. Optical and thermotropic data.

Rg(Th-m,n)	Solution $\lambda_{max, abs}$ (nm)	Solution $\lambda_{max, em}$ (nm)	Thermal transitions[a]	Transition temp. (°C)[b]	Liquid crystalline?
Rn(Th-5,4)[d]	--[f]	--[f]	0[g]	--[g]	No
Rg(Th-5,4)[c]	--[f]	--[f]	2	165-174, 180-196	Yes
Rg(Th-5,6)[c]	--[f]	--[f]	1	174-196	No
Rg(Th-5,8)[c]	--[f]	--[f]	2	185-202, 206-223	Yes
Rg(Th-8,3)[d]	444	564	2	112-122, 123-141	No
Rg(Th-8,4)[d]	--[f]	--[f]	1	104-123	No
Rg(Th-11,4)[e]	435	557	1	70-100	No
Rg(Th-11,6)[d]	--[f]	--[f]	2	103-123, 163-178	Yes
Rg(Th-11,8)[d]	--[f]	--f	1	145-161	No
Rg(Th-8,0)[d]	448	567	2	180-192 196-202	No

[a] single heating scan
[b] temperature range of broad transitions for DSCs shown in Appendix D
[c] 1,2-dichlorobenzene fraction
[d] $CHCl_3$ fraction
[e] hexanes fraction
[f] unable to analyze due to insolubility at room temperature
[g] no evidence of melting below 275 °C

solid state and orange in solution. This evidence confirms that the $(CH_2)_m$ spacer between the backbone and the $(CF_2)_nF$ segment insulates the backbone from the electron-withdrawing effects of the fluoroalkyl group.

3.3.2: Characterization of Solid-state Polymer Properties

The thermal properties of **Rg(Th-m,n)** homologues were evaluated by differential scanning calorimetry (DSC). Each sample was heated and cooled to erase any thermal history before being subjected to repeated heating and cooling cycles; hence, the thermograms corresponding to first cycles are often anomalous. Three of the eight homologues exhibit a single melting endotherm upon heating and a corresponding slightly supercooled crystallization exotherm upon cooling (Table 3.1, thermograms in Appendix D). For example, the thermogram for **Rg(Th-11,4)** shows a single endotherm upon heating, corresponding to a semicrystalline-isotropic transition (Figure 3.1). A single exotherm is seen upon cooling, corresponding to the isotropic-semicrystalline transition. The same behavior is demonstrated by **Rg(Th-8,4)** and **Rg(Th-11,8)** (Appendix D, Figures D.1 and D.6).

Two homologues, **Rg(Th-5,4)** and **Rg(Th-11,6)**, display multiple transitions upon heating and cooling (Table 3.2). For example, the thermogram for **Rg(Th-11,6)** (Figure 3.2) shows two endotherms upon heating, which correspond to semicrystalline-liquid crystalline and liquid crystalline-isotropic transitions. This thermogram displays two

Table 3.2. Thermal transitions for liquid crystalline homologues of **Rg(Th-m,n)**.

	Heating		**Cooling**	
Rg(Th-m,n)	$T_{SC\rightarrow LC}$ (ºC)	$T_{LC\rightarrow I}$ (ºC)	$T_{I\rightarrow LC}$ (ºC)	$T_{LC\rightarrow SC}$ (ºC)
Rg(Th-5,4)	165 – 174	180 – 196	153 – 165	
Rg(Th-5,8)	185 – 202	206 – 223	184 – 197	
Rg(Th-11,6)	103 – 123	163 – 178	92 – 124	137 – 149

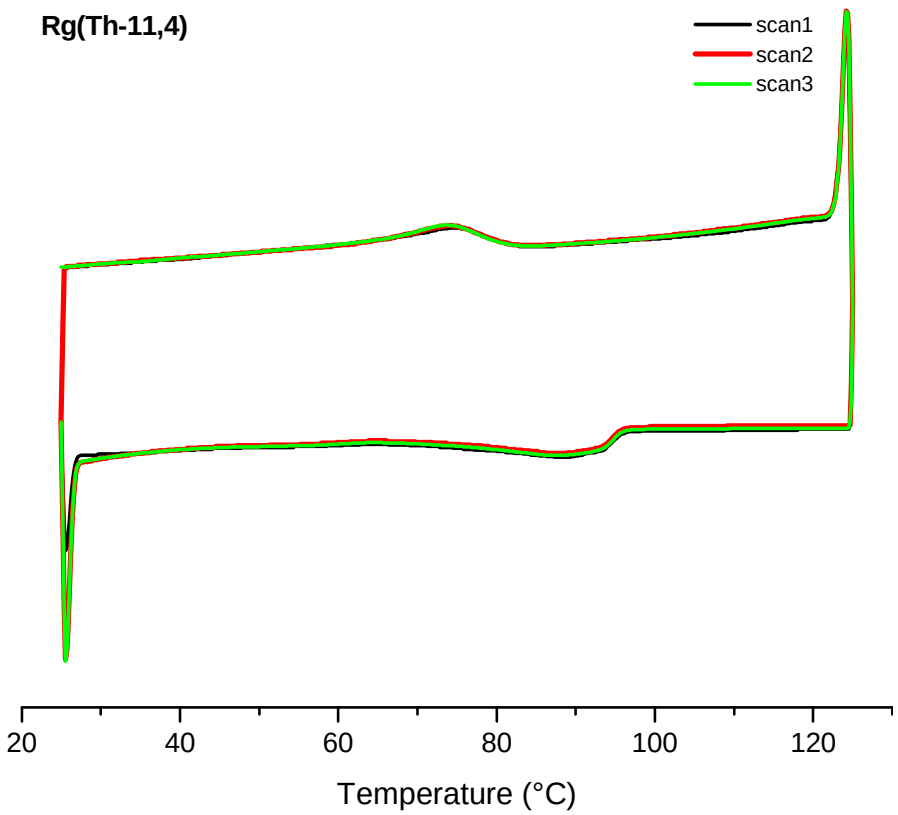

Figure 3.1. DSC thermogram of regioregular **Rg(Th-11,4)** (heating and cooling at 10 ºC/min).

exotherms upon cooling, consistent with slightly supercooled isotropic to liquid crystalline (I→LC) and liquid crystalline to semicrystalline (LC→SC) transitions. The thermogram of **Rg(Th-5,4)** (Appendix D, Figure D.2) also exhibits two endotherms upon heating, but the transitions occur over a small temperature range. Cooling this homologue resulted in a single, relatively sharp exotherm equal in area to the sum of the two heating endotherms, indicating a single, supercooled crystallization transition. Both of these homologues are orange and fluid to the naked eye at mesophase temperatures when compressed between glass slides on a hot plate.

The two endotherms of **Rg(Th-5,8)** (Appendix D, Figure D.4) are relatively weak and broad compared to the **Rg(Th-5,4)** and **Rg(Th-11,6)** counterparts. However, this

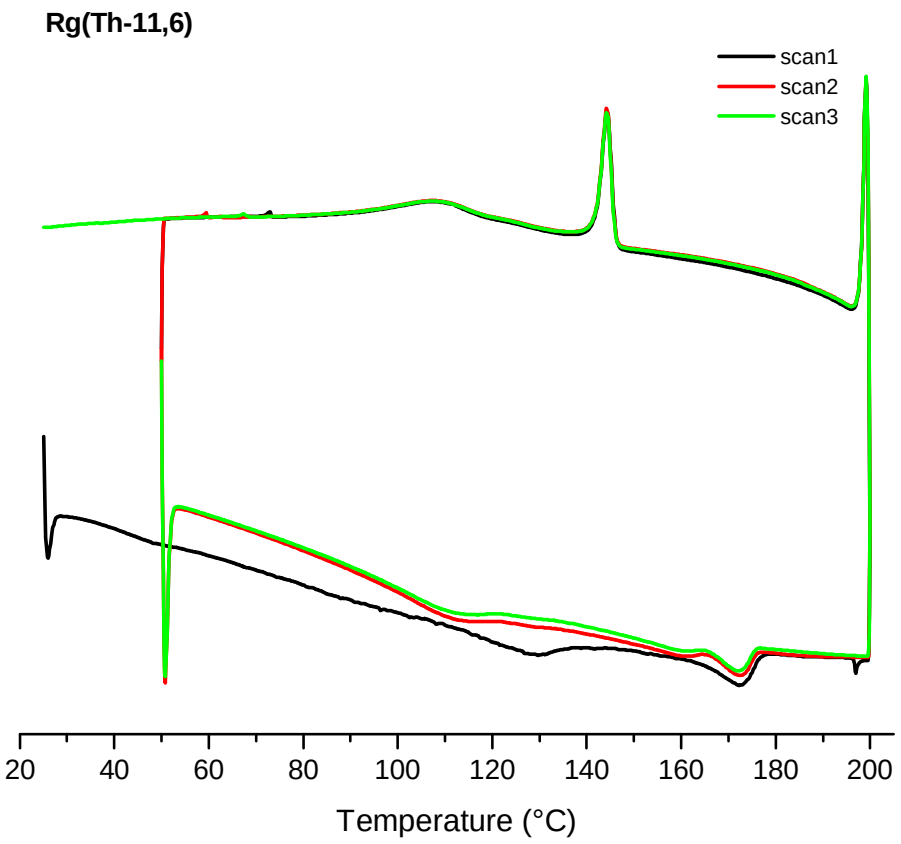

Figure 3.2. DSC thermogram of regioregular **Rg(Th-11,6)** (heating and cooling at 10 ºC/min). First scan is anomalous.

material is orange and fluid to the naked eye when compressed between glass slides on a hot plate and held at mesophase temperatures (beginning at approximately 185 ºC), suggesting that **Rg(Th-5,8)** is also liquid crystalline.

The **Rg(Th-8,3)** homologue and the **Rg(Th-8,0)** reference polymer each exhibit two endotherms upon heating and a single, slightly supercooled exotherm upon cooling (Appendix D, Figures D.3 and D.7), yet they are not believed to be liquid crystalline. Unlike its liquid crystalline counterparts, **Rg(Th-8,3)** is a purple, non-flowing solid over the temperature range corresponding to the first thermal transition (112-122 °C) and does not become orange and fluid to the naked eye (when compressed between glass slides on

a hot plate) until it reaches 127-140 °C, which corresponds to the second temperature range. Thus, it is likely that the first transition can be attributed to a solid-solid reorganization transition, rather than to a semicrystalline-liquid crystalline transition. **Rg(Th-8,0)** demonstrates similar phenomena, remaining a purple, non-flowing solid until the second thermal transition temperature range (196-202 °C) is reached.

While the first two heating segments for **Rg(Th-5,6)** (Appendix D, Figure D.3) display two endotherms, the third scan exhibits only one endotherm (at a temperature similar to the first transition seen during the first two cycles). The lack of a higher-temperature transition in the third scan may indicate that two scans were required to completely erase thermal history. Based on the data obtained, it is believed that **Rg(Th-5,6)** is not liquid crystalline.

The X-ray diffractogram of **Rg(Th-11,6)** (Figure 3.2) at 90 ºC shows sharp signals at d = 19.0 Å, 12.83 Å, and 7.70 Å (2θ = 4.54º, 6.77º, and 11.3º), which is consistent with the (200), (300), and (500) Bragg reflections of a lamellar architecture with an interlayer spacing of approximately 38 Å (Figure 3.3). The signals at 4.87 Å and 2.32 Å (18.2º and 38.7º) may be assigned to relatively disordered packing of the alkyl portion of the side chain. The shoulder corresponding to 5.4 Å (16.5º) can be attributed to packing of the fluoroalkyl side chain segments.[1] The reflection at 3.79 Å (23.5º) is ascribed in literature to π-stacking.[2-6] The diffractogram is consistent with the three-dimensional organization previously described for poly(3-alkylthiophene)s.[2,5,6]

The effect of temperature on the microstructure in each of these liquid crystalline homologues was determined by variable temperature wide-angle X-ray scattering on powder samples. Thermal history was erased by heating above the clearing temperature and allowing to cool to room temperature. Diffractograms were obtained at temperatures corresponding to the three phases described above. The diffractograms for **Rg(Th-11,6)**

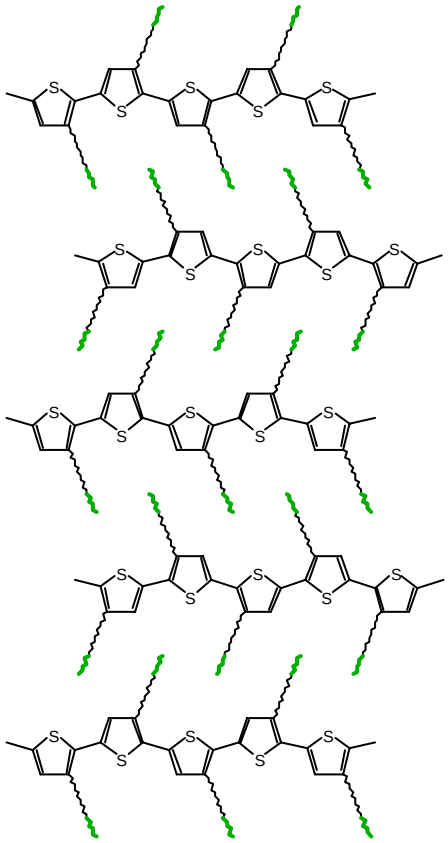

Figure 3.3. Interdigitated lamellar architecture for **Rg(Th-11,6)** consistent with X-ray diffraction data. Fluoroalkyl segments are shown in bold.

(Figure 3.4, *d*-spacings given in Table 3.3) demonstrate that a significant degree of order, characteristic of semicrystalline poly(3-substituted thiophene)s,[2-6] is present at 90 ºC, below the first thermal transition. This order is largely retained in the liquid crystalline mesophase at 140 ºC, but it diminishes substantially in the melt at 210 ºC. The loss of

Table 3.3. Polymer **Rg(Th-11,6)** *d*-spacing as a function of temperature.

Temperature (ºC)	*d*-spacing (Å)					
90	2.32	3.79	4.87	7.82	13.06	19.46
140	2.32	3.79	5.24	7.87	13.25	19.64
210	2.30	--	7.72	7.72	12.96	18.52

order is particularly noticeable in the 3.8 Å (23.4º) region. The lamellar spacing increases from 19.46 Å (4.54º) in the semicrystalline phase to 19.64 Å (4.50º) in the liquid crystalline mesophase and decreases to 18.52 Å (4.77º) in the isotropic phase.

Thermochromism of poly(3-alkylthiophene)s has previously been ascribed to melting transitions,[7] and the appearance of isosbestic points in these spectra have been attributed to the existence of an equilibrium between two distinct polymer backbone conformations.[8,9] Thermochromism of solvent cast films of **Rg(Th-5,4)** was examined by variable-temperature UV-visible spectroscopy. As expected, the absorption maximum, λ_{max}, of the film decreases from 510 to 487 nm upon heating. This change is reversed upon subsequent cooling (Figure 3.5). The decrease in λ_{max} upon heating represents a reduction of conjugation length associated with SC→LC and LC→I transitions. Two isosbestic points appear in the spectra, at 485 and 457 nm (Figure 3.5).

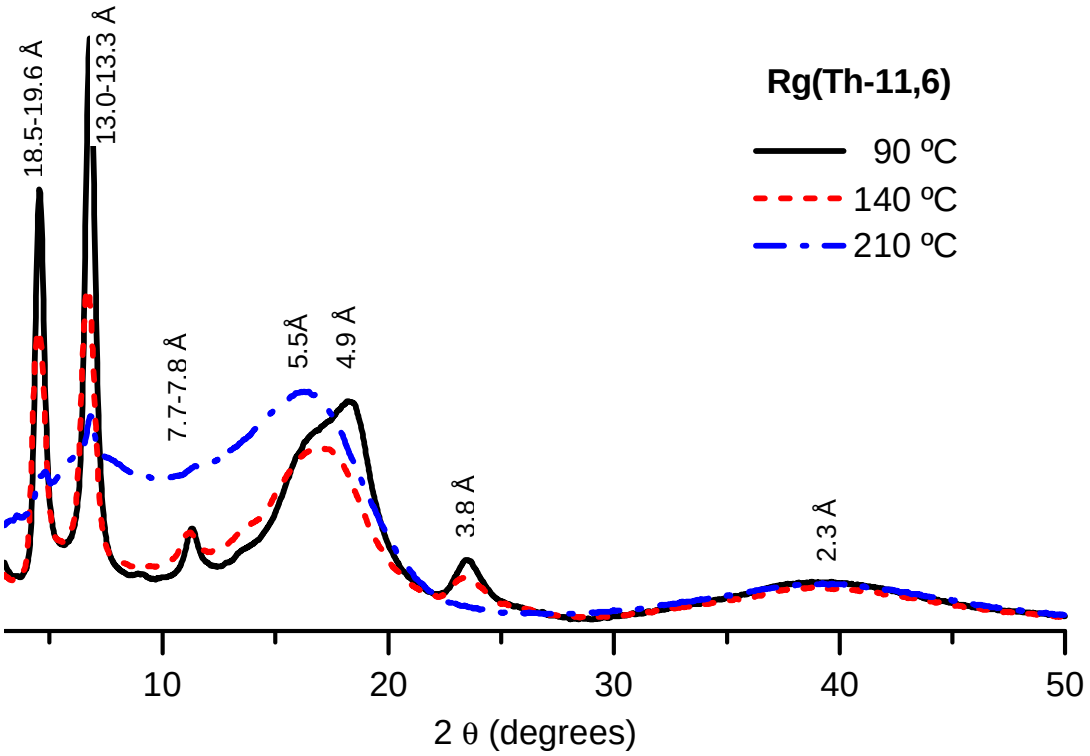

Figure 3.4. Wide-angle X-ray diffractogram of **Rg(Th-11,6)** powder, heating from 90 ºC to 210 °C.

The isosbestic points at 485 nm and 457 nm, respectively, are defined by the spectra obtained between 61-175 ºC and between 194-245 ºC. The two temperature ranges are consistent with the phase transitions seen by DSC, confirming the temperature-dependent equilibrium between phases.

Polarized optical microscopy provides further evidence for liquid crystallinity. Micrographs of **Rg(Th-11,6)** (Figure 3.6) exhibit birefringence from 40-165 ºC. The birefringence decreases gradually between 130-165 ºC and disappears entirely between 170-176 ºC, confirming that **Rg(Th-11,6)** is ordered in the two lower temperture ranges (crystalline phase and mesophase), but not in the isotropic phase. These transitions are also consistent with the DSC transitions described above.

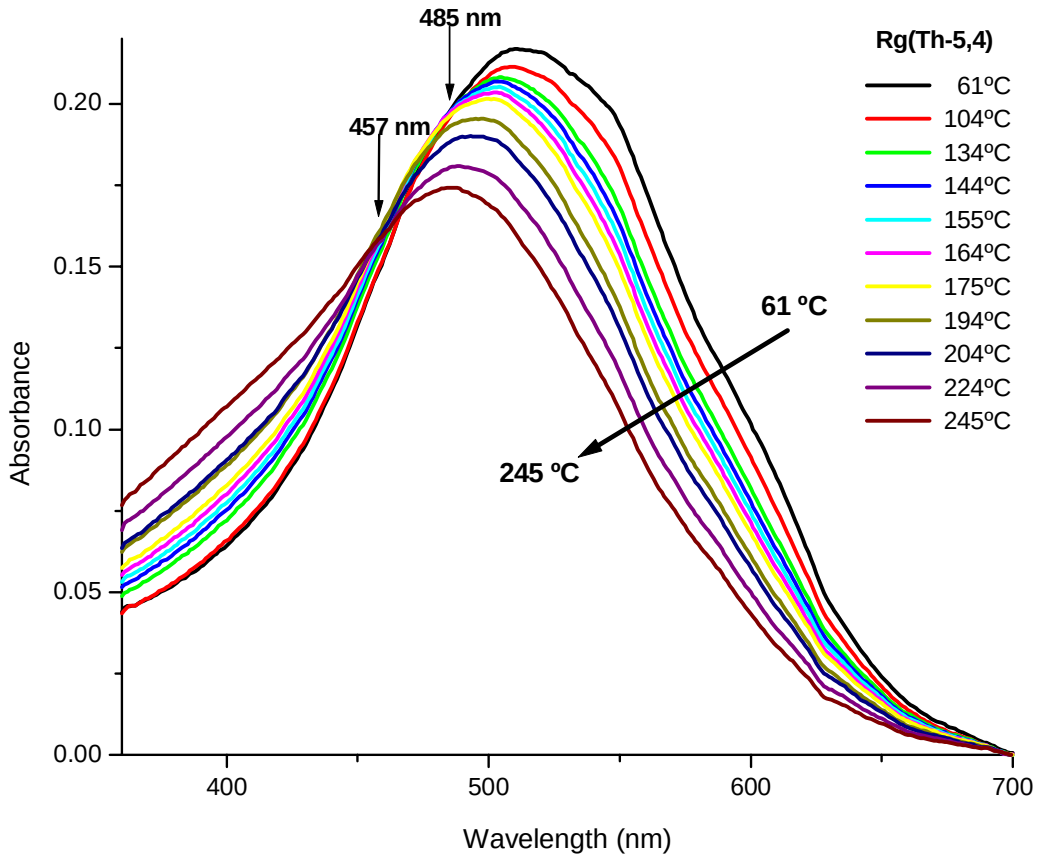

Figure 3.5. UV-visible spectra of a **Rg(Th-5,4)** thin film, cooling from 245 ºC to 61 ºC.

3.4: Conclusions

The semifluorinated **Rg(Th-m,n)** homologues synthesized in Chapter 2 exhibit optical properties similar to those of their alkyl-substituted counterparts. Of the homologues prepared, only **Rg(Th-5,4)**, **Rg(Th-5,8)**, and **Rg(Th-11,6)** display liquid crystallinity. However, there is no simple correlation between thermotropic behavior and side chain length or m:n block ratio. One possible reason for this result could be the variation in molecular weight between various **Rg(Th-m,n)** homologues.

This body of evidence demonstrates that **Rg(Th-5,4)**, **Rg(Th-5,8)**, and **Rg(Th-11,6)** are liquid crystalline materials, each with an ordered, fluid mesophase between semicrystalline and isotropic phases. While conjugation length decreases during the

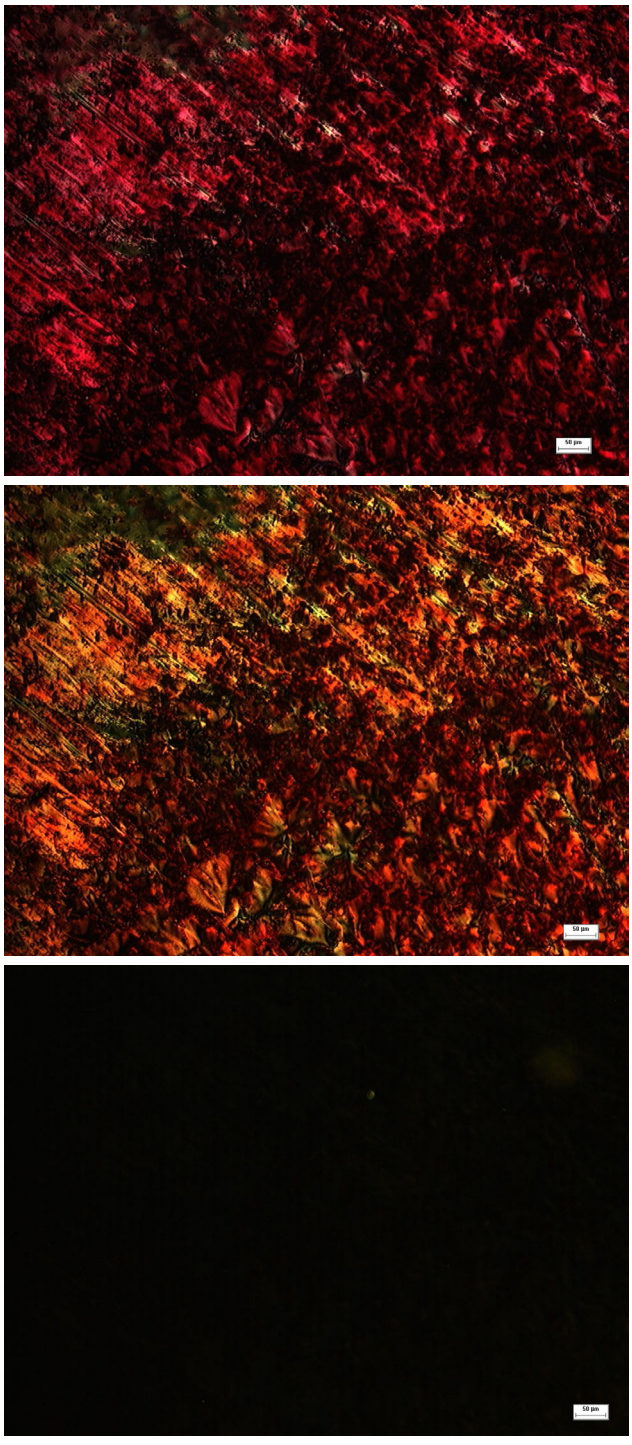

Figure 3.6. Polarized optical micrographs of a **Rg(Th-11,6)** thin film, at 40 ºC (top), 140 ºC (middle), and 176 ºC (bottom). Scale bar corresponds to 50 μm.

formation of the liquid crystalline phase, X-ray scattering confirms that this fluid, thermotropic mesophase is still significantly ordered.

3.5: References

1. Fujiwara, M.; Satoh, K.; Konda, S.; Ujiie, S. *Macromolecules* **2006**, *39*, 5836.

2. McCullough, R. D.; Tristram-Nagle, S.; Williams, S. P.; Lowe, R. D.; Jayaraman, M. *J. Amer. Chem. Soc.* **1993**, *115*, 4910.

3. McCullough, R. D.; Belot, J. A.; Williams, S. P. *NATO ASI Series, Series C: Mathematical and Physical Sciences* **1995**, *456*, 349.

4. McCullough, R. D.; Williams, S. P.; Tristram-Nagle, S.; Jayaraman, M.; Ewbank, P. C.; Miller, L. *Synth. Met.* **1995**, *69*.

5. Prosa, T. J.; Winokur, M. J.; McCullough, R. D. *Macromolecules* **1996**, *29*, 3654.

6. Skotheim, T. A.; Elsenbaumer, R. L.; Reynolds, J. R.; Editors *Handbook of Conducting Polymers, Second Edition, Revised and Expanded*; Marcel Dekker: New York, N. Y., **1997**.

7. Faied, K.; Frechette, M.; Ranger, M.; Mazerolle, L.; Levesque, I.; Leclerc, M.; Chen, T.-A.; Rieke, R. D. *Chem. Mater.* **1995**, *7*, 1390.

8. Gallazzi, M. C.; Toscano, F.; Montoneri, E. *J. Mater. Sci. Lett.* **1999**, *18*, 971.

9. Hong, X. M.; Collard, D. M. *Macromolecules* **2000**, *33*, 6916.

CHAPTER 4: SYNTHESIS AND CHARACTERIZATION OF COFACIAL 1,8-BIS(OLIGOTHIOPHENE)-SUBSTITUTED NAPHTHALENES AS MODELS FOR INTERCHAIN CHARGE TRANSFER

4.1: Background

As discussed in Chapter 1, characterization of the redox states of two-dimensional conjugated systems might be an approach to develop a greater understanding of the nature of charge carriers in conjugated polymer films. A number of reports have discussed models for charge transport involving discrete, two-dimensional oligomeric systems covalently linked by rigid or flexible units (see Section 1.4). One such system, designed by Nakayama, is based on 1,8-disubstituted naphthalene 'cores' and various short α-oligothiophene 'arms'.[1-4]

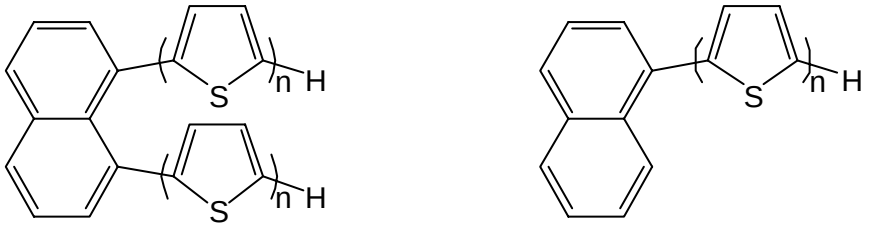

Figure 4.1. Hydrogen terminated oligomers synthesized by Nakayama: cofacial bis (oligomers) (left) and mono(oligomers) (right).

Nakayama examined a series of 1,8-bis(oligothienyl)naphthalenes (Figure 4.1, left) and 1-(oligothienyl)naphthalene analogues (Figure 4.1, right) with hydrogen-terminated 'arms' ranging in length from one to four thiophene units.[1-3] Nakayama refers to the former systems as 'stacked' and 'cofacial'. NMR spectra indicate that free rotation occurs around the naphthalene-thiophene bond in solution. It is posited that the preferred conformation of the molecules involves the thiophene rings being cofacial to each other. The X-ray crystal structure of the bis(dithienyl)-substituted compound shows the planes

of the inner thiophene ring to be twisted by 57º from the plane of the naphthalene ring. The torsion angles (16-28º) between the inner and outer thiophene rings indicate that the oligomeric arms are not entirely planar.

Nakayama demonstrated the effects of conjugation length and π-stacking through a series of spectroscopic and electrochemical measurements.[1,2] Cyclic voltammetry experiments confirmed the expected decrease in oxidation potential for the longer oligomeric arms, consistent with an enhanced ability to stabilize charge. The oxidation potentials of the bis-substituted naphthalenes were lower than those of the corresponding mono-substituted naphthalenes, indicating that the resulting radical cation is stabilized through π-interactions with the thiophene ring on the adjacent oligomer. UV-vis spectra of the di-substituted naphthalenes exhibit a red-shift in λ_{max} as the oligomeric arm increases in length, which is consistent with the stabilization of the excited state due to delocalization along the oligomer.

However, the cyclic voltammetry experiments also revealed a significant limitation of these molecules.[1,2] Because the oligomers are terminated with hydrogen atoms, the oxidized form is unstable towards arene-arene coupling. Consequently, each molecule undergoes only a single oxidation before undergoing irreversible oxidative polymerization. A number of structural variations with additional substituents were claimed in a patent,[3] but no indication exists that these functionalities render the oligomers stable to oxidation.

Nakayama later extended the disubstituted naphthalene system to include multi-stacked compounds (Figure 4.2).[4] These materials exhibit solid-state packing, optical transitions, electrochemical behavior, and oxidative polymerization similar to the molecules described above. Iyoda examined a multi-stacked variation on this system (Figure 4.3), again with similar optical transitions, electrochemical behavior, and oxidative polymerization.[5] In all cases, the presence of an adjacent conjugated oligomer

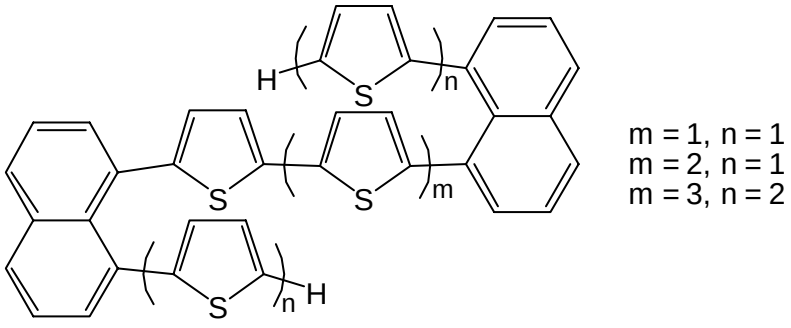

Figure 4.2. Hydrogen-terminated multi-stacked oligomers examined by Nakayama.

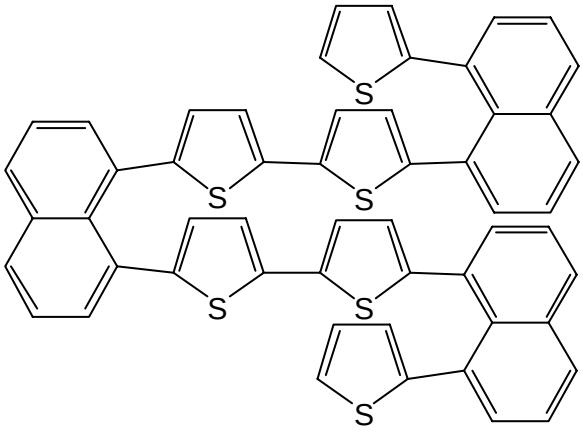

Figure 4.3. Hydrogen terminated multi-stacked system examined by Iyoda.

was found to increase the stabilization of oxidized states compared to mono-substituted counterparts.

While the systems described by Nakayama and Iyoda exhibit a number of intriguing properties, the charged states of these molecules are unstable and therefore unsuitable as models for charge carriers in conjugated polymers. Accordingly, we set out to stabilize the oxidized states against oxidative polymerization by installation of methyl groups at the two α-termini of the 1,8-bis(oligothienyl)naphthalenes examined by Nakayama (Figure 4.4). The effect of methylation on oxidative properties and stability is discussed below.

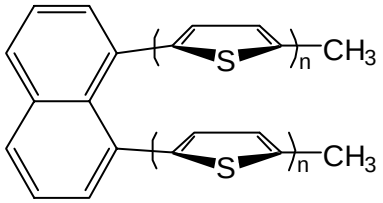

n = 1: **N-(ThMe)$_2$**
n = 2: **N-(Th$_2$Me)$_2$**
n = 3: **N-(Th$_3$Me)$_2$**

Figure 4.4. Structure of methyl-terminated 1,8-bis(oligothienyl)naphthalenes.

4.2: Experimental

General Methods. Et_2O and THF were purified by distillation from sodium or potassium benzophenone ketyl. All reagents were used as received from Fisher, VWR, or Aldrich. Organometallic cross-coupling reactions were carried out with anhydrous solvents under N_2 atmosphere using standard Schlenk techniques. Column chromatography was performed using silica gel (60 Å, 230 x 400 mesh, Sorbent Technologies). Room temperature ^{1}H NMR spectra were recorded on a Varian Mercury Vx 300 MHz instrument using $CDCl_3$ as a solvent. ^{13}C NMR spectra were obtained at 75.5 MHz. Variable temperature ^{1}H and ^{13}C NMR spectra were obtained on a Bruker AMX400 instrument at 400 MHz and 100 MHz, respectively, using $CDCl_3$. Two-dimensional and NOE NMR spectra were recorded on a Bruker DRX500 instrument at 500 MHz and 125 MHz, respectively, using $CDCl_3$. Chemical shifts for ^{1}H and ^{13}C spectra are reported relative to the corresponding residual nuclei in deuterated solvents. Infrared spectra were recorded on a Thermo Electron Nicolet 4700 FTIR as neat solids or liquids. Elemental analyses were performed by Atlantic Microlabs (Norcross, GA). GC-MS spectra and HRMS data were recorded on a Hewlett-Packard 5890 GC coupled to a VG 70SE EI spectrometer with split (100/1 split ratio) injections. Cyclic voltammetry experiments were performed on a BAS100B electrochemical analyzer at a scan rate of 100 mV/s, using 2-6 mM analyte and 0.1 M *n*-Bu_4NPF_6 electrolyte in CH_2Cl_2, an Au working electrode, a Pt auxiliary electrode, and an Ag/Ag^+ reference electrode.

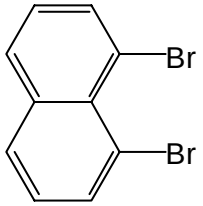

1,8-Dibromonaphthalene N-(Br)$_2$, 1. $NaNO_2$ (66.41 g, 962.5 mmol) was carefully dissolved in concentrated H_2SO_4 (500 mL) in a 4 L beaker equipped with overhead stirrer. The solution was cooled to 0 ºC, and a solution of 1,8-diaminonaphthalene (50.06 g, 316.4 mmol) in AcOH (1 L) was added dropwise over 2.75 h. After stirring for 1 h, a solution of CuBr (146.84 g, 1.0236 mol) in HBr (425 mL) was added over 1 h. The solution was allowed to warm to room temperature, stirred at 40-50 ºC for 20 h, and allowed to cool to room temperature. CH_2Cl_2 (800 mL) and H_2O (500 mL) were added, and the mixture was filtered to remove a black, insoluble material. The organic and aqueous layers were separated, and the aqueous layer was washed with CH_2Cl_2 (2 x 100 mL). The combined organic layers were washed with 5% aqueous $NaHCO_3$ (2 x 500 mL) and dried over Na_2SO_4. The solvent was removed on a rotary evaporator. The residue was recrystallized from hexanes followed by EtOH. Column chromatography (silica gel, 3:1 hexanes:$CHCl_3$) afforded **1** as a white powder (18.9 g, 21%), mp 107.5-109.5 ºC. ^{1}H NMR (300 MHz, $CDCl_3$): 7.25 (dd, J = 8.1, 7.5 Hz, 2H, H-3 and H-6), 7.80 (dd, J = 8.1, 1.2 Hz, 2H, H-2 and H-7), 7.92 (dd, J = 7.5, 1.5 Hz, 2H, H-4 and H-5). ^{13}C NMR (75 MHz, $CDCl_3$): δ 119.6 (C-1 and C-8), 126.4 (C-3 and C-6), 130.0 (C-9), 129.6 (C-4 and C-5), 135.4 (C-2 and C-7), 137.1 (C-10). IR (powder): 3055 (w), 1594, 1542, 1352, 1185 (s), 1138, 847, 806, 743 cm^{-1}. HRMS (EI) calculated for $C_{10}H_6Br_2$: 283.88362. Observed 283.88304 (Δ = 2.1 ppm). Elem. anal. calculated for $C_{10}H_6Br_2$: C 42.00% H 2.11% Br 55.88%. Observed: C 42.22% H 2.19% Br 55.59%.

1,8-Bis(2-thienyl)naphthalene, N-(Th)$_2$, 2. Using Schlenk techniques, a solution of 2-bromothiophene (28.5 mL, 48.5 g, 297 mmol) in anhydrous Et_2O (125 mL) was

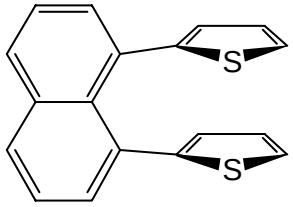

added slowly to Mg° turnings (10.82 g, 423.0 mmol) and anhydrous Et_2O (125 mL) in a 500 mL 3-neck round-bottomed flask at a rate that initiated Grignard formation and sustained gentle reflux. After the addition was complete, the mixture was heated at reflux for 2 h. The resulting Grignard reagent was transferred via cannular to an addition funnel and added slowly to a solution of 1,8-bisbromonaphthalene (14.15 g, 68.32 mmol) and Ni(dppp)Cl_2 (482.7 mg, 890.5 μmol) in anhydrous Et_2O (125 mL) in a 1 L round-bottomed flask under an N_2 atmosphere. The solution was stirred at reflux for 16 h, allowed to cool to room temperature, and poured into ice water (300 mL). The aqueous and organic layers were separated, and the aqueous layer was extracted with Et_2O (3 x 300 mL). The combined organic layers were dried over $MgSO_4$, and the solvent was removed on a rotary evaporator. Preliminary fractionation by column chromatography (silica/hexanes) afforded impure product and a mixture of mono-substituted, bis-substituted, and unreacted material. This latter mixture was subjected to re-reaction under conditions similar to those described above (Grignard reagent prepared from 15.39 mL 2-bromothiophene and 5.85 g Mg° was added to 13.88 g of isolated mixture and 0.392 g Ni(dppp)Cl_2). The crude residue from the second reaction was combined with the crystals isolated previously by column chromatography and isolated by filtration. Recrystallization from hexanes, followed by column chromatography (silica/hexanes) afforded **2** as a waxy, pale yellow solid (4.65 g, 32.4%), mp 104-105 °C. ^{1}H NMR (300 MHz, $CDCl_3$): 6.49 (dd, *J* = 3.6, 1.5 Hz, 2H, H-3'), 6.65 (dd, *J* = 5.1, 3.6 Hz, 2H, H-4'), 7.04 (dd, *J* = 5.1, 1.5 Hz, 2H, H-5'), 7.53 (dd, *J* = 8.1, 6.9 Hz, 2H, H-3 and H-6), 7.61 (dd, *J* = 6.9, 1.8 Hz, 2H, H-2 and H-7), 7.93 (dd, *J* = 8.1, 1.8 Hz, 2H, H-4 and H-5). ^{13}C

NMR (75 MHz, $CDCl_3$): δ 123.9 (2C), 125.1 (2C), 126.7 (2C), 127.6 (2C), 129.2 (2C), 130.5 (2C), 132.3 (2C), 132.5 (2C), 135.4 (2C), 144.2 (2C). IR (powder): 3080 (w), 1591, 1428, 1367, 1265, 1167, 1043, 842, 820, 686 cm^{-1}. HRMS (EI) calculated for $C_{18}H_{12}S_2$: 292.03804. Observed 292.03763 (Δ = 1.4 ppm). Elem. anal. calculated for $C_{18}H_{12}S_2$: C 73.93% H 4.14% S 21.93%. Observed: C 74.08% H 4.10% S 21.83%.

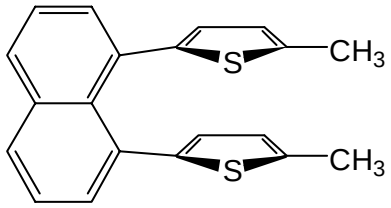

1,8-Bis(5-methyl-2-thienyl)naphthalene, N-(ThMe)$_2$, 3. *n*-Butyllithium (24.6 mL of a 2.5 M solution in hexanes, 61.6 mmol) was added to a solution of TMEDA (9.24 mL, 7.16 g, 61.6 mmol) in anhydrous THF (20 mL) in a 500 mL round-bottomed flask at –78 ºC using Schlenk techniques. The solution was stirred at –78 ºC for 20 min, and 2-methylthiophene (5.4 mL, 5.5 g, 56 mmol) was added. The solution was stirred at –78 ºC for 30 min then allowed to warm to room temperature. A slurry of $MgBr_2 \cdot Et_2O$ (19.24 g, 74.51 mmol) in anhydrous THF (80 mL) was added slowly (exothermic!), and the resulting mixture was stirred for 1 h. A solution of **N-Br$_2$, 1** (4.00 g, 14.0 mmol), and Ni(dppp)Cl_2 (152 mg, 280 μmol) in anhydrous THF (30 mL) was added slowly. The mixture was stirred at reflux for 16 h, then allowed to cool to room temperature. The mixture was poured onto ice water (150 mL) and acidified with 5% aqueous HCl (50 mL). The organic and aqueous layers were separated, and the aqueous layer was extracted with Et_2O (3 x 200 mL). The combined organic layers were dried over $MgSO_4$, and the solvent was removed on a rotary evaporator. Column chromatography (silica/hexanes) followed by recrystallization from hexanes afforded **3** as a beige solid

(260 mg, 5.8%), mp 83.5-84.5 ºC. ^{1}H NMR (300 MHz, $CDCl_3$): 2.39 (d, *J* = 1.0 Hz, 6H, CH_3), 6.28 (d, *J* = 3.4 Hz, 2H, H-3'), 6.31 (dq, *J* = 3.4, 1.0 Hz, 2H, H-4'), 7.49 (dd, *J* = 8.1, 7.2 Hz, 2H, H-3 and H-6), 7.56 (dd, *J* = 7.1, 1.4 Hz, 2H, H-2 and H-7), 7.88 (dd, *J* = 8.1, 1.3 Hz, 2H, H-4 and H-5). ^{13}C NMR (75 MHz, $CDCl_3$): δ 15.1 (CH_3), 124.7 (C-4'), 125.0 (C-3), 127.4 (C-3'), 128.9 (C-4), 130.5 (C-9), 132.0 (C-2), 132.8 (C-1), 135.4 (C-10), 138.5 (C-5'), 141.9 (C-2'). IR (powder): 3057 (w), 2912 (w), 2853 (w), 1446, 1365, 1174, 1028, 821, 785, 773 cm^{-1}. HRMS (EI) calculated for $C_{20}H_{16}S_2$: 329.06934. Observed 320.06955 (Δ = -0.7 ppm). Elem. anal. calculated for $C_{20}H_{16}S_2$: C 74.96% H 5.03% S 20.01%. Observed: C 75.18% H 5.12% S 19.94%.

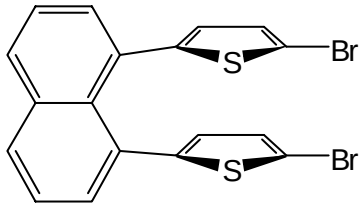

1,8-Bis(5-bromo-2-thienyl)naphthalene, N-(ThBr)$_2$, 4. *N*-bromosuccinimide (4.36 g, 24.6 mmol) was added to a solution of **N-(Th)$_2$**, **2** (3.58 g, 12.3 mmol), in $CHCl_3$ (90 mL) at –10 ºC. The reaction mixture was stirred at –10 ºC for 16 h, allowed to warm to room temperature, and poured into water (50 mL). The organic and aqueous layers were separated, and the aqueous layer was extracted with $CHCl_3$ (3 x 50 mL). The combined organic layers were dried over $MgSO_4$, and the solvent was removed on a rotary evaporator. The residue was triturated with hexane, and the solvent was removed from hexane-soluble material by rotary evaporation. Recrystallization from 9:1 hexanes:CH_2Cl_2 afforded **4** as a beige solid (2.12 g, 38.4%), mp 105-108 ºC (dec.). ^{1}H NMR (300 MHz, $CDCl_3$): 6.25 (d, *J* = 3.9 Hz, 2H, H-3'), 6.67 (d, *J* = 3.9 Hz, 2H, H-4'), 7.44-7.60 (m, 4H, H-3, H-4, H-5, and H-6), 7.87-8.01 (m, 2H, H-2 and H-7). ^{13}C NMR

(75 MHz, $CDCl_3$): δ 110.9, 125.2, 128.0, 129.4, 130.0, 130.6, 131.0, 132.6, 135.3, 145.5. IR (powder): 3048 (w), 1439, 1042, 960, 817, 794, 765 cm^{-1}. HRMS (EI) calculated for $C_{18}H_{10}S_2Br_2$: 447.85907. Observed 447.85754 (Δ = 3.4 ppm). Elem. anal. calculated for $C_{18}H_{10}S_2Br_2$: C 48.00% H 2.24% S 14.28% Br 35.48%. Observed: C 48.25% H 2.27% S 14.28% Br 35.48%.

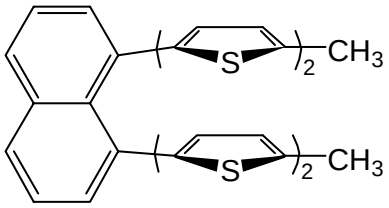

1,8-Bis(5'-methyl-5,2'-bithiophen-2-yl)naphthalene, N-($Th_2Me)_2$, 5. *n*-Butyllithium (2.94 mL of a 2.5 M solution in hexanes, 7.35 mmol) was added to a solution of TMEDA (1.10 mL, 0.853 g, 7.34 mmol) in anhydrous THF (4 mL) in a 500 mL round-bottomed flask at –78 ºC using Schlenk conditions. The solution was stirred at –78 ºC for 30 min, and 2-methylthiophene (0.64 mL, 0.65 g, 6.6 mmol) was added. The solution was stirred at –78 ºC for 30 min then allowed to warm to room temperature. $ZnCl_2$ (7.32 mL of a 1.0 M solution in Et_2O, 7.32 mmol) was added slowly (exothermic!), and the resulting mixture was stirred for 1 h. A solution of **N-($ThBr)_2$**, **4** (1.00 g, 2.22 mmol), and $Pd(PPh_3)_4$ (45 mg, 39 μmol) in anhydrous THF (15 mL) was added slowly. The mixture was stirred at reflux for 2 d, allowed to cool to room temperature, poured onto ice H_2O (50 mL), and filtered to remove insoluble material. The resulting solution was acidified with 0.5% aqueous HCl (20 mL). The organic and aqueous layers were separated, and the aqueous layer was extracted with Et_2O (3 x 100 mL). The combined organic layers were dried over $MgSO_4$, and the solvent was removed on a rotary evaporator. Column chromatography (silica/hexanes) afforded **5** as a light yellow solid

(230 mg, 21.4%), mp 132.5-136 ºC. ^{1}H NMR (300 MHz, $CDCl_3$): 2.47 (s, 6H, CH_3), 6.39 (d, *J* = 3.6 Hz, 2H, H-3'), 6.60-6.66 (m, 4H, H-4' and H-4"), 6.84 (d, *J* = 3.4 Hz, 2H, H-3"), 7.52 (dd, *J* = 8.1, 7.0 Hz, 2H, H-3 and H-6), 7.62 (dd, *J* = 7.0, 1.1 Hz, 2H, H-2 and H-7), 7.92 (dd, *J* = 8.1, 1.0 Hz, 2H, H-4 and H-5). ^{13}C NMR (75 MHz, $CDCl_3$): δ 15.3 (CH_3), 123.1 (C-4'), 123.2 (C-3"), 125.1 (C-3), 125.7 (C-4"), 128.4 (C-3'), 129.4 (C-4), 130.6 (C-9), 131.9 (C-1), 132.1 (C-2), 135.3 (C-2"), 135.4 (C-10), 136.5 (C-5'), 138.8 (C-5"), 142.7 (C-2'). IR (powder): 2913 (w), 2848 (w), 1440, 1261, 866, 786, 769 cm^{-1}. HRMS (EI) calculated for $C_{28}H_{20}S_4$: 484.04479. Observed 484.04504 (Δ = -0.5 ppm). Elem. anal. calculated for $C_{28}H_{20}S_4$: C 69.38% H 4.16% S 26.46%. Observed: C 69.52% H 4.27% S 26.21%.

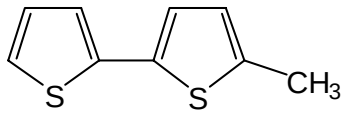

5-Methyl-2,2'-bithiophene, 5-MeTh$_2$, 6. Pulverized KOH flakes (722 mg, 13.0 mmol), 2,2'-bithiophene-5-carbaldehyde (5.03 g, 25.9 mmol), and hydrazine hydrate (14.3 mL of a 64% aqueous solution, 28.5 mmol) were added to di(ethylene glycol) (35 mL) in a 250 mL round-bottomed flask. The mixture was stirred at 120-130 ºC for 2 h, and water was allowed to evaporate. The solution was allowed to cool to room temperature, and 5% aqueous HCl (100 mL) and $CHCl_3$ (100 mL) were added. The organic and aqueous layers were separated, and the aqueous layer was extracted with $CHCl_3$ (5 x 200 mL). The combined organic layers were washed with H_2O (5 x 400 mL) and dried over $MgSO_4$. and the solvent was removed on a rotary evaporator. The residue was dissolved in hexanes, and the solution was passed through a short plug of silica. The solvent was removed on a rotary evaporator to afford **6** as a pale yellow liquid (3.55 g, 76.0%). ^{1}H NMR (300 MHz, $CDCl_3$): 6.65-6.75 (m, 1H), 6.97-7.06 (m, 2H), 7.08 (dd, *J*

= 3.3, 1.1 Hz), 7.15 (dd, J = 5.5, 1.1 Hz). ^{13}C NMR (75 MHz, $CDCl_3$): δ 15.0, 122.8, 123.4, 123.5, 125.7, 127.5, 134.9, 137.7, 138.8. IR (powder): 3066 (w), 2914 (w), 2856 (w), 1519, 1425, 1230, 1203, 1048, 835, 790, 687 cm^{-1}. HRMS (EI) calculated for $C_9H_8S_2$: 180.00674. Observed 180.00602 (Δ = 4.0 ppm). Elem. anal. calculated for $C_9H_8S_2$: C 59.96% H 4.47% S 35.57%. Observed: C 60.05% H 4.63% S 35.58%.

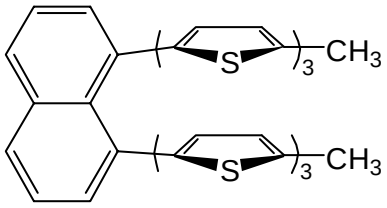

1,8-Bis(5”-methyl-5,2’:5’,2”-terthiophen-2-yl)naphthalene, N-($Th_3Me)_2$, 7. *n*-Butyllithium (2.94 mL of a 2.5 M solution in hexanes, 7.35 mmol) was added to a solution of TMEDA (1.10 mL, 0.853 g, 7.34 mmol) in anhydrous THF (4 mL) in a 500 mL round-bottomed flask at –78 ºC using Schlenk techniques. The solution was stirred at –78 ºC for 30 min, and 5-methyl-2,2’-bithiophene (1.2 g, 6.7 mmol) was added. The solution was stirred at –78 ºC for 30 min and allowed to warm to room temperature. $ZnCl_2$ (7.32 mL of a 1.0 M solution in Et_2O, 7.32 mmol) was added slowly (exothermic!), and the resulting mixture was stirred for 1 h. A solution of **N-($ThBr)_2$, 4** (1.00 g, 2.22 mmol) and $Pd(PPh_3)_4$ (45 mg, 39 μmol) in THF (15 mL) was added slowly. The mixture was stirred at reflux for 4 h, allowed to cool to room temperature, poured onto ice water (50 mL), and acidified with 0.5% aqueous HCl (50 mL). The organic solvent was removed by rotary evaporation, Et_2O (50 mL) was added, and the mixture was filtered to remove insoluble material. The organic and aqueous layers were separated, and the aqueous layer was extracted with Et_2O (3 x 100 mL). The combined organic layers were dried over $MgSO_4$, and the solvent was removed on a rotary evaporator. Column

chromatography (silica/hexanes) and subsequent recrystallization from 1:1 hexanes:CH_2Cl_2 afforded **7** as a dark orange powder (74 mg, 3.4%), mp 168-171 °C. ^{1}H NMR (300 MHz, $CDCl_3$): 2.46 (s, 6H, CH_3), 6.41 (d, *J* = 3.7 Hz, 2H, H-3'), 6.60 (dq, *J* = 3.4, 0.9 Hz, 2H, H-4"'), 6.70 (d, *J* = 3.7 Hz, 2H), 6.88 (d, *J* = 3.5 Hz, 2H, H-4'), 6.91 (d, *J* = 3.7 Hz, 2H, H-3"'), 6.93 (d, *J* = 3.7 Hz, 2H), 7.53 (dd, *J* = 8.1, 7.0 Hz, 2H, H-3 and H-6), 7.62 (dd, *J* = 7.0, 1.1 Hz, 2H, H-2 and H-7), 7.93 (dd, *J* = 8.1, 1.1 Hz, 2H, H-4 and H-5). ^{13}C NMR (75 MHz, $CDCl_3$): δ 15.4 (CH_3), 123.4 (C-3"'), 123.5, 123.6 (C-4'), 123.9, 125.2 (C-3), 125.9 (C-4"'), 128.7 (C-3'), 129.6 (C-4), 130.7 (C-9), 131.8 (C-1), 132.1 (C-2), 135.0 (C-2"'), 135.5 (C-10), 135.7 (C-2"), 136.2 (C-5'), 136.5 (C-5"), 139.0 (C-5"'), 143.4 (C-2'). IR (powder): 3061 (w), 2908 (w), 1442, 819, 785 cm^{-1}. HRMS (EI) calculated for $C_{36}H_{24}S_6$: 648.02023. Observed 648.01978 (Δ = 0.7 ppm). Elem. anal. calculated for $C_{36}H_{24}S_6$: C 66.63% H 3.73% S 29.65%. Observed: C 66.60% H 3.89% S 29.50%.

4.3: Results and Discussion

4.3.1: Synthetic Approaches to 1,8-Bis(oligothiophene)-substituted Naphthalenes

1,8-Bisbromonaphthalene, **1**, was synthesized from 1,8-diaminonaphthalene via a Sandmeyer reaction (Figure 4.5). Previous reports[6-10] detail a variety of experimental procedures, including dissolving 1,8-diaminonaphthalene in various concentrations of

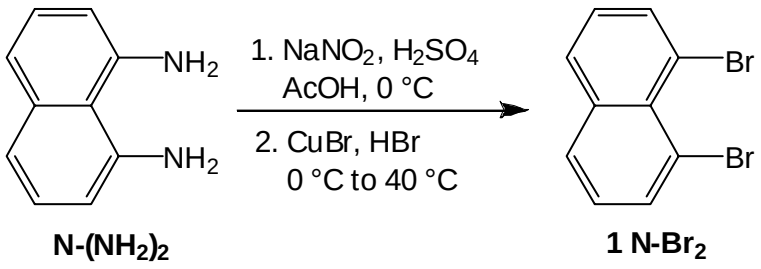

Figure 4.5. Synthesis of 1,8-dibromonaphthalene **1** via a Sandmeyer reaction.

H_2SO_4; dissolving $NaNO_2$ in H_2O or adding solid $NaNO_2$ to the diaminonaphthalene solution; and extracting the reaction mixture after neutralization with NaOH, as opposed to extracting the acidic mixture. Since H_2SO_4 was found to be a poor solvent for 1,8-diaminonaphthalene, we chose to slowly add a solution of 1,8-diaminonaphthalene in AcOH[6,9] to a solution of $NaNO_2$ in concentrated H_2SO_4. The reaction mixture was diluted with CH_2Cl_2 and filtered to remove insoluble material before being subjected to organic/aqueous extraction. This method was found to promote both the formation of the bis(diazo) intermediate and the most facile workup. Reactions using H_2SO_4 as the solvent for 1,8-diaminonaphthalene resulted primarily in the isolation of starting material. Attempts to neutralize the crude reaction mixture with NaOH resulted in the formation of a thick sludge, which precluded the extraction of product.

Bis(5-methyl-2-thienyl)naphthalene, **3 N-(ThMe)$_2$**, was synthesized by the nickel-catalyzed Kumada[11] coupling of 5-methyl-2-thienylmagnesium bromide and 1,8-bisbromonaphthalene (Figure 4.6). 2-Methylthiophene was lithiated with *n*-butyllithium in the presence of tetramethylethylenediamine (TMEDA). Transmetallation with $MgBr_2 \cdot Et_2O$ gave 5-methyl-2-thienylmagnesium bromide,[12] which was added to a solution of 1,8-bisbromonaphthalene in the presence of $Ni(dppp)Cl_2$. The low yield of this reaction (5.8%) can be attributed to the low solubility of $MgBr_2 \cdot Et_2O$ in THF and a competitive side reaction (homocoupling), which forms 5,5'-dimethyl-2,2'-bithiophene

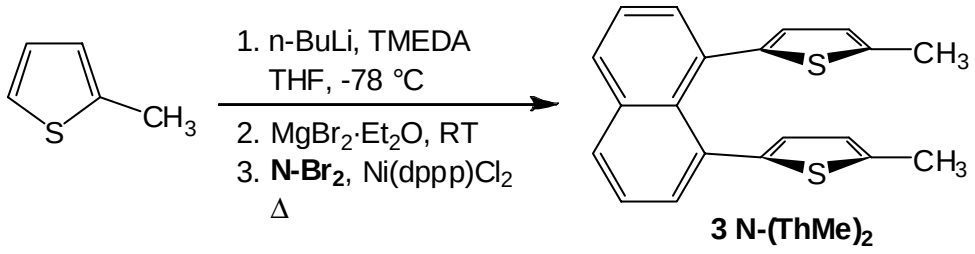

Figure 4.6. Synthesis of **3 N-(ThMe)$_2$** by Kumada coupling. Structure is not intended to indicate a specific conformation.

byproduct. To mitigate the challenge of transmetallation with a relatively insoluble reagent, future transmetallations were done with more soluble $ZnCl_2$ as part of a Negishi coupling (below).[13,14] A significant yield (45%) of mono-reacted 1-bromo-8-(5-methyl-2-thienyl)naphthalene was also isolated. Although it was not attempted, this compound could be re-reacted to increase overall yield, if desired.

The analogous bis(dithienyl)- and bis(terthienyl)-substituted naphthalenes, **5 N-(Th$_2$Me)$_2$** and **7 N-(Th$_3$Me)$_2$**, were synthesized using a divergent approach. 1,8-Bis(2-thienyl)naphthalene, **2 N-(Th)$_2$**, was prepared by Kumada coupling of 2-bromothiophene and 1,8-dibromonaphthalene (Figure 4.7).[1,2,11] Due to the consumption of Grignard reagent by the competitive formation of 2,2'-bithiophene, conversion of starting material to the desired 1,8-bis substituted product was incomplete. This situation can be mitigated somewhat, but not completely, by the use of excess Grignard reagent. According to GC-MS analysis, the crude product mixture contained 1,8-dibromonaphthalene, 1-bromo-8-(2-thienyl)naphthalene, and 1,8-bis(2-thienyl)naphthalene in a ratio of 20:45:35. Consequently, the crude reaction mixture was separated from 2,2'-bithiophene by column chromatography before being re-reacted under similar Kumada conditions to increase conversion.

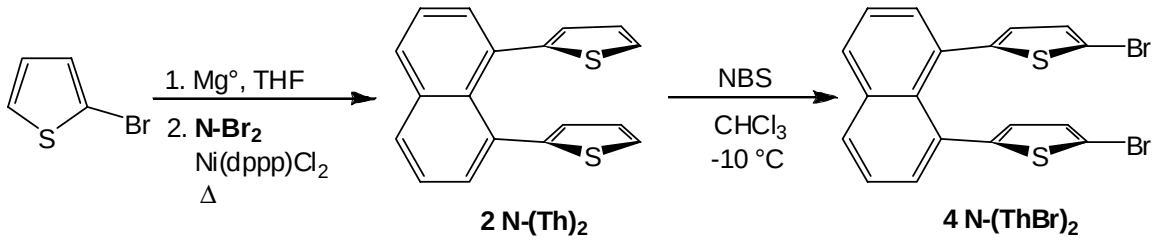

Figure 4.7. Synthesis of 1,8-bis(2-thienyl)naphthalene **2** and 1,8-bis(5-bromo-2-thienyl) naphthalene **4**.

The 1,8-bis(2-thienyl)naphthalene, **2 N-(Th)$_2$**, was subjected to dibromination

using 2.0 equivalents of *N*-bromosuccinimide (NBS), Figure 4.7. Precise stoichiometry and low temperature (-10 ºC) avoid overbromination and formation of regioisomers. The desired 1,8-bis(5-bromo-2-thienyl)naphthalene, **4 N-(ThBr)$_2$**, product was separated from mono-brominated material by recrystallization. This key intermediate was used in two subsequent Negishi reactions to afford the above mentioned compounds.

1,8-Bis(5'-methyl-5,2'-bithiophen-2-yl)naphthalene, **5 N-(Th$_2$Me)$_2$**, was formed by lithiation and subsequent transmetallation of 2-methylthiophene, which was then coupled to **4 N-(ThBr)$_2$** in a palladium-catalyzed Negishi reaction (Figure 4.8).[13,14] The crude product contained a mixture of starting material **4** (approximately 10%), mono-reacted 1-(5-bromo-2-thienyl)-8-(5'-methyl-5,2'-bithiophen-2-yl)naphthalene (approximately 50%), and desired product **5 N-(Th$_2$Me)$_2$** (approximately 40%). As with the cross-coupling reactions described above, mono-reacted material could be subjected to re-reaction to increase yield. The yield could also be increased by optimizing reaction conditions.

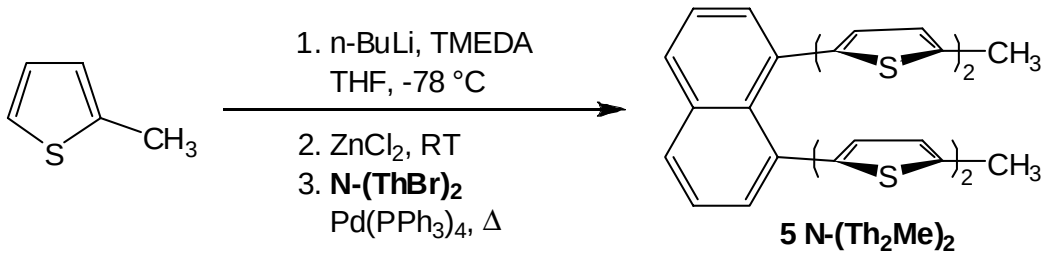

Figure 4.8. Synthesis of **5 N-(Th$_2$Me)$_2$**, by Negishi coupling.

A key intermediate in the synthesis of **7 N-(Th$_3$Me)$_2$** was 5-methyl-2,2'-bithiophene, **6 5-MeTh$_2$**. Attempts to synthesize **6 5-MeTh$_2$** via Negishi coupling of 2-methyl thiophene and 2-bromothiophene resulted in an inseparable mixture of the desired product, 2,2'-bithiophene, and 5,5'-dimethyl-2,2'-bithiophene from homocouplings. The Wolff-Kischner reduction[15,16] of 2,2'-bithiophene-5-carbaldehyde (Figure 4.9) afforded **6**

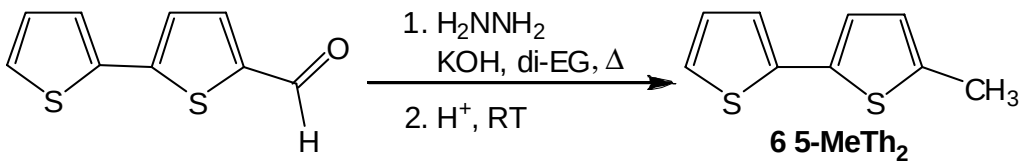

Figure 4.9. Wolff-Kischner synthesis of 5-methyl-2,2'-bithiophene, **6**.

in reasonable yield and avoided byproduct formation.

The Negishi coupling[13,14] (Figure 4.10) of **6 5-MeTh$_2$**, and **4 N-(ThBr)$_2$** under conditions similar to those described above afforded **7 N-(Th$_3$Me)$_2$**. Both starting materials were recovered, in addition to the expected byproducts, 5,5"'-2,2',2",2'"-quarterthiophene and 1-(5-bromo-2-thienyl)-8-(5"-methyl-5,2':5',2"-terthiophen-2-yl)naphthalene. The recovery of starting materials indicates incomplete lithiation of **6 5-MeTh$_2$**, accounting for the lower yield observed. This yield could be increased by optimizing reaction conditions and by re-reacting mono-reacted material.

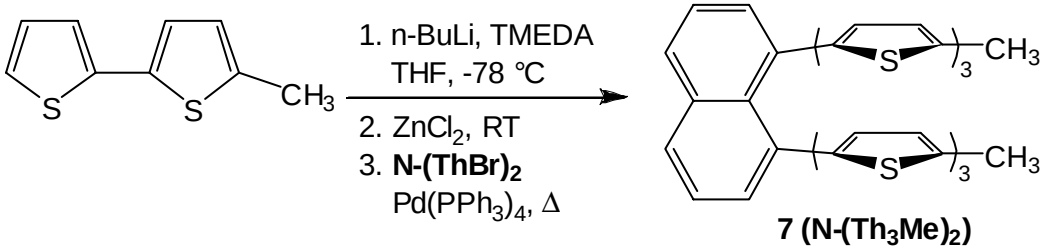

Figure 4.10. Synthesis of **7 N-(Th$_3$Me)$_2$** by Negishi coupling.

4.3.2: Structural Characterization of 1,8-Bis(oligothiophene)-substituted Naphthalenes

The identity and purity of all compounds were verified by NMR spectroscopy. Due to subtle variations in each of the thiophene moieties in **3 N-(ThMe)$_2$**, **5 N-(Th$_2$Me)$_2$**, and **7 N-(Th$_3$Me)$_2$**, additional NMR experiments were performed to definitively assign the signals arising from each of these subunits. Because each of these

molecules is symmetrically substituted, each ^{1}H or ^{13}C signal corresponds to two hydrogen or carbon nuclei, respectively. For clarity, only one half of each symmetric molecule is labeled in Figures 4.11-4.26.

Heteronuclear Single Quantum Correlation (HSQC) spectroscopy was used to assign ^{1}H and ^{13}C signals corresponding to the aromatic hydrogen nuclei directly bonded to the aromatic carbon nuclei of **3 N-(ThMe)$_2$** (Figure 4.11). Signals A and a (7.6 and 133 ppm); B and b (7.5 and 126 ppm); and C and c (7.9 and 130 ppm) correspond, respectively, to the hydrogen and carbon nuclei at the 2, 3, and 4 positions of the naphthalene ring. Resonances D and d (6.3 and 128 ppm) and E and e (6.35 and 125 ppm) correspond to the hydrogen and carbon nuclei at the 3' and 4' positions of the thiophene ring, respectively. No other signals are present because no other aromatic protons and carbons are coupled. Heteronuclear Multiple Bond Correlation (HMBC) spectroscopy, which allows for correlation between hydrogen nuclei coupled to carbon nuclei two or three bonds removed, was used to definitively assign all remaining aromatic ^{13}C signals (Figure 4.12). Based on HMBC, resonances f, g, h, i, and j (at 133, 131, 136, 143, and 149 ppm) correspond to carbon nuclei 1, 9, 10, 2', and 5', respectively.

Double-Quantum Filtered ^{1}H-^{1}H Correlation Spectroscopy (COSY) was used to confirm the assignment of the ^{1}H signals arising from the aromatic hydrogen nuclei of **5 N-(Th$_2$Me)$_2$** (Figure 4.13). According to this spectrum, resonances A (doublet of doublets at 7.6 ppm), B (doublet of doublets at 7.5 ppm), and C (doublet of doublets at 7.9 ppm) correspond, respectively, to the hydrogen nuclei at the 2, 3, and 4 positions of the naphthalene ring. The doublet G (6.9 ppm) and the doublet of quartets F (6.6 ppm) arise from the 3" and 4" hydrogen nuclei of the outer thiophene ring. Doublets E (6.7 ppm) and D (6.4 ppm) arise from the two hydrogen nuclei on the inner thiophene ring, but they cannot be definitively assigned without further information. A Nuclear Overhauser Effect (NOE) difference spectrum, with selective irradiation of the hydrogen

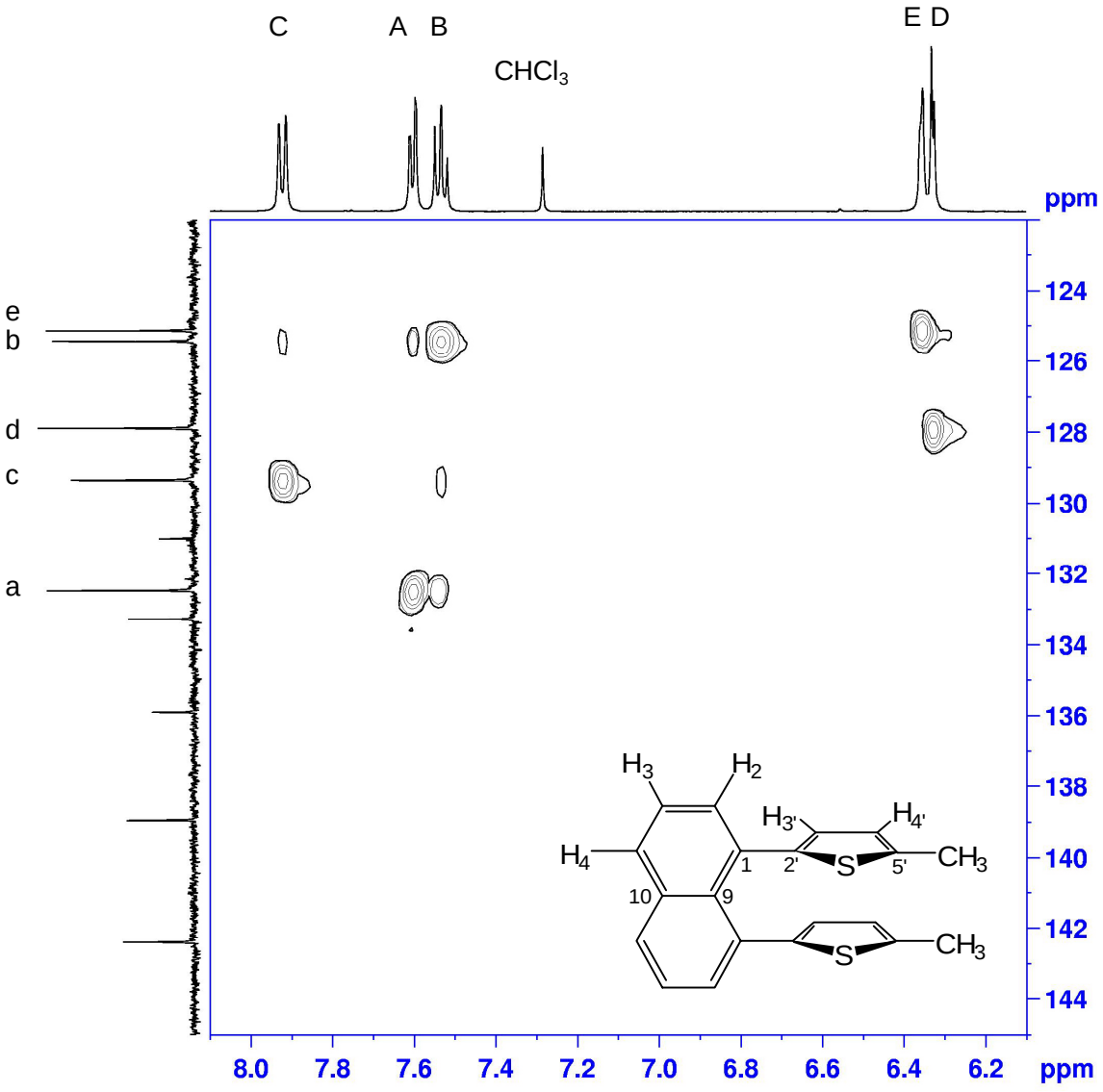

Figure 4.11. HSQC spectrum of the aromatic region of **3 N-(ThMe)$_2$**.

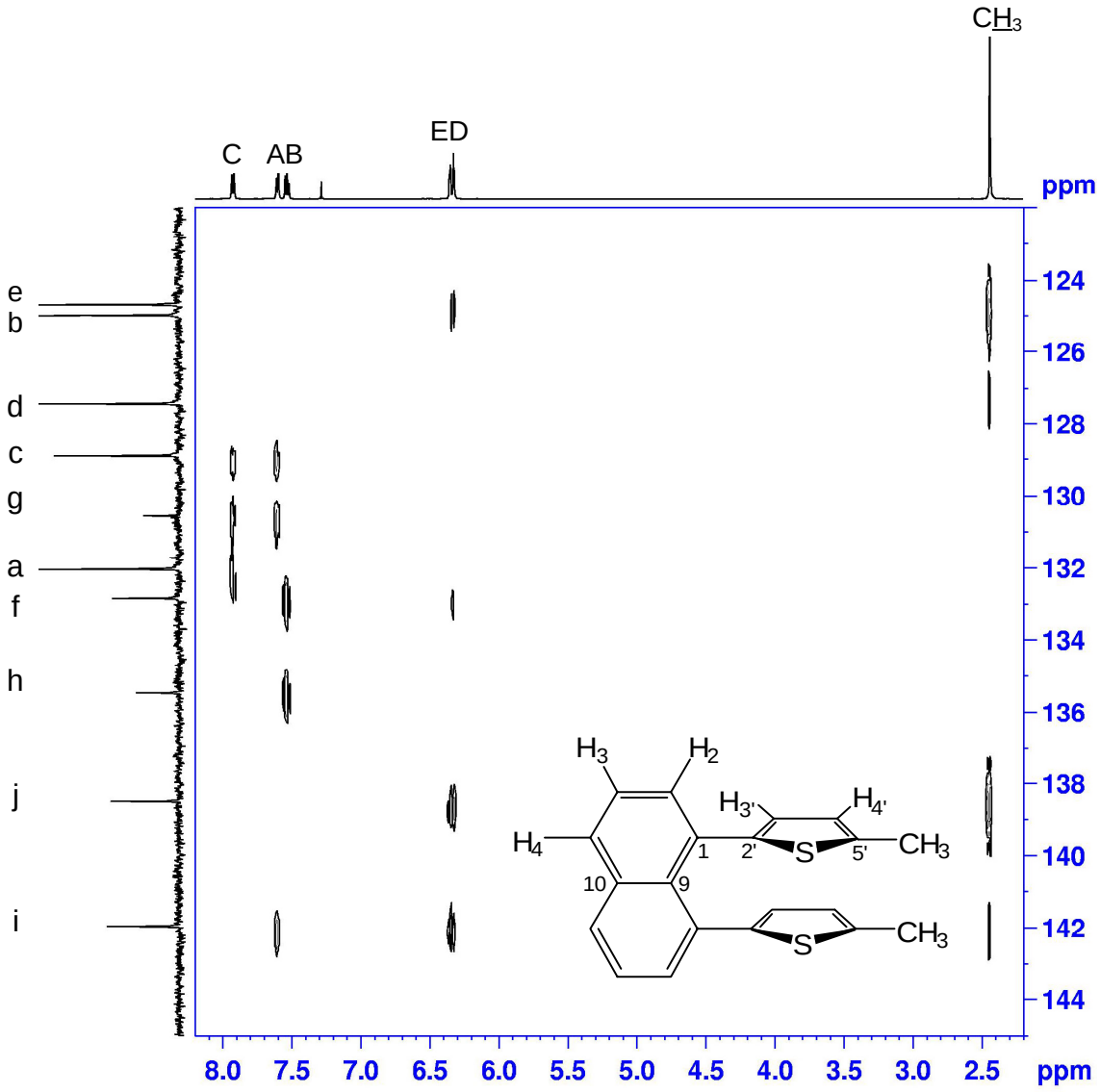

Figure 4.12. HMBC spectrum of **3 N-(ThMe)$_2$**.

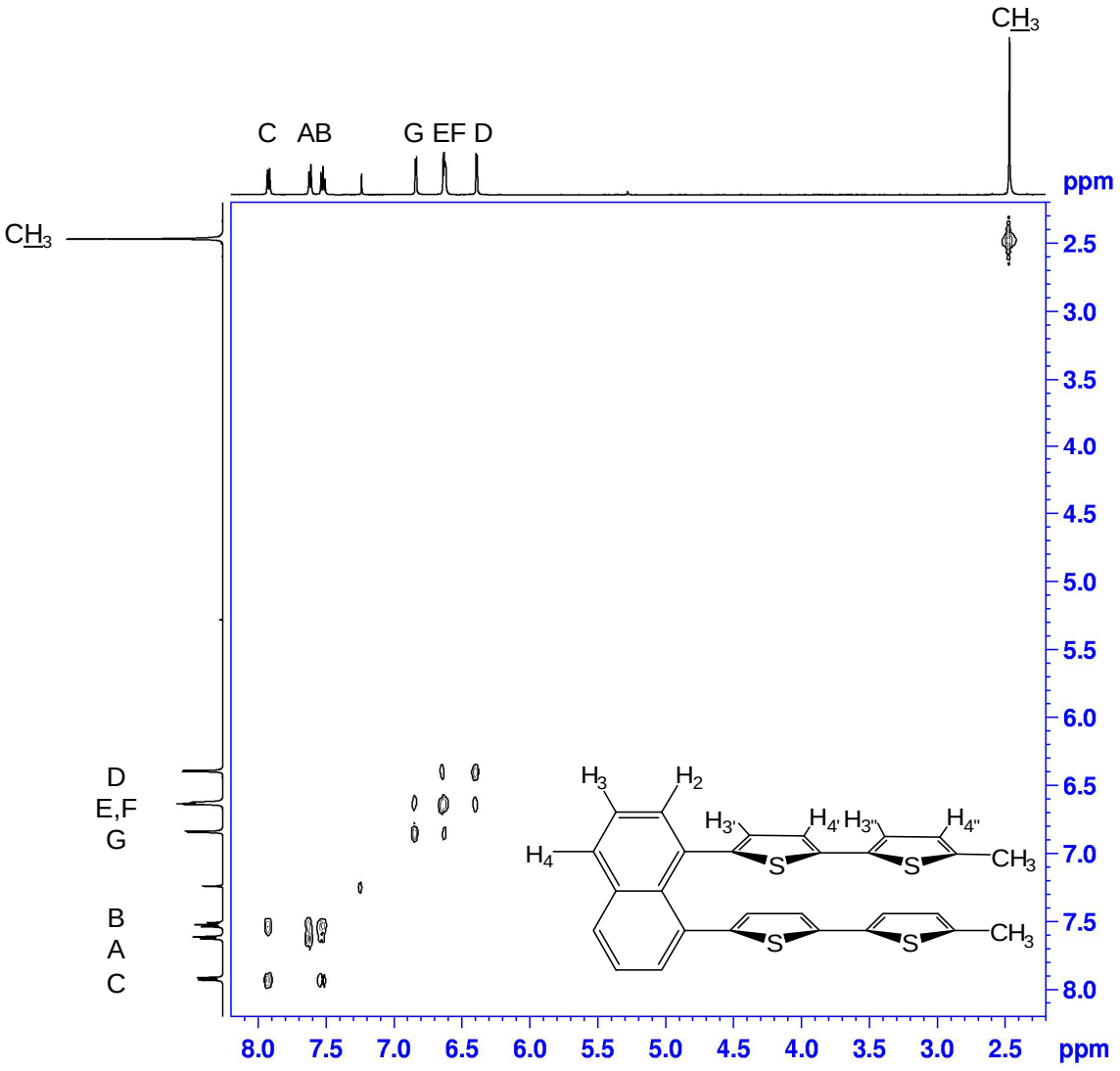

Figure 4.13. COSY spectrum of **5 N-($Th_2Me)_2$.**

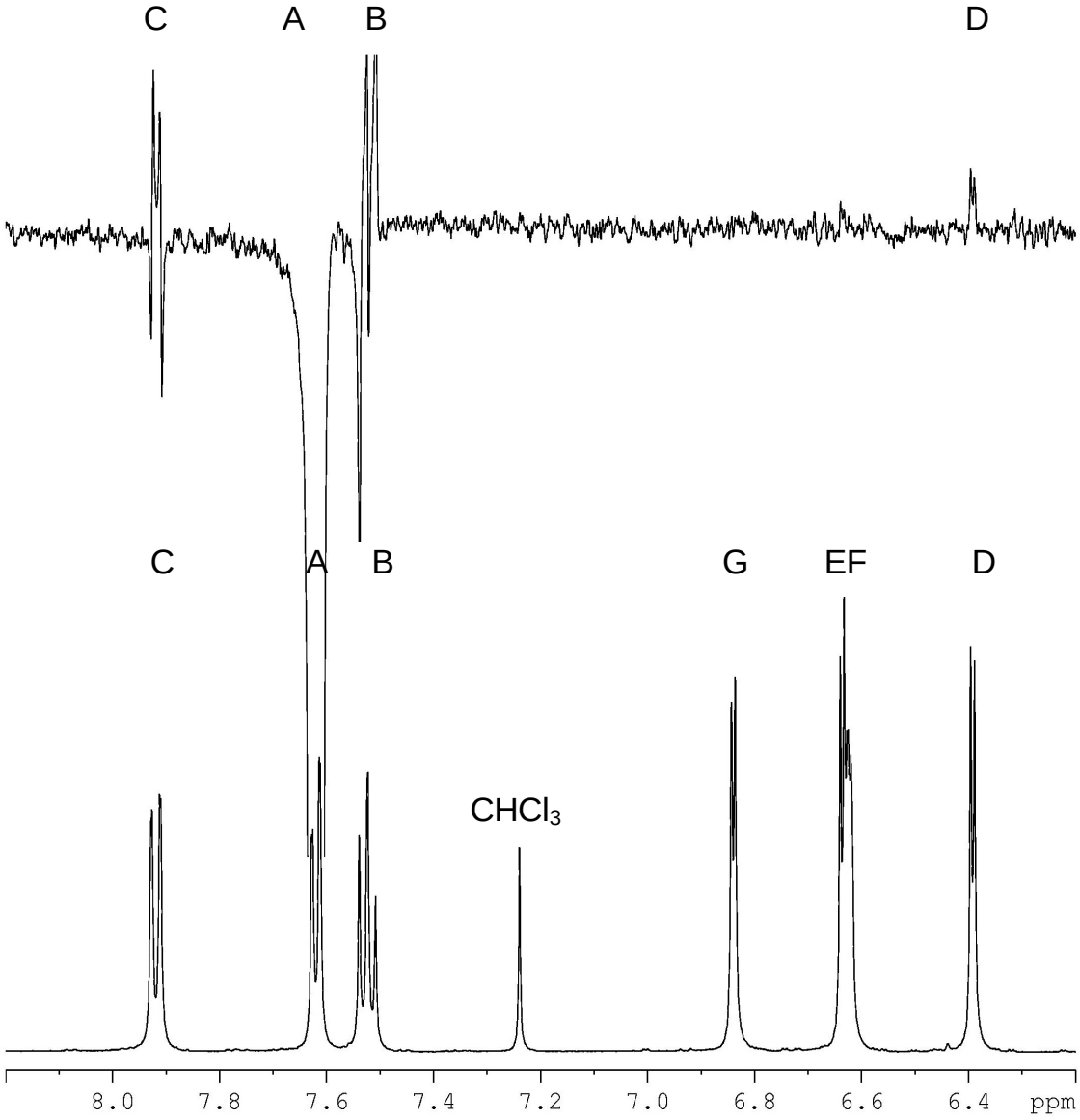

Figure 4.14. NOE (top) and ^{1}H NMR (bottom) spectra of **5 N-(Th$_2$Me)$_2$**.

nucleus at the 2 position (signal A, 7.6 ppm), facilitates the assignment of resonance D (Figure 4.14). Because the selective irradiation of A gives rise to a signal associated with the hydrogen nuclei closest in space to the irradiated nucleus, signal D (6.4 ppm) must be associated with the hydrogen nucleus at the 3' position of thiophene. As a result, signal E (6.7 ppm) is assigned to the hydrogen nucleus at the 4' thiophene position. Thus, all ^{1}H signals were definitively assigned based on a combination of COSY and NOE spectra.

HSQC spectroscopy (Figure 4.15) facilitated the assignment of resonances a, b, and c (each singlets at 133, 126, 130 ppm) to the carbon nuclei at the 2, 3, and 4 positions of the naphthalene ring. Signals d and e (singlets at 129 and 123.7 ppm) are associated with the carbon nuclei at the 3' and 4' positions of the inner thiophene ring. Signals f and g (singlets at 126 and 123.8 ppm) correspond to the carbon nuclei at the 4" and 3" positions of the outer thiophene ring. HMBC spectroscopy (Figure 4.16) was used to assign all remaining carbon resonances. Signals h, i, j, k, l, m, and n (at 132, 131, 135.5, 143, 136.5, 135.4, 139 ppm) correspond to carbon nuclei at the 1, 9, and 10 positions of the naphthalene ring and at the 2', 5', 2", 5" positions of the thiophene rings, respectively.

The same method was applied to assign resonances for **7 N-($Th_3Me)_2$**. The COSY spectrum was used to assign signals A (doublet of doublets at 7.6 ppm), B (doublet of doublets at 7.5 ppm), C (doublet of doublets at 7.9 ppm), H (doublet at 6.87 ppm), and I (doublet of quartets at 6.6 ppm) as the hydrogen nuclei at the 2, 3, and 4 positions of naphthalene and the 3"' and 4"' positions of the outer thiophene, respectively (Figure 4.17). The COSY spectrum also indicates that signals F and G (a pair of doublets at 6.92 ppm) correspond to hydrogen nuclei on adjacent carbons of one thiophene ring. Similarly, signals E and D (a pair of doublets at 6.4 and 6.7 ppm) correspond to hydrogen nuclei on adjacent carbons of a different thiophene ring. An NOE spectrum with selective irradiation at δ 7.6 ppm, corresponding to the 2 position of the naphthalene,

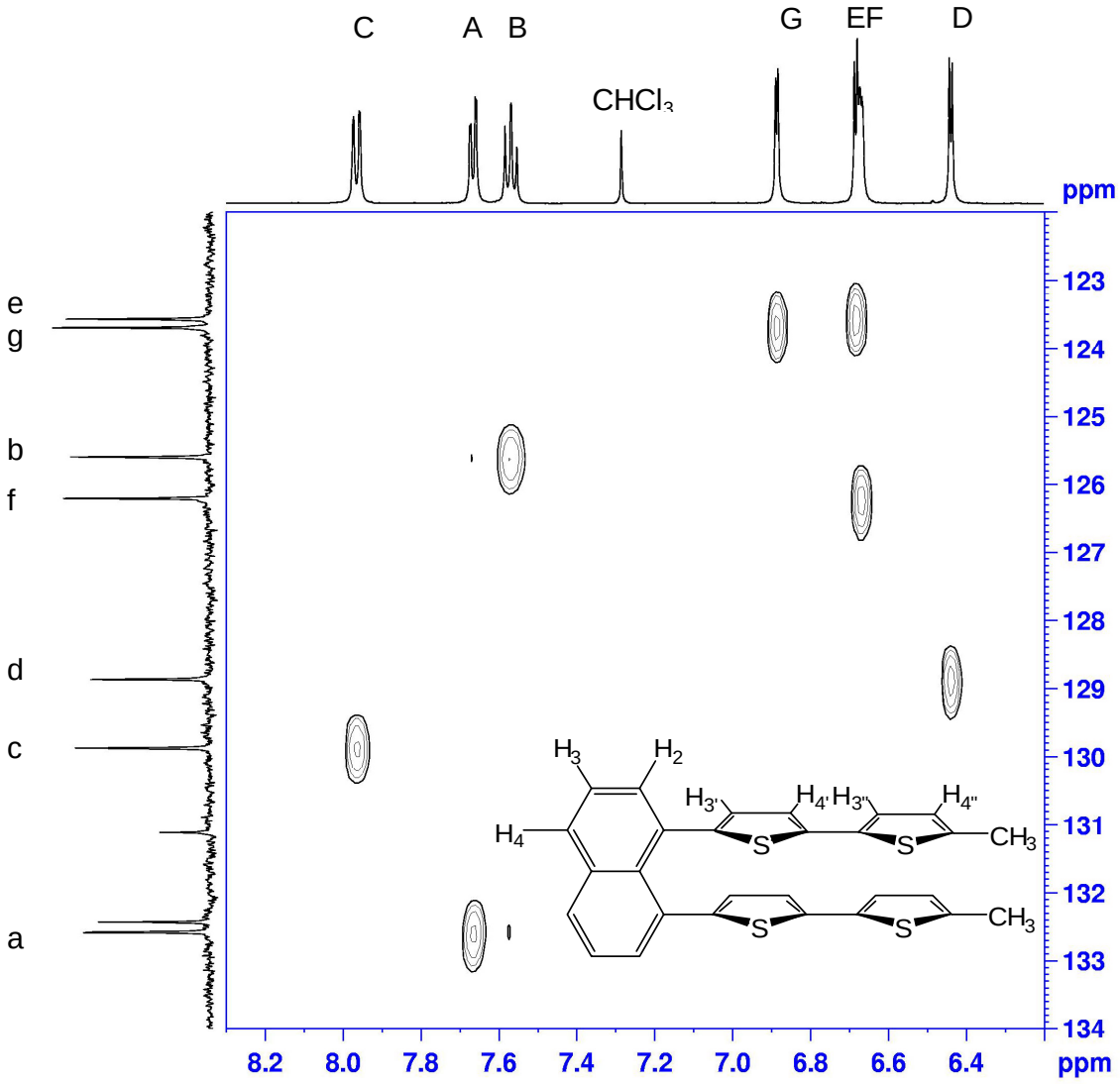

Figure 4.15. Relevant portion of the HSQC spectrum of **5 N-(Th_2Me)$_2$**.

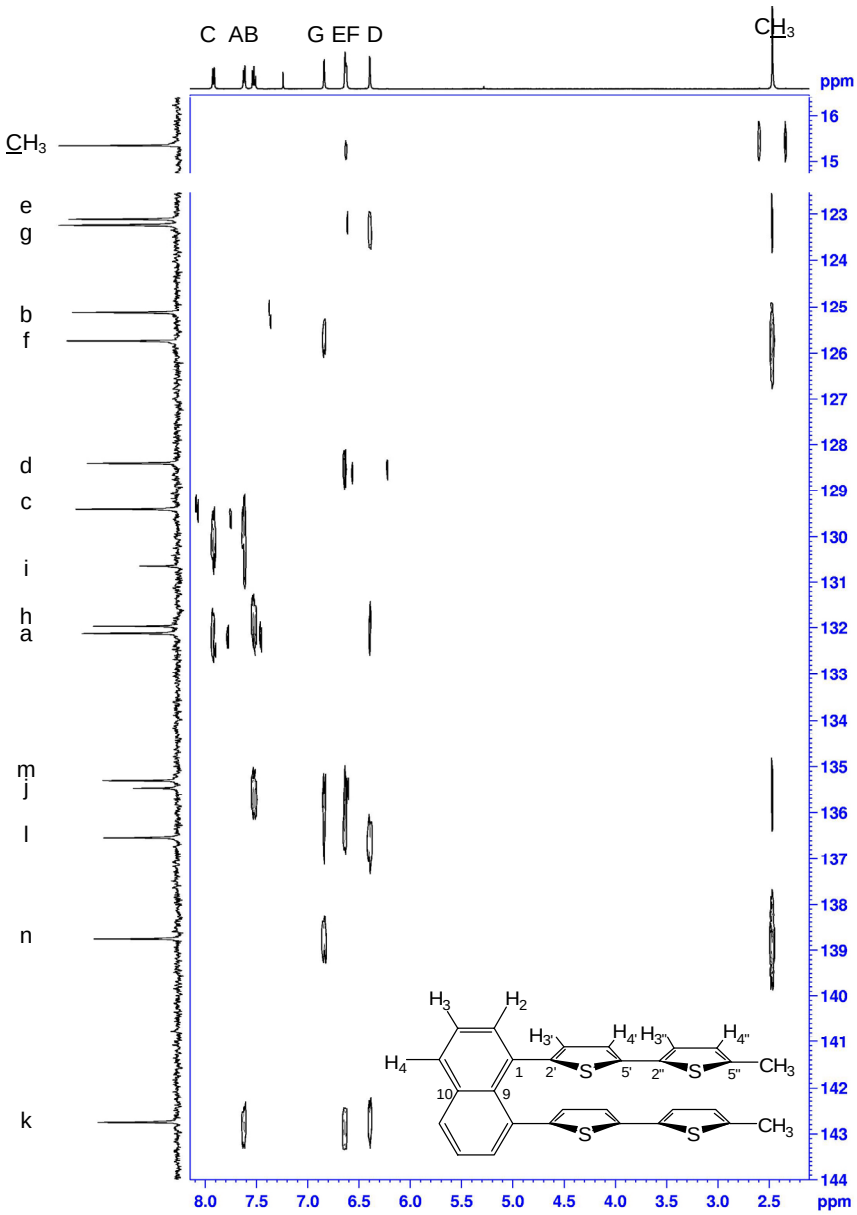

Figure 4.16. HMBC spectrum of **5 N-($Th_2Me)_2$.**

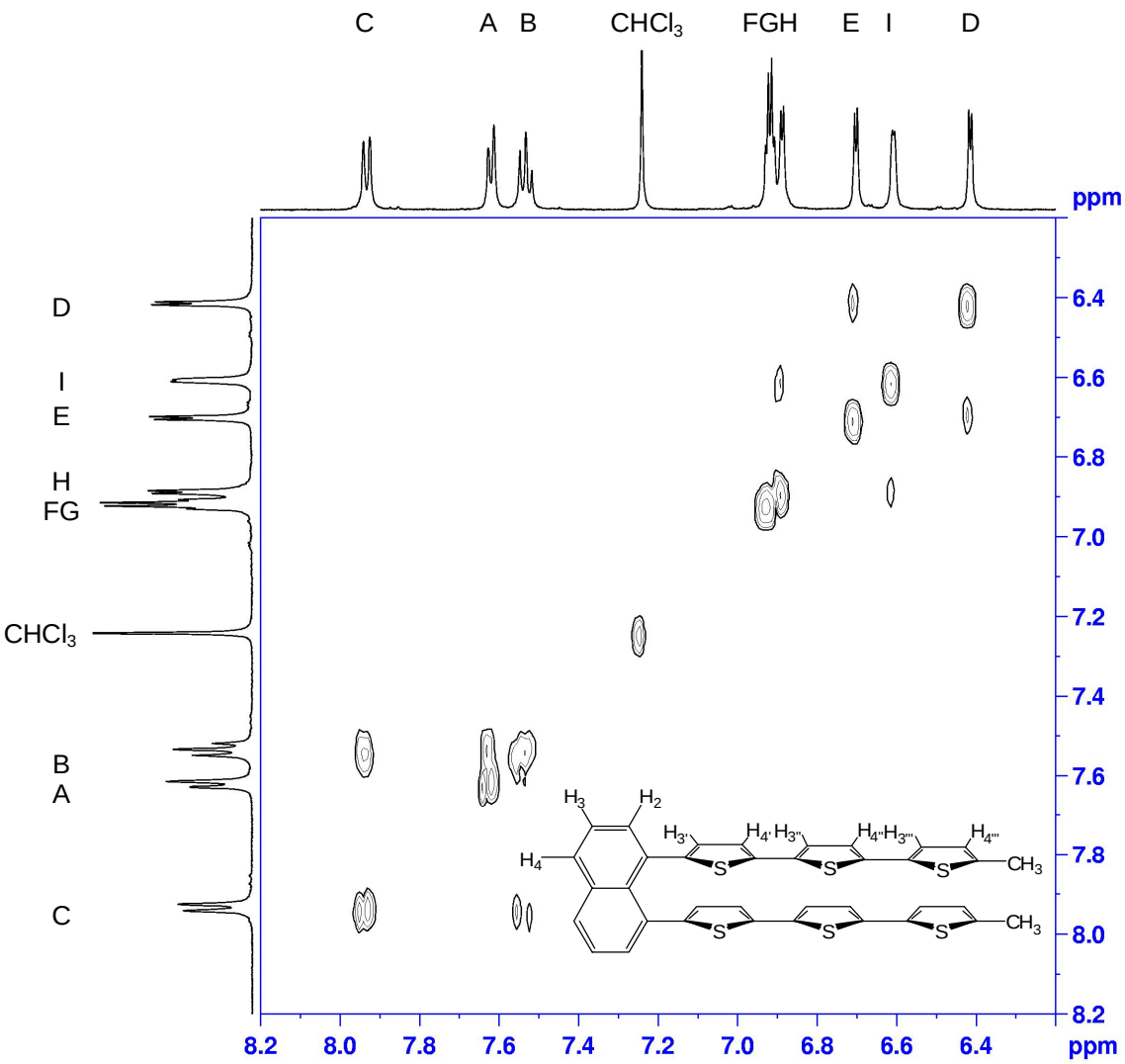

Figure 4.17. COSY spectrum of **7 N-(Th_3Me)$_2$**.

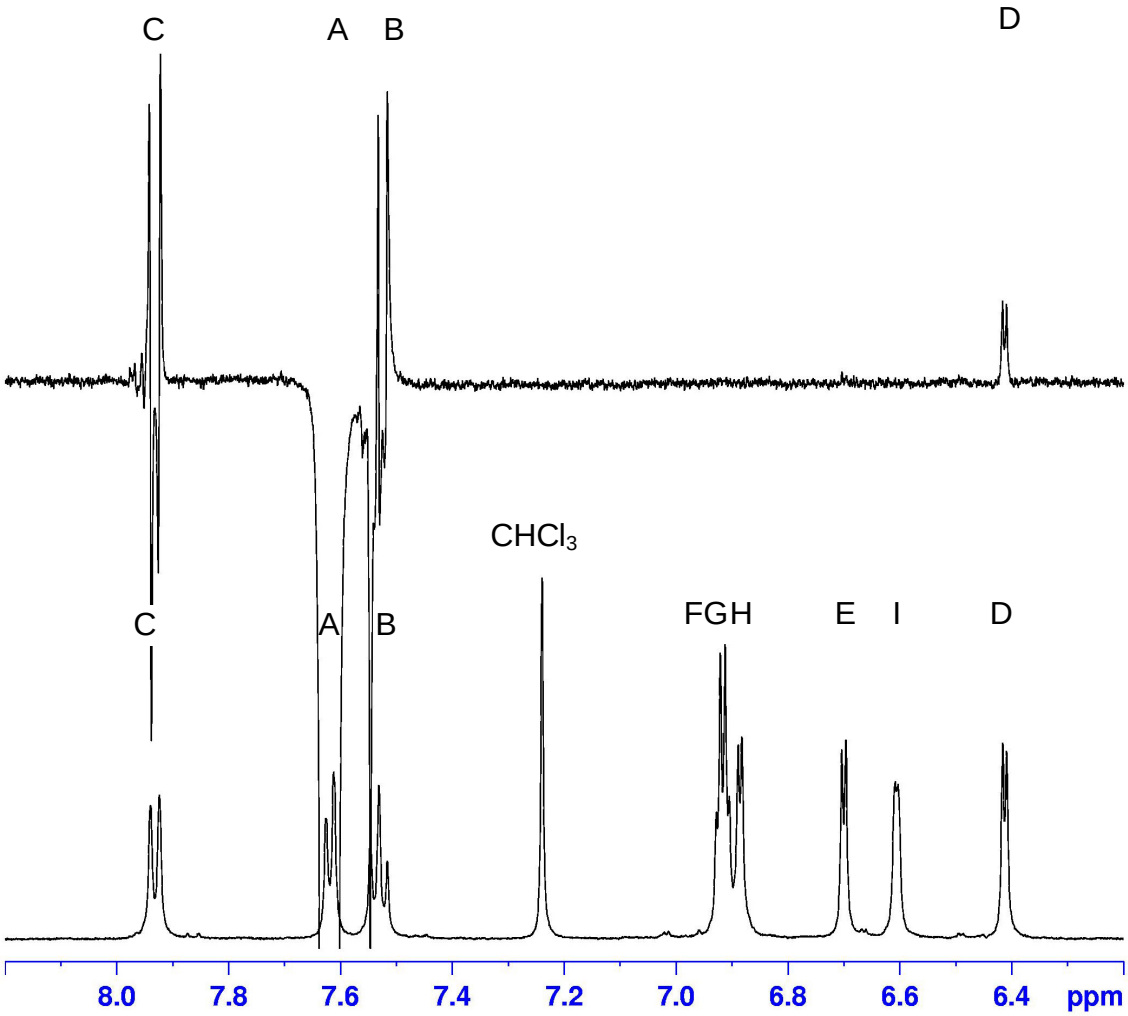

Figure 4.18. NOE (top) and ^{1}H NMR (bottom) spectra of **7 N-(Th$_3$Me)$_2$**.

demonstrates that signal D arises from the hydrogen nucleus at the 3' position of the inner thiophene ring (Figure 4.18). Consequently, signal E must be assigned to the hydrogen nucleus at the 4' position of the same ring. Additional attempts, using NOE techniques with selective excitation at δ 6.7 ppm, to further identify signals F and G as corresponding to specific 3" and 4" hydrogen nuclei were unsuccessful.

HSQC spectroscopy (Figure 4.19) was used to assign ^{13}C resonances a, b, and c (at 133, 126, and 130 ppm) as arising from the carbon nuclei at the 2, 3, and 4 positions of the naphthalene ring, respectively. Similarly, signals d, e, h, and i correspond to the carbon nuclei at the 3', 4', 3"', and 4"' positions of the innermost and outermost thiophene rings. While the signals at 124.0 and 124.4 ppm must each be assigned to one of the carbon nuclei at the β (3" and 4") positions of the center thiophene ring, it is not possible to definitively assign them specifically to f or to g due to the uncertainty of the ^{1}H signal assignment. HMBC spectroscopy (Figure 4.20) resulted in the assignment of signals j, k, and l (at 132.2, 131.2, and 135.3 ppm) as the carbon nuclei at the 1, 9, and 10 positions of naphthalene. Similarly, resonances m, n, o, p, q, and r (at 144, 136.8, 136.2, 137.0, 135.5, and 139 ppm) correspond to the 2', 5', 2", 5", 2"', and 5"' positions of the thiophene rings.

The conformational freedom of **3 N-(ThMe)$_2$**, **5 N-(Th$_2$Me)$_2$**, and **7 N-(Th$_3$Me)$_2$** was evaluated by variable temperature NMR spectroscopy. The sharp signals displayed in the ^{1}H spectrum of **3 N-(ThMe)$_2$** obtained at 60 °C (Figure 4.21, top) indicate that the thiophene rings are free to rotate about the thiophene-naphthalene bond. This rotational freedom is curtailed somewhat at room temperature, as evidenced by the broadening and divergence of the ^{1}H signals at 6.25 and 6.32 ppm, which correspond to the hydrogen nuclei at the 4' and 3' thiophene positions, respectively (Figure 4.21, center). As the sample temperature approaches –40 °C, **3 N-(ThMe)$_2$** begins to precipitate out of solution (as suggested by the broad $CHCl_3$ signal at 7.24 ppm, Figure 4.21, bottom), resulting in

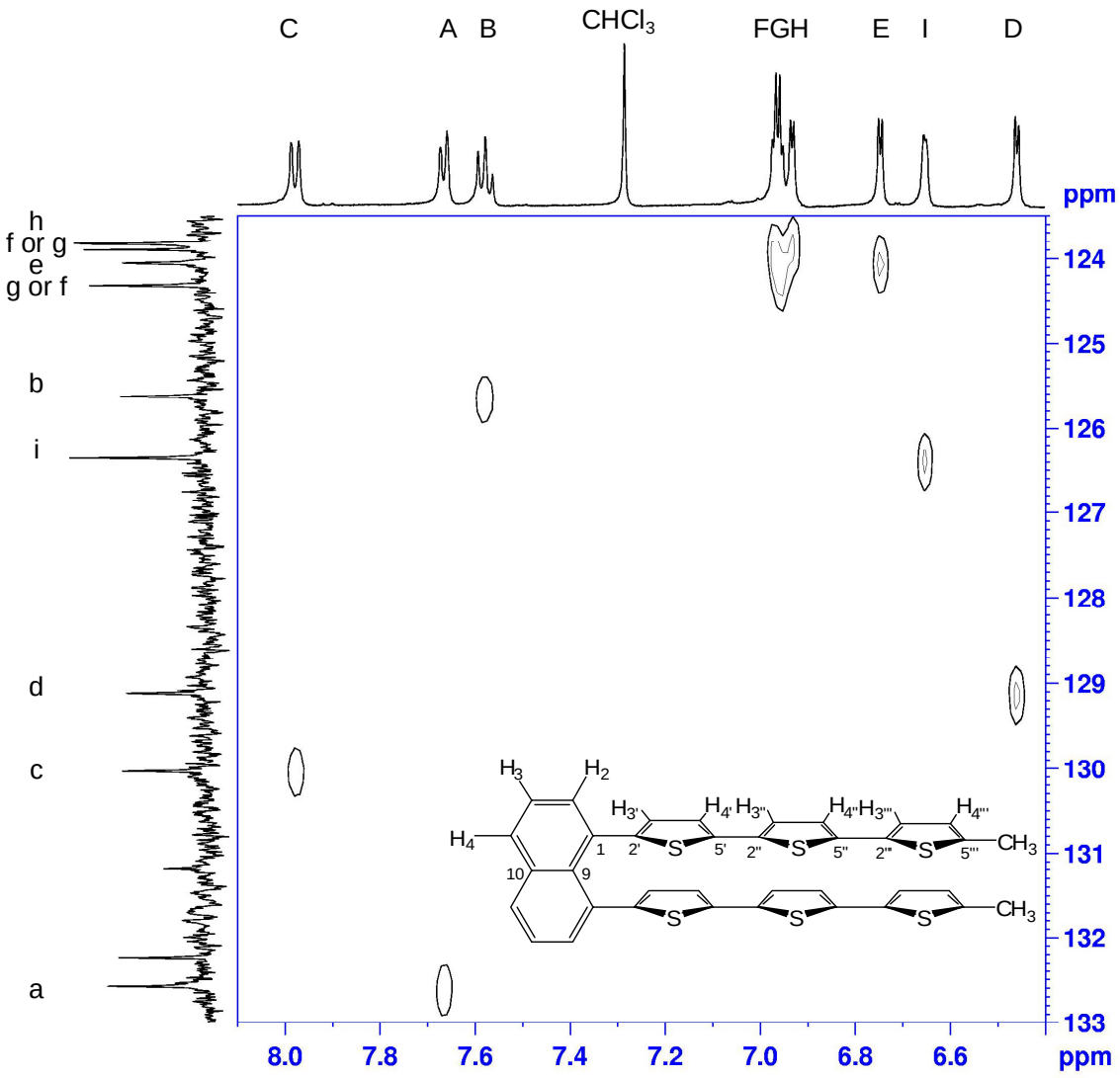

Figure 4.19. HSQC spectrum of **7 N-($Th_3Me)_2$**.

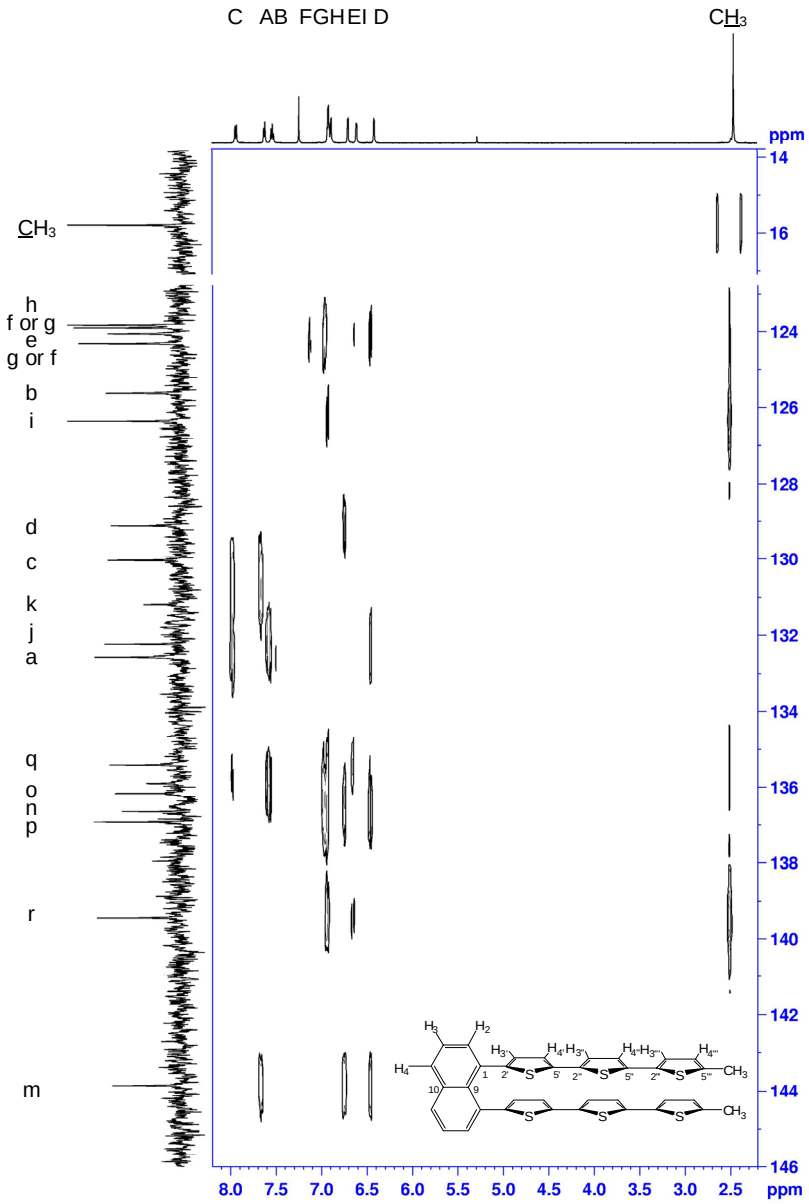

Figure 4.20. HMBC spectrum of **7 N-($Th_3Me)_2$**.

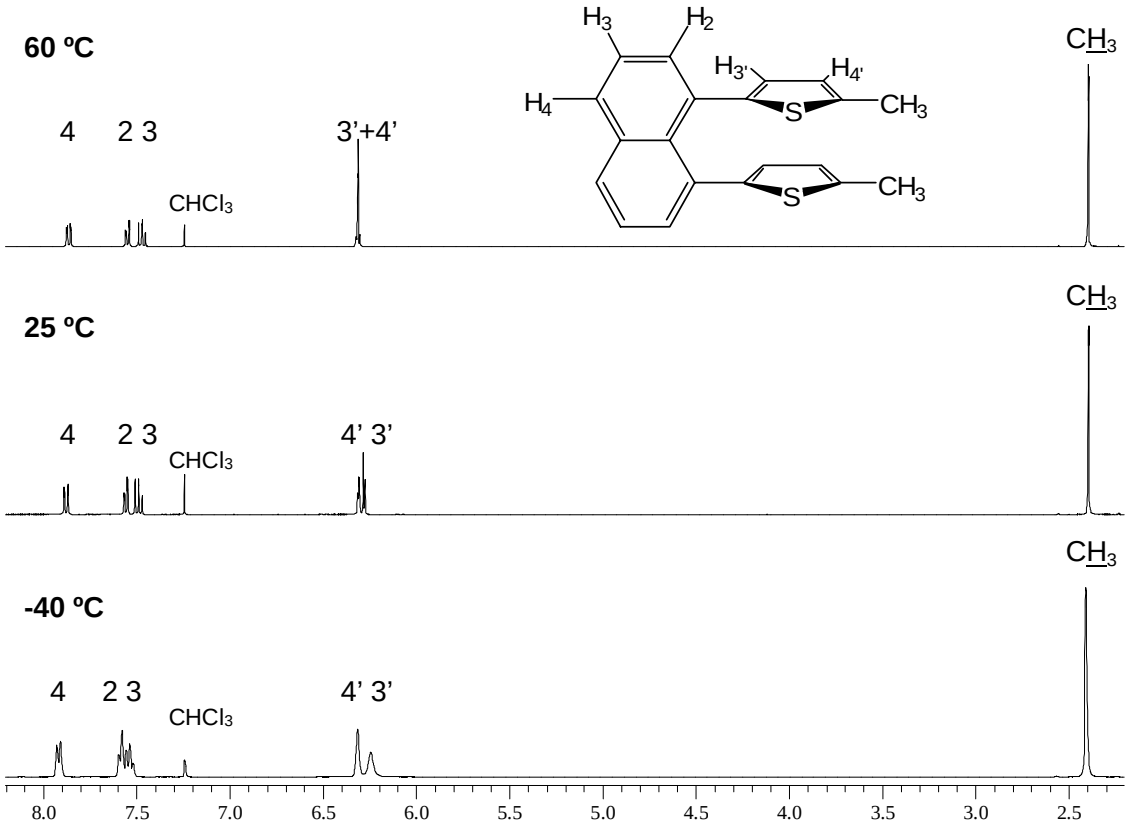

Figure 4.21. ^{1}H NMR spectra of **3 N-(ThMe)$_2$** at 60 ºC (top), 25 ºC (center), and –40 ºC (bottom).

all of the peaks undergoing significant broadening.

The presence of sharp singlet resonances in the ^{13}C spectrum of **3 N-(ThMe)$_2$** obtained at 60 ºC (Figure 4.22, top) provides additional evidence for free rotation at elevated temperature. At room temperature (Figure 4.22, center), ^{13}C signals at 132, 125, 127.5, and 124.5 ppm broaden from singlets to give multiple peaks. These signals correspond to the carbon nuclei at the 2 and 3 positions of naphthalene and the 3' and 4' positions of thiophene, respectively (Figure 4.22, dotted blue lines). With the exception of the singlet at 129 ppm (which is assigned to the carbon nucleus at the 4 position of naphthalene), all remaining signals exhibit a change in chemical shift (Figure 4.22, solid red lines). Further changes in chemical shift arise when the sample is cooled to low temperature (Figure 4.22, bottom, solid red lines). At low temperature, the previously

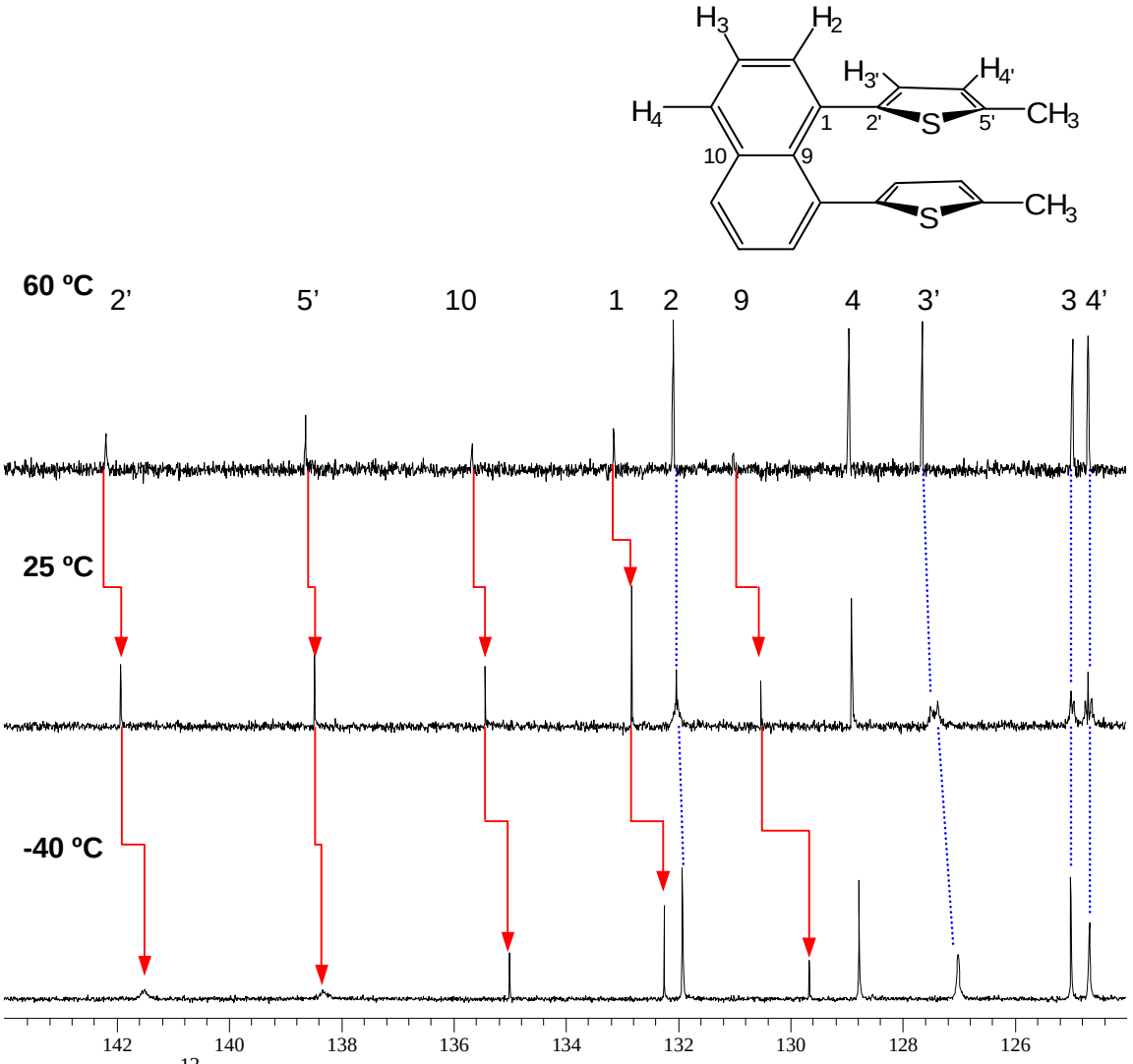

Figure 4.22. ^{13}C NMR spectra of **3 N-(ThMe)$_2$** at 60 ºC (top), 25 ºC (center), and –40 ºC (bottom).

broadened resonances at 132, 125, 127.5, and 124.5 ppm coalesce and become sharper (Figure 4.22, bottom, dotted blue lines). However, signals at 141.5 and 138.5, which are assigned to the 2' and 5' positions of the thiophene ring, broaden substantially (Figure 4.22, bottom, dotted blue lines). One possible rationale for this data is that two rotamers undergo fast interconversion at 25 °C and significantly slower interconversion at –40 °C.

Additional degrees of rotational freedom are introduced in **5 N-($Th_2Me)_2$**, where there is the possibility of rotation around the bond between the 5' and 2" carbons of the adjacent thiophene rings. In this case, the molecule rotates freely in solution at room temperature, as evidenced by the sharp resonances in the ^{1}H spectrum (Figure 4.23, top). Broadening of the signals at 2.5, 6.3, 6.6, 6.7, and 6.9 ppm, which arise from the hydrogen nuclei on the methyl group and the thiophene rings, indicates a reduction in rotational freedom at low temperature (Figure 4.23, bottom). The same phenomenon occurs in a less concentrated sample, indicating that the broadening is likely not due to aggregation or crystallization. The reduction in rotational freedom is supported by broadening (Figure 4.24, dotted blue lines) and changes in chemical shift in the ^{13}C

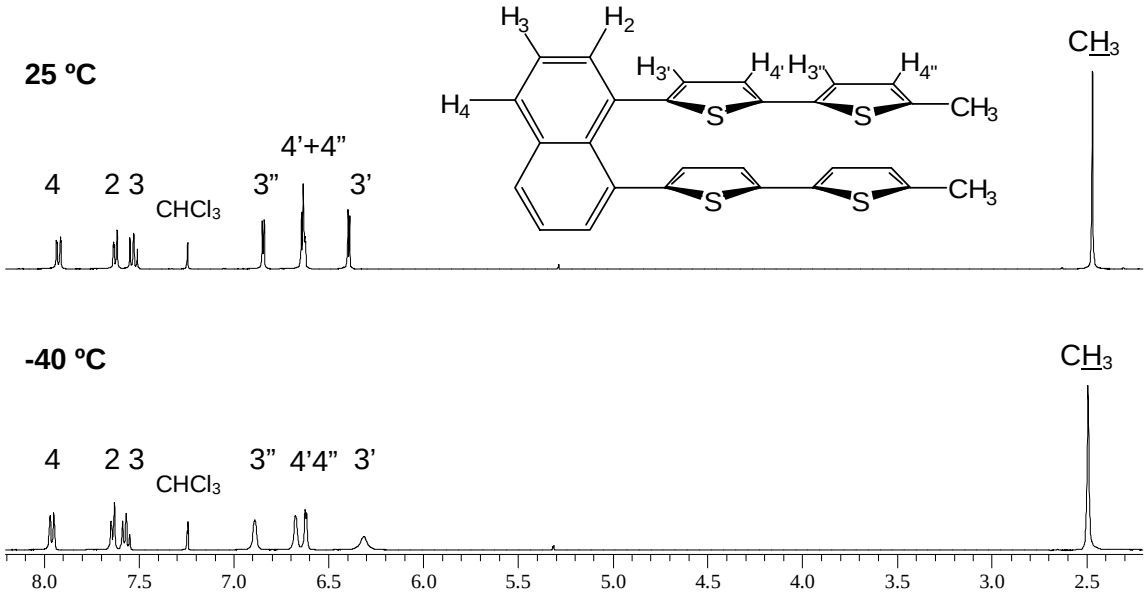

Figure 4.23. ^{1}H NMR spectra of **5 N-($Th_2Me)_2$** at 25 ºC (top) and –40 ºC (bottom).

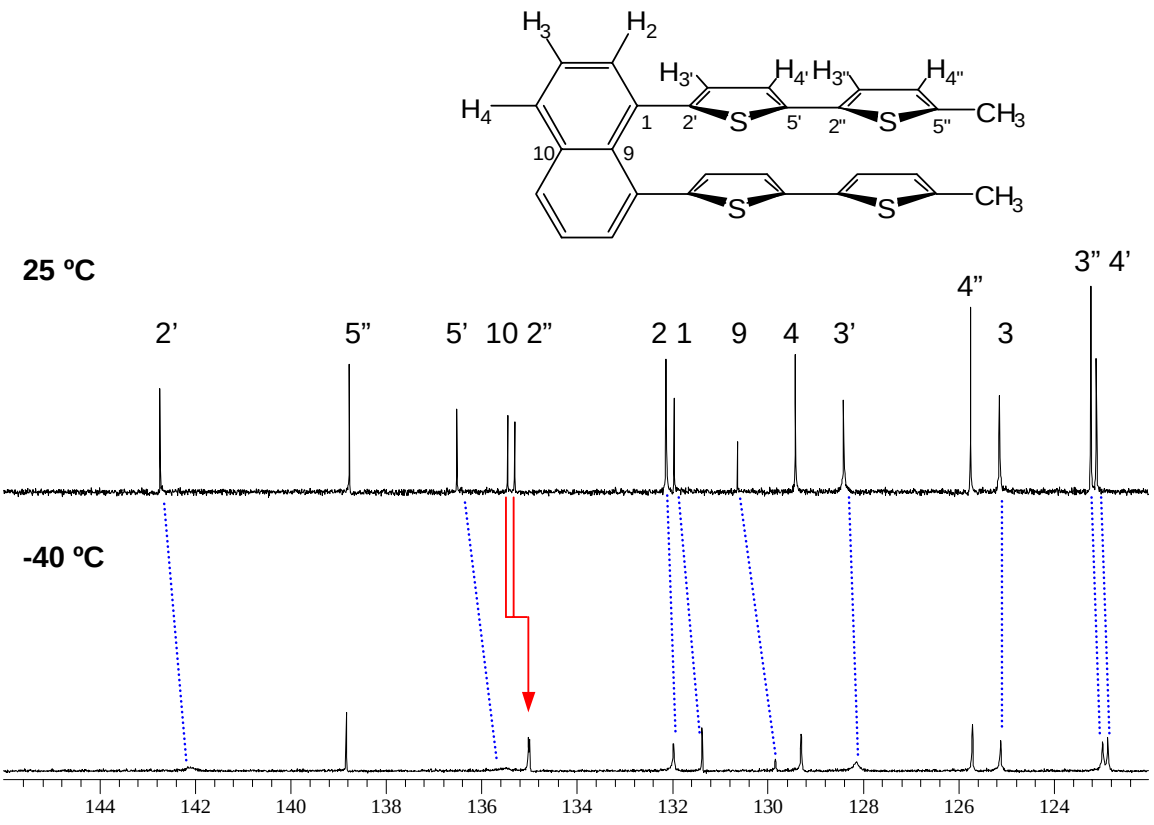

Figure 4.24. ^{13}C NMR spectra of **5 N-(Th$_2$Me)$_2$** at 25 ºC (top) and –40 ºC (bottom).

spectra (Figure 4.24, solid red lines) similar to those described above.

The ^{1}H and ^{13}C spectra of **7 N-(Th$_3$Me)$_2$** exhibit similar behavior to **5 N-(Th$_2$Me)$_2$**. Sharp ^{1}H signals at room temperature are consistent with a fully averaged conformation (Figure 4.25, top). Reduced rotational freedom at –40 °C is indicated by broadening of the signals at 2.5, 6.3, 6.61, 6.65, 6.88, and 6.95 ppm, which are assigned to the methyl and thienyl hydrogen nuclei (Figure 4.25, bottom). Changes in the ^{13}C spectra (Figure 4.26) again provide additional insight into molecular rotation. Upon cooling, resonances corresponding to the carbon nuclei at the 2, 3, and 4 position of the naphthalene (132, 125.3, and 129.5 ppm) and the 2', 3', and 4' positions of the innermost thiophene ring (142.7, 128.3, and 124.6 ppm) are significantly broadened (Figure 4.26, dotted lines). Signals corresponding to the thienyl carbon nuclei of the two outer

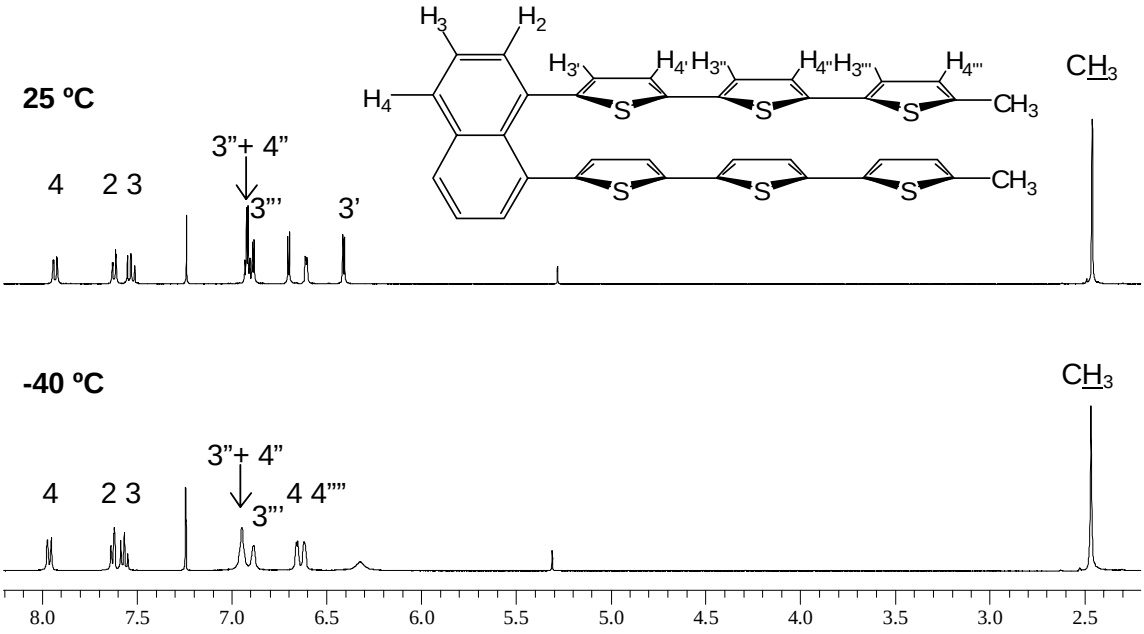

Figure 4.25. ^{1}H NMR spectra of **7 N-(Th$_3$Me)$_2$** at 25 ºC (top) and –40 ºC (bottom).

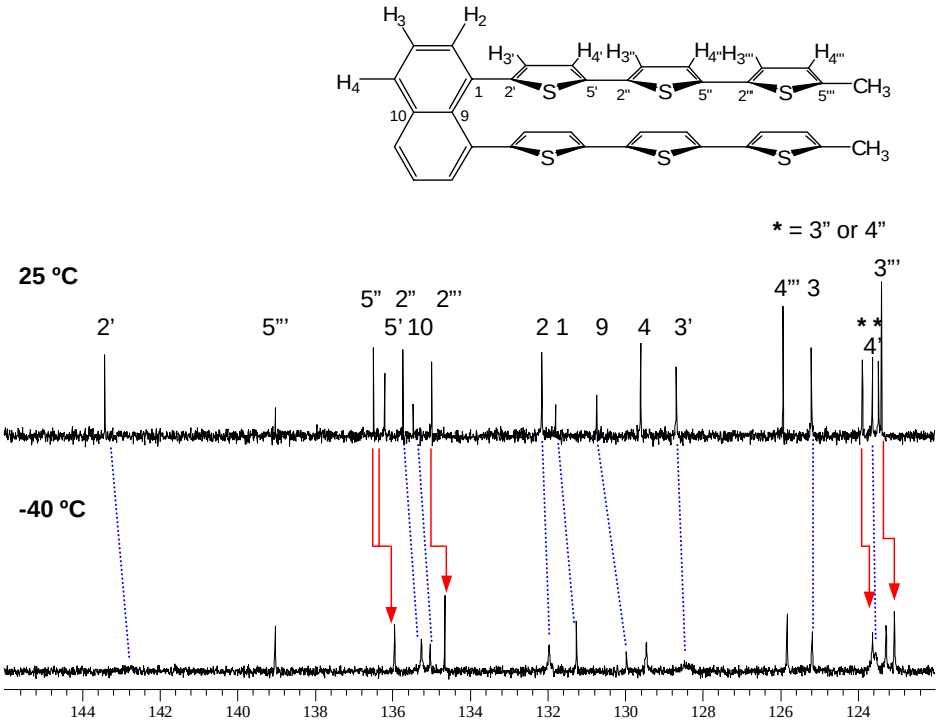

Figure 4.26. ^{13}C NMR spectra of **7 N-(Th$_3$Me)$_2$** at 25 ºC (top) and –40 ºC (bottom).

thiophene rings also exhibit broadening, but to a lesser degree (Figure 4.26, dotted lines). This is consistent with the model proposed for **5 N-($Th_2Me)_2$**, in which the more sterically-constrained inner thiophene ring rotates at a slower rate than the outer two thiophene rings, which are subject to fewer rotational constraints.

The energy of ring rotation for **5 N-($Th_2Me)_2$** was calculated with Spartan 04 (v. 1.01) using the AM1 semi-empirical method. The ground state geometry was optimized in an all-anti conformation. Separate calculations determined the energetics of anti-to-syn rotation around the naphthalene-thiophene bond and the thiophene-thiophene bond (corresponding to the inner and outer rings, respectively).

The energy profile for the rotation of the *inner* thiophene ring from a dihedral angle of -80 to -260° (Figure 4.27) reveals an energy barrier of approximately 3.6

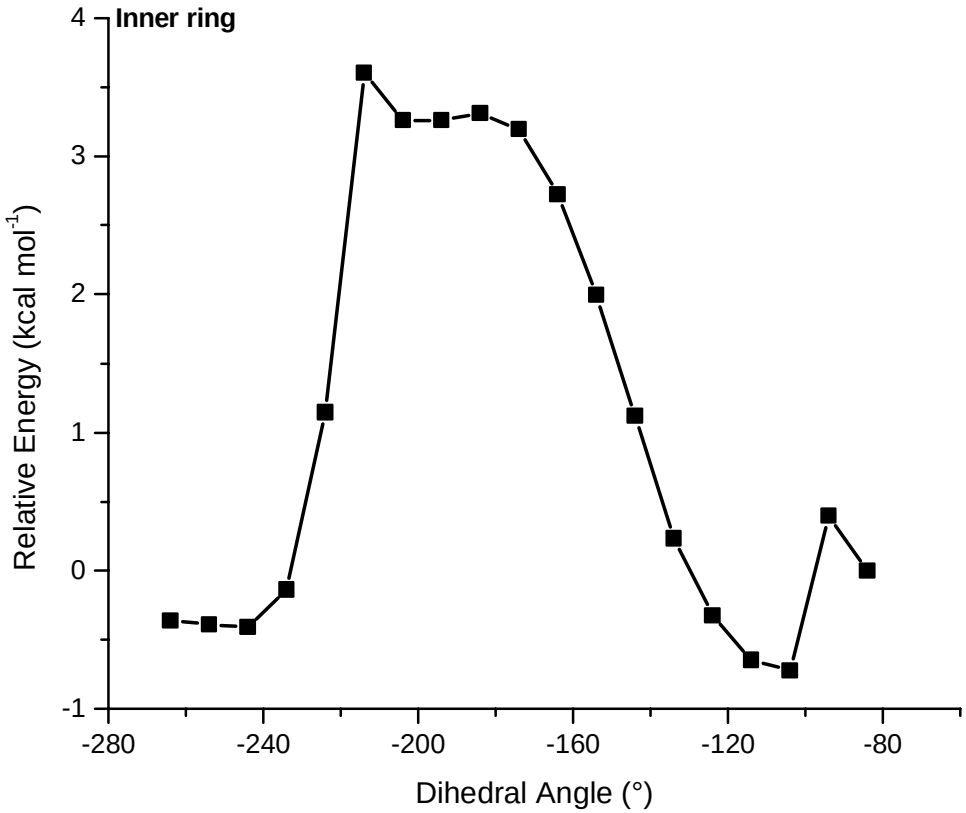

Figure 4.27. Calculated energy barrier to inner thiophene ring rotation for **5 N-($Th_2Me)_2$**.

kcal/mol at 25 °C, which is approximately $6k_bT$. This barrier is relatively low, indicating that the molecule is likely to sample all rotational states at room temperature. As the temperature of the sample decreases, the increase in conformational constraints results in a significant decrease in the rate of rotation. This decrease in rotation speed gives rise to the spectral broadening demonstrated by NMR (Figures 4.23 and 4.24). While the theoretical coalescence temperature (corresponding to complete resolution of two conformers, as seen by NMR) for a 3.6 kcal/mol barrier is likely to be very low (approximately –180 to -200 °C), it is reasonable to expect the broadening phenomenon seen in Figures 4.23 and 4.24.

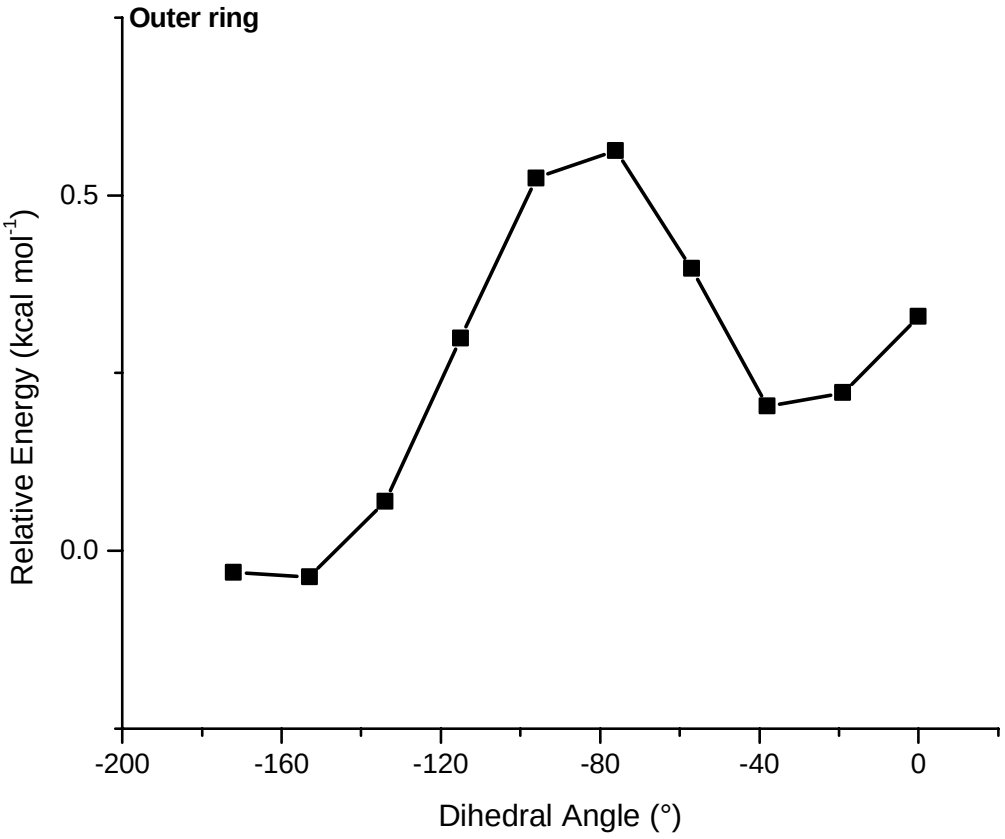

Figure 4.28. Calculated energy barrier to outer thiophene ring rotation for **5 N-(Th$_2$Me)$_2$**.

The energy profile for the rotation of the *outer* thiophene ring from -173 to 0° (Figure 4.28) reveals a much smaller energy barrier of approximately 0.56 kcal/mol at 25 °C, which is comparable to k_bT even at -40 °C. This supports the conclusion that the outer thiophene ring encounters a significantly smaller barrier to rotation than does the inner thiophene ring. This result is consistent with the variable temperature NMR data, which indicate that the outer thiophene is relatively free to rotate at both 25 and -40 °C. Due to a relatively small decrease in conformational constraints upon cooling, the small decrease in the speed of rotation gives rise to NMR signals that are only slightly broadened at -40 °C.

4.3.3: Absorption and Emission Spectroscopy of 1,8-Bis(oligothiophene)-substituted Naphthalenes

UV-visible and fluorescence spectroscopy, respectively, were used to examine the effect of oligomer length on absorption and emission properties. As expected, the λ_{max} values for absorption and emission each shift to higher wavelength as the oligomer length increases (Table 4.1). This red-shift is consistent with a decreased HOMO-LUMO transition due to increased conjugation length.

4.3.4: Effects of Structure on Electronic Properties of 1,8-Bis(oligothiophene)-substituted Naphthalenes

Cyclic voltammetry (CV) was used to determine the effect of molecular structure

Table 4.1. Absorption and emission maxima for **3 N-(ThMe)$_2$**, **5 N-(Th$_2$Me)$_2$**, and **7 N-(Th$_3$Me)$_2$**.

	$\lambda_{max, abs}$ (nm)	$\lambda_{max, em}$ (nm)
N-(ThMe)$_2$	318	365
N-(Th$_2$Me)$_2$	336	478
N-(Th$_3$Me)$_2$	371	497

Table 4.2. Oxidation and reduction potentials of **3 N-(ThMe)$_2$**, **5 N-(Th$_2$Me)$_2$**, and **7 N-(Th$_3$Me)$_2$**.

	Potential (V, vs. Ag/Ag$^+$ in CH$_2$Cl$_2$)											
	E_{1ox}	**E_{1red}**	**$E_{1,1/2}$**	**E_{2ox}**	**E_{2red}**	**$E_{2,1/2}$**	**E_{3ox}**	**E_{3red}**	**$E_{3,1/2}$**	**E_{4ox}**	**E_{4red}**	**$E_{4,1/2}$**
N-(ThMe)$_2$	1.28	1.16	1.22	1.53	1.42	1.48	--	--	--	--	--	--
N-(Th$_2$Me)$_2$	0.97	0.89	0.93	1.23	1.13	1.18	1.59[a]	1.48[a]	1.54[a]	--[a]	--[a]	--[a]
N-(Th$_3$Me)$_2$	0.82	--[b]	--[c]	1.03	0.96	1.00	1.33	1.24	1.29	1.46	--[b]	--[c]

[a] 3rd and 4th oxidations occur at similar potentials, resulting in a single, two electron signal at $E_{1/2}$ = 1.54 V
[b] peak not well-defined due to steep slope of the curve
[c] not calculable in the absence of well-defined reduction peak

on the electronic properties of **3 N-(ThMe)$_2$**, **5 N-(Th$_2$Me)$_2$**, and **7 N-(Th$_3$Me)$_2$** (Table 4.2). All experiments were performed using 2-6 mM analyte and 0.1 M *n*-Bu_4NPF_6 electrolyte in CH_2Cl_2 with an Au working electrode, Pt auxiliary electrode, and Ag/Ag^+ reference electrode at a scan rate of 100 mV/s. Hydrogen-terminated oligomers examined by Nakayama exhibit irreversible one electron oxidations ascribed to oxidative polymerization.[1-4] This is to be expected of oligothiophenes with unblocked α-termini.

The CV of **7 N-(Th$_3$Me)$_2$** (Figure 4.29) exhibits a first oxidation at E_{1ox} = + 0.82 V vs. Ag/Ag^+ in CH_2Cl_2 (Appendix E, Figure E.1), compared to + 0.5 V vs. Ag/Ag^+ in CH_3CN seen by Nakayama for the ummethylated analogue. It is reasonable to see an increase in E_{1ox} in a less polar solvent due to a decreased ability to solvate charged species. While Nakayama only observed one oxidation wave, a second oxidation wave

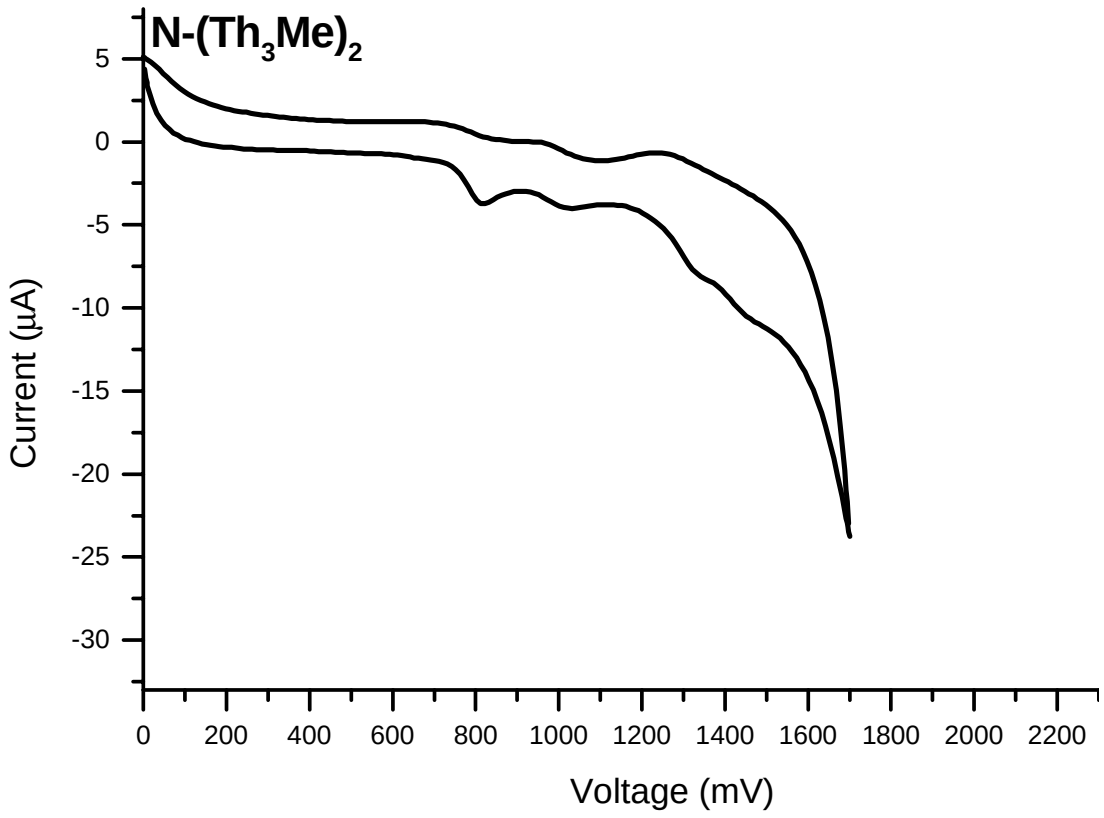

Figure 4.29. CV of **7 N-(Th$_3$Me)$_2$**.

(E_{2ox} = + 1.03 V) is observed in the case of **7 N-($Th_3Me)_2$**. Whereas it is difficult to say if E_{1ox} is reversible, the second oxidation *is* reversible based on the comparable areas under the E_{2ox} and E_{2red} peaks (Appendix E, Figure E.2.). Small waves in Figure 4.29 (E_{ox} = + 1.33 V and E_{4ox} = + 1.46 V) could be attributed to separate third and fourth oxidations; however, only one broad reverse wave is observed at +1.24 V (Appendix E, Figure E.3).

One possible interpretation of this data is that either: (i) sequential oxidation of **7 N-($Th_3Me)_2$** results in two waves, the first of which is only quasi-reversible, or (ii) an ECE process occurs after the first oxidation. As no evidence for the latter process (e.g, a highly colored solution or coating of the electrode) is observed, it is likely that the first explanation is valid.

The CV of **5 N-($Th_2Me)_2$** (Figure 4.28) displays similar behavior. A first

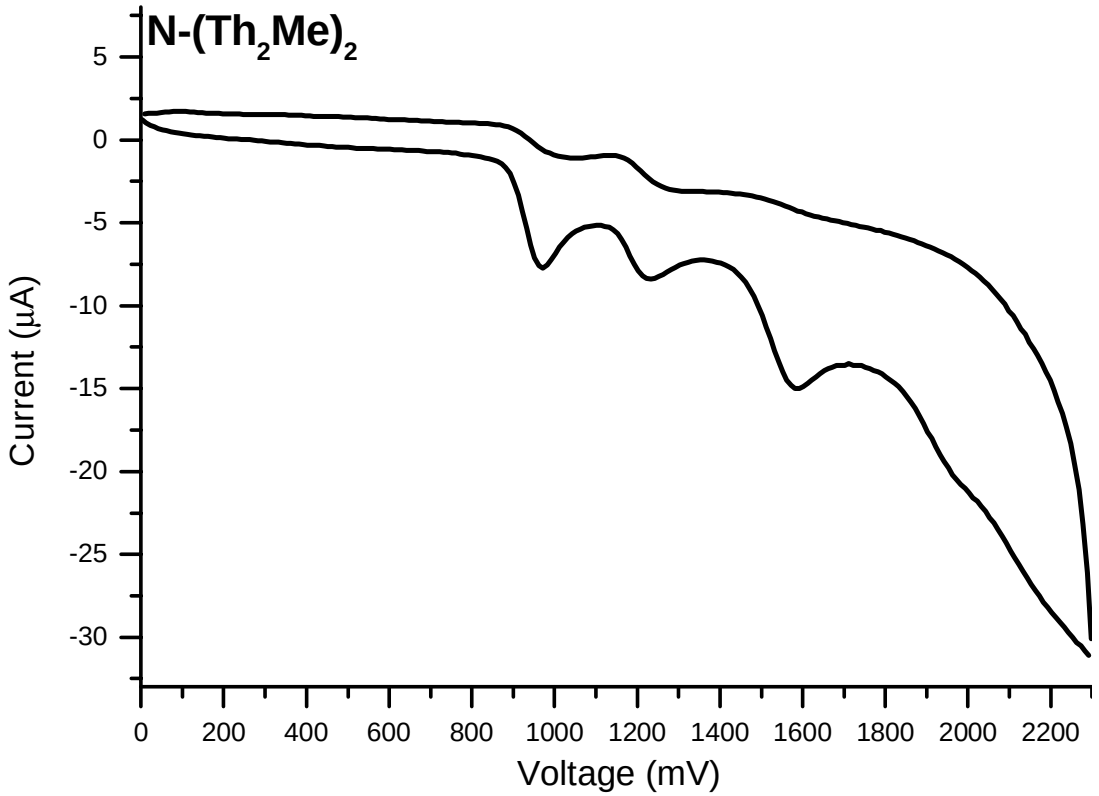

Figure 4.30. CV of **5 N-($Th_2Me)_2$**.

oxidation at E_{1ox} = + 0.97 V is likely to be quasi-reversible (Appendix E, Figure E.4). A second oxidation at E_{2ox} = + 1.23 V appears to be reversible (Appendix E, Figure E.5). As expected, both of these oxidation potentials are higher than the corresponding oxidation potentials of **7 N-($Th_3Me)_2$**, due to the lower conjugation length and ability to delocalize charge over the shorter oligomer chain length. An additional wave at E_{ox} = + 1.59 V could arise from a third and/or fourth oxidation process; however, only one reverse wave is observed at +1.48 V (Appendix E, Figure E.6).

The CV of **3 N-$(ThMe)_2$** (Figure 4.27, multiple cycles shown in Appendix E, Figure E.9) exhibits oxidation at E_{1ox} = + 1.28 V (Appendix E, Figure E.7). A second oxidation is visible at E_{2ox} = + 1.53 V, although no reverse wave is apparent (Appendix E, Figure E.8). As expected, both of these oxidation potentials are higher than the corresponding oxidation potentials of **5 N-($Th_2Me)_2$** and **7 N-($Th_3Me)_2$**, due to the further

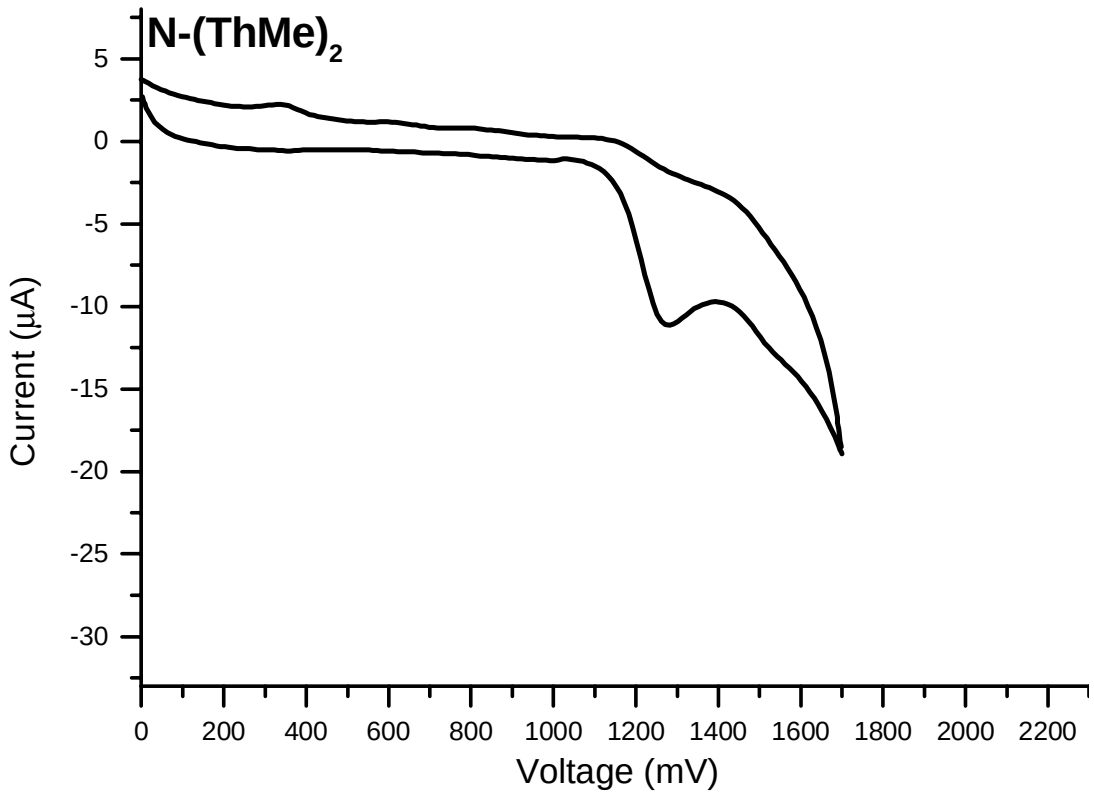

Figure 4.31. CV of **3 N-$(ThMe)_2$**.

decrease in conjugation length and ability to delocalize charge over the shorter oligomer chain length. Analysis of the cyclic voltammagrams precludes determination of reversibility vs. quasi-reversibility. While third and fourth oxidations may occur at high potential, no evidence of these processes is apparent.

Thus, although the two bithiophene tiers of the stacked compound are identical, they undergo separate one electron oxidations at different potentials. The ability of **3 N-(ThMe)$_2$**, **5 N-(Th$_2$Me)$_2$**, and **7 N-(Th$_3$Me)$_2$** to undergo multiple oxidations demonstrates that installation of blocking methyl groups at the α-termini of each oligomer arm prevents oxidative polymerization. This represents a significant enhancement in properties compared to the systems examined by Nakayama, as this stability is key to the use of such materials in electronic devices.

4.4: Conclusions

A family of 1,8-bis(oligothiophene) substituted naphthalenes, **3 N-(ThMe)$_2$**, **5 N-(Th$_2$Me)$_2$**, and **7 N-(Th$_3$Me)$_2$**, have been synthesized. Each structure was completely characterized using a variety of NMR techniques. Variable temperature ^{1}H and ^{13}C spectroscopy confirmed that each molecule undergoes a decrease in rotational freedom with decreasing temperature. Additionally, these spectra revealed that multiple rates of rotation exist in **5 N-(Th$_2$Me)$_2$** and **7 N-(Th$_3$Me)$_2$**, based on the proximity of a given thiophene ring to the 1,8-bis substituted naphthalene core. Cyclic voltammetry confirmed that the installation of methyl groups at the terminus of each thiophene oligomer prevents oxidative polymerization, a key property not observed in previously reported compounds.[1-3] As expected, oxidation potentials decrease with increases in oligomer length. These results will form the basis for expansion of this work, as discussed in Chapter 5.

4.5: References

1. Kuroda, M.; Nakayama, J.; Hoshino, M. *Tetrahedron Lett.* **1992**, *33*, 7553.

2. Kuroda, M.; Nakayama, J.; Hoshino, M.; Furusho, N.; Kawata, T.; Ohba, S. *Tetrahedron* **1993**, *49*, 3735.

3. Kuroda, M.; Kosho, N.; Nakayama, J.; Hoshino, T. *Jpn. Kokai Tokkyo Koho* **1993**, *Patent JP 92-52963 19920312*.

4. Kuroda, M.; Nakayama, J.; Hoshino, M.; Furusho, N.; Ohba, S. *Tetrahedron Lett.* **1994**, *35*, 3957.

5. Iyoda, M.; Nakao, K.; Kondo, T.; Kuwatani, Y.; Yoshida, M.; Matsuyama, H.; Fukami, K.; Nagase, S. *Tetrahedron Lett.* **2001**, *42*, 6869.

6. Hodgson, H. H.; Whitehurst, J. S. *J. Chem. Soc.* **1947**, 80.

7. Bossenbroek, B.; Sanders, D. C.; Curry, H. M.; Shechter, H. *J. Amer. Chem. Soc.* **1969**, *91*, 371.

8. Seyfirth, D.; Vick, S. C. *J. Organomet. Chem.* **1977**, *141*, 173.

9. Vyskocil, S.; Meca, L.; Tislerova, I.; Cisarova, I.; Polasek, M.; Harutyunyan, S. R.; Belokon, Y. N.; Stead, R. M. J.; Farrugia, L.; Lockhart, S. C.; Mitchell, W. L.; Kocovsky, P. *Chem. Eur. J.* **2002**, *8*, 4633.

10. House, H. O.; Koepsell, D. G.; Campbell, W. J. *J. Org. Chem.* **1972**, *37*, 1003.

11. Tamao, K.; Kodama, S.; Nakajima, I.; Kumada, M.; Minato, A.; Suzuki, K. *Tetrahedron* **1982**, *38*, 3347.

12. McCullough, R. D.; Lowe, R. D. *J. Chem. Soc., Chem. Commun.* **1992**, 70.

13. Garnier, F.; Yassar, A.; Hajlaoui, R.; Horowitz, G.; Deloffre, F.; Servet, B.; Ries, S.; Alnot, P. *J. Amer. Chem. Soc.* **1993**, *115*, 8716.

14. Li, L.; Counts, K. E.; Kurosawa, S.; Teja, A. S.; Collard, D. M. *Adv. Mater.* **2004**, *16*, 180.

15. MacEachern, A.; Soucy, C.; Leitch, L. C.; Arnason, J. T., Morand, P. *Tetrahedron* **1988**, *44*, 2403.

16. Nakayama, J.; Nakamura, Y.; Tajiri, T.; Hoshino, M. *Heterocycles* **1986**, *24*, 637.

CHAPTER 5: FUTURE WORK

5.1: Future Directions for Poly(3-semifluoroalkylthiophene)s

Aspects of the work discussed in Chapters 2 and 3 could potentially be expanded upon. Based on existing data, it is still not possible to make *a priori* structure-property predictions of the liquid crystallinity of a given semifluoroalkyl-substituted homopolymer based on m and n values. Additional **RgTh(m,n)** homologues could be synthesized in an attempt to gain additional insights. However, it should be noted that even the best synthetic route to these polymers is particularly low-yielding (5-10% overall yield) and labor intensive due to difficulty in purifying synthetic intermediates. Moreover, a predictive model is by no means a guaranteed result.

The use of semifluoroalkyl-substituted homopolymers and copolymers in (opto)electronic devices is complicated by the limited solubility of these materials in common organic solvents at room temperature. This insolubility is incompatible with standard FET fabrication methods. Block copolymerization of the semifluoroalkyl-substituted, rigid rod segment with a solubilizing, aliphatic block may increase the solubility of these materials while imparting an additional degree of control over their physical and thermal properties.[1-3] The advances in block copolymerization of regioregular poly(3-alkylthiophene)s by McCullough and others establishes ample precedent for this approach.[1-5] Depending on the identity of the second block, these copolymers could be used in FETs, LEDs, solar cells, or sensors.[6-8] Additional fabrication techniques could be developed or modified for compatibility with semifluoroalkyl-substituted materials.

5.2: Future Directions for Cofacial 1,8-Bis(oligothiophene)-Substituted Naphthalenes

Solubility is also expected to play a role in future generations of stacked oligothiophenes, especially as the number of aromatic rings increases. Substitution of the rings at the β-position(s) with methyl or other alkyl groups would increase solubility; introduce a rotational barrier that should encourage π-stacking; and allow electrochemical tuning.[9,10] Additional alkyl functionality could be introduced at the termini of the oligomers or on the naphthalene core for the purposes of solubility; alternatively, functional end groups could be added at these positions to facilitate later coupling.[11-13] Synthesis of unstacked oligomers (examples shown in Figure 5.1) would provide an additional set of model compounds to elucidate the effect of π-π interactions in comparison to stacked analogues.

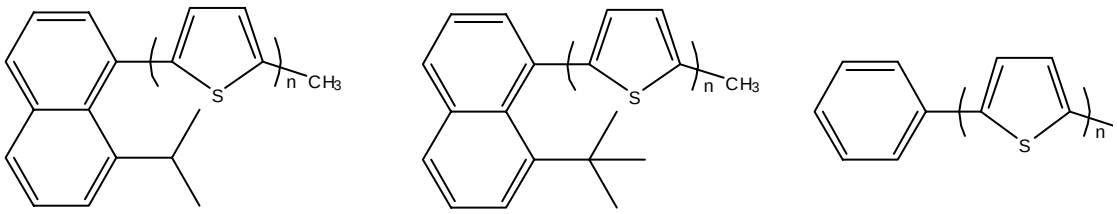

Figure 5.1. Possible unstacked oligomer model compounds.

As discussed in Chapter 4, Nakayama and Iyoda have each examined hydrogen-terminated multi-stacked systems. As is true of the two-arm oligomer systems, the unsubstituted α-termini of these multi-stacked molecules render them susceptible to oligomerization upon oxidation and therefore unsuitable for examination of excited states.[11, 12] The first generation of molecules described in Chapter 4 could evolve into a

more complex second generation of extended, multi-stacked oligomers (Figure 5.2), which could self-assemble to form supramolecular wires useful in (opto)electronic applications.

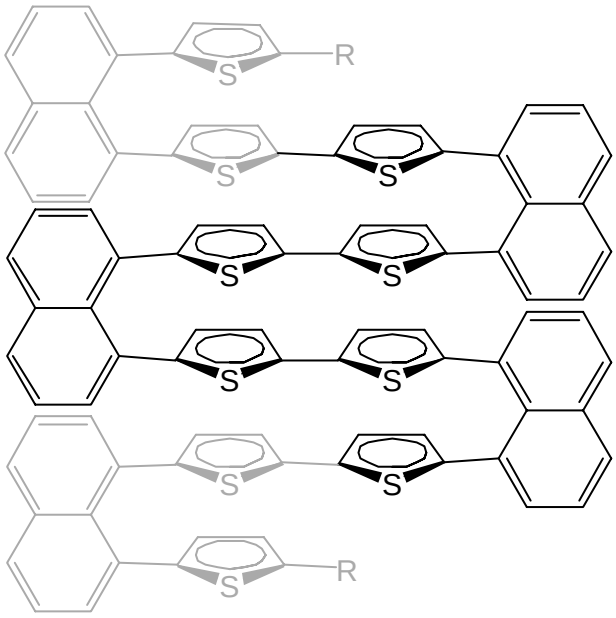

Figure 5.2. Example of a proposed multi-stacked system, which extends (gray) Iyoda's existing system (black). R = alkyl.

5.3: References

1. Iovu, M. C.; Craley, C. R.; Jeffries-El, M.; Krankowski, A. B.; Zhang, R.; Kowalewski, T.; McCullough, R. D. *Macromolecules* **2007**, *40*, 4733.

2. Iovu, M. C.; Jeffries-El, M.; Zhang, R.; Kowalewski, T.; McCullough, R. D. *J. Macromol. Sci., Part A: Pure Appl. Chem.* **2006**, *43*, 1991.

3. Liu, J.; Sheina, E.; Kowalewski, T.; McCullough, R. D. *Angew. Chem., Int. Ed.* **2002**, *41*, 329.

4. Radano, C. P.; Scherman, O. A.; Stingelin-Stutzmann, N.; Mueller, C.; Breiby, D. W.; Smith, P.; Janssen, R. A. J.; Meijer, E. W. *J. Amer. Chem. Soc.* **2005**, *127*, 12502.

5. Iovu, M. C.; Jeffries-El, M.; Sheina, E. E.; Cooper, J. R.; McCullough, R. D.

Polymer **2005**, *46*, 8582.

6. Sauve, G.; McCullough, R. D. *Adv. Mater.* **2007**, *19*, 1822.

7. Sauve, G.; Zhang, R.; Jia, S.; Kowalewski, T.; McCullough, R. D. *Proceedings of SPIE-The International Society for Optical Engineering* **2006**, *6336*, 633614/1.

8. Li, B.; Sauve, G.; Iovu, M. C.; Jeffries-El, M.; Zhang, R.; Cooper, J.; Santhanam, S.; Schultz, L.; Revelli, J. C.; Kusne, A. G.; Kowalewski, T.; Snyder, J. L.; Weiss, L. E.; Fedder, G. K.; McCullough, R. D.; Lambeth, D. N. *Nano Lett.* **2006**, *6*, 1598.

9. Clough, R. L.; Roberts, J. D. *J. Amer. Chem. Soc.* **1976**, *98*, 1018.

10. Kuroda, M.; Nakayama, J.; Hoshino, M.; Furusho, N.; Kawata, T.; Ohba, S. *Tetrahedron* **1993**, *49*, 3735.

APPENDIX A: STUDENTS REPAIRING THE LEAKY PIPELINE: THE GEORGIA TECH WOMEN IN CHEMISTRY COMMITTEE

A.1: Introduction

Although women and minorities currently earn 34% and 7%, respectively, of Ph.D.s in Chemistry,[1,2] they remain underrepresented at the highest levels of academia, industry, and government. Table A.1 shows the percentage of female faculty at top 50 research-active Chemistry departments over a six year period.[3] Underrepresented racial minorities comprise approximately 4% of tenure-track faculty members at such institutions.[4] Similar underrepresentation at increasing levels of responsibility is also present in industrial and government organizations.[5] Gender and racial equity is a business and economic imperative, especially as the United States faces a shortage in the domestic chemistry workforce and increased global competition in the chemistry sector.[6] The number of Ph.D.s earned by U.S. citizens and permanent residents decreased from 1,170 to 1,131, a 3.3% decline, between 1996 and 2005. Over the same period, the percentage of total Ph.D.s earned by international students increased from 28.7% to 37.5%.[7] Because employers in the chemical sciences are currently obliged to meet their hiring needs with qualified non-U.S. citizens, the implications of such educational trends on the domestic workforce are numerous. As the population of Caucasian male

Table A.1. Percentage of female tenure-track faculty at top 50 funded chemistry departments.[2]

	2000	*2001*	*2002*	*2003*	*2004*	*2005*	*2006*
Assistant Professor	18%	20%	21%	21%	20%	21%	21%
Associate Professor	21%	20%	20%	20%	19%	21%	22%
Full Professor	6%	7%	7%	8%	8%	9%	10%
All Professors	10%	11%	12%	12%	12%	13%	14%

chemists—who have historically comprised the majority of the field's workforce—is on the decline,[7] it is critical to engage women and underrepresented minorities to fill this void. A diverse workforce, however, is *more* than economically driven—it is also a moral and ethical imperative.

The dearth of females in science, technology, engineering, and mathematics (STEM) has often been attributed to few women pursuing careers in technical fields, or insufficient 'lag time' to allow the employment rates to 'catch up' to the educational rates. However, these suggestions are not supported by statistics. Women have earned greater than 25% of all Ph.D.s in Chemistry since the late 1980s—rising to 34% by the mid-2000s—yet after nearly three tenure cycles comprise only 10% of full professors.[1,3,8] Therefore, the underrepresentation of women at higher levels of STEM careers is best explained by the leaky pipeline hypothesis (Figure A.1), whereby qualified candidates

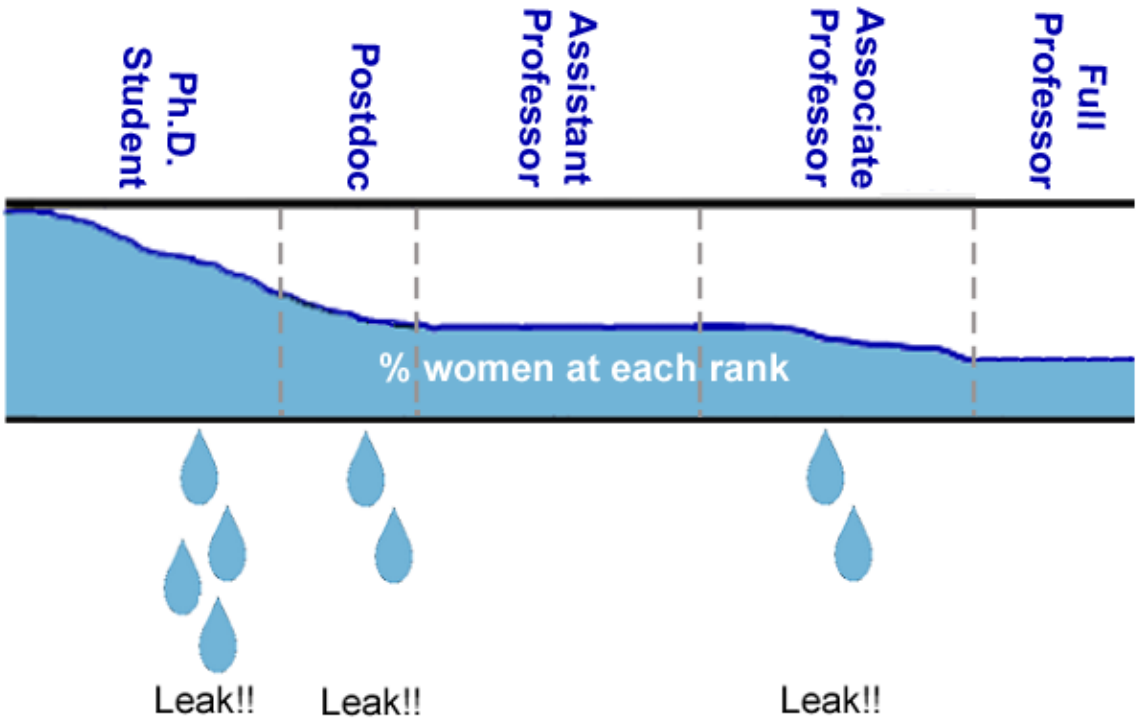

Figure A.1. Representation of the 'leaky pipeline' characterizing the exodus of women from careers in STEM. Here, a 'full' pipeline corresponds to 50% women entering Ph.D. programs.

self-select out of careers in STEM due to an accumulation of disadvantages compared to their male counterparts. This takes place when considering graduate study, during graduate study, and at the conclusion of Ph.D. work. Although the pipeline for minorities is significantly less full to begin with,[2] the trend still holds; members of underrepresented racial minorities constitute a tiny fraction of the tenure-track faculty at research institutions (52 of 1484 total professors in FY2003).[4] As the rate of women earning tenure is comparable to the rate of women beginning tenure-track positions (Table A.1), programs that focus on the retention of existing faculty members—such as the NSF ADVANCE initiative and the Committee on the Advancement of Women Chemists (COACh)—appear to be effective. The number of similar programs to retain and promote women and minorities in industry is on the rise.

Women and minorities remain underrepresented in the ranks of research faculty and upper-level industry leadership because the pipeline to careers in STEM fields hemorrhages before, during, and immediately following the Ph.D. due to self-selection.[8,9] Successful programs exist to promote and support women in science from preschool through the workplace, but they are rare at the graduate school level. The scarcity of endeavors focused on encouraging graduate women and minorities to continue in the sciences after earning their Ph.D.s is a major contributor to the leak in the pipeline. As these students already 'in the pipeline' face imminent decisions about pursuing STEM careers, it is imperative that programs are created to repair this leak, retain students who obtain advanced degrees, and establish underrepresented groups in scientific careers. Such endeavors must focus on developing programs and practices that engage, enable, and inspire female and minority Ph.D.-scientists-in-training to achieve their full potential. As members of these populations continue through the pipeline, attain high-level positions, and influence future generations of scientists, it is reasonable to expect an autocatalytic effect on climate that will ultimately change the face of academic,

industrial, and government chemistry.

A.2: Program Description

The Georgia Tech Women in Chemistry Committee was founded in 2004 by a group of graduate students and postdoctoral associates in the School of Chemistry and Biochemistry to provide support for female scientists and to raise awareness of and propose solutions to challenges faced by women in science, specifically chemistry. In its first year, the Committee expanded selected initiatives to include undergraduates, faculty, and staff from a variety of colleges and universities in the metro Atlanta area. The Committee has created programs that address a broad range of female scientists' needs, ranging from hosting workshops and symposia to advocating for family-friendly parental leave and childcare policies. With initiatives aimed at leveling the playing field for women and other minorities, the Committee works to create a more inclusive, supportive environment for all chemists.

A.3: Committee Accomplishments

A.3.1. The Georgia Tech Women in Chemistry Committee raises awareness of and promotes solutions to challenges faced by female and minority scientists.

The inaugural Women in Chemistry Symposium (October 2005) was a full-day event for over 100 undergraduate and graduate students; faculty and administrators; and government and industry scientists from the greater Atlanta area. Participants were affiliated with fifteen companies, government labs, and educational institutions, including two Historically Black Colleges and Universities (HBCUs) and a women's college. The Committee obtained funding from the Georgia Tech NSF ADVANCE Program, the College of Sciences, the School of Chemistry and Biochemistry, the Center for Organic Photonics and Electronics, and an alumni donation. Events included networking sessions and a series of issue-focused panel discussions and roundtable talks featuring 21 regional

and national speakers. Keynote addresses were given by Professors Mary Frank Fox (co-director of the Georgia Tech NSF ADVANCE program), Geraldine Richmond (chair of the Committee on the Advancement of Women Chemists), and Karen Wooley (Washington University in St. Louis). Each participant was given a folder containing information on resources and suggested readings. Results of small-group roundtable discussions were summarized and disseminated to all participants by email. Feedback generated by surveys and evaluations established focus areas for future Committee activities. Funding for future programs was obtained; execution of these activities has established the Committee as a sustainable program in metro Atlanta.

The Committee co-hosted, with the School of Chemistry and Biochemistry, a town hall-style meeting for female graduate students to learn more about their challenges and concerns. Discussion topics included raising a family while in school; developing appropriate personal and professional skills; and encountering particular challenges as racial minorities. Committee members presented the summarized information at a School faculty meeting and followed up with department-wide surveys about programming and family-friendly policies.

A.3.2. WIC advocates for institutional policies that benefit all graduate students and postdoctoral associates.

Committee representatives worked with the School to establish accommodation guidelines for maternity and paternity leave, personal illness or injury, and family emergencies. These are the first such guidelines at Georgia Tech. To the best of our knowledge, fewer than 10 other Chemistry programs in the nation have such a initiative. WIC members—in conjunction with the School Chair, Dean of Students, and Women's Resource Center—advocate for accessible, affordable, on-campus childcare for the children of students and postdoctoral associates.

A.3.3. The Committee develops activities to promote personal and professional development, based on constituent feedback.

WIC promoted interaction between students and faculty, inspiring several students, postdocs, and faculty to establish an informal lunch group. The Committee hosted informal mentoring receptions to allow graduate students to meet potential senior student, postdoc, and faculty mentors. Committee representatives worked with the School of Chemistry and Biochemistry to design a formal mentoring program for all incoming Chemistry graduate students.

WIC arranged the funding and logistics necessary to sponsor a COACh (Committee on the Advancement of Women Chemists) professional development workshop for 43 graduate students in October 2006. Funding was obtained from the School of Chemistry and Biochemistry, from the Center for Organic Photonics and Electronics, and through a competitive grant from COACh. This negotiation skills workshop was paired with workshops on thesis and grant writing. Participants included graduate students and postdoctoral associates from several majors at Georgia Tech, Georgia State University, the University of Arizona, and the University of Washington. Feedback from participants indicated that this workshop was an empowering, formative step in their professional development. This event was recognized with the 2007 American Chemical Society's Women Chemists Committee ChemLuminary Award for Outstanding Single Event Promoting Women.

The Committee proposed a collaboration with the Georgia Tech Women's Resource Center (WRC) and established informal, topical monthly lunches for graduate women in a variety of majors. The pilot program incorporating chemistry, physics, and math students was very successful and has expanded to include all graduate majors. This initiative has led the WRC to establish a Graduate Women's Council and additional programming to specifically serve graduate women.

A.3.4. Women in Chemistry sponsors activities to benefit the local community.

Food remaining after Committee events has been donated to the Atlanta Day Shelter for women and children. The Committee sponsored a School-wide food drive to benefit the Atlanta Community Food Bank.

A.3.5. WIC disseminates relevant information from local and national sources.

A web page (http://web.chemistry.gatech.edu/~wic) was created to serve as a repository for Committee information, local activities, and resource material. An email list communicates timely announcements about news and events to subscribing graduate students and postdoctoral associates.

A.3.6. WIC encourages others to establish similar programs.

The Committee's work was presented at the American Association for the Advancement of Science Annual Meeting (February 2006, St. Louis); in the Workforce of the Future Symposium at the ACS National Meeting (March 2006, Atlanta); and at the Southeastern Regional Meeting of the American Chemical Society (November 2006, Augusta, GA). The organization's successes have catalyzed the formation of a similar organization in the Georgia Tech Woodruff School of Mechanical Engineering.

Thus, WIC has created an embryonic program with the aim of developing a sustainable initiative to repair the leaky pipeline for minorities and women at the graduate level. Receipt of the American Chemical Society's 2006 Stanley C. Israel Award for Advancing Diversity in the Chemical Sciences focused attention on student-driven contributions to this important, ongoing effort.

A.4: Future Work

The Women in Chemistry Committee will continue to establish itself as a sustainable, student-driven entity in the School of Chemistry and Biochemistry. Existing partnerships (e.g., with the Women's Resource Center and Center for Organic Photonics

and Electronics) may continue, and new partnerships (e.g., with two newly formed entities, the Georgia Tech chapter of the National Organization of Black Chemists and Chemical Engineers, NOBCChE, and the local American Chemical Society's Women Chemists Committee) may be developed. The Committee's focus and programs will evolve as necessary, based on the needs of graduate students in the School. New programs, such as an annual guest lecture by a prominent female chemist, will continue the transformation of the Georgia Tech School of Chemistry and Biochemistry into a diverse, supportive environment.

A.5: Conclusion

A diverse workforce approaches challenges from a range of perspectives, fostering creativity and driving innovation. Repairing the leaky pipeline and retaining existing students will strengthen the domestic technology workforce, thereby enhancing U.S. competition in the technology sector and boosting the national economy. Broader representation of underrepresented minorities in chemical professions will provide positive role models for the next generation of scientists and engineers. The Georgia Tech Women in Chemistry Committee's lasting contribution to institutional transformation will continue to benefit *all* chemists, the chemical profession, and society at large.

A.6: References

1. Heylin, M. *Chem. Eng. News* **2006**, *84*, 43.
2. Heylin, M. *Chem. Eng. News* **2006**, *84*, 57.
3. Marasco, C. *Chem. Eng. News* **2006**, *84*, 58.
4. Nelson, D. *A national analysis of diversity of science and engineering faculties at research universities,* **2005**. http://cheminfo.chem.ou.edu/~djn/diversity/briefings/Diversity%20Report%20Final.pdf.
5. Tullo, A. *Chem. Eng. News* **2006**, *84*, 22.

6. *Rising above the gathering storm: energizing and employing America for a brighter economic future*, National Academies Press, **2006**.

7. *Survey of earned doctorates*, National Science Foundation, **2005**. http://www.nsf.gov/statistics/srvydoctorates/.

8. Marasco, C. *Chem. Eng. News* **2003**, *81*, 58.

9. Handelsman, J.; Cantor., N.; Carnes, M.; Denton, D.; Fine, E.; Grosz, B.; Hinshaw, V.; Marrett, C.; Rosser, S.; Shalala, D.; Sheridan, J. *Science* **2005**, *309*, 1190.

APPENDIX B: DETAILED PROCEDURES FOR THE SYNTHESIS OF 3-(IODO SEMIFLUOROALKYL) THIOPHENES, 2(m,n)

General method for synthesis of 3-(iodo semifluoroalkyl) thiophenes

A mixture of **1(m)**, AIBN, and the corresponding perfluoroalkyl iodide was stirred under N_2 for 30 minutes in a 50 mL round-bottomed flask and then heated to 70-80 ºC. (Reactions containing perfluorobutyl iodide were heated to 60°C with a condenser to prevent loss of reagent.) Synthesis of **2(8,4)** and **2(8,3)** was carried out in a sealed Schlenk tube under N_2. In some cases, the reaction was initially catalyzed by BPO, but sluggish conversion necessitated replacement by AIBN. The degree of conversion was monitored by ^{1}H NMR, and additional AIBN and perfluoroalkyl iodide were added as shown in Tables B.1-B.7 to ensure continued reaction. In some cases, decomposed or unreacted catalyst, perfluoroalkyl iodide, and/or perfluoroalkyl byproduct were removed during the course of the reaction under reduced pressure or by filtering the mixture through silica gel with petroleum ether and removing the solvent, excess reagent, and byproduct under reduced pressure. The separation of product from the **1(m)** starting material proved particularly challenging; in most cases, the purification was discontinued after a sufficient amount of pure product was obtained to proceed with the next step in the reaction sequence. This accounts for the discrepancy between the moderately high degree of conversion and the relatively modest yields. Column chromatography (silica gel, petroleum ether) gave product **2(m,n)** as either a clear, colorless liquid or a white solid.

3-(4-Iodo-6,6,7,7,8,8,9,9,10,10,11,11,12,12,13,13,13-heptadecafluorotridecyl) thiophene, 2(5,8). Treatment of **1(5)** (5.92 g, 39.0 mmol) with AIBN (322 mg, 1.96 mmol) and perfluorooctyl iodide (2.83 mL, 10.7 mmol) was followed by treatment as described in Table B.1. The reaction mixture was subjected to reduced pressure to remove any unreacted $F(CF_2)_8I$. Column chromatography (silica gel, petroleum ether) gave **2(5,8)** as a white solid (12.5 g, 46.1%), mp 44–46 °C.

Table B.1. Reaction progress for the synthesis of **2(5,8)**.

Time (h)	% conversion	Catalyst added (g)	$F(CF_2)_8I$ added (mL)	Notes
0	0	0.3218	2.83	AIBN as catalyst
15	--	--	2.83	
22	--	--	2.83	
38	--	--	2.83	
68	26	0.3200	2.83	
118	50	0.3200	2.83	
142	62	--	--	
166	--	--	--	pumped down at RT for 4 h and let stand at RT overnight
182	--	0.3200	2.18	
206	78	--	2.18	
302	78			
378	--	0.1600	1.25	
382	--	--	1.25	
406	--	0.1600	1.25	
429	81	0.3223	3.28	
477	85	--	--	pumped down overnight
501	--	0.3237	1.70	
549	86	--	--	cooled to RT, pumped down

3-(4-Iodo-6,6,7,7,8,8,9,9,10,10,11,11,11-tridecafluoroundecyl)thiophene, 2(5,6). Treatment of **1(5)** (6.11 g, 40.2 mmol) with AIBN (330 mg, 2.01 mmol) and perfluorohexyl iodide (2.40 mL, 11.0 mmol) was followed by treatment as described in Table B.2. The reaction mixture was subjected to reduced pressure to remove any unreacted $F(CF_2)_6I$. Column chromatography (2 successive columns, silica gel, petroleum ether) gave **2(5,6)** as a clear, colorless liquid (5.86 g, 24.4%).

Table B.2. Reaction progress for the synthesis of **2(5,6)**.

Time (h)	% conversion	Catalyst added (g)	$F(CF_2)_6I$ added (mL)	Notes
0	0	0.3298	2.40	AIBN as catalyst
15	--	--	2.40	
22	--	--	2.40	
38	--	--	2.40	
68	27	0.3300	2.40	
118	45	0.3300	2.64	
190	57			
214	--	--	--	cooled to RT, pumped down, let stand
238	67	0.3300	2.10	
257	--	--	2.10	
353	69	--	--	
425	--	0.1650	1.58	
430	--	--	1.58	
478	--	0.1680	1.58	
501	72	0.3381	1.96	
525	73	--	--	
549	--	--	--	cooled to RT, pumped down, let stand
573	--	0.3288	1.90	
645	86	--	--	cooled to RT, pumped down

3-(10-Iodo-12,12,13,13,14,14,15,15,16,16,17,17,18,18,19,19,19-heptadecafluorononadecyl) thiophene, 2(11,8). Treatment of **1(11)** (1.58 g, 5.87 mmol) with BPO (74 mg, 305 μmol) and perfluorooctyl iodide (1.70 mL, 6.44 mmol) was followed by treatment as described in Table B.3. The reaction mixture was subjected to reduced pressure to remove any unreacted $F(CF_2)_8I$. Column chromatography (2 columns, silica gel, petroleum ether) gave **2(11,8)** as a white solid (863 mg, 18.0%).

Table B.3. Reaction progress for the synthesis of **2(11,8)**.

Time (h)	% conversion	Catalyst added (g)	$F(CF_2)_8I$ added (mL)	Notes
0	0	0.0740	1.70	BPO as catalyst
72	10	--	--	
96	10	0.0490		switched to AIBN catalyst
120	41	--	--	
144	41	0.0460	1.02	
168	54	--	--	
192	66	0.0490	0.78	
264	67	0.0474	0.56	
336	73	--	--	
360	--	0.0497	0.23	
384	--	--	0.23	
432	--	0.0480	0.30	cooled to RT, pumped down for 2 h prior to next addition
456	--	--	0.30	
480	85	0.0400	0.13	
528	86			
672	--	0.0400	0.12	cooled to RT, filtered through silica plug, pumped down prior to next addition
696	87	--	0.12	
888	87	--	--	cooled to RT, filtered, pumped down

3-(10-Iodo-12,12,13,13,14,14,15,15,16,16,17,17,17-tridecafluoroheptadecyl)thiophene, 2(11,6). Treatment of **1(11)** (4.17 g, 15.9 mmol) with BPO (195 mg, 804 μmol) and perfluorohexyl iodide (3.80 mL, 17.5 mmol) was followed by treatment as described in Table B.4. The reaction mixture was subjected to reduced pressure to remove any unreacted $F(CF_2)_6I$. Column chromatography (silica gel, petroleum ether) gave **2(11,6)** as a clear, colorless liquid (2.31 g, 20.5%).

Table B.4. Reaction progress for the synthesis of **2(11,6)**.

Time (h)	% conversion	Catalyst added (g)	$F(CF_2)_6I$ added (mL)	Notes
0	0	0.1946	3.80	BPO as catalyst
72	12	0.1360	--	switched to AIBN catalyst
96	40	--	--	
120	42	0.1308	2.20	
144	51	--	--	
168	51	0.1352	1.90	
240	57	0.1362	1.63	
312	63	--	--	
336	--	0.1320	0.70	
360	--	--	0.70	
408	--	0.1336	0.57	cooled to RT, pumped down for 2 h prior to addition
432	--	--	0.57	
456	75	0.1318	0.48	
504	80	--	--	
576	--	0.1308	0.38	cooled to RT, filtered through short silica plug to remove catalyst residue, then pumped down prior to addition
600	--	--	0.38	
624	81	--	0.29	
672	84	--	0.29	
840	85			cooled to RT, pumped down

3-(10-Iodo-12,12,13,13,14,14,15,15,15-nonafluoropentadecyl)thiophene, 2(11,4). Treatment of **1(11)** (4.30 g, 16.4 mmol) with AIBN (137 mg, 837 μmol) and perfluorobutyl iodide (3.10 mL, 18.3 mmol) was followed by treatment as described in Table B.5. The reaction mixture was subjected to reduced pressure to remove any unreacted $F(CF_2)_4I$ and perfluorooctane. Column chromatography (silica gel, petroleum ether) gave **2(11,4)** as a clear, colorless liquid (1.96 g, 20.2%).

Table B.5. Reaction progress for the synthesis of **2(11,4)**.

Time (h)	% conversion	Catalyst added (g)	$F(CF_2)_4I$ added (mL)	Notes
0	0	0.1375	3.10	used a water-jacketed condenser, AIBN as catalyst
72	39	0.1382	--	
96	50	--	--	
120	57	0.1360	1.34	
168	66	0.1355	1.05	
240	73	0.1368	0.83	
336	--	0.1377	0.46	cooled to RT, pumped down prior to addition
360	--	0.1359	0.46	cooled to RT, pumped down prior to addition
408	85	0.1368	0.28	
432	--	--	0.28	
456	86	0.1318	0.22	
624	87	--	--	cooled to RT, pumped down, let stand
672	89	0.1368	0.21	
680	--	--	0.21	
696	90	--	--	cooled to RT, pumped down

3-(7-Iodo-9,9,10,10,11,11,12,12,12-nonafluorododecyl)thiophene, 2(8,4). Treatment of **1(8)** (5.92 g, 30.5 mmol) with AIBN (1.25 g, 7.62 mmol) and perfluorobutyl iodide (7.71 mL, 45.7 mmol) in a sealed Schlenk flask equipped with a water-jacketed condenser was followed by treatment as described in Table B.6. The reaction mixture was subjected to reduced pressure to remove any unreacted $F(CF_2)_4I$ and perfluorooctane. Column chromatography (silica gel, petroleum ether) gave **2(8,4)** as a clear, colorless liquid (4.90 g, 29.8%).

Table B.6. Reaction progress for the synthesis of **2(8,4)**.

Time (h)	% conversion	Catalyst added (g)	$F(CF_2)_4I$ added (mL)	Notes
0	0	1.25	7.71	used a water-jacketed condenser, AIBN as catalyst
1.5	--	--	3.00	
16	--	--	--	cooled to RT, pumped down

3-(7-Iodo-9,9,10,10,11,11,11-nonafluorododecyl)thiophene, 2(8,3). Treatment of **1(8)** (5.70 g, 29.3 mmol) with AIBN (1.20 g, 7.33 mmol) and perfluoropropyl iodide (6.35 mL, 44.0 mmol) in a sealed Schlenk tube was followed by treatment as described in Table B.7. The reaction mixture was subjected to reduced pressure to remove any unreacted $F(CF_2)_3I$ and perfluorohexane. Column chromatography (silica gel, petroleum ether) gave **2(8,3)** as a clear, colorless liquid (5.48 g, 38.1%).

Table B.7. Reaction progress for the synthesis of **2(8,3)**.

Time (h)	% conversion	Catalyst added (g)	$F(CF_2)_4I$ added (mL)	Notes
0	0	1.20	6.35	AIBN as catalyst
22.5	75	0.60	3.00	cooled to RT prior to addition and heating
49	>80	--	--	cooled to RT, pumped down

APPENDIX C: ^{1}H AND ^{13}C NMR SPECTRA OF INTERMEDIATES IN THE SYNTHESIS OF POLY(3-SEMIFLUOROALKYLTHIOPHENE)S

^{1}H NMR spectra were recorded on a Varian Mercury Vx 300 MHz instrument using $CDCl_3$ as a solvent. ^{13}C NMR spectra were obtained at 75.5 MHz.

Figure C.1	^{1}H (top) and ^{13}C (bottom) spectra of **1(5)**.	122
Figure C.2	^{1}H (top) and ^{13}C (bottom) spectra of **1(11)**.	123
Figure C.3	^{1}H (top) and ^{13}C (bottom) spectra of **1(8)**.	124
Figure C.4	^{1}H (top) and ^{13}C (bottom) spectra of **2(5,4)**.	125
Figure C.5	^{1}H (top) and ^{13}C (bottom) spectra of **2(5,8)**.	126
Figure C.6	^{1}H (top) and ^{13}C (bottom) spectra of **2(5,6)**.	127
Figure C.7	^{1}H (top) and ^{13}C (bottom) spectra of **2(11,8)**.	128
Figure C.8	^{1}H (top) and ^{13}C (bottom) spectra of **2(11,6)**.	129
Figure C.9	^{1}H (top) and ^{13}C (bottom) spectra of **2(11,4)**.	130
Figure C.10	^{1}H (top) and ^{13}C (bottom) spectra of **2(8,4)**.	131
Figure C.11	^{1}H (top) and ^{13}C (bottom) spectra of **2(8,3)**.	132
Figure C.12	^{1}H (top) and ^{13}C (bottom) spectra of **3(5,4)**.	133
Figure C.13	^{1}H (top) and ^{13}C (bottom) spectra of **3(5,8)**.	134
Figure C.14	^{1}H (top) and ^{13}C (bottom) spectra of **3(5,6)**.	135
Figure C.15	^{1}H (top) and ^{13}C (bottom) spectra of **3(11,8)**.	136
Figure C.16	^{1}H (top) and ^{13}C (bottom) spectra of **3(11,6)**.	137
Figure C.17	^{1}H (top) and ^{13}C (bottom) spectra of **3(11,4)**.	138
Figure C.18	^{1}H (top) and ^{13}C (bottom) spectra of **3(8,4)**.	139
Figure C.19	^{1}H (top) and ^{13}C (bottom) spectra of **3(8,3)**.	140
Figure C.20	^{1}H (top) and ^{13}C (bottom) spectra of **4(5,4)**.	141
Figure C.21	^{1}H (top) and ^{13}C (bottom) spectra of **4(5,8)**.	142
Figure C.22	^{1}H (top) and ^{13}C (bottom) spectra of **4(5,6)**.	143
Figure C.23	^{1}H (top) and ^{13}C (bottom) spectra of **4(11,8)**.	144
Figure C.24	^{1}H (top) and ^{13}C (bottom) spectra of **4(11,6)**.	145
Figure C.25	^{1}H (top) and ^{13}C (bottom) spectra of **4(11,4)**.	146
Figure C.26	^{1}H (top) and ^{13}C (bottom) spectra of **4(8,4)**.	147
Figure C.27	^{1}H (top) and ^{13}C (bottom) spectra of **4(8,3)**.	148

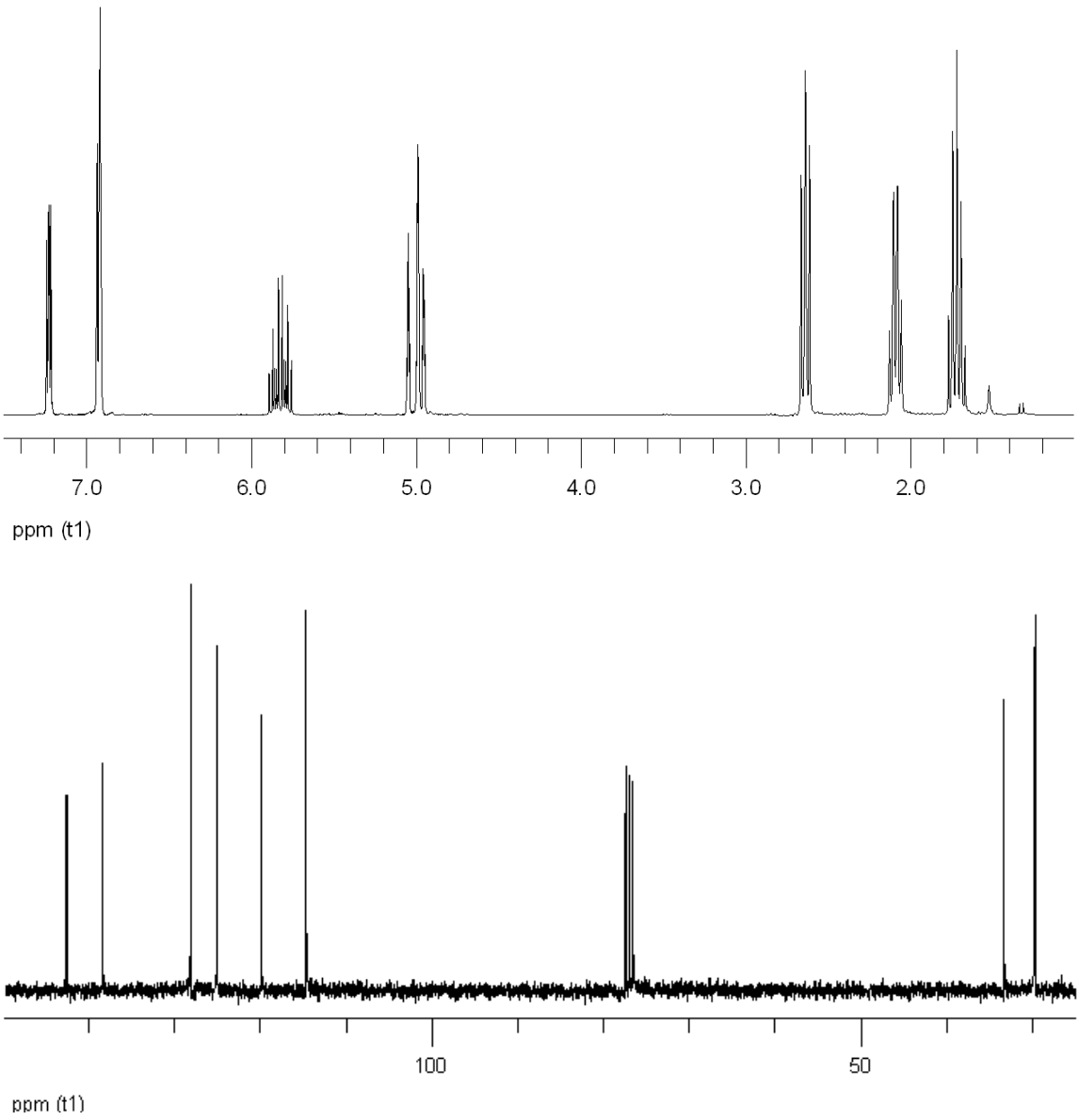

Figure C.1. ^{1}H (top) and ^{13}C (bottom) spectra of **1(5)**.

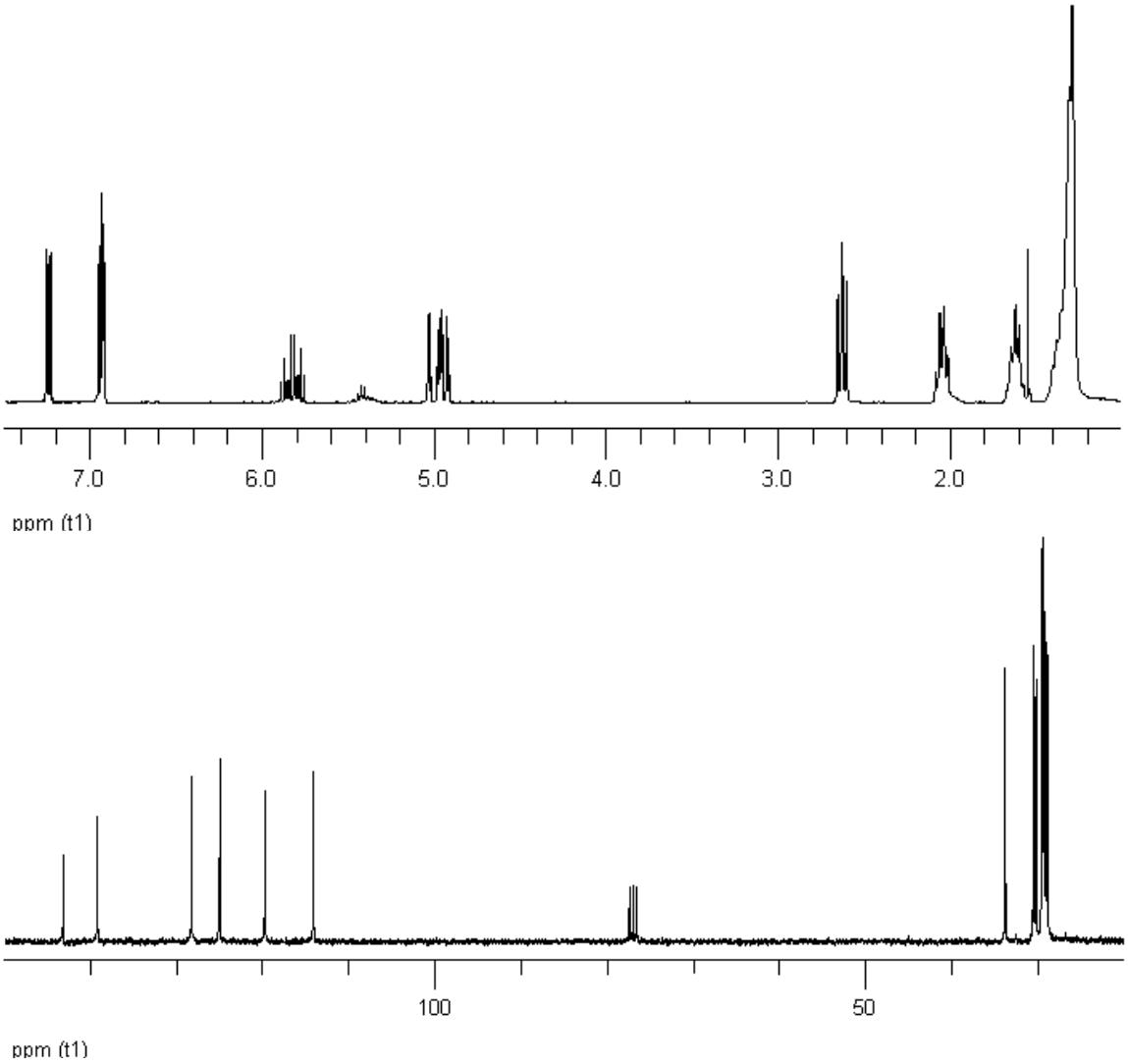

Figure C.2. ^{1}H (top) and ^{13}C (bottom) spectra of **1(11)**. Signal from 5.3-5.5 ppm in the ^{1}H spectrum is due to the internal alkene regioisomer (discussed in Section 2.3.1).

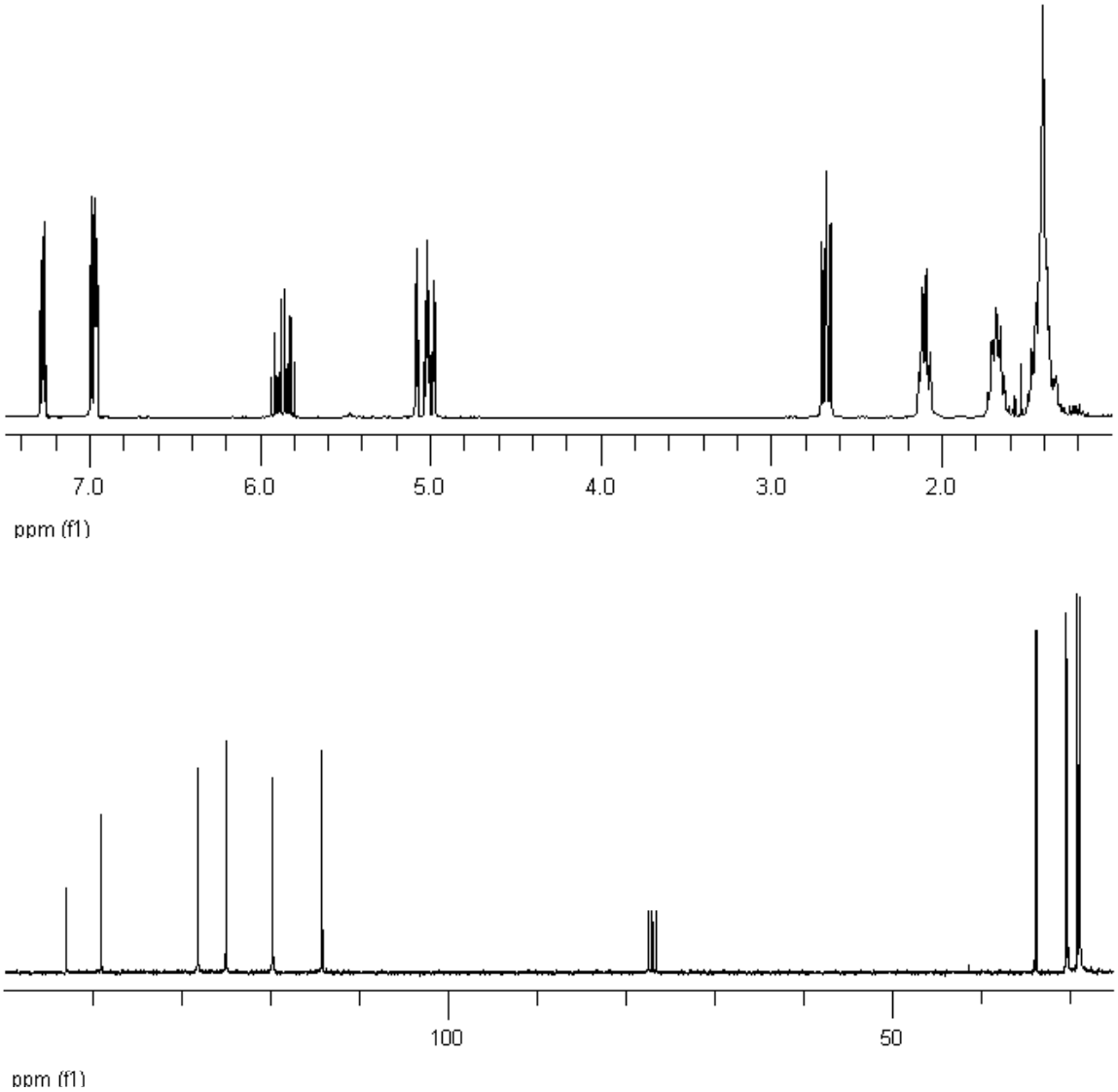

Figure C.3. ^{1}H (top) and ^{13}C (bottom) spectra of **1(8)**.

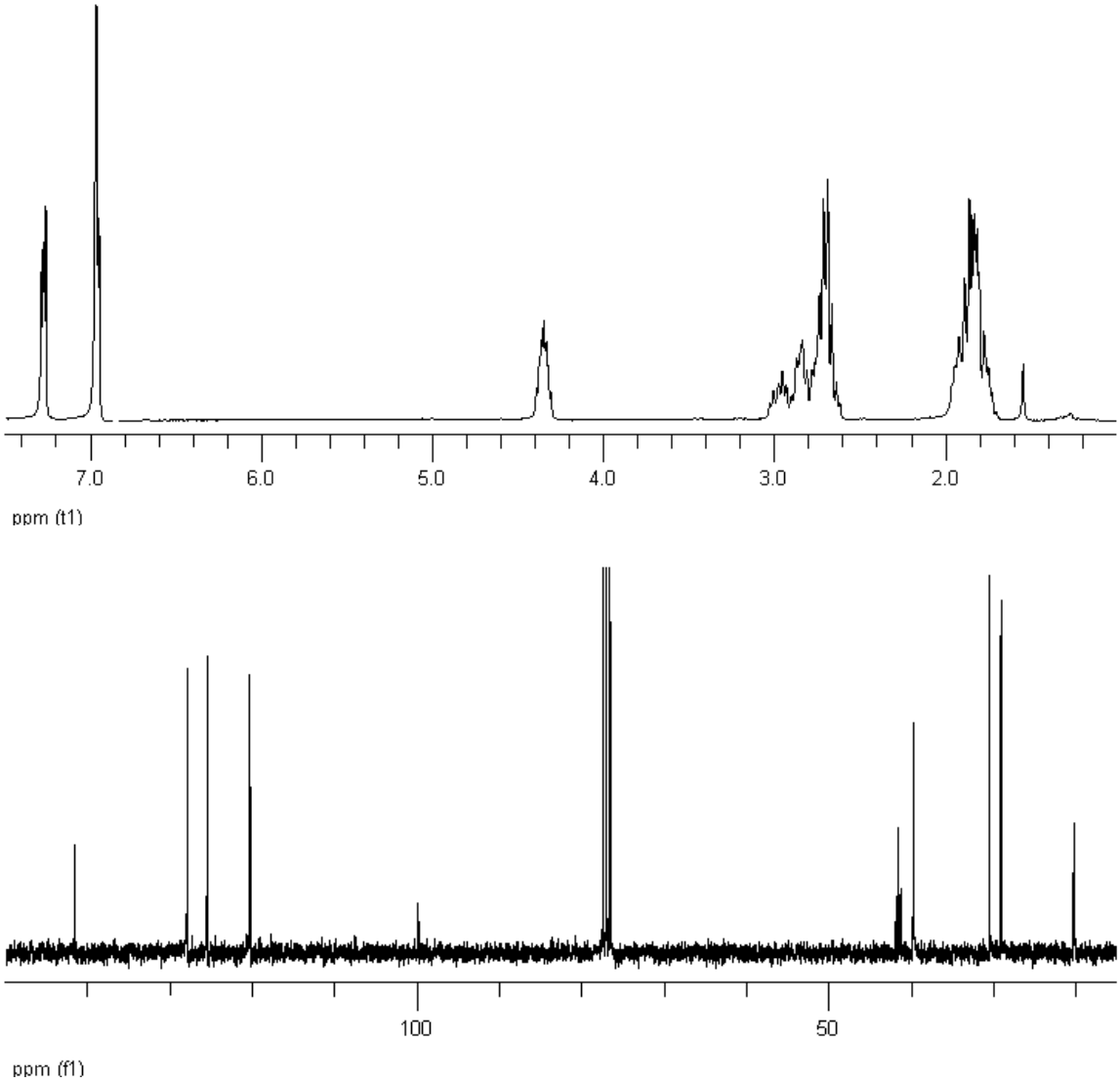

Figure C.4. ^{1}H (top) and ^{13}C (bottom) spectra of **2(5,4)**.

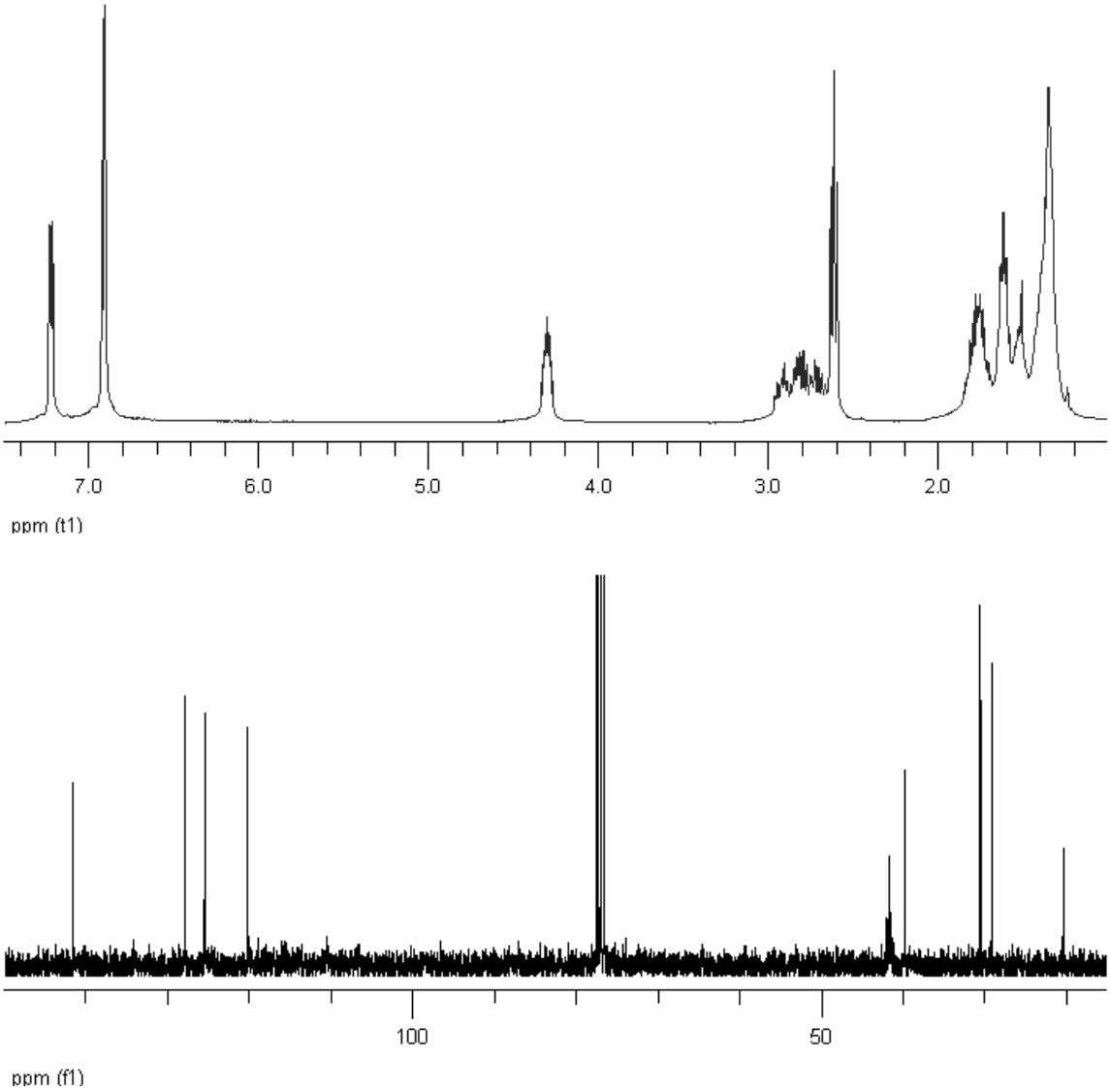

Figure C.5. ^{1}H (top) and ^{13}C (bottom) spectra of **2(5,8)**.

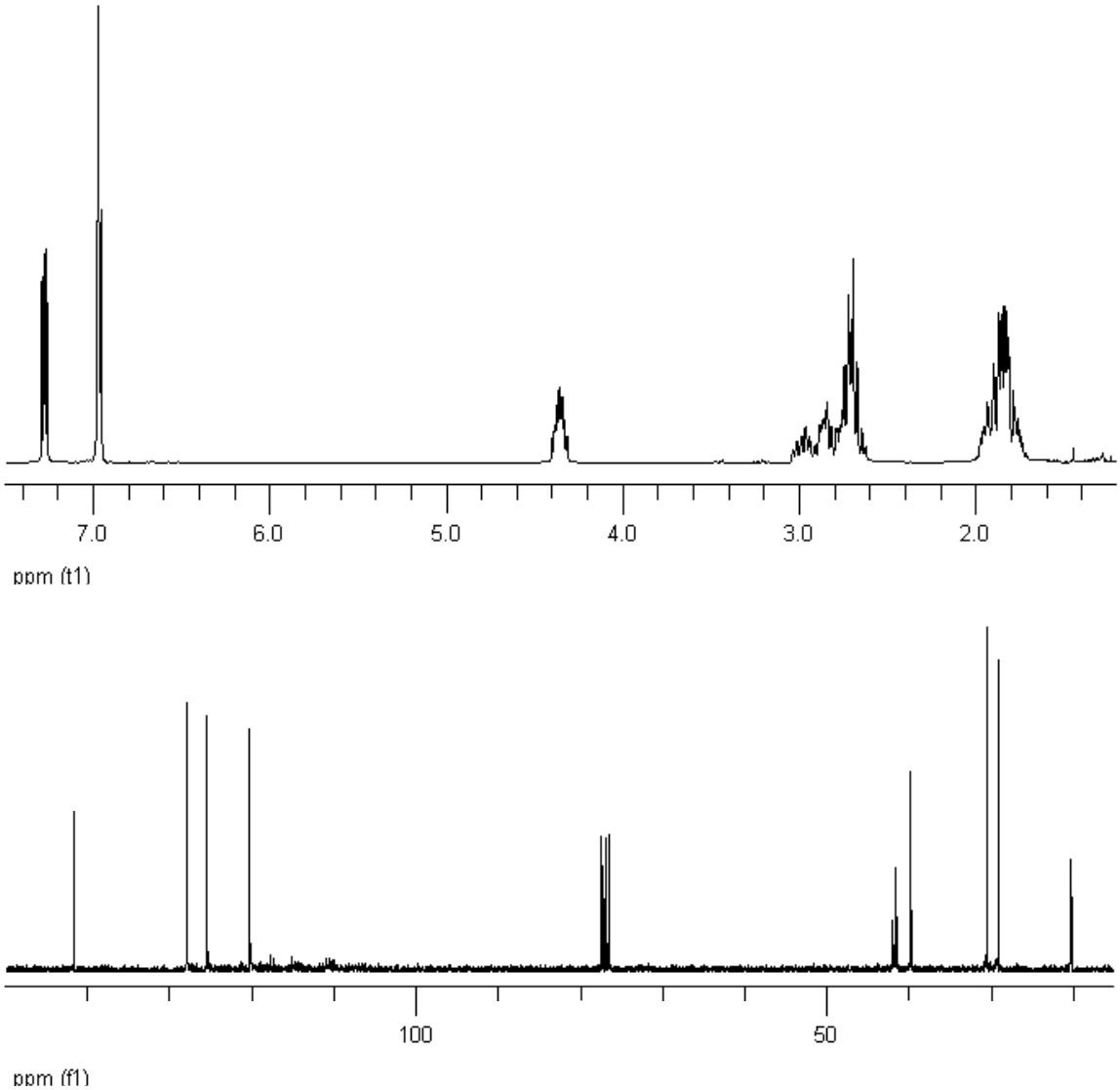

Figure C.6. ^{1}H (top) and ^{13}C (bottom) spectra of **2(5,6)**.

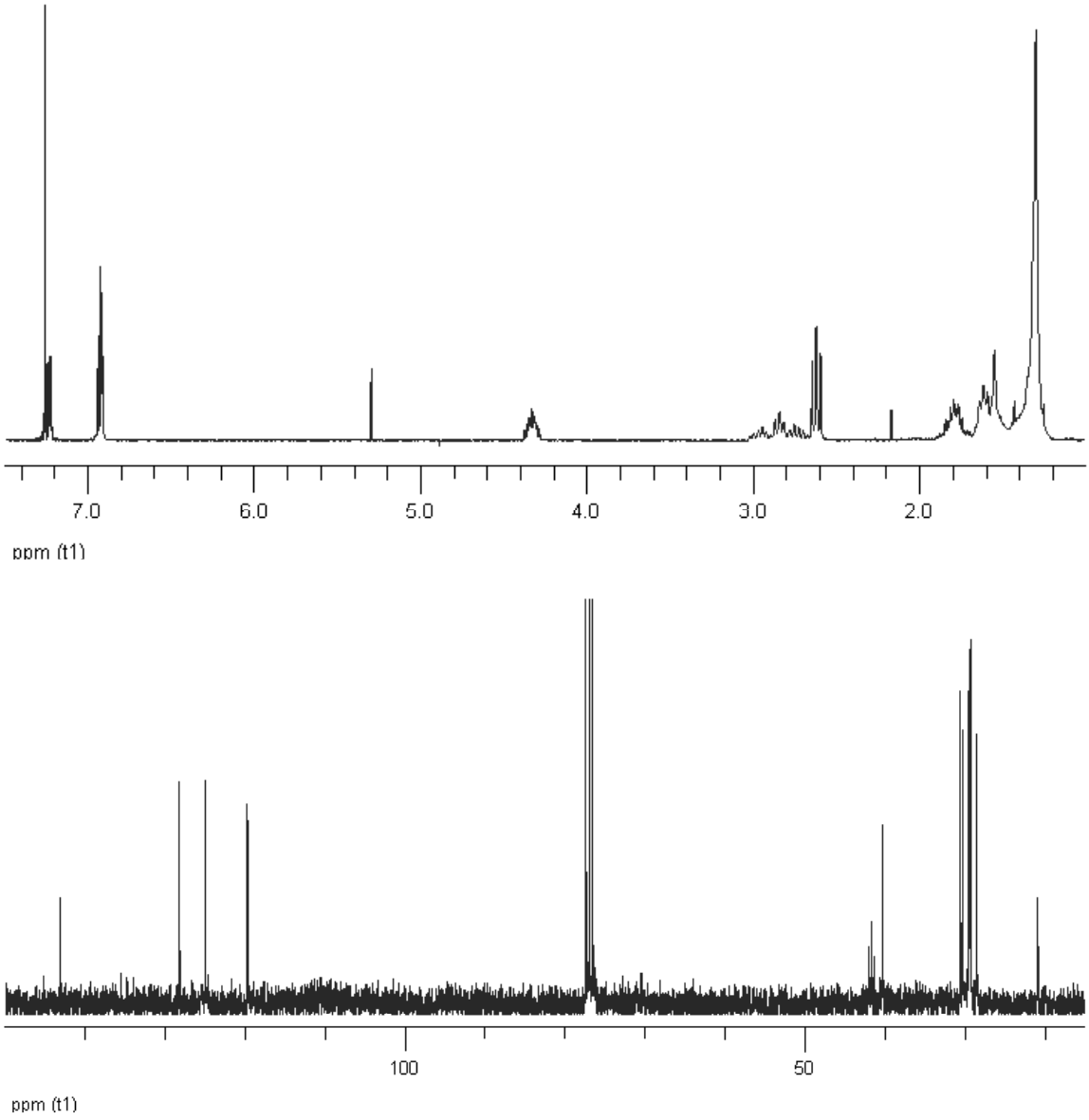

Figure C.7. ^{1}H (top) and ^{13}C (bottom) spectra of **2(11,8)**. ^{1}H spectrum contains residual CH_2Cl_2 (5.3 ppm) and acetone (2.1 ppm).

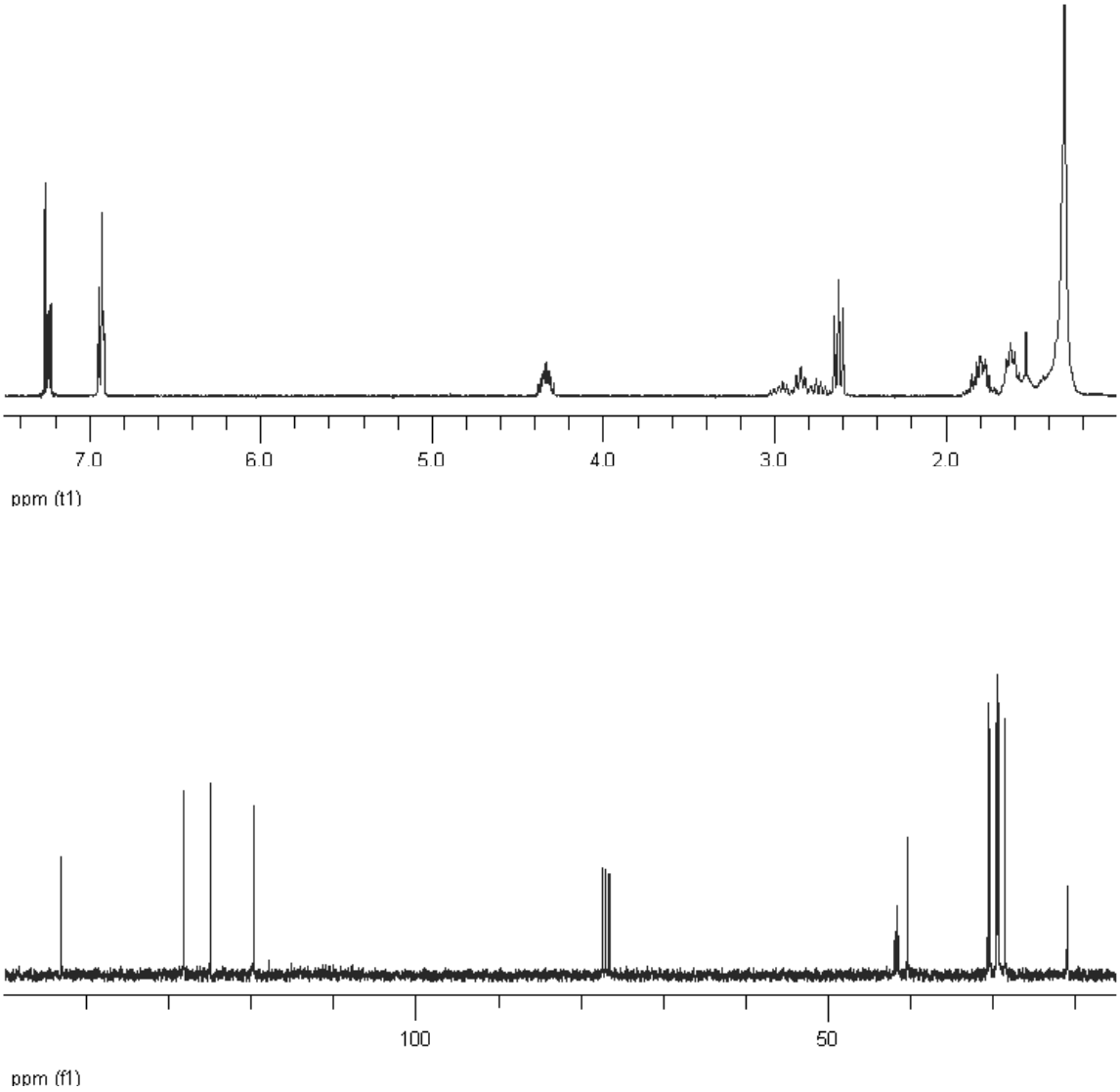

Figure C.8. ^{1}H (top) and ^{13}C (bottom) spectra of **2(11,6)**.

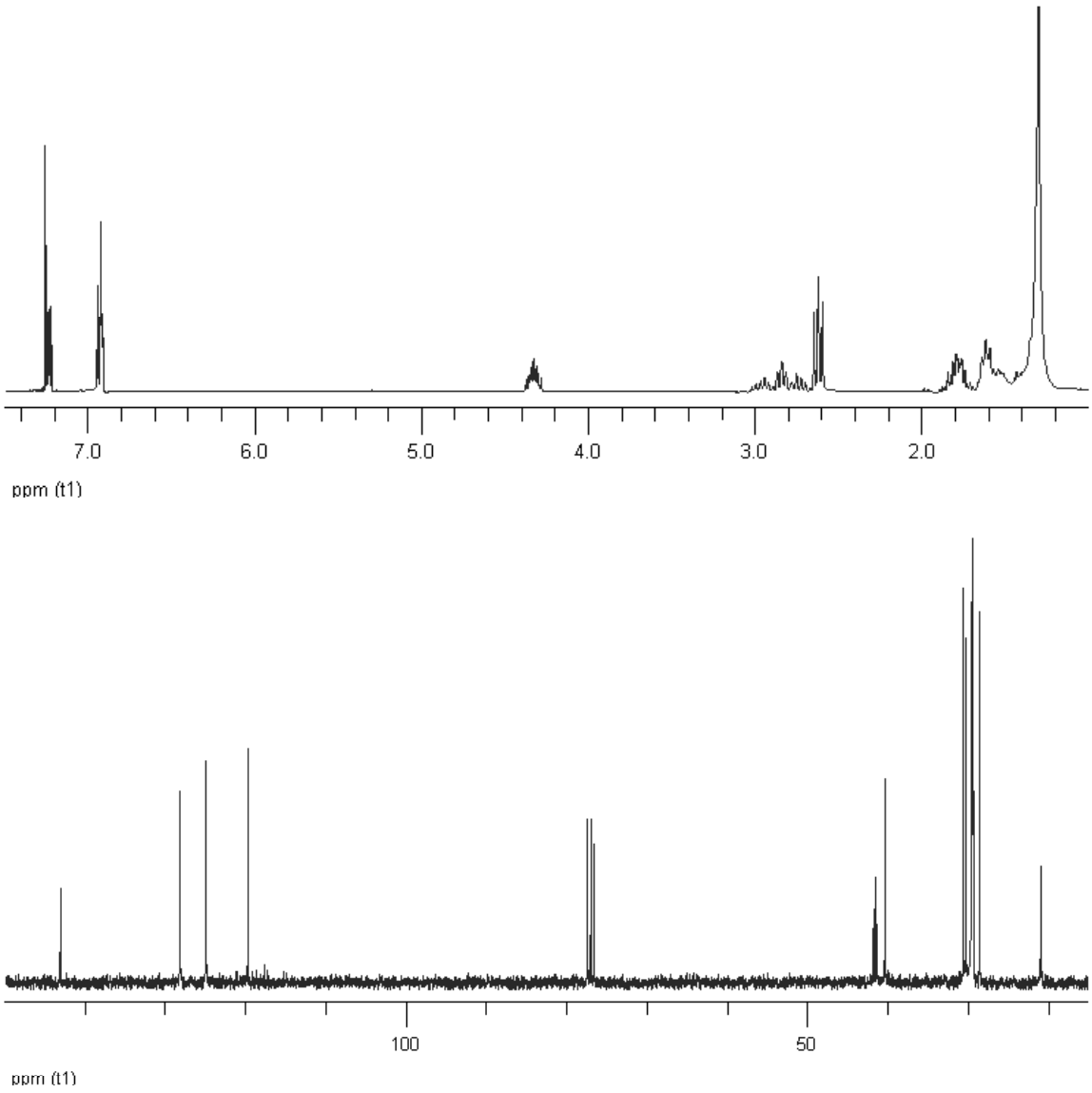

Figure C.10. ^{1}H (top) and ^{13}C (bottom) spectra of **2(11,4)**.

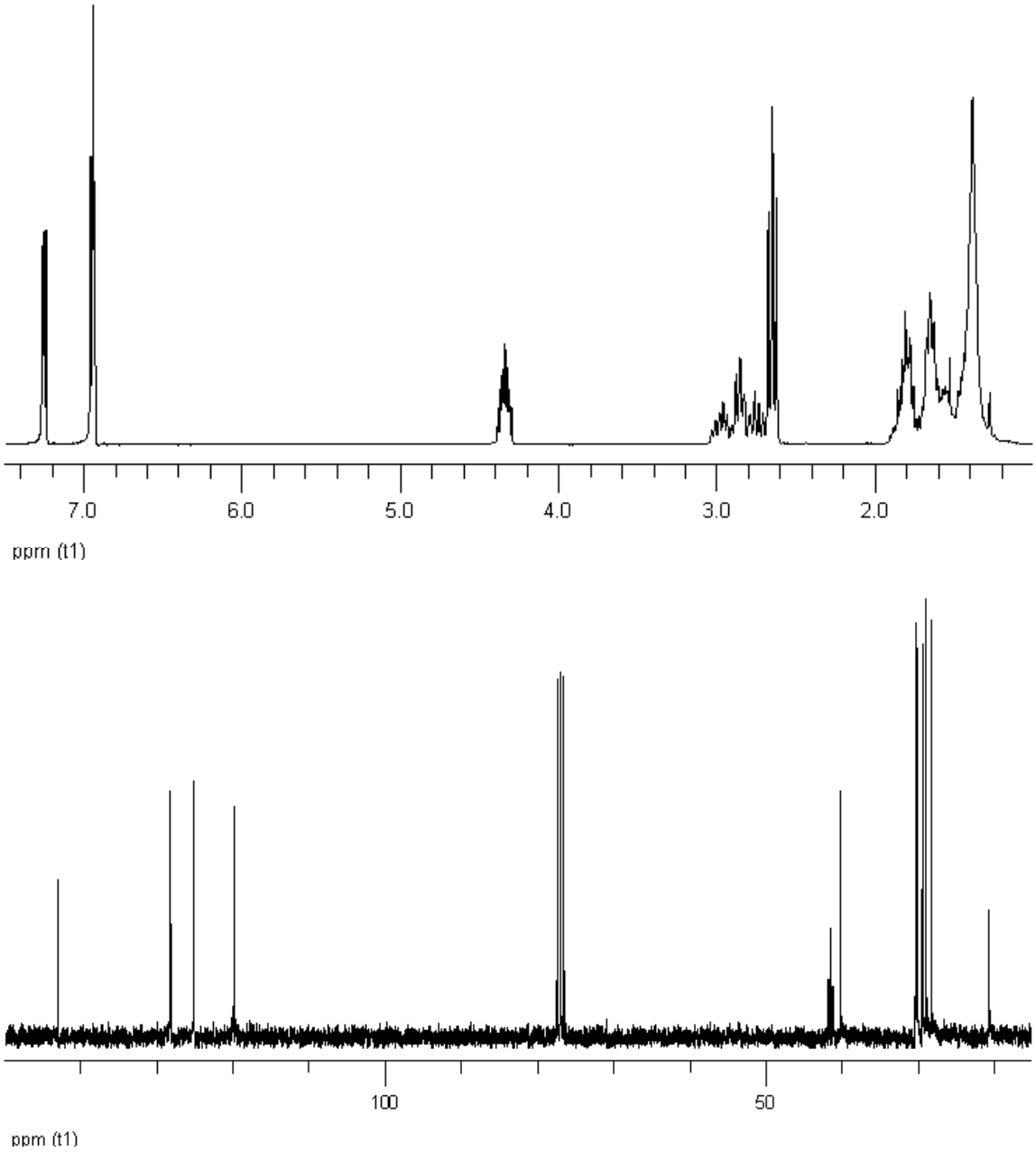

Figure C.10. ^{1}H (top) and ^{13}C (bottom) spectra of **2(8,4)**.

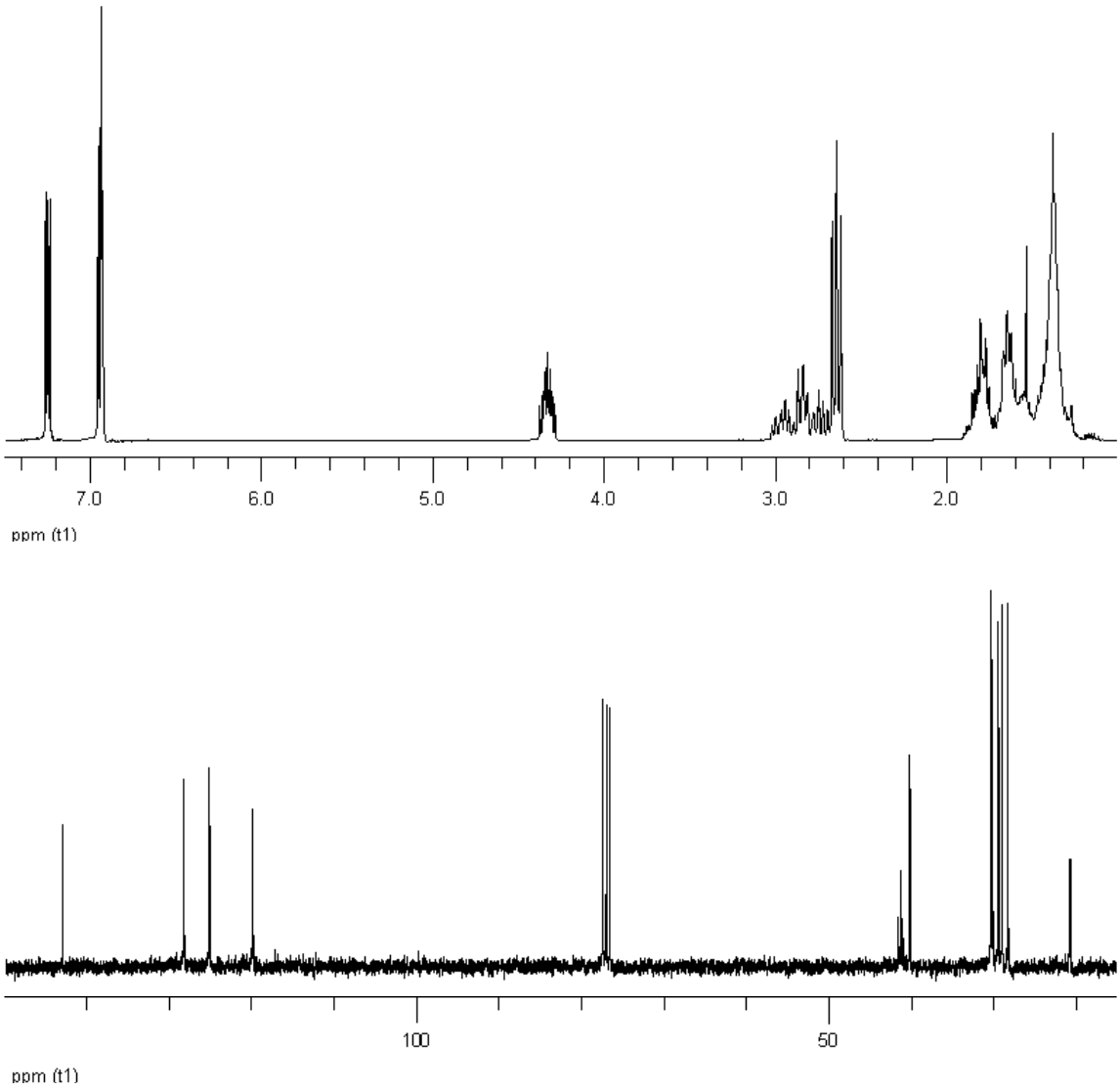

Figure C.11. ^{1}H (top) and ^{13}C (bottom) spectra of **2(8,3)**.

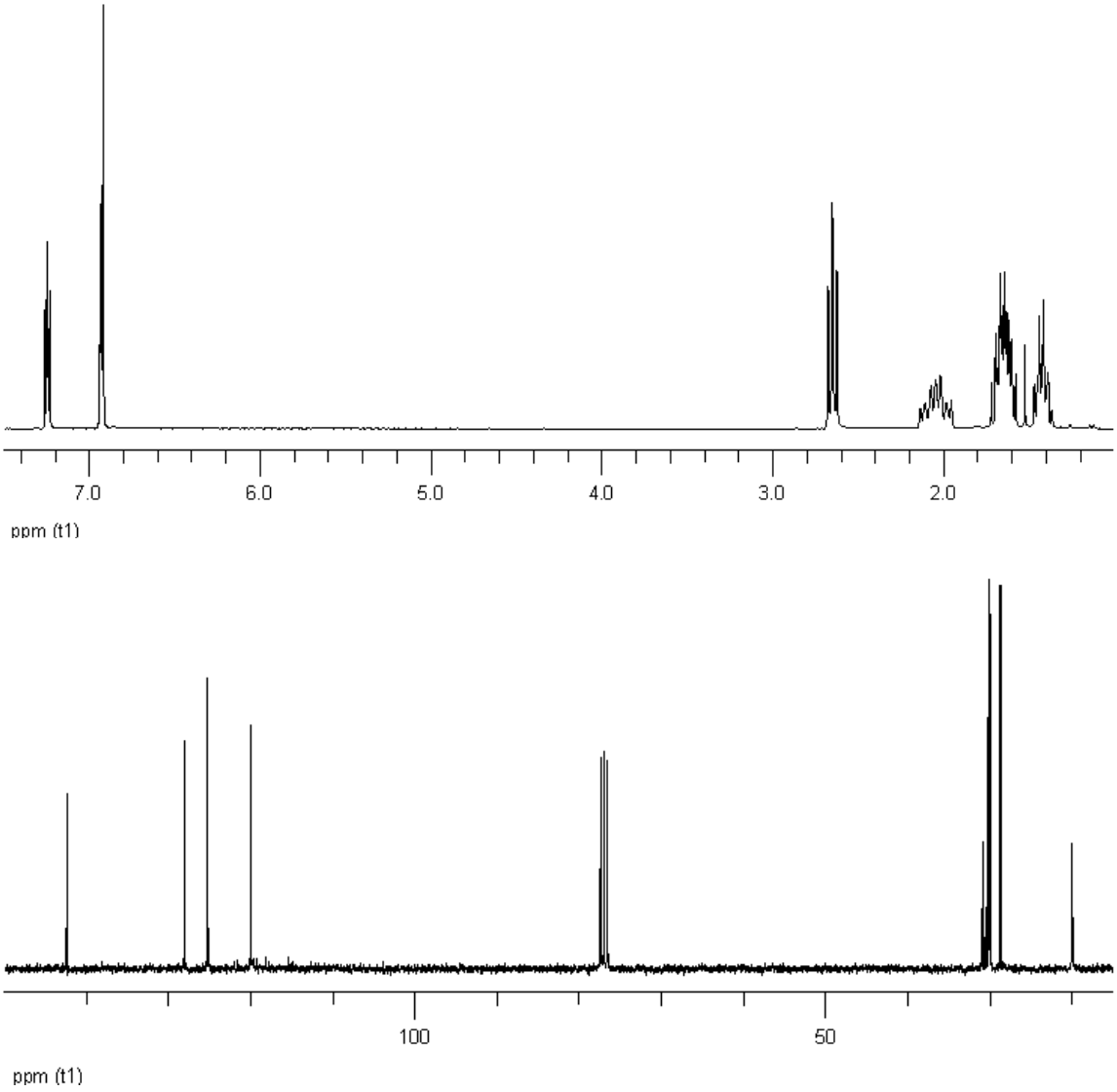

Figure C.12. ^{1}H (top) and ^{13}C (bottom) spectra of **3(5,4)**.

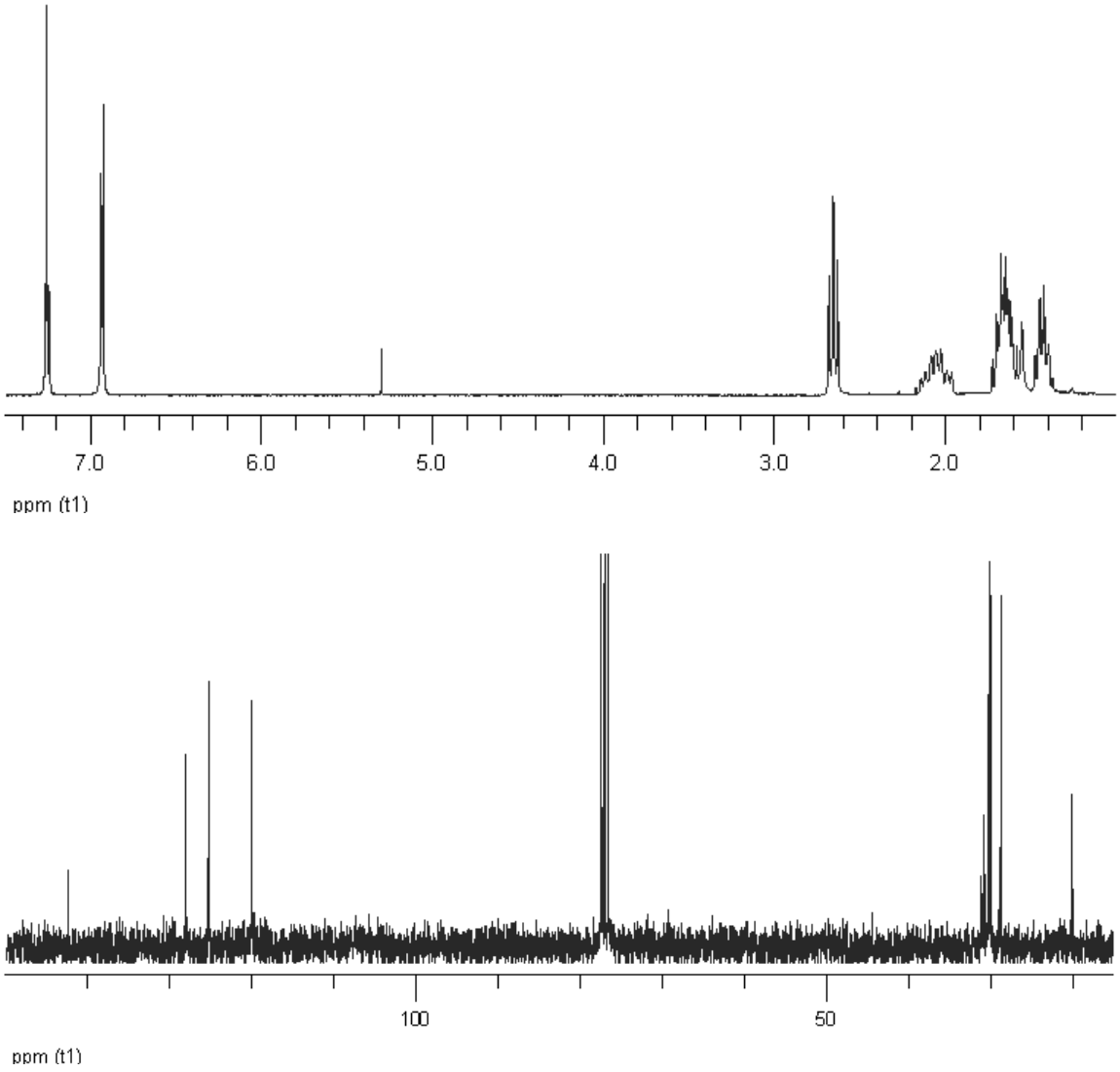

Figure C.13. ^{1}H (top) and ^{13}C (bottom) spectra of **3(5,8)**. ^{1}H spectrum contains residual CH_2Cl_2 (5.3 ppm)

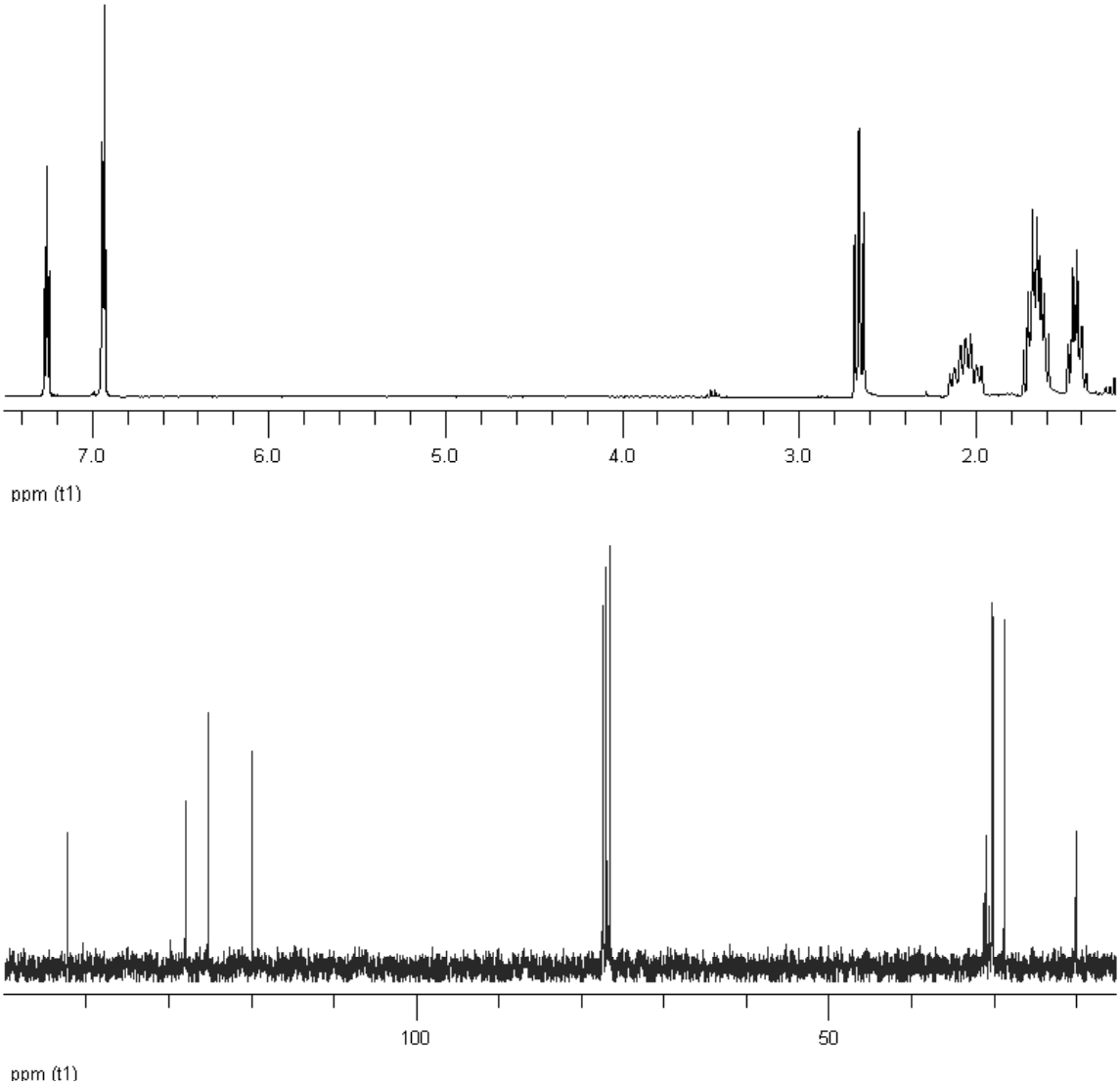

Figure C.14. ^{1}H (top) and ^{13}C (bottom) spectra of **3(5,6)**. ^{1}H spectrum contains residual Et_2O (3.45, 1.2 ppm).

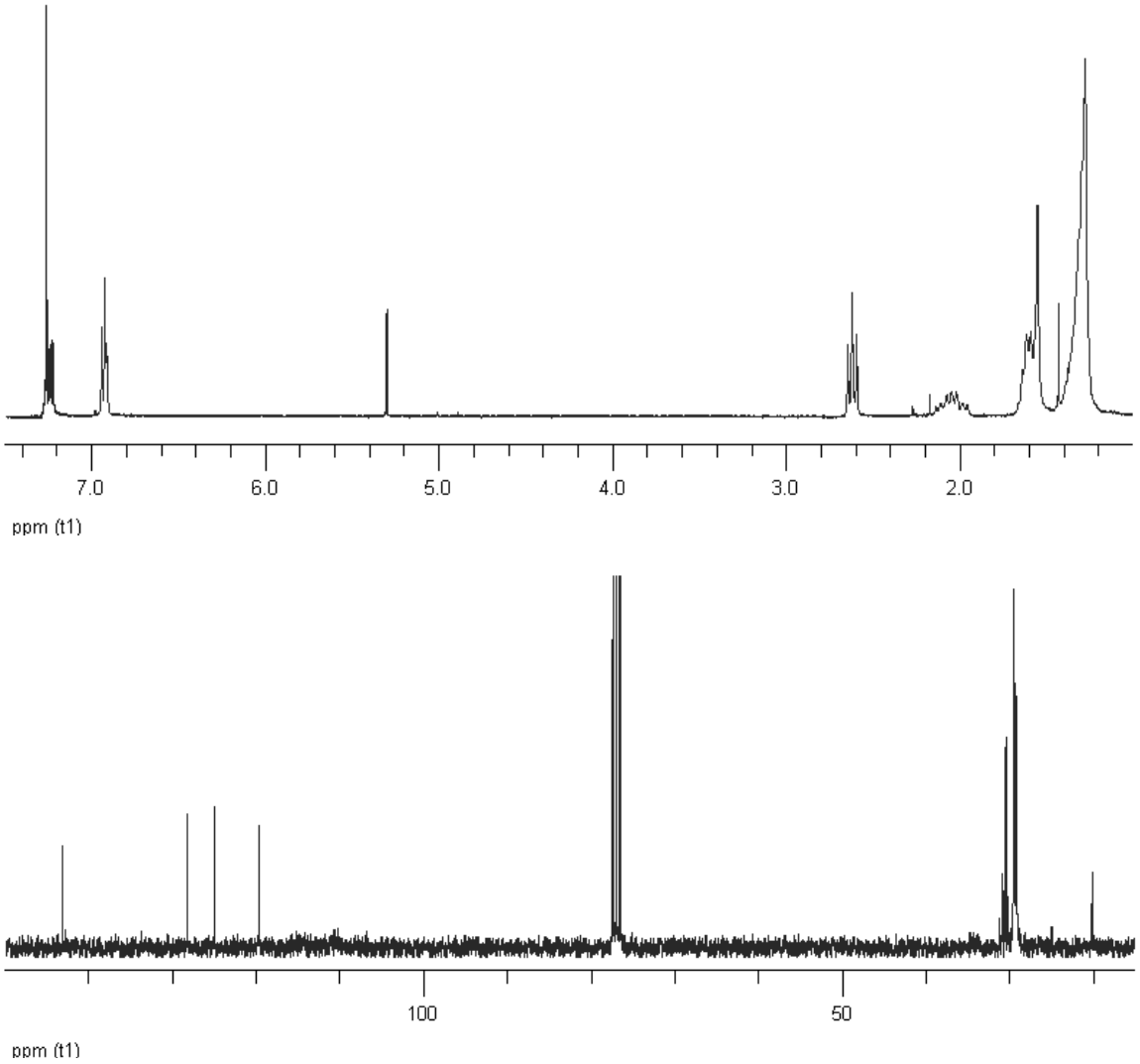

Figure C.15. ^{1}H (top) and ^{13}C (bottom) spectra of **3(11,8)**. ^{1}H spectrum contains residual CH_2Cl_2 (5.3 ppm) and acetone (2.1 ppm).

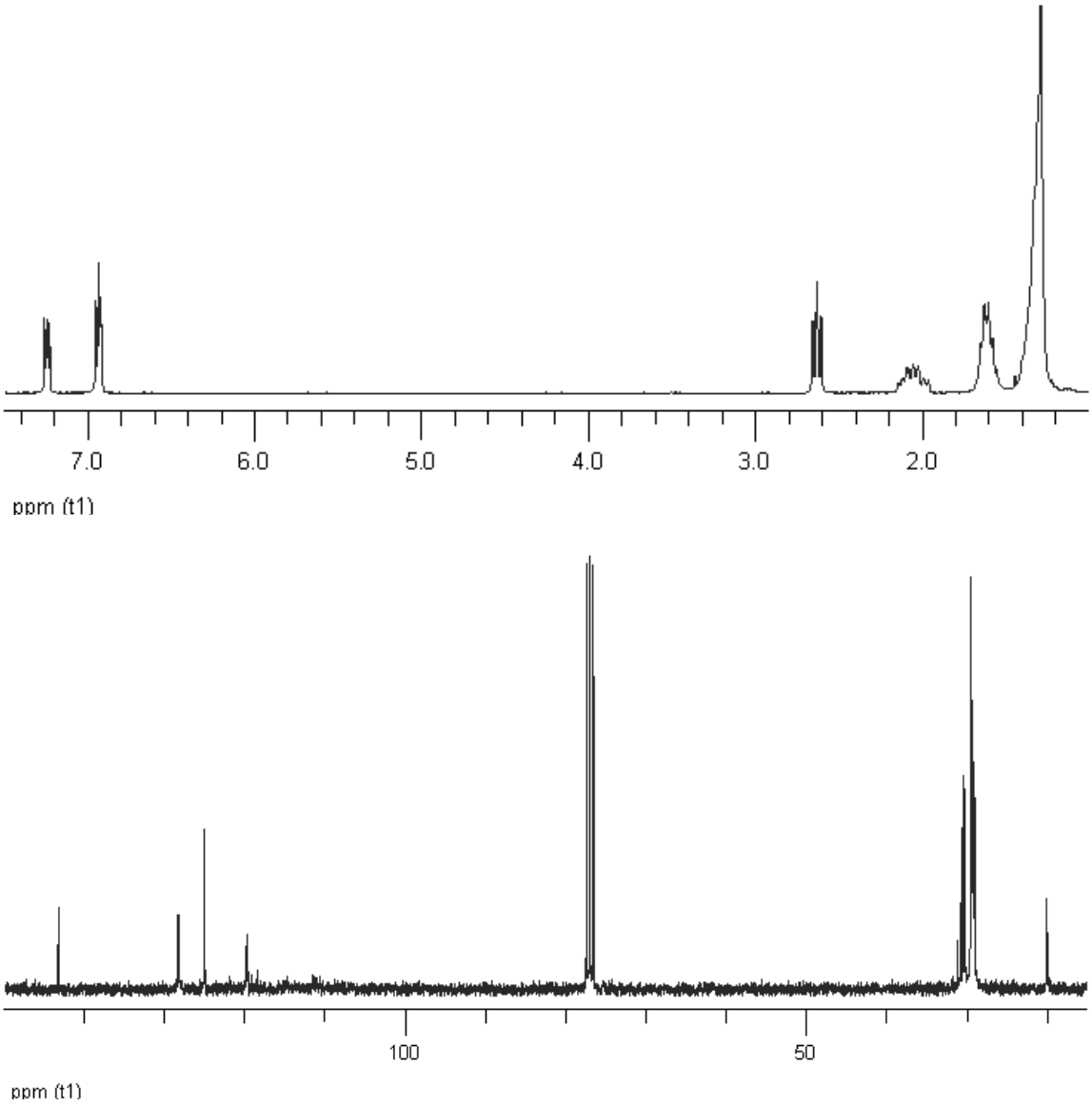

Figure C.16. ^{1}H (top) and ^{13}C (bottom) spectra of **3(11,6)**.

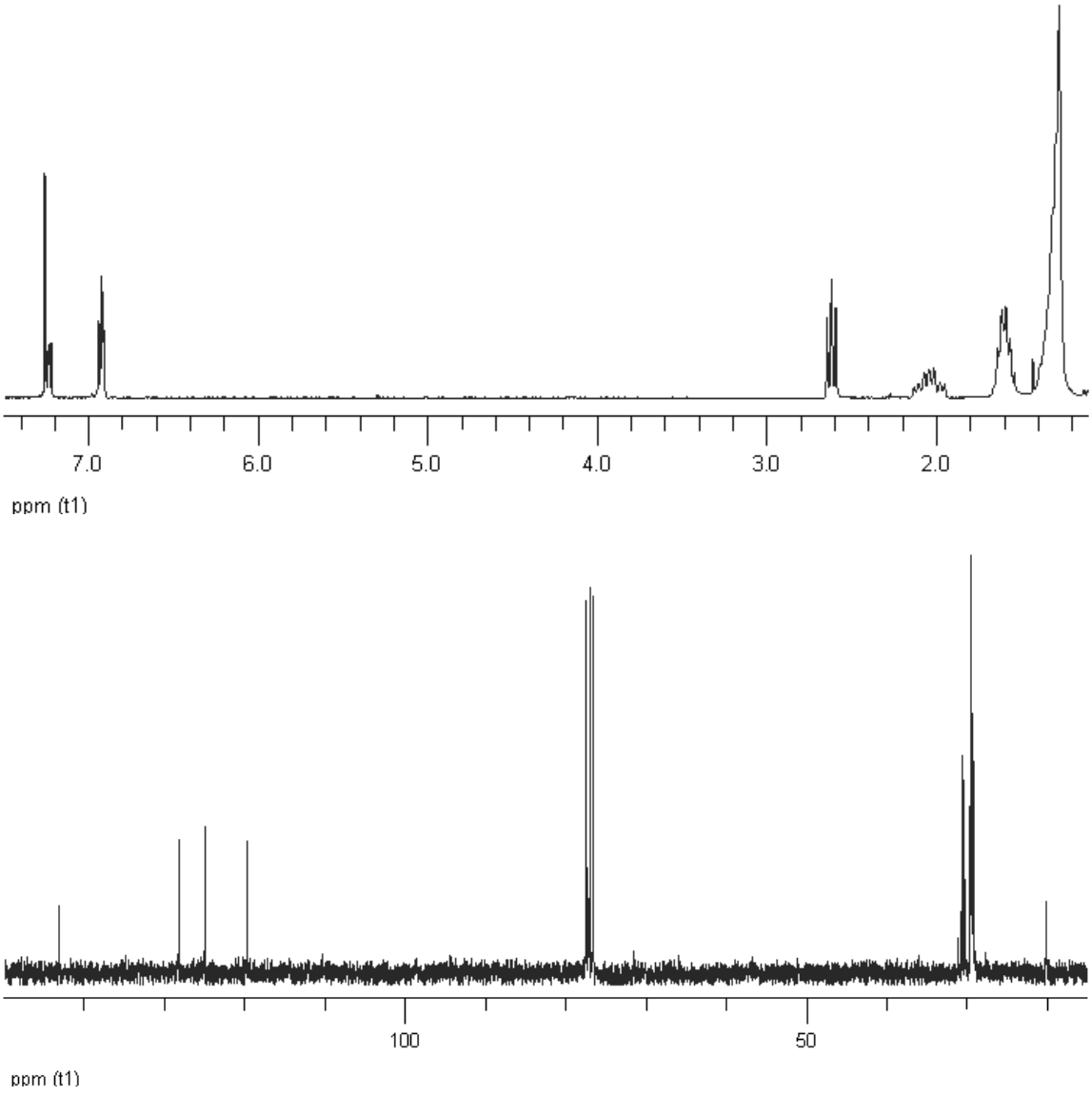

Figure C.17. ^{1}H (top) and ^{13}C (bottom) spectra of **3(11,4)**.

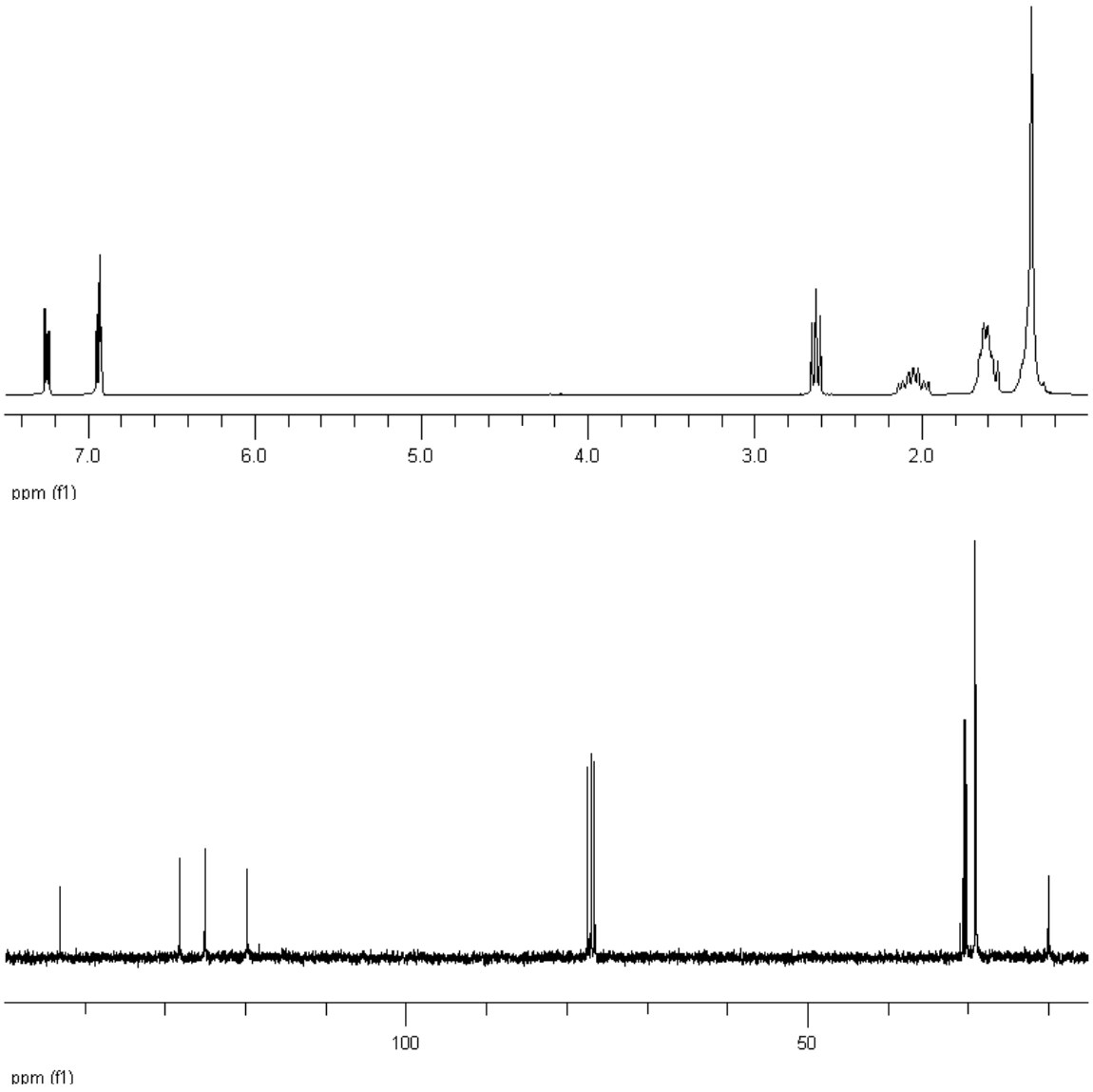

Figure C.18. ^{1}H (top) and ^{13}C (bottom) spectra of **3(8,4)**.

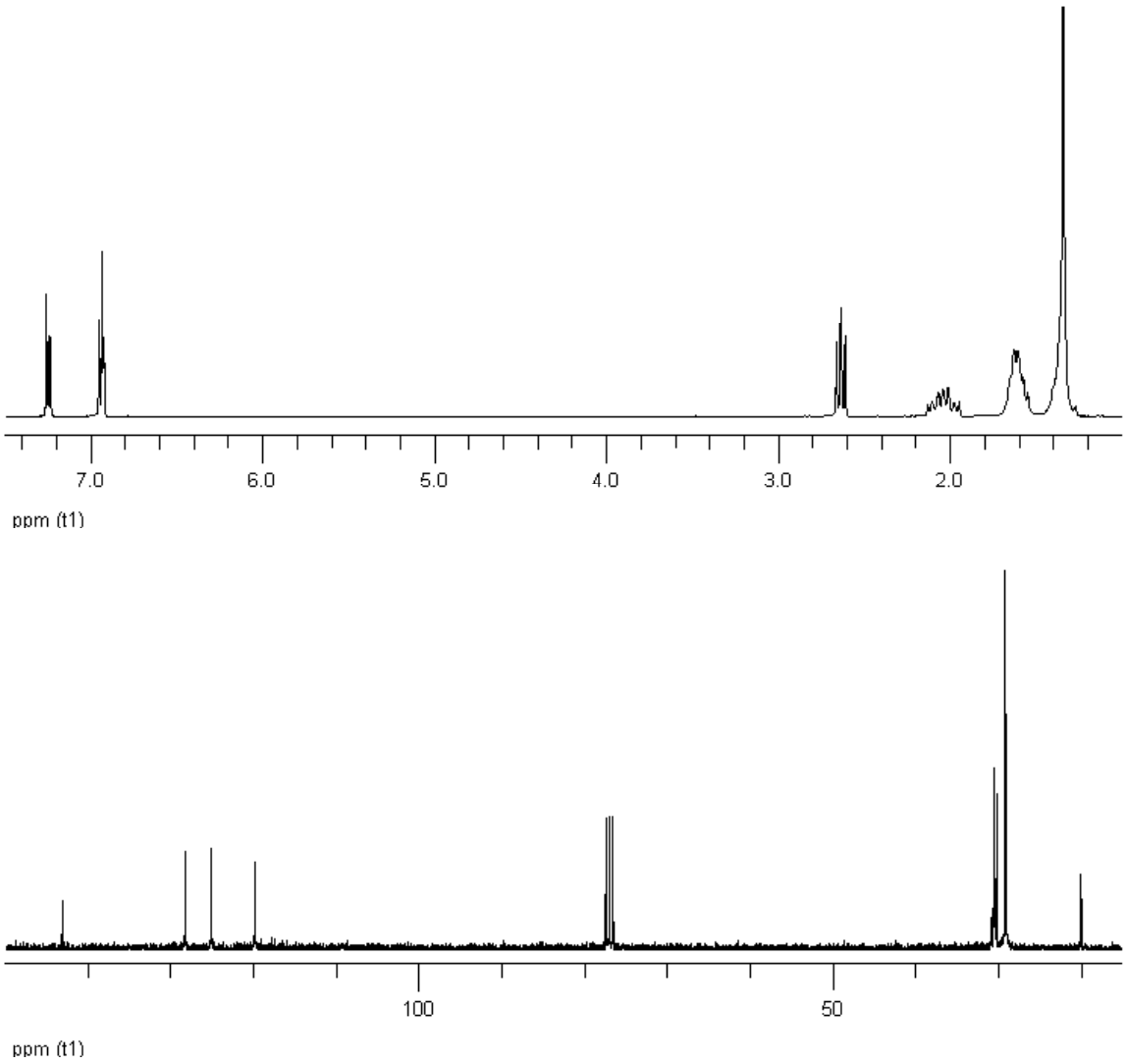

Figure C.19. ^{1}H (top) and ^{13}C (bottom) spectra of **3(8,3)**.

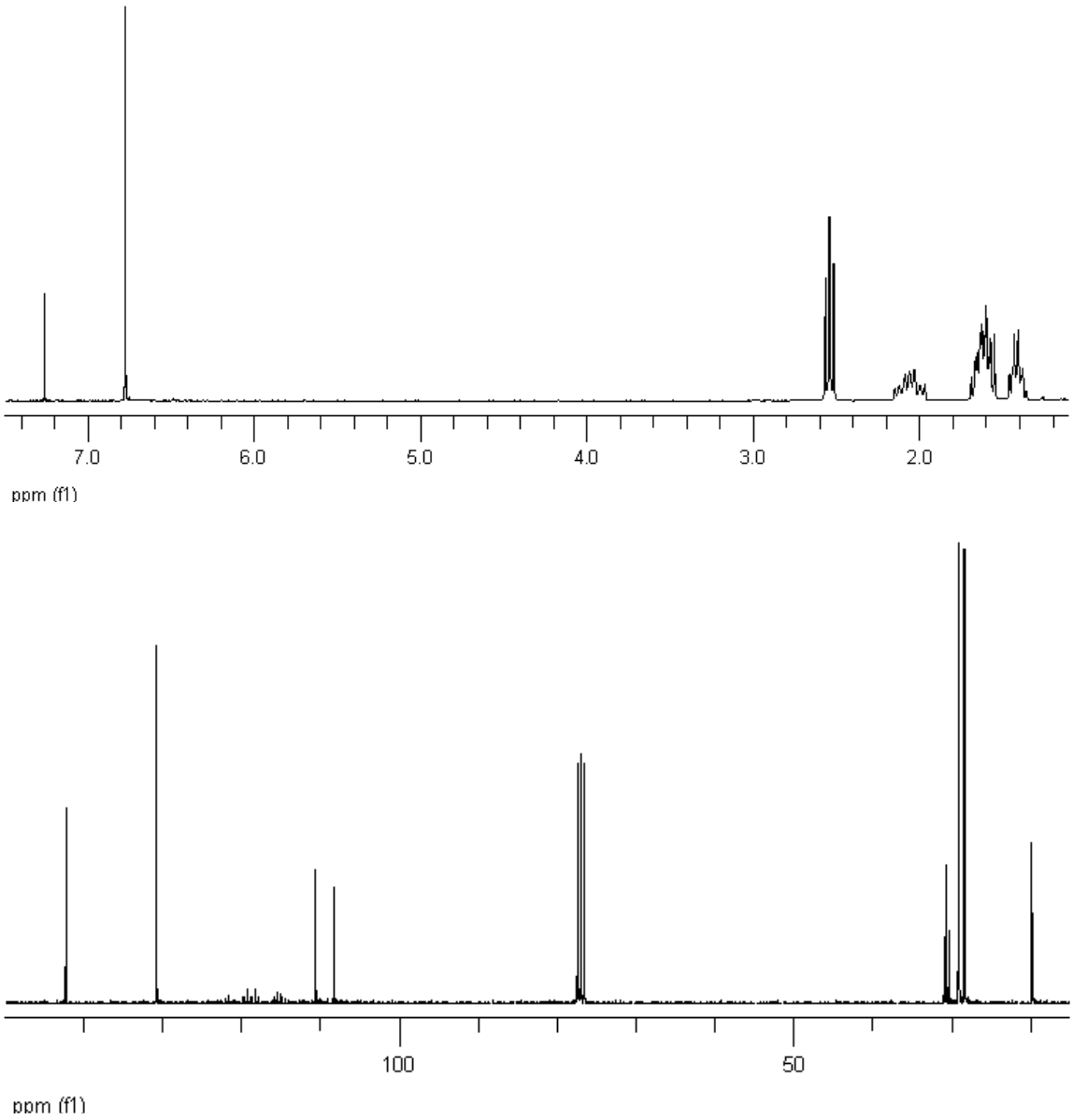

Figure C.20. ^{1}H (top) and ^{13}C (bottom) spectra of **4(5,4)**, with CF_2 resonances at 115-120 ppm in the ^{13}C spectrum.

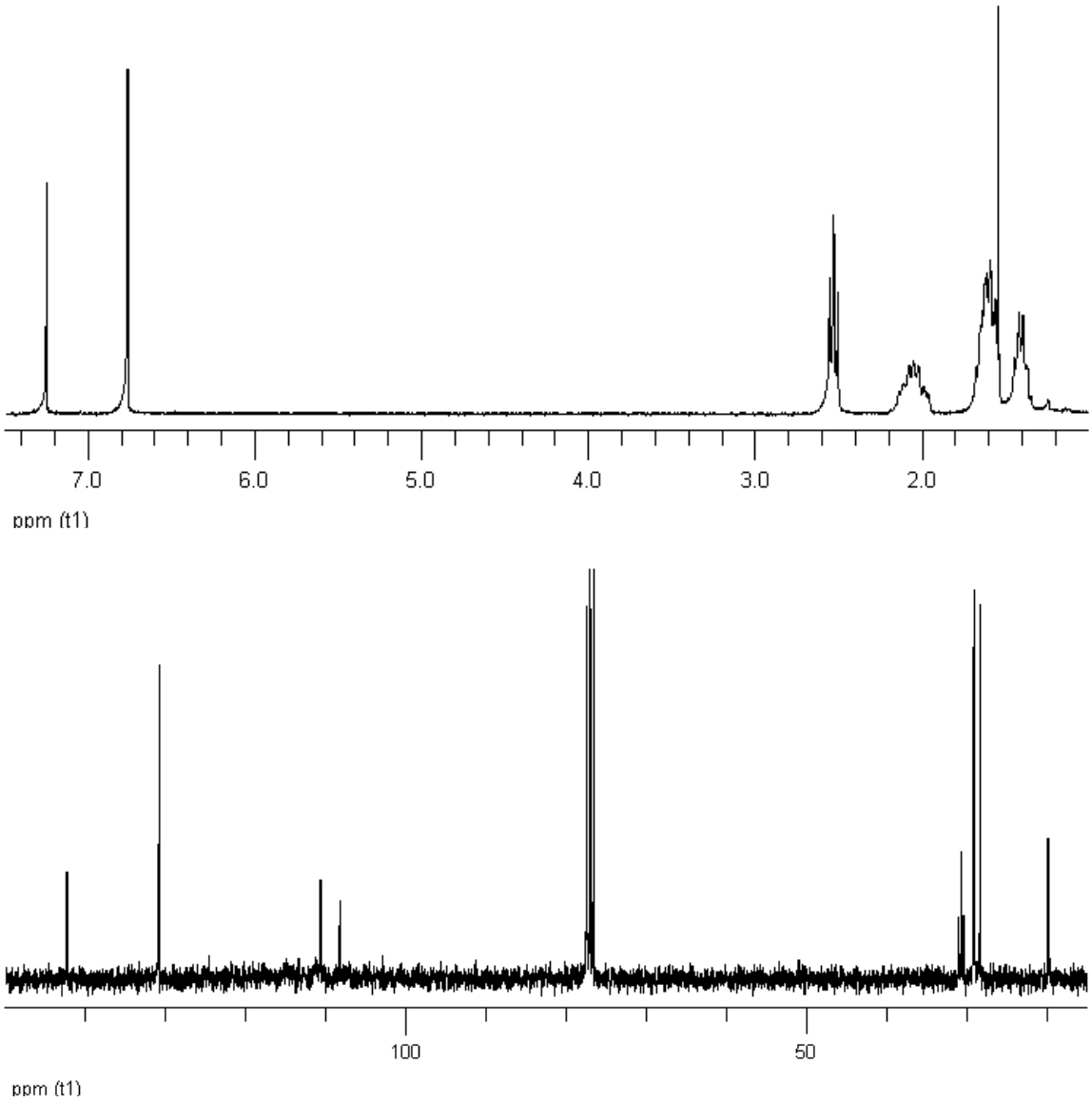

Figure C.21. ^{1}H (top) and ^{13}C (bottom) spectra of **4(5,8)**.

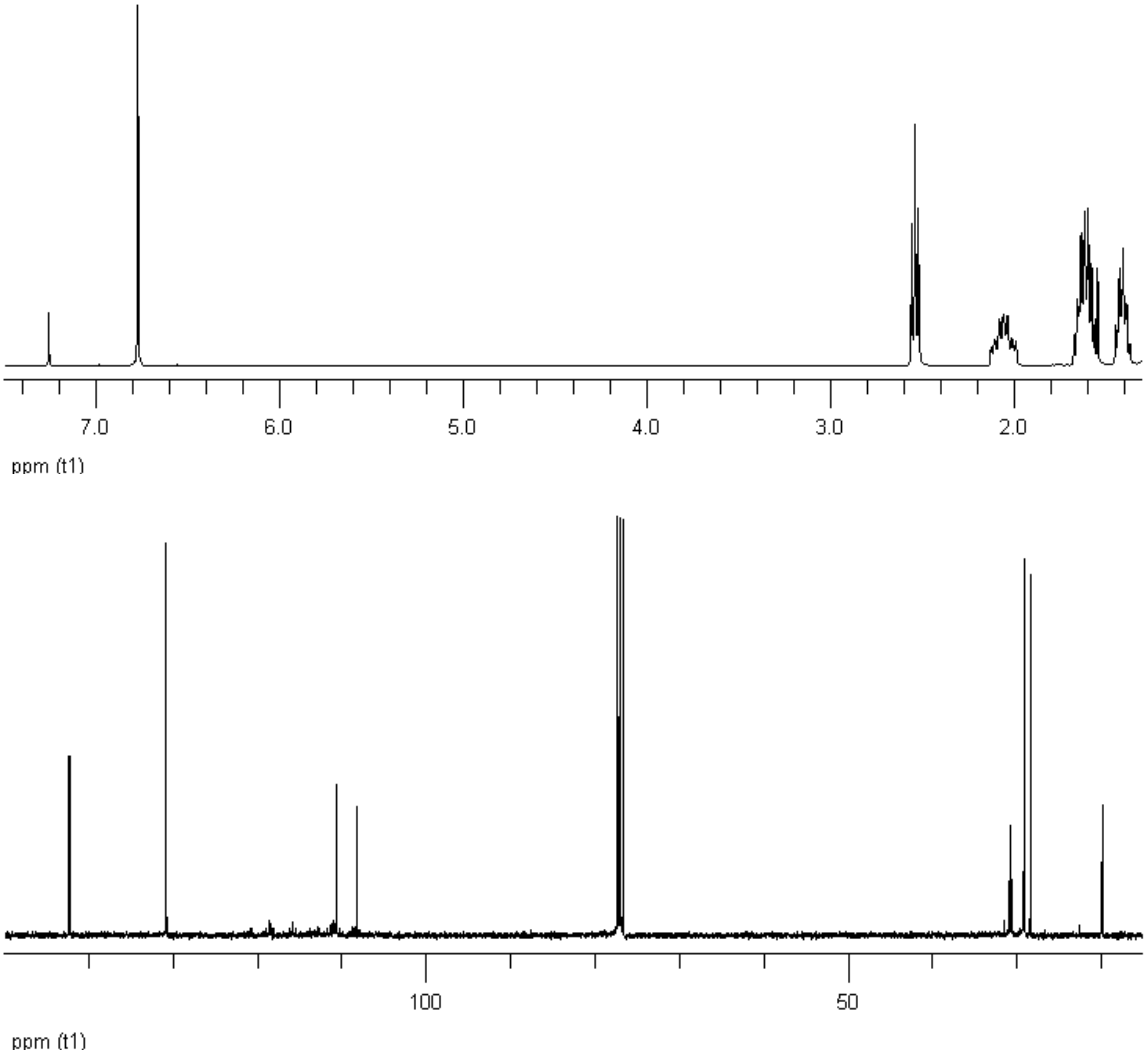

Figure C.22. ^{1}H (top) and ^{13}C (bottom) spectra of **4(5,6)**, with CF_2 resonances at 107-122 ppm in the ^{13}C spectrum.

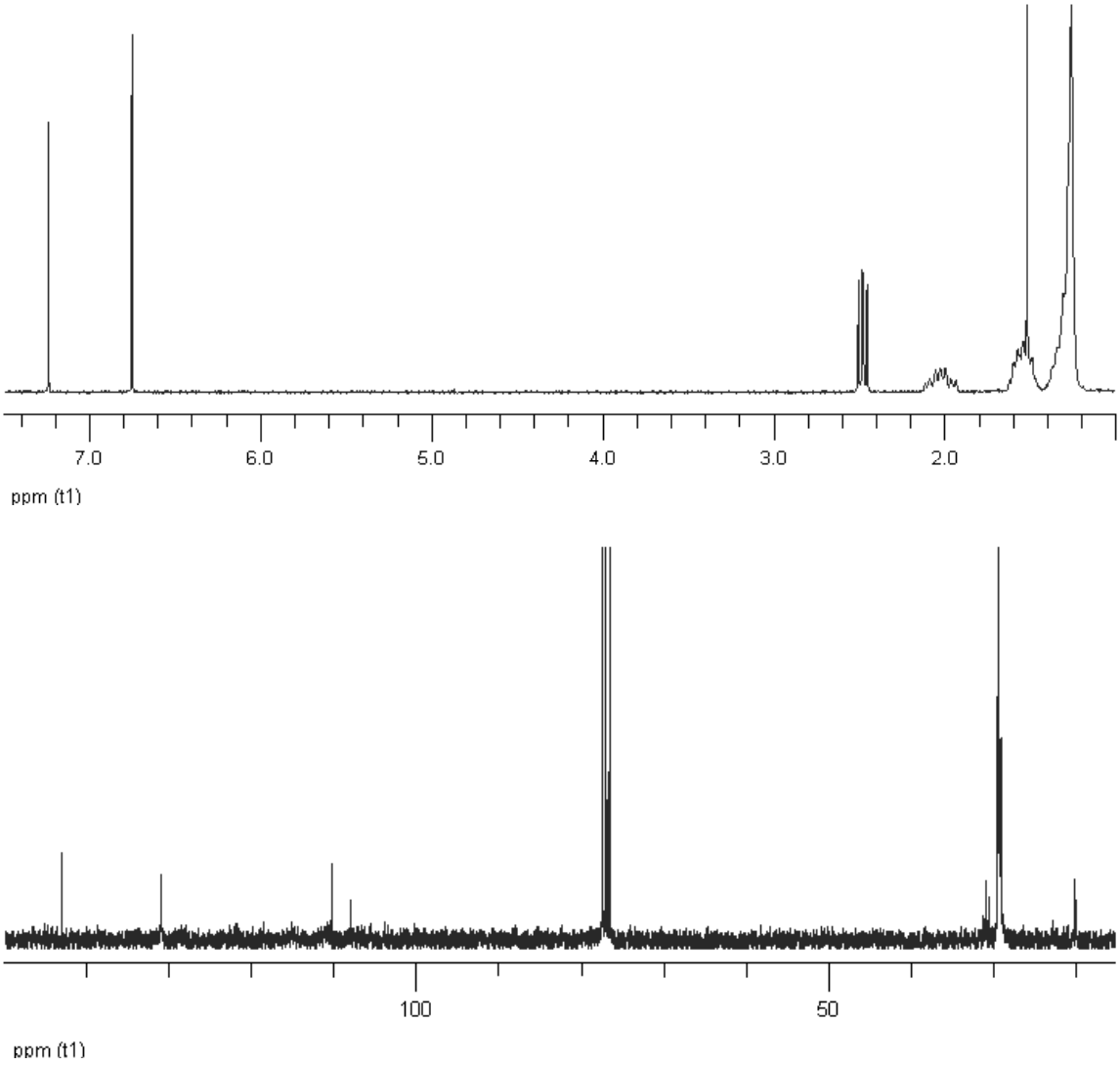

Figure C.23. ^{1}H (top) and ^{13}C (bottom) spectra of **4(11,8)**.

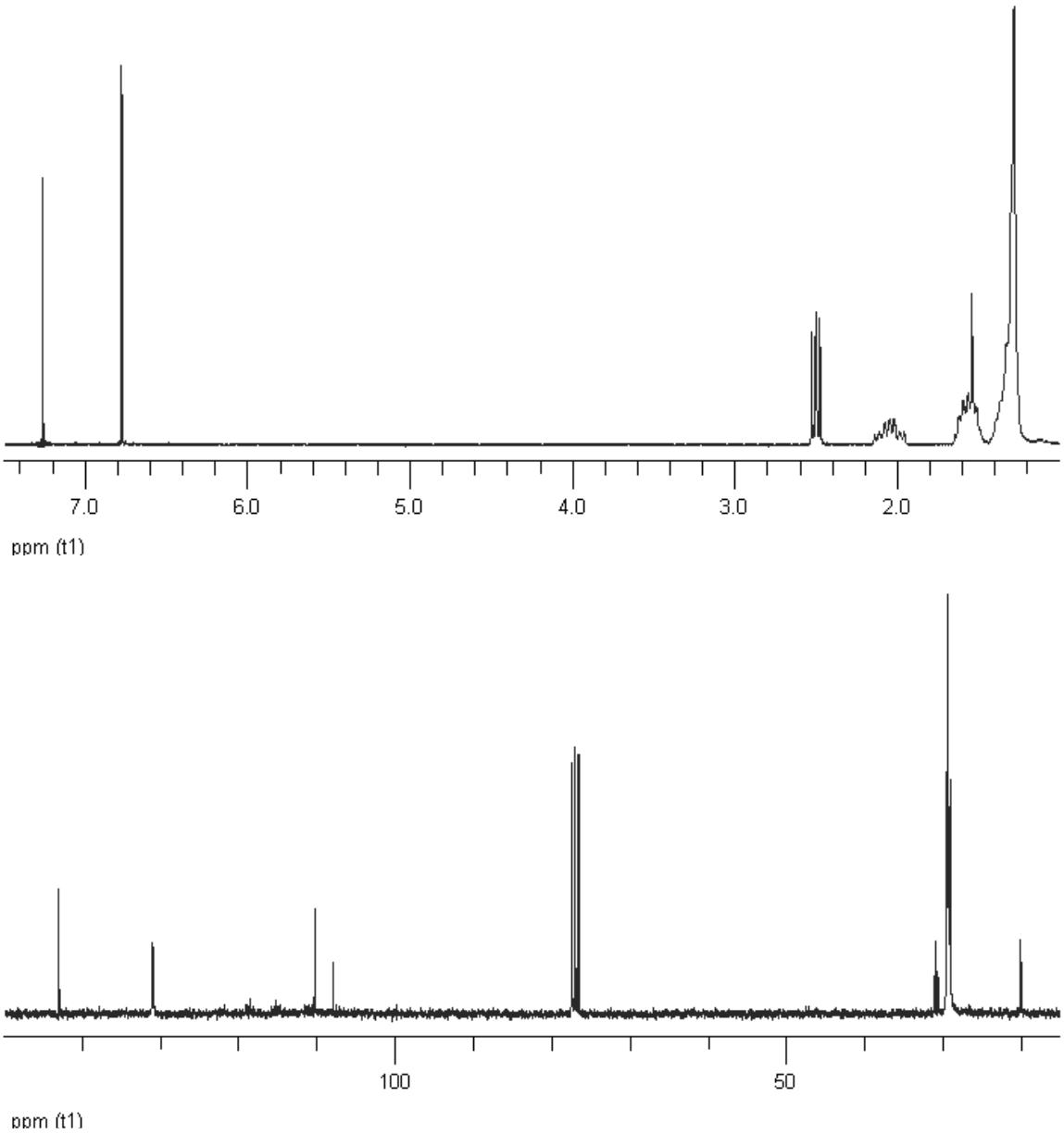

Figure C.24. ^{1}H (top) and ^{13}C (bottom) spectra of **4(11,6)**.

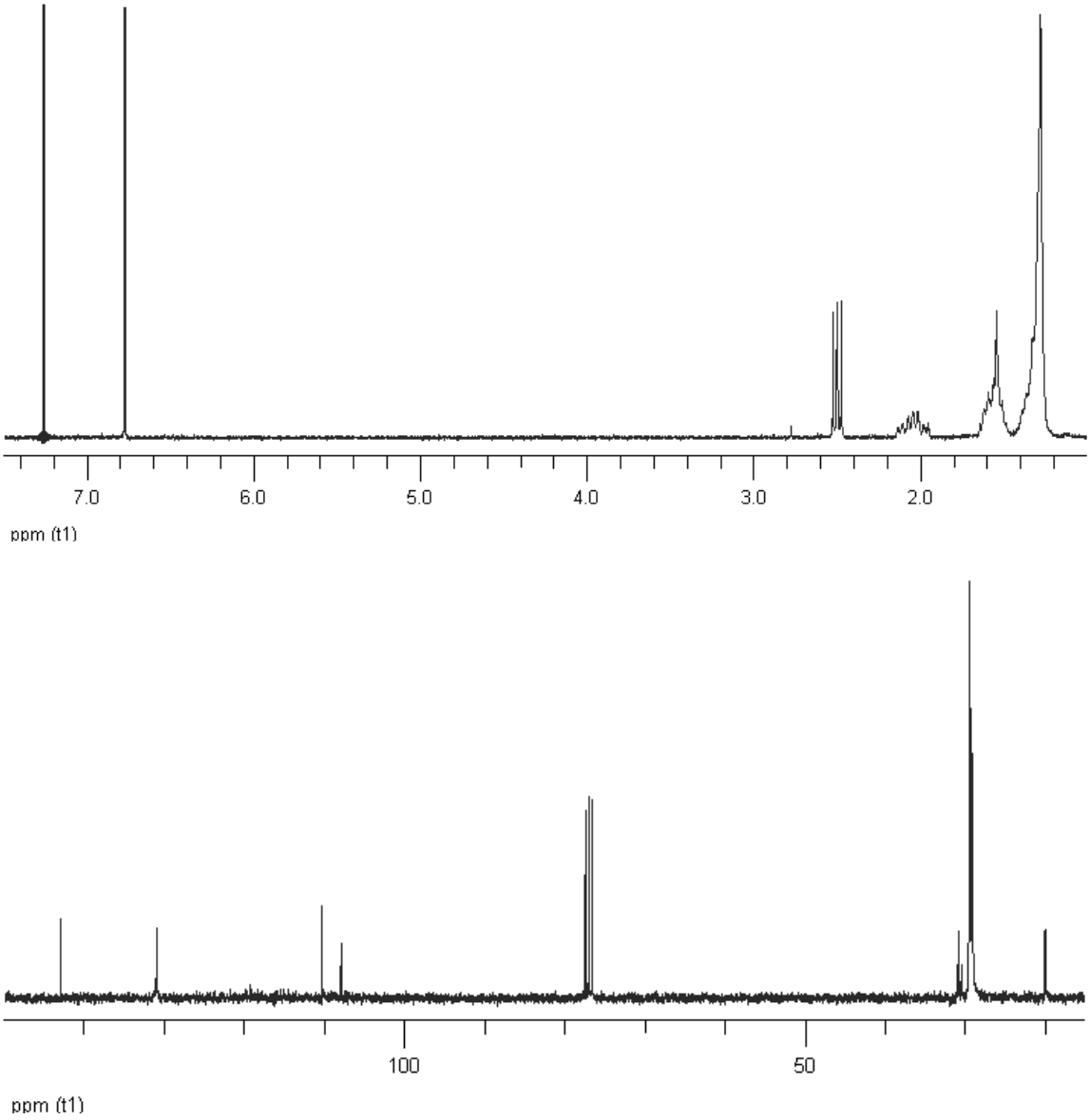

Figure C.25. ^{1}H (top) and ^{13}C (bottom) spectra of **4(11,4)**.

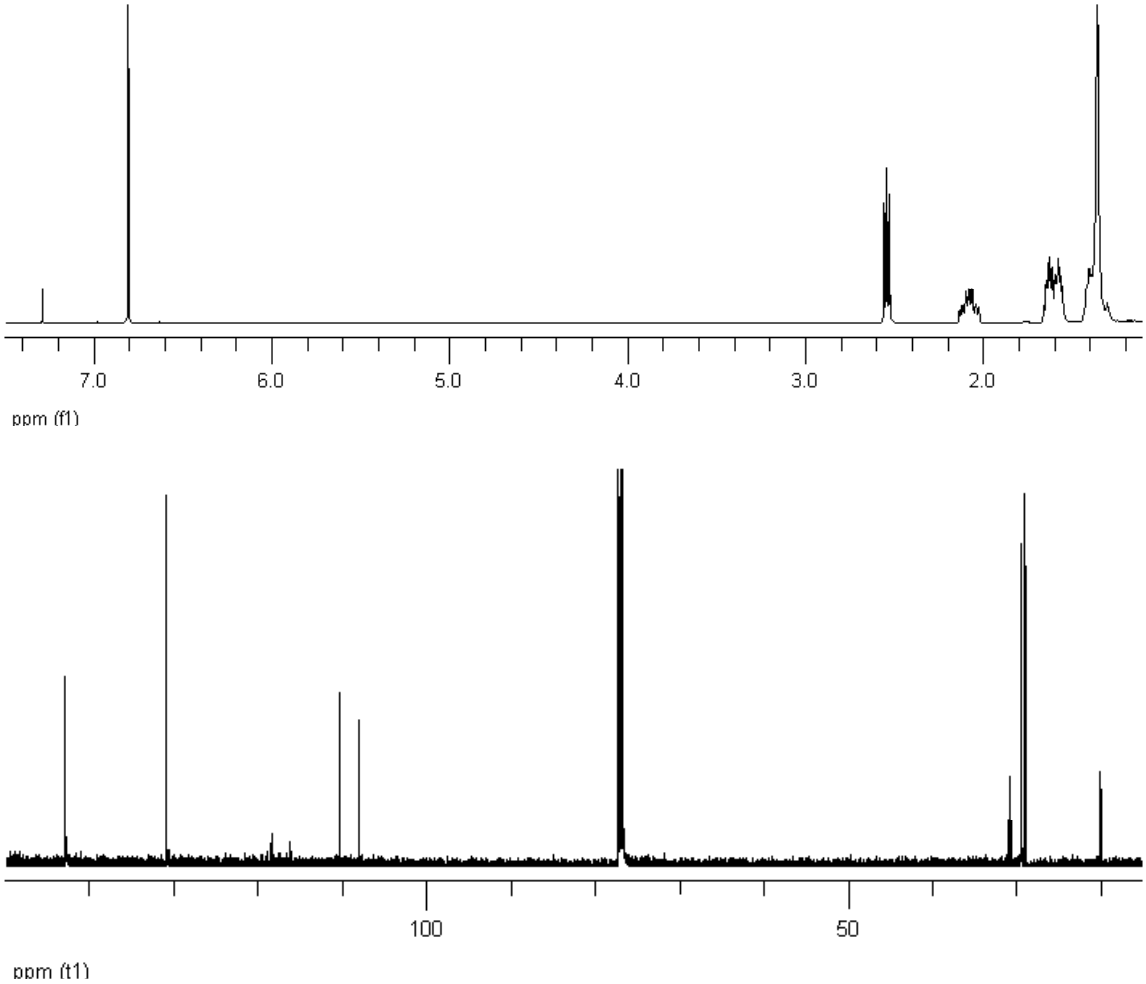

Figure C.26. ^{1}H (top) and ^{13}C (bottom) spectra of **4(8,4)**, with CF_2 resonances at 115-120 ppm in the ^{13}C spectrum.

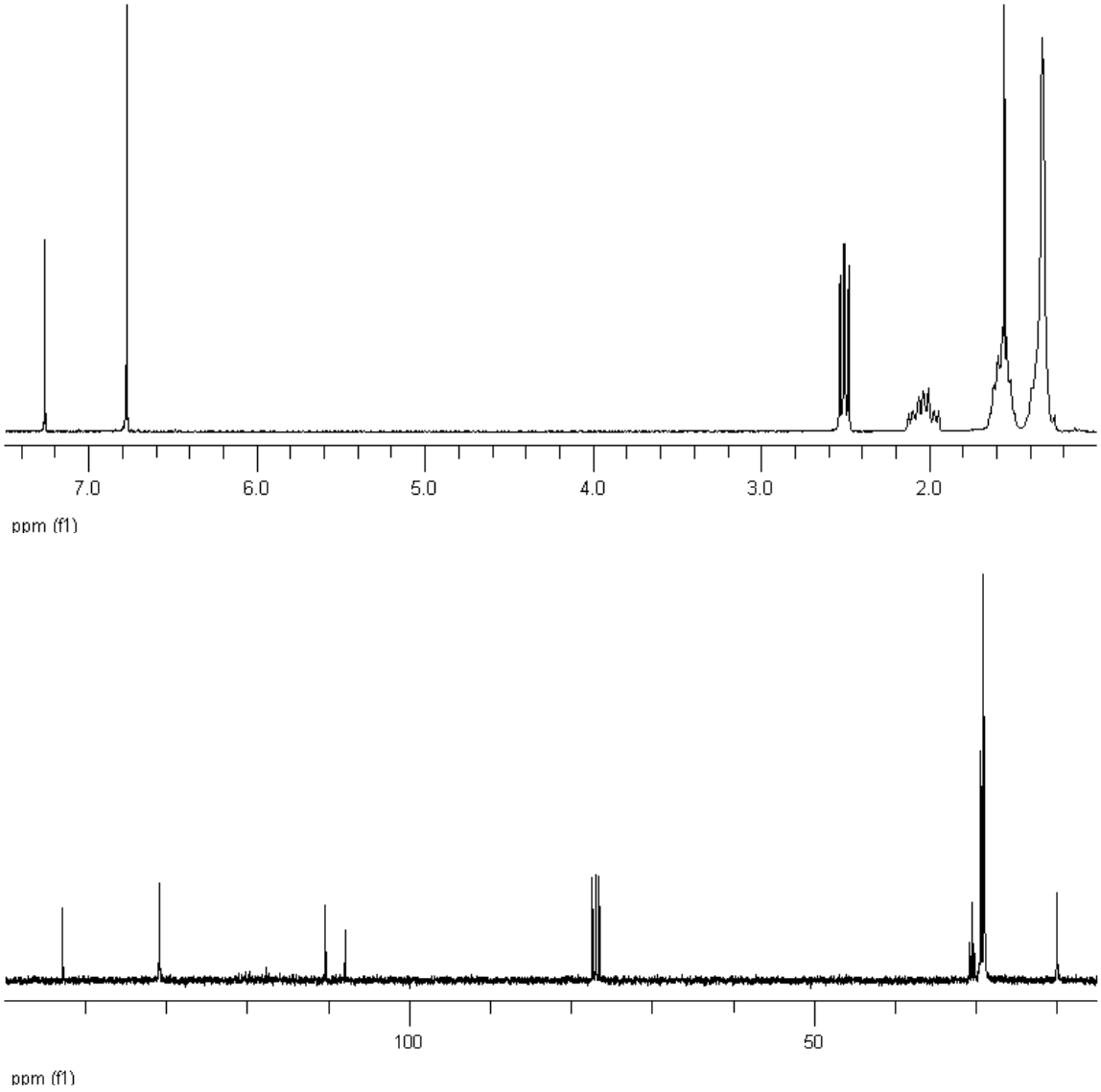

Figure C.27. ^{1}H (top) and ^{13}C (bottom) spectra of **4(8,3)**.

APPENDIX D: DSC THERMOGRAMS OF SIX POLY(3-SEMIFLUOROALKYL THIOPHENE) HOMOLOGUES

This appendix includes DSC thermograms for the six **Rg(Th-m,n)** compounds whose thermograms were not shown in Chapter 3. In general, the first scan of each thermogram is anomalous compared to subsequent scans. This is not unusual, as the first heating and cooling cycle is affected by any metastable states that arise from processing. Subsequent scans are generally quite similar to each other. A decrease in intensity upon subsequent scans occurs for some samples; this may be attributed to slight decomposition at relatively high temperatures. The results and conclusions associated with these figures are discussed in Chapter 3.

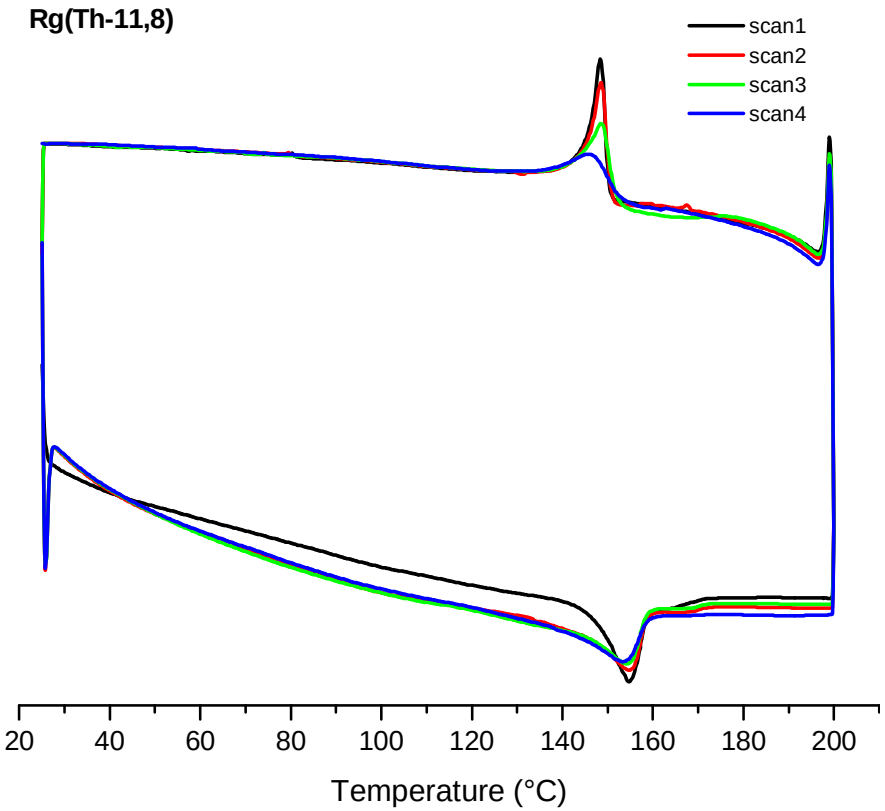

Figure D.1. DSC thermogram of regioregular **Rg(Th-11,8)** (heating and cooling at 10ºC/min). First scan is anomalous.

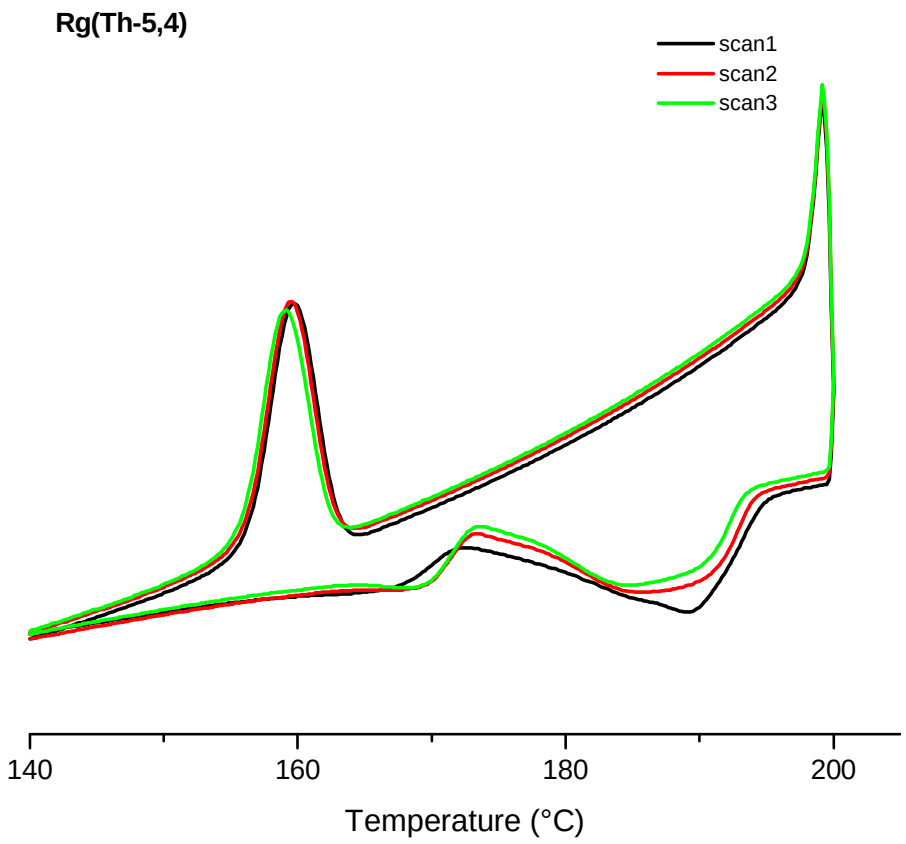

Figure D.2. DSC thermogram of regioregular **Rg(Th-5,4)** (heating and cooling at 10ºC/min). First scan is anomalous.

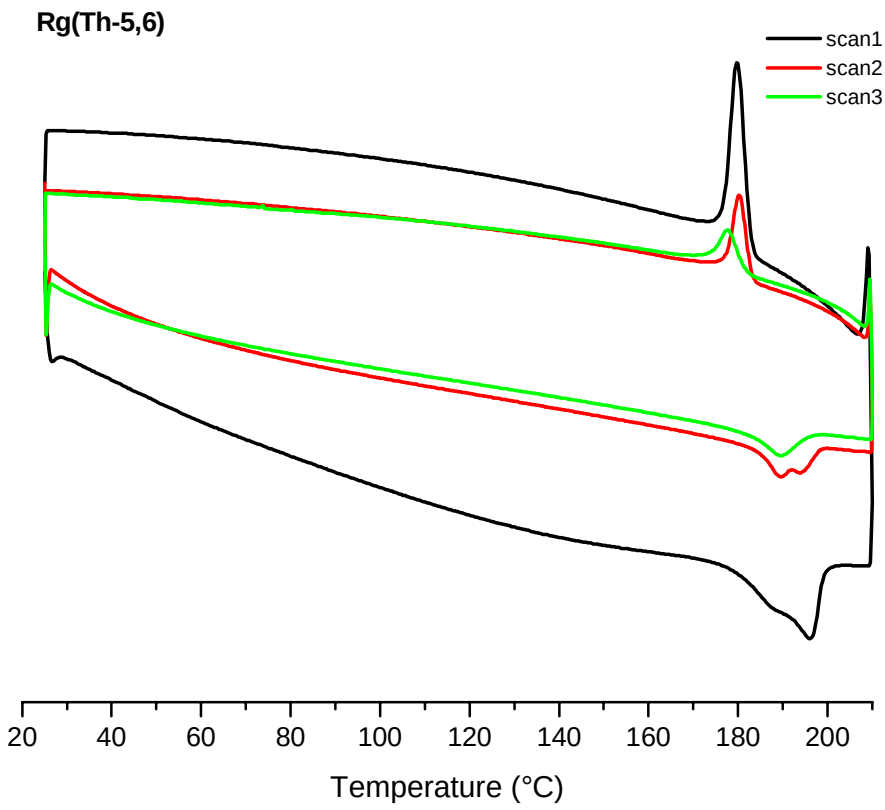

Figure D.3. DSC thermogram of regioregular **Rg(Th-5,6)** (heating and cooling at 10ºC/min).

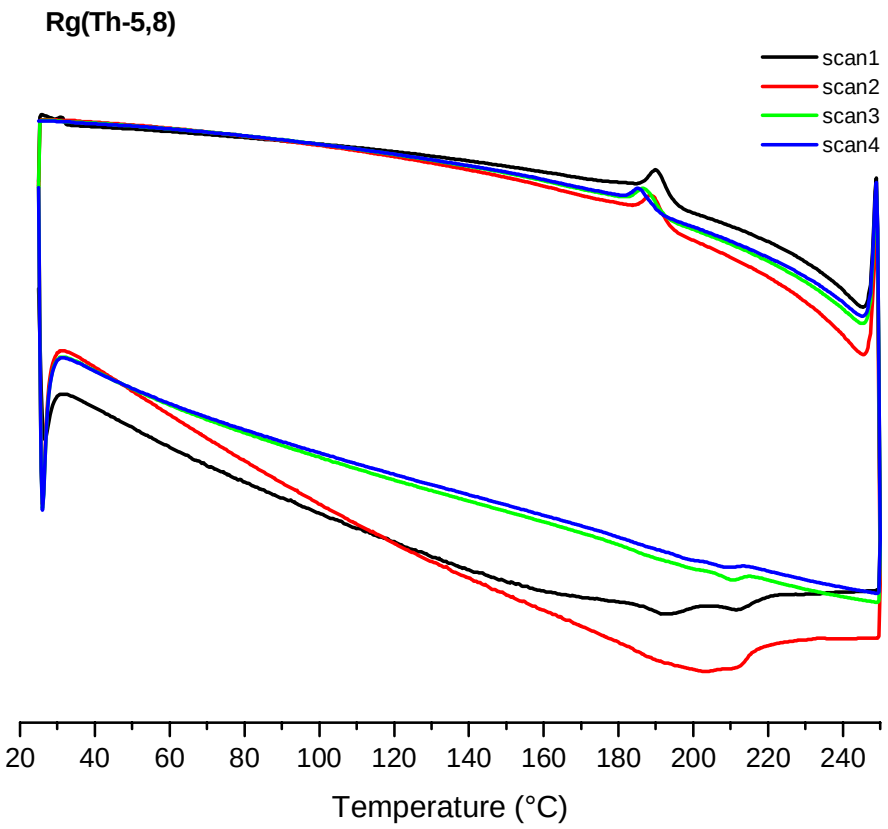

Figure D.4. DSC thermogram of regioregular **Rg(Th-5,8)** (heating and cooling at 10ºC/min).

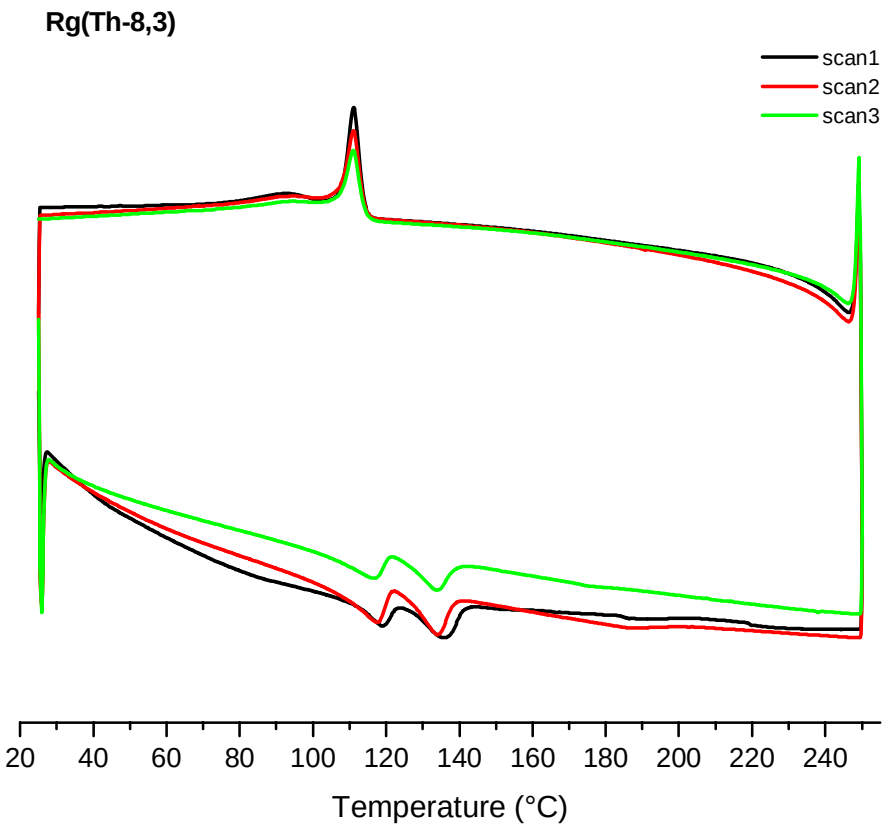

Figure D.5. DSC thermogram of regioregular **Rg(Th-8,3)** (heating and cooling at 10ºC/min).

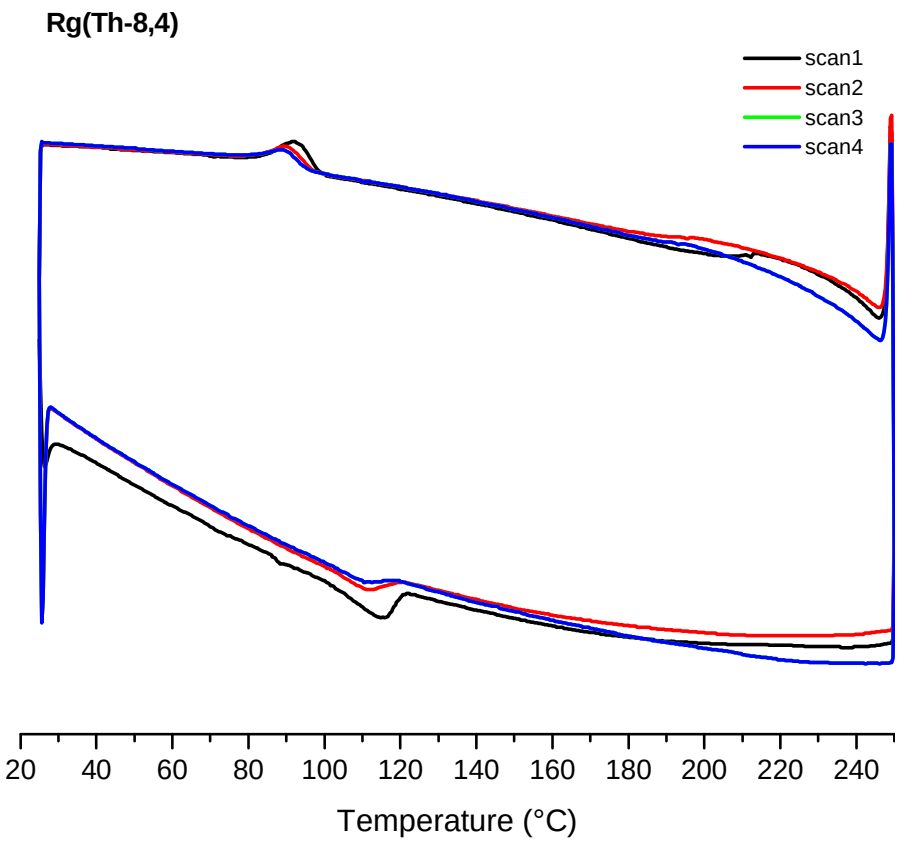

Figure D.6. DSC thermogram of regioregular **Rg(Th-8,4)** (heating and cooling at 10ºC/min). First scan is anomalous.

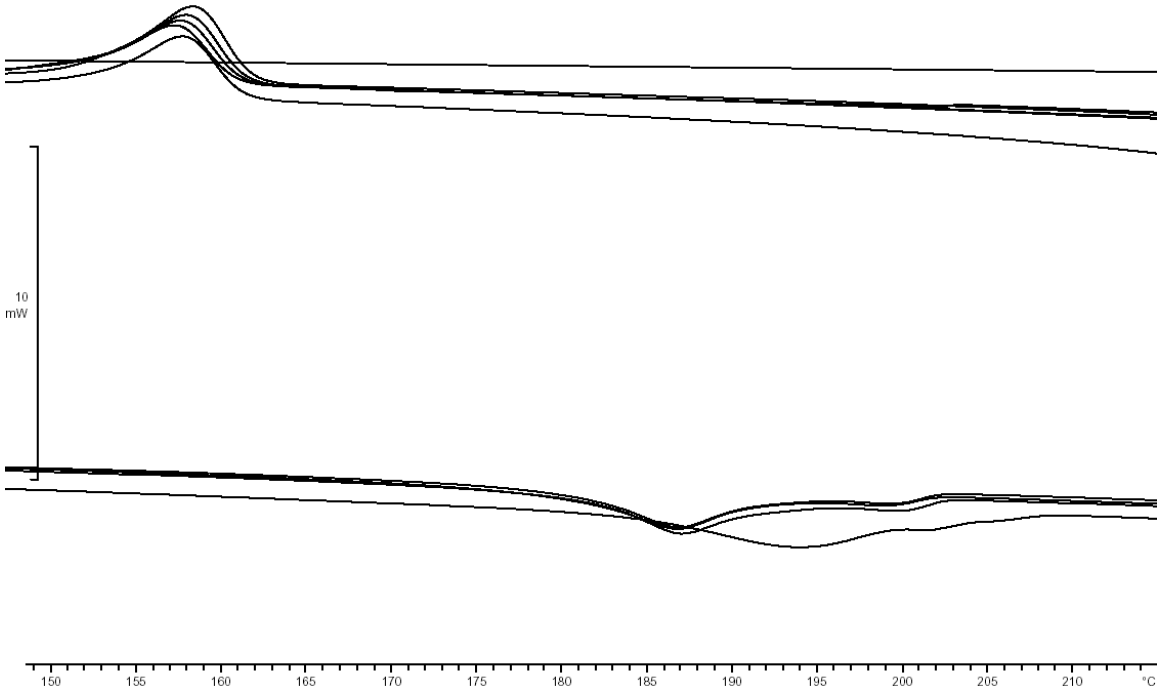

Figure D.7. DSC thermogram of regioregular **Rg(Th-8,0)** (heating and cooling at 10ºC/min). First scan is anomalous.

APPENDIX E: CYCLIC VOLTAMMAGRAMS OF 1,8- BIS(OLIGOTHIENYL) NAPHTHALENES

All experiments were performed using 2-6 mM analyte and 0.1 M *n*-Bu_4NPF_6 electrolyte in CH_2Cl_2 with an Au working electrode, Pt auxiliary electrode, and Ag/Ag^+ reference electrode at a scan rate of 100 mV/s.

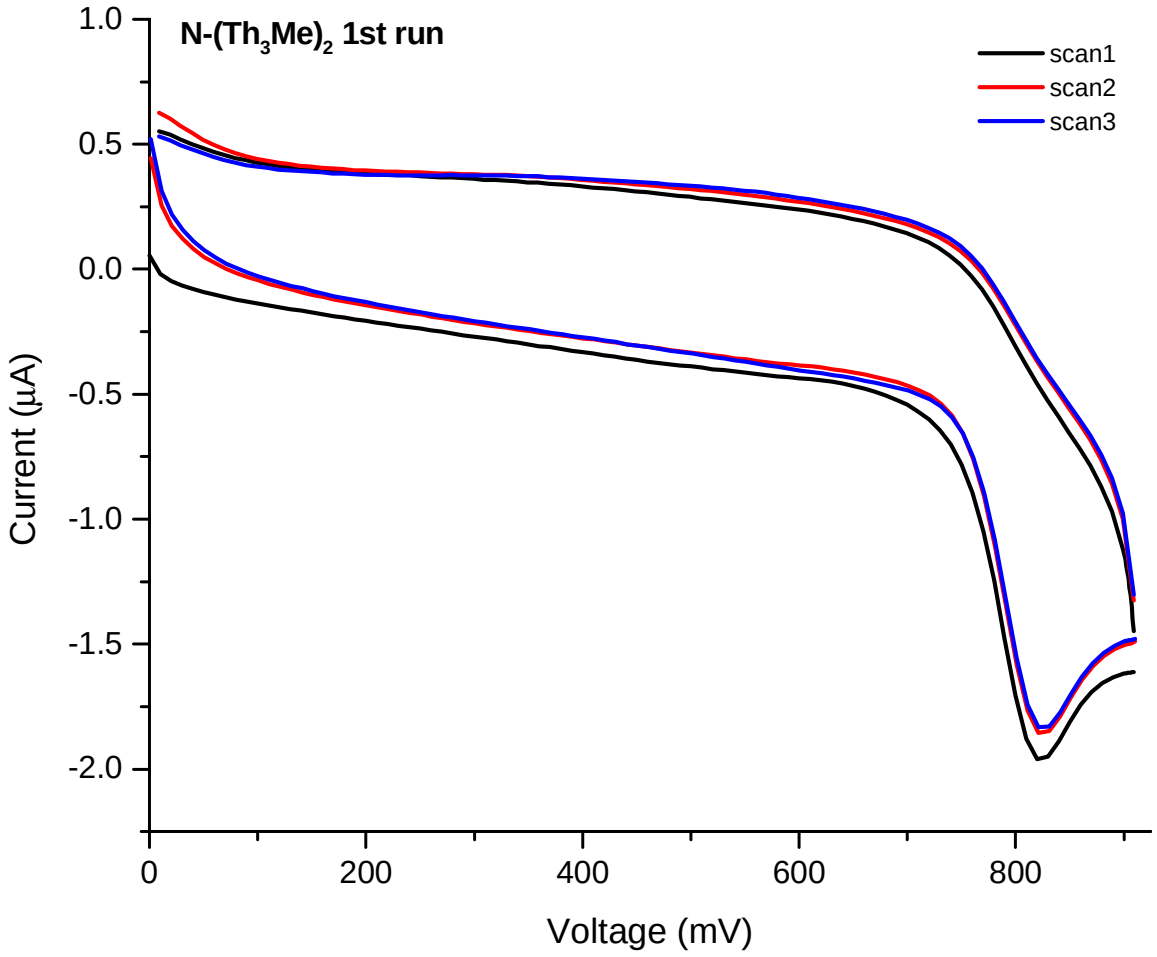

Figure E.1. CV of **7 N-($Th_3Me)_2$**, first run.

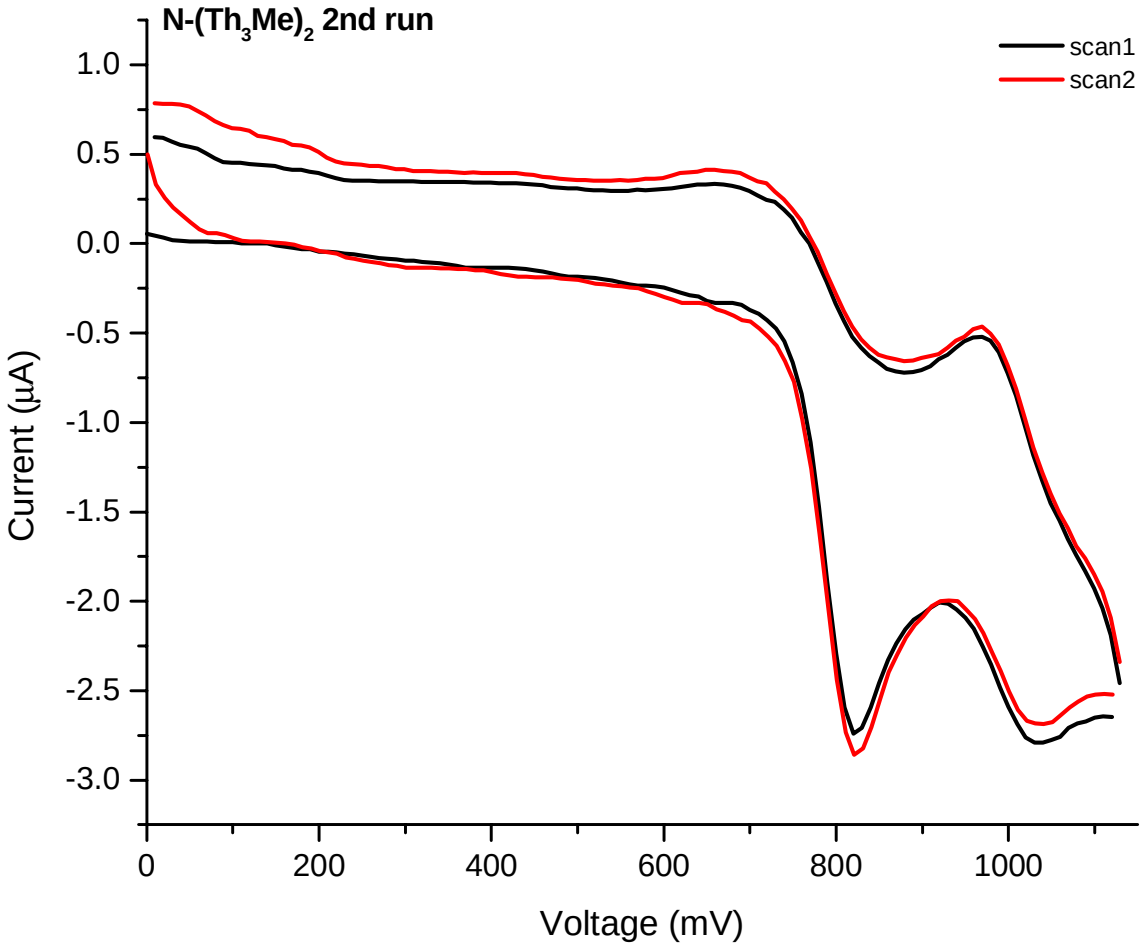

Figure E.2. CV of **7 N-(Th$_3$Me)$_2$**, second run.

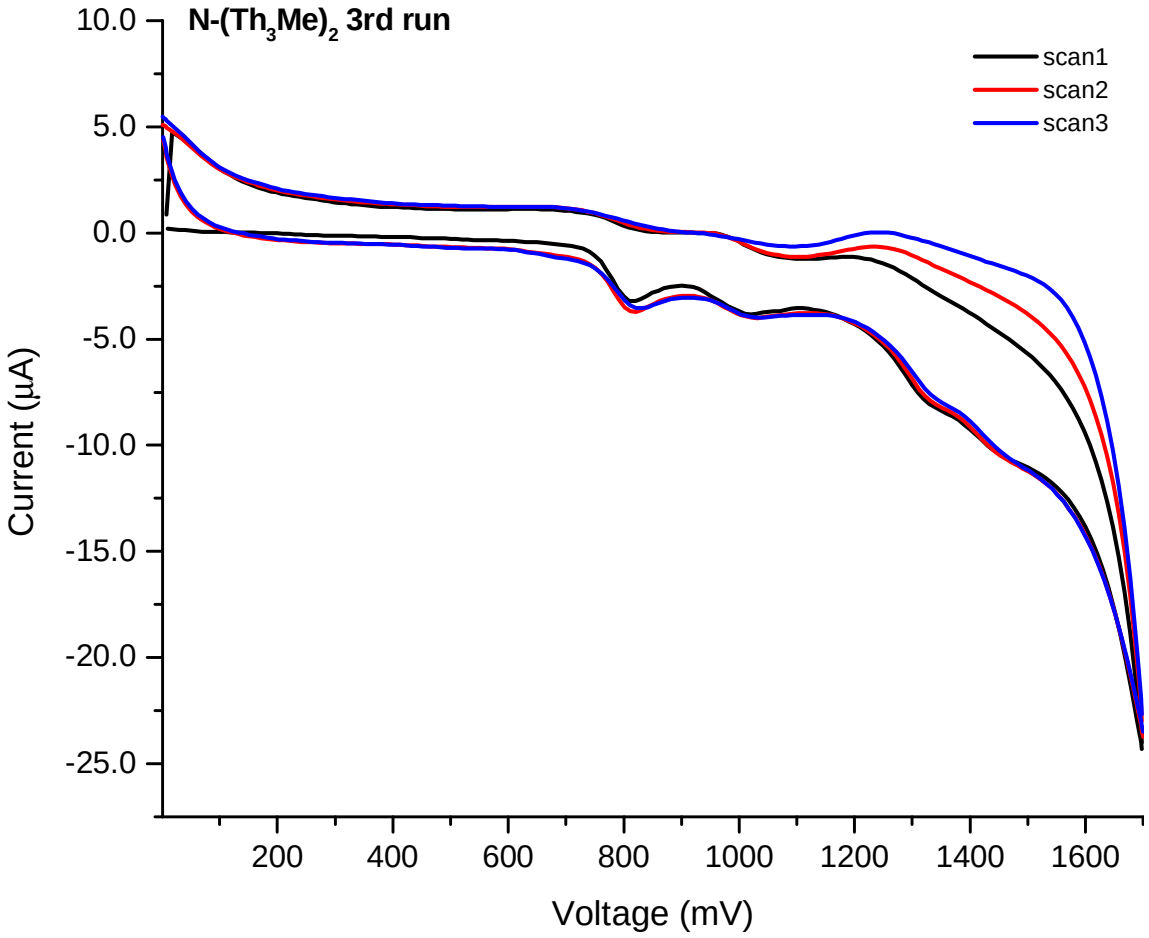

Figure E.3. CV of **7 N-($Th_3Me)_2$**, third run.

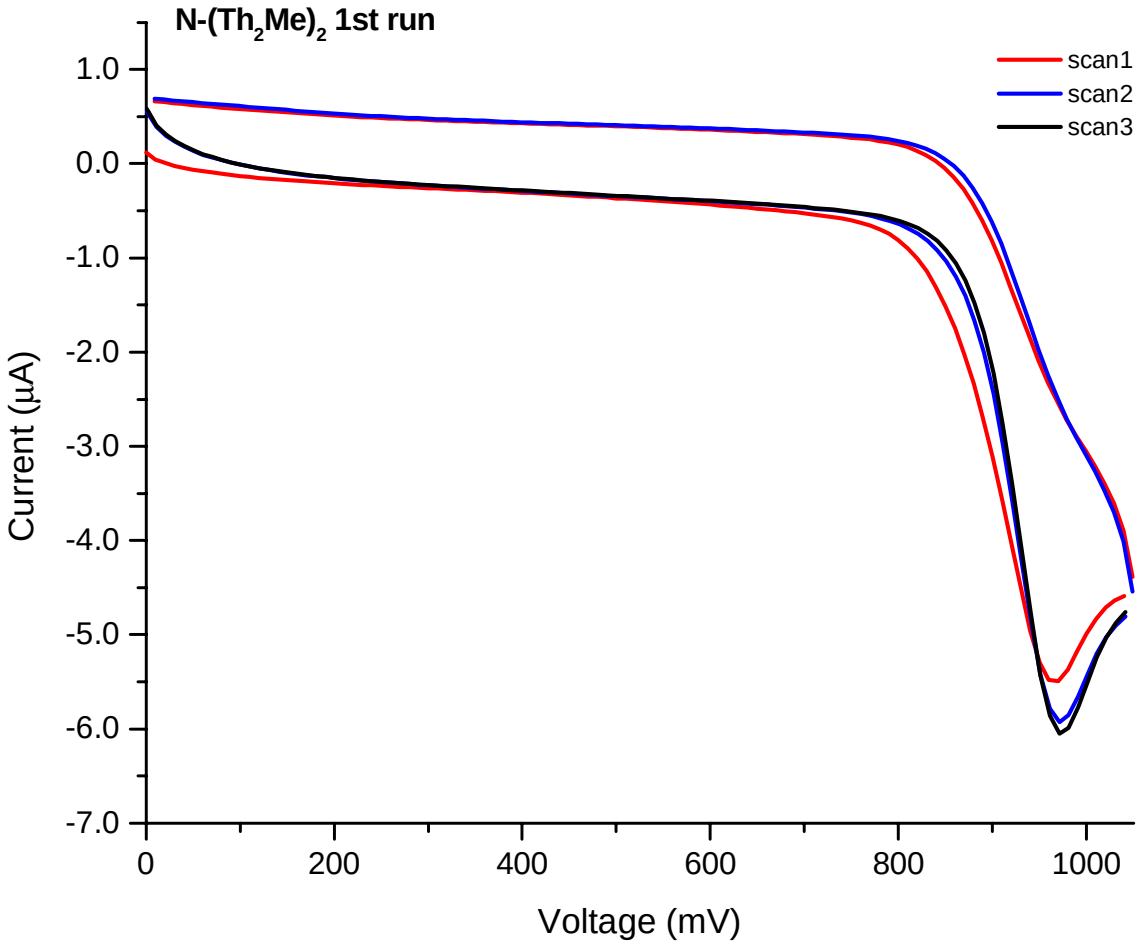

Figure E.4. CV of **5 N-($Th_2Me)_2$**, first run.

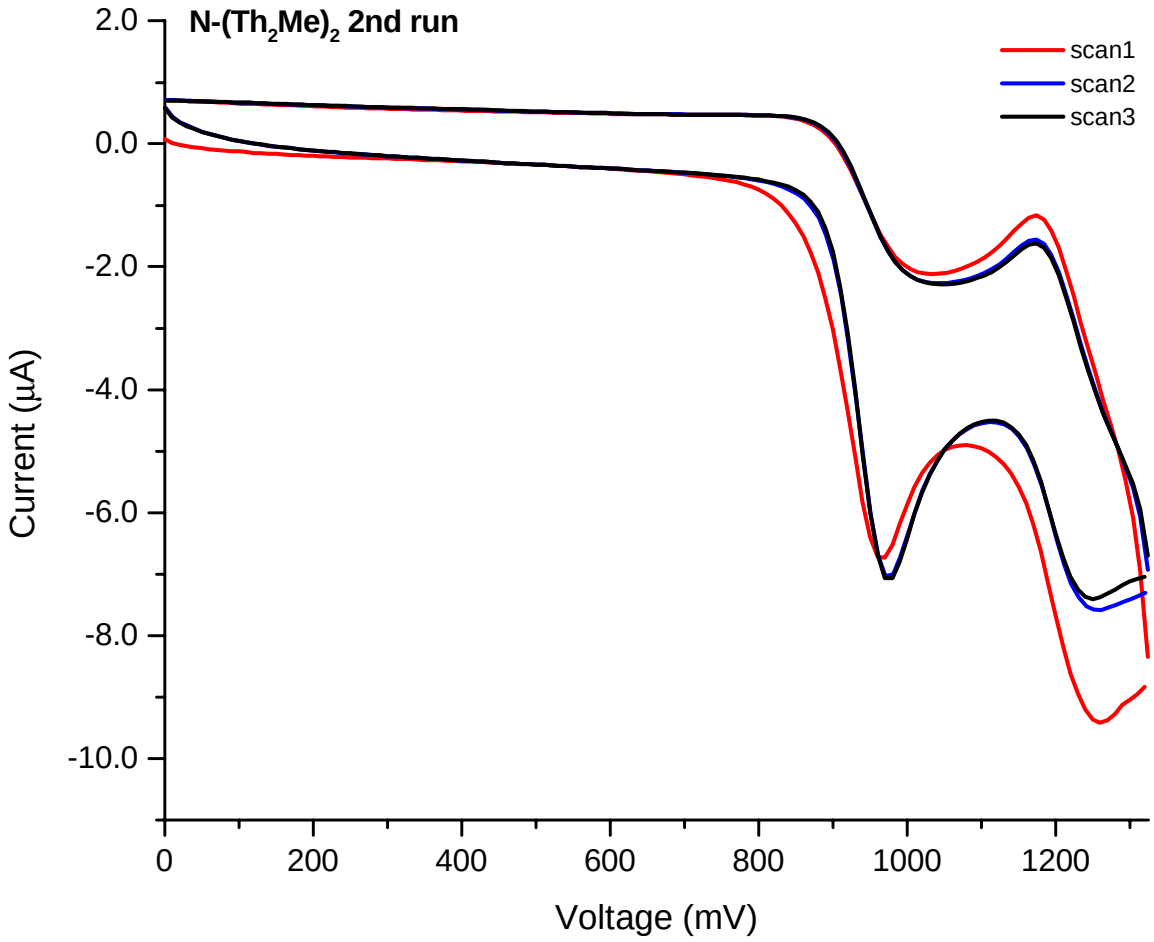

Figure E.5. CV of **5 N-($Th_2Me)_2$**, second run.

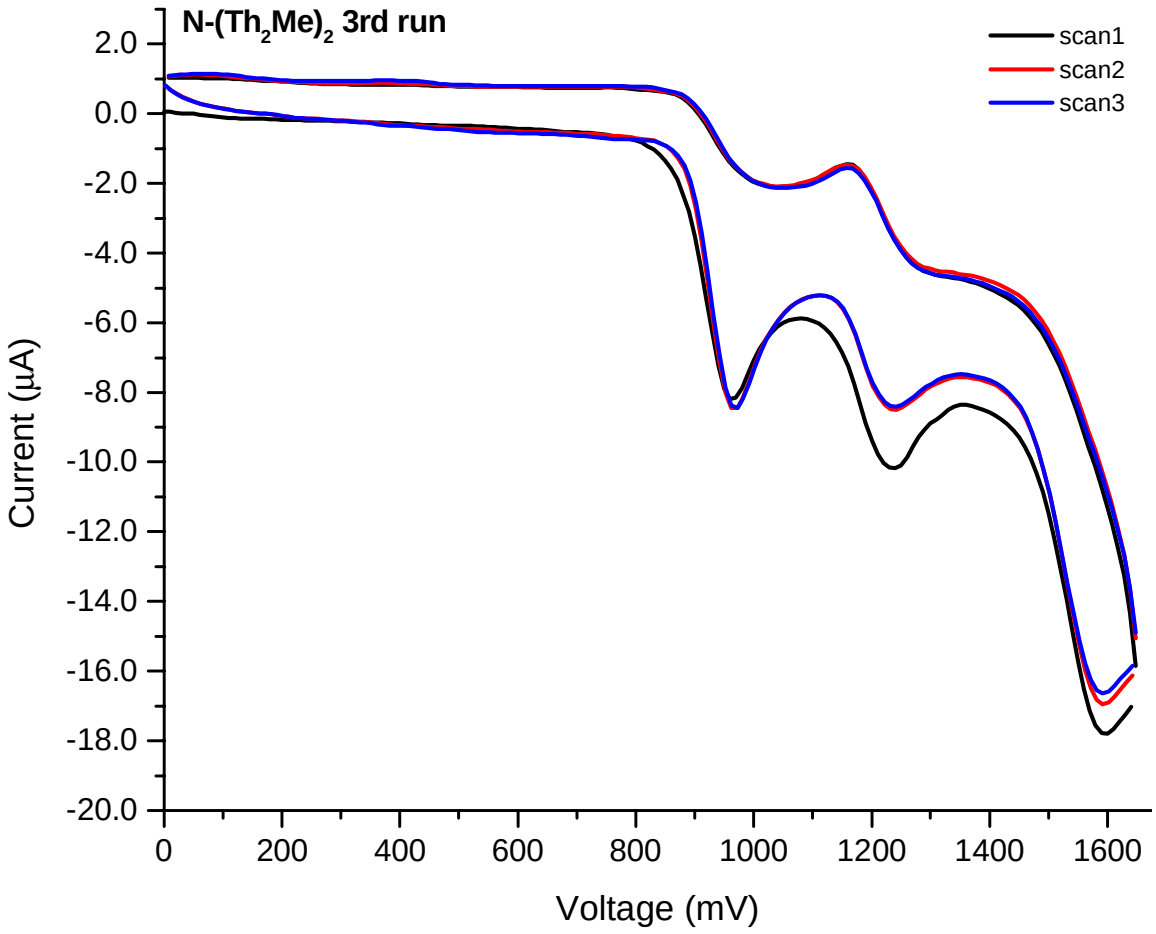

Figure E.6. CV of **5 N-($Th_2Me)_2$**, third run.

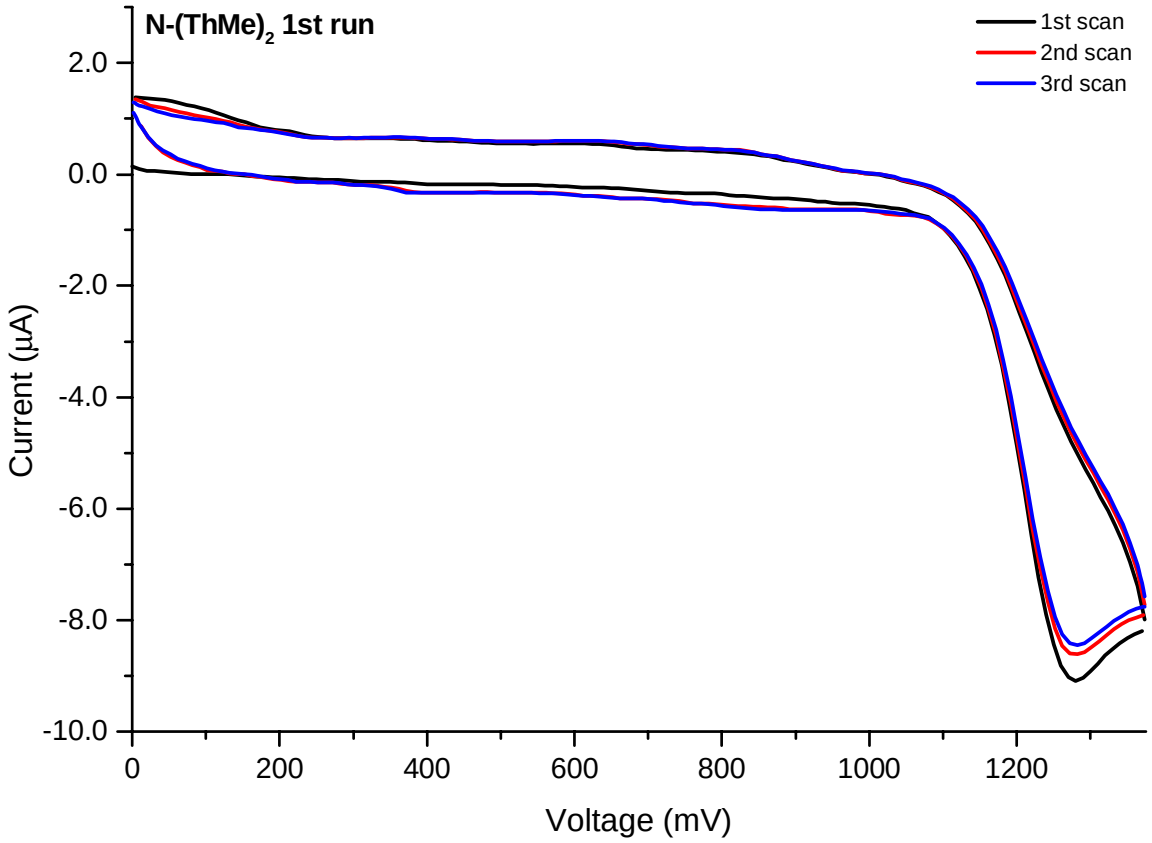

Figure E.7. CV of **3 N-(ThMe)$_2$**, first run.

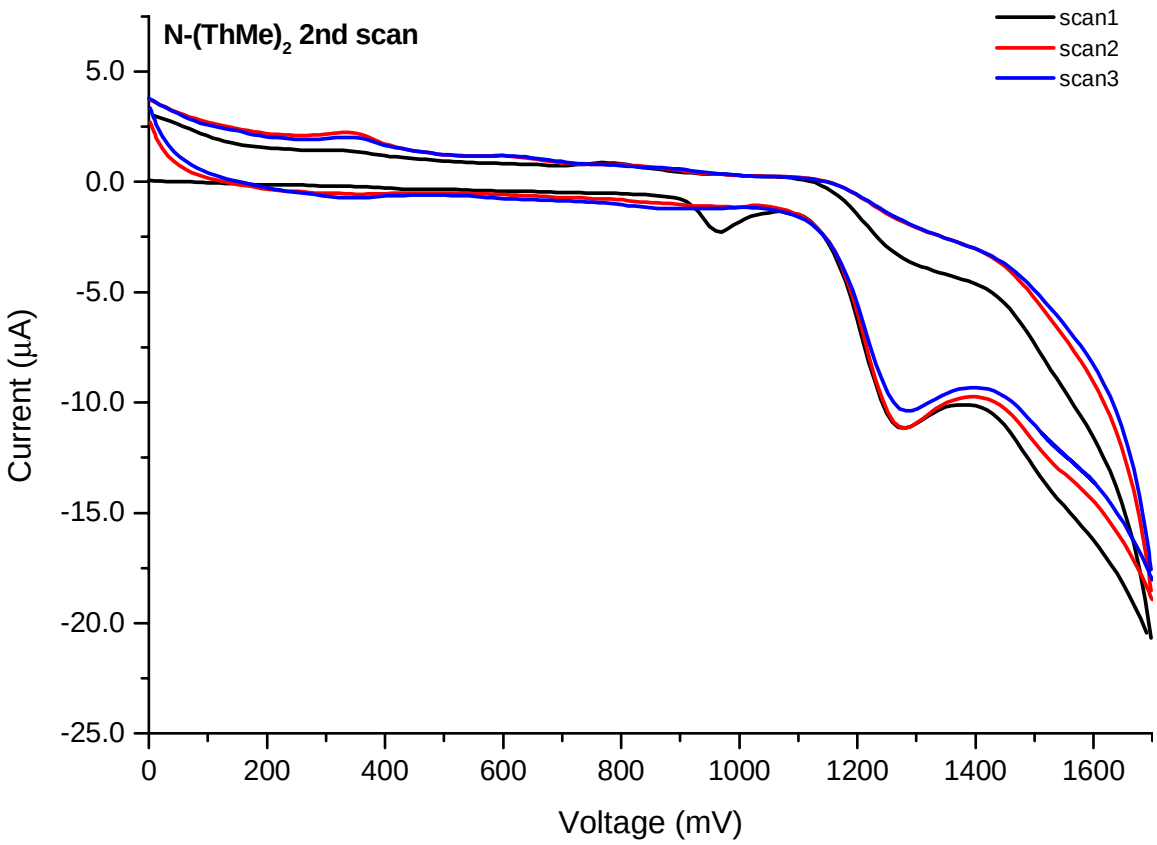

Figure E.8. CV of **3 N-(ThMe)$_2$**, second run.

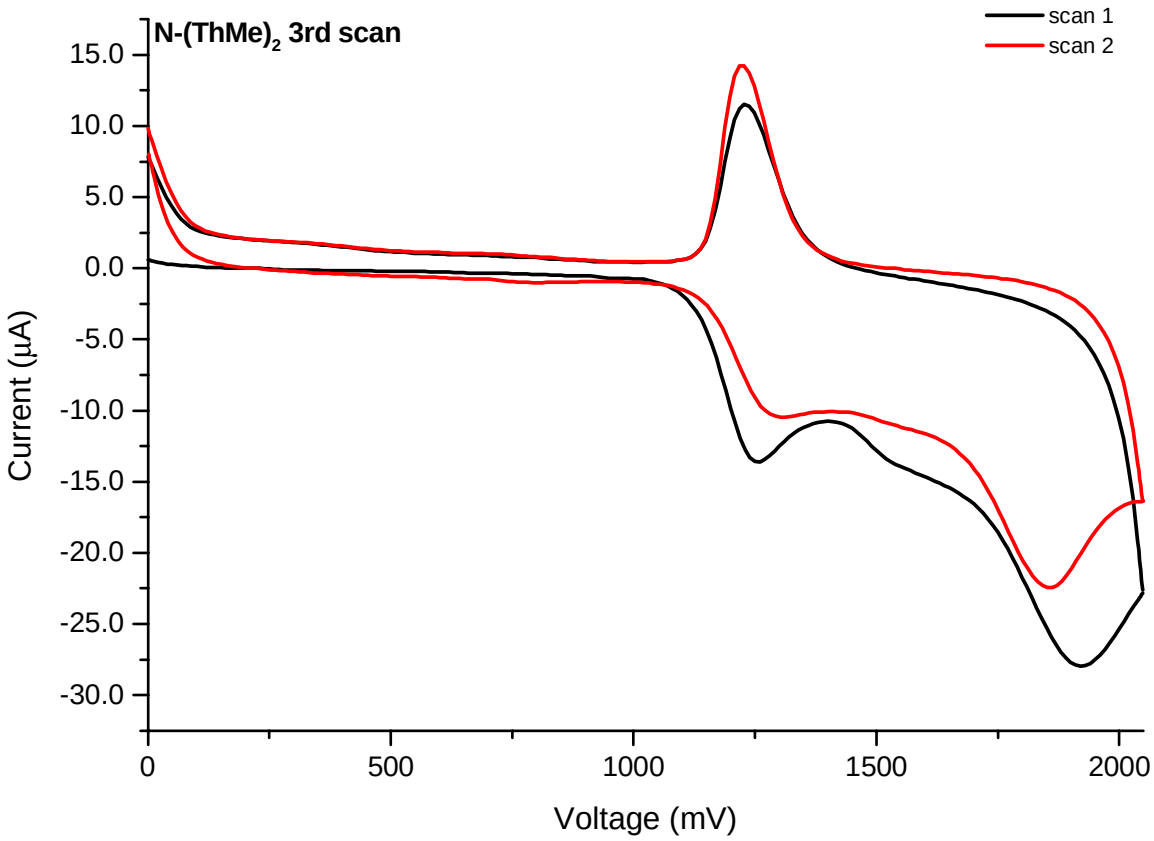

Figure E.9. CV of **3 N-(ThMe)$_2$**, third run.

APPENDIX F: SUPPLEMENTAL INFORMATION FOR CONFORMATIONAL ANALYSIS OF N-($Th_2Me)_2$ BY NMR

Table F.1. Possible conformations of **5 N-($Th_2Me)_2$** and maximum number of corresponding NMR signals.

Conformer	Max. # NMR signals	Conformer	Max. # NMR signals
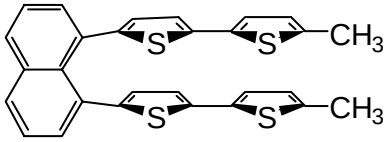	8 ^{1}H, 15 ^{13}C	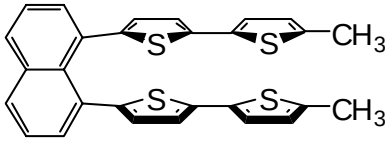	8 ^{1}H, 15 ^{13}C
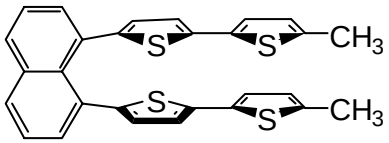	16 ^{1}H, 28 ^{13}C	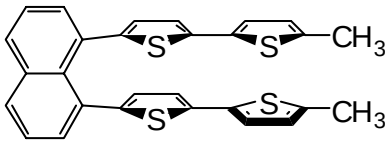	16 ^{1}H, 28 ^{13}C
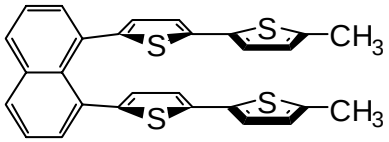	8 ^{1}H, 15 ^{13}C	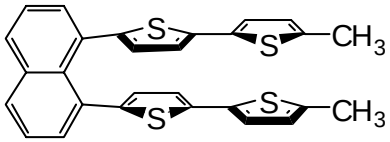	8 ^{1}H, 15 ^{13}C

The coalescence rate constant k_c is given by the equation

$$k_c = \frac{\pi \Delta \nu}{\sqrt{2}} = 2.22 \Delta \nu$$

where $\Delta\nu$ is the separation (in Hz) between the NMR signals corresponding to each of the two conformers. The coalescence temperature T_c can be calculated from the free enthalpy of activation (in units of cal mol^{-1}) using the equation

$$\Delta G_c = 4.58 T_c \left(10.32 + \log \frac{T_c}{k_c} \right)$$

Because k_c—and, consequently, T_c—is determined by the magnitude of $\Delta\nu$, it varies with the NMR frequency and with the separation between NMR signals. Table F.2 illustrates the effect of ΔG_c, field strength, and signal separation on k_c and T_c.[1]

Table F.2. Effect of various parameters on coalescence temperature T_c

ΔG_c (cal mol^{-1})	NMR frequency ν (MHz)	Δν (ppm)	k_c (Hz)	T_c (°C)
3500	400	0.2	177.6	-196.4
3500	100	0.2	44.4	-200.6
3500	100	2.0	444	-193.4
500	400	0.2	177.6	-261.3
500	100	0.2	44.4	-262.0
500	100	2	444	-260.7

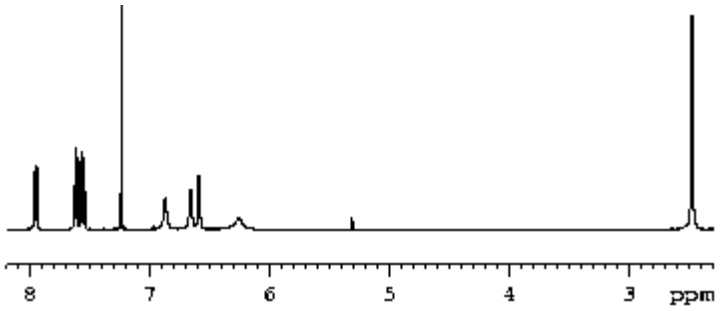

Figure F.1. ^{1}H NMR of a dilute (5 mg/mL) sample of **5 N-(Th_2Me)$_2$** at –50 °C.

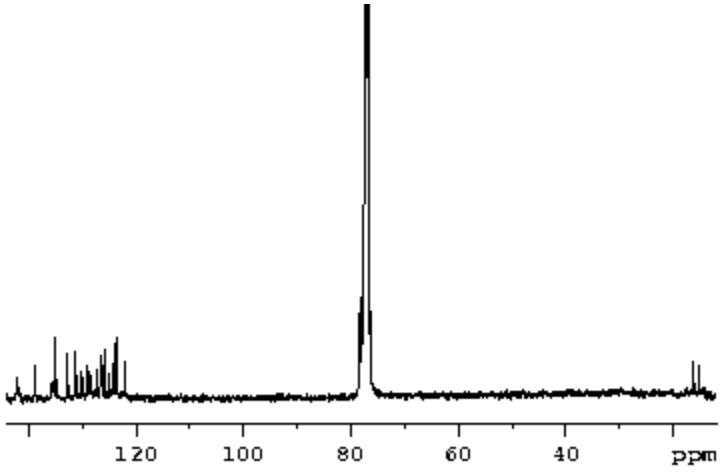

Figure F.2. ^{13}C NMR of a dilute (5 mg/mL) sample of **5 N-(Th_2Me)$_2$** at –40 °C.